TRITA-ETS-2002-07
ISSN 1650-674X

Synchronous Voltage Reversal Control of Thyristor Controlled Series Capacitor

Lennart Ängquist

Royal Institute of Technology
Department of Electrical Engineering

TRITA-ETS-2002-07
ISSN 1650-674X

Synchronous Voltage Reversal Control of Thyristor Controlled Series Capacitor

Lennart Ängquist

Stockholm 2002
Doctoral Dissertation
Royal Institute of Technology
Department of Electrical Engineering

Nothing is as practical as a good theory
Kurt Lewin (1890-1947)

Abstract

Series compensation of transmission lines is an effective and cheap method of improving the power transmission system performance. Series capacitors virtually reduces the length of the line making it easier to keep all parts of the power system running in synchronism and to maintain a constant voltage level throughout the system. In Sweden this technology has been in use since almost 50 years.

The possibility to improve the performance of the AC transmission system utilizing power electronic equipment has been discussed a lot since about ten years. Some new semiconductor based concepts have been developed beside the since long established HVDC and SVC technologies. The Thyristor Controlled Series Capacitor (TCSC) is one such concept. By varying the inserted reactance an immediate and well-defined impact on the active power flow in the transmission line is obtained. Several potential applications, specifically power oscillation damping, benefit from this capability. The concept implied the requirement to design a semiconductor valve, which can be inserted directly in the high-voltage power circuit. This certainly presented a technical challenge but the straightforward approach appeared to be a cost-effective alternative with small losses.

It was also realized that the TCSC exhibits quite different behaviour with respect to subsynchronous frequency components in the line current as compared to the fixed series capacitor bank. This was a very interesting aspect as the risk of subsynchronous resonance (SSR), which just involves such line current components, has hampered the use of series compensation in power systems using thermal generating plants.

The thesis deals with the modelling and control aspects of TCSC. A simplifying concept, the equivalent, instantaneous voltage reversal, is introduced to represent the action of the thyristor controlled inductive branch, which is connected in parallel with the series capacitor bank in the TCSC. The ideal voltage reversal is used in the thesis in order to describe and explain the TCSC dynamics, to investigate its apparent impedance at various frequencies, as a platform for synthesizing the boost control system and as the base element in deriving a linear, small-signal dynamical model of the three-phase TCSC. Quantitative Feedback Theory (QFT) then has been applied to the TCSC model in order to tune its boost regulator taking into account the typical variation of parameters that exists in a power system. The impact of the boost control system with respect to damping of SSR is finally being briefly looked at.

Keywords: Thyristor Controlled Series Capacitor, TCSC, FACTS, reactive power compensation, boost control, phasor estimation, Quantitative Feedback Theory, subsynchronous resonance, SSR.

Acknowledgements

First I would like to thank my advisor, Professor Åke Ekström, for giving me support in the work with the thesis. We met already in 1969 when I was a trainee in the HVDC depertment in ASEA and Åke Ekström was head of the system department. My work at that time was to modify a technical memorandum about transfer functions for HVDC converters according to the concept of "equidistant" triggering. I found this kind of work most fascinating and I have kept my interest for mathematical modelling of converters ever since. Many years later I met Åke Ekström again, when he had taken up the Professor chair in Stockholm, and he has encouraged me to make this thesis. I am very grateful for his help and interest.

My work with the Thyristor Controlled Series Capacitor started already in 1989, when it was first decided that an outdoor thyristor valve should be constructed and tested in the AEP network in Kanawha River Series Capacitor station, West Virginia, USA. Then I have been involved in TCSC work in Stöde, Sweden, and in Imperatríz, Brazil. So I have had the possibility to follow the development from the first idea to the implementation, testing and commissioning. In this process I have worked together with many colleagues within ABB. I would like to thank them all for giving ideas, help and support in all phases of the work. It is not possible to mention all, and I will only address two persons who have been specially important for me in this work: Mr Per Halvarsson, with whom I have worked through all these years. He combines wise technical judgement, practical skill and good administrative talents in one person. Mr Erik Hansson, who has guided me in the work with computer control systems and who has been a trustworthy companion in work in the field.

In order to do the thesis work and to attend the courses I have had the support from my company ABB. I would like to thank the managers Hans-Åke Jönsson and Mikael Norin for their support.

Finally I would like to thank my wife, who has encouraged me to finalize this work, which took a lot more time than I could ever foresee.

Lennart Ängquist
Enköping, August 2002

List of Acronyms

Acronyms	Description
FACTS	Flexible AC Systems
PLL	Phase-Locked-Loop
PWM	Pulse-Width Modulation
POD	Power Oscillation Damping
QFT	Quantitative Feedback Theory
rms	Root Mean Square
RLS	Recursive Least Square
SSR	Subsynchronous Resonance
SSSC	Static Synchronous Series Compensator
STATCOM	Static Synchronous Compensator
SVC	Static Var Compensator
SVR	Synchronous Voltage Reversal
TI	Torsional Interaction (SSR)
TCR	Thyristor Controlled Reactor
TCSC	Thyristor Controller Series Capacitor
TSSC	Thyristor Switched Series Capacitor
UPFC	Unified Power Flow Controller
VSC	Voltage-Source Converter

List of Contents

CHAPTER 1
OVERVIEW OF THE THESIS

1.1 BACKGROUND

For many years the use of power electronic equipment in power transmission systems was restricted to High Voltage Direct Current (HVDC). But in the 1970'ies the Static Var Compensator (SVC) was introduced as a means to provide reactive power support and voltage control in the network. It found wide-spread application in transmission systems as well as in large industrial plants. The fast development of high-power semiconductors during the 80'ies brought forward rugged thyristors capable of handling high voltages and heavy short-circuit currents. As a result intense research efforts were initiated in many places with the overall objective to improve the AC transmission technology by introducing power electronics to control voltage, phase and current in such systems. The well-known FACTS program was launched by EPRI in USA around 1990. Many new concepts were proposed, among them the Thyristor Controlled Series Capacitor (TCSC).

The first proposed use of TCSC was related to power flow control, but it was soon realized that the device is also a very effective means for providing damping of electromechanical power oscillations. A third possible application of TCSC emerged from the insight that it can provide series compensation without causing the same risk for subsynchronous resonance (SSR) as a fixed series capacitor.

In the TCSC concept the thyristor valve is connected directly in series with the transmission line and accordingly it becomes fully exposed to all overvoltages occurring in the system. Thus the main circuit, including the cooling system, requires full insulation relative ground level, which means that it shall withstand impulse tests with voltage amplitudes well exceeding 1000 kV. This was a challenge as earlier power electronic apparatus had always been connected to the high voltage circuit through their own dedicated transformers. However, the challenge also brings about an opportunity, because eliminating the need for an

interfacing transformer, which would represent substantial cost and losses, makes the TCSC an economically attractive device with low losses.

1.2 OBJECTIVES

The purpose of this thesis is to present a general overview of the TCSC concept. The steady-state characteristics are well known from the literature and a number of dynamical models also have been presented in different papers. However, in the author's opinion, the dynamical models presented so far turn into mathematics very fast. The engineer is left without any good description making it easy to understand the dynamics of the TCSC.

- *it is an objective of the present thesis to present a conceptual description, a "theory", of the function of the TCSC, giving an intuitive insight into its dynamical behaviour*

For design and tuning of the control system a good dynamical model is also needed.

- *it is an objective of the present thesis to derive a dynamical model, based on the presented description, having sufficient accuracy and bandwidth*

Any apparatus that shall be installed in the power transmission system must be designed so that it can cope with the parameter variation that normally occurs when the system is in operation.

- *it is a further objective of the thesis to investigate a method to design a robust control system taking such parameter variations into consideration*

1.3 METHODS AND RESULTS

1.3.1 Use of the capacitor voltage zero-crossing angle

In thyristor converter technology the firing angle with respect to the driving voltage, often denoted as α, has traditionally been considered as the natural converter control signal. This convention also has been inherited into other fields of power electronic equipment, like SVC and TCSC. In all literature presented so far this traditional method has been applied. It is certainly well adapted to describe the characteristics of the TCSC in steady state operation. However, the same approach it is not very helpful, when one tries to describe the dynamical behaviour of the TCSC in a comprehensive way. There is simply no general principle to connect the change of firing angle to the change of the operating state in the TCSC.

In this thesis the focus has been changed from the thyristor firing angle to the angle related to the capacitor voltage zero-crossing. The reason is that during steady state conditions the capacitor voltage zero-crossing must occur at one

uniquely determined equilibrium angle relative the line current, and any displacement of the capacitor voltage zero-crossing from this equilibrium position has a well-defined impact on the state of the TCSC. Many main characteristics of the TCSC, even quantitative ones, can easily be related to the displacement of the capacitor voltage zero-crossing angle from its equilibrium position.

1.3.2 Equivalent instantaneous voltage reversals

The insight of the importance of the capacitor voltage zero-crossing angle permits an idealisation, where we consider an equivalent TCSC circuit, which performs **instantaneous** voltage reversals as a substitute for the real voltage reversals that needs **finite** time to be executed in the main circuit. This idealisation is extensively used in this thesis as a base for modelling and simulation. It generates a new theory of TCSC control, which is developed further as described below.

1.3.3 Synchronous Voltage Reversal (SVR) control scheme

The concept of equivalent instantaneous voltage reversals serves as a platform for synthesis of a new control system for the TCSC. The boost control system has a structure, where the regulator provides a timing reference for the capacitor voltage zero-crossing instants and a subsystem finally determines the thyristor firing instant taking into account the timing reference and the measured instantaneous capacitor voltage and line current values.

1.3.4 TCSC characteristics at subsynchronous frequencies

It is possible to derive the basic, inherent characteristics of the TCSC at subsynchronous frequencies from a simple analysis using the concept of the equivalent instantaneous voltage reversals.

1.3.5 Three-phase TCSC model

Using the concept of equivalent instantaneous voltage reversals a small-signal, three-phase model of the TCSC can be derived. It has a sampling rate of 300/360 Hz in a 50/60 Hz network. The high sampling rate means that frequencies covering the whole subsynchronous frequency range can be dealt with without violating the Nyquist frequency limit.

1.4 CONTRIBUTIONS IN THE WORK

The present work provides the following contributions:

- description of the TCSC using the concept of equivalent capacitor voltage reversals as described in chapter 4.1

- derivation of boost dynamics as described in chapter 4.4
- SVR control system architecture as described in chapter 4.5
- control equation for the fire pulse generating subsystem as described in chapter 4.6
- derivation of the apparent impedance of the TCSC for subsynchronous frequencies as described in chapter 5.3, 5.4 and 5.5
- incorporation of the homopolar component in the "converter-oriented" coordinate system as described in chapter 6
- three-phase dynamical model of the TCSC as described in chapter 7

1.5 THESIS ORGANIZATION

The main purpose of this thesis is to discuss the problems related to modelling of the TCSC and the associated control problems. However, it seems appropriate to give a short introduction about reactive power in general and series compensation in particular. Hopefully this will provide a proper insight in the potential of application of the TCSC and a basic idea of what requirements that must be fulfilled by the device. Thus chapter 2 starts by presenting the physical background for the reactive power consumption in the network. The theoretical principle for reactive power series compensation is described. Further the applications and the implementation of series capacitors is explained.

Chapter 3 summarizes the steady state characteristics of the TCSC. This material is not new, but has been incorporated for reference.

Chapter 4 describes the main contribution of this thesis. The Synchronous Voltage Reversal scheme, is being presented.

Chapter 5 contains a simple derivation of the apparent characteristics of the TCSC at subsynchronous frequencies. A single-phase approach is utilized.

In chapter 6 the representation of three-phase converters is investigated. The concept of "converter-oriented" coordinate system is presented. The three-phase space vector representing the TCSC capacitor voltage including its homopolar component is presented and visualized.

Chapter 7 starts with summarizing some dynamical models of the TCSC which have been described in the literature. The motivation for developing a three-phase model is given and then the derivation of the three-phase TCSC model using the instantaneous voltage reversals as an idealising approximation is presented.

Chapter 8 describes the main characteristics of the derived model.

Chapter 9 very shortly discusses the outline of boost control system in the TCSC.

Chapter 10 deals with the topic of phasor estimation. Power electronic converters typically are utilized to control the fundamental frequency component of some

quantity like voltage or current. The problem to extract this component in real-time from measured signals is discussed. Models in the frequency and time domains are given.

In Chapter 11 the phasor estimation algorithms are used to get the response value of TCSC boost factor from the measured capacitor voltage and line current. The synchronization system, using the estimated line current phasor as input, also is investigated.

Chapter 12 describes the boost control problem for stiff line current. The boost regulator is tuned for some defined uncertainties using the Quantitative Feedback Theory (QFT) approach. The impact of the synchronization for improving the suppression of line current phases shifts is described. Comparison of the results from the idealized model used for tuning and a complete model that has fully implemented models of the main circuit shows a very good agreement.

In chapter 13 the control of the TCSC is investigated when it is inserted in a transmission line. Some uncertainties with respect to line resistance variation and source impedance variation are defined and the control system is tuned for these conditions.

Chapter 14 describes very briefly how one can investigate the electrical damping at subsynchronous frequencies of a generator connected to a radial transmission line that incorporates a TCSC.

Finally in chapter 15 the result of the work is summarized together with a short outlook.

CHAPTER 2
REACTIVE POWER AND TCSC

2.1 PHYSICS OF REACTIVE POWER

The subject of this thesis is Thyristor Controlled Series Capacitors and it deals mainly with the control of such devices. Specifically a certain control scheme named Synchronous Voltage Reversal will be dealt with in detail. However, before entering this rather particular topic it seems appropriate to give a broad background on the problems related to reactive power consumption in power transmission systems in general.

Many people regard **reactive power** as a diffuse concept, more or less artificially created from mathematical considerations. The rest of this section presents an interpretation of what reactive power is in terms of physical phenomena. The explanation immediately clarifies what reactive power compensation means and how it may be implemented.

In this thesis the discussion will be restricted to the inductive reactive power consumption in transmission lines caused by the load current. A similar interpretation may be worked out for the capacitive reactive power generation emerging from the electrical field between the phase conductors when the line is energized with high voltage.

2.1.1 Magnetic fields associated with transmission lines

Physics teaches that transfer of electrical power along a transmission line is always associated with magnetic and electrical field energy. A magnetic field surrounds the phase conductor whenever any current flows in that phase. The field strength is proportional to the current and the field is distributed in space so that the field strength is high close to the conductor surface and it lessens fast with the distance from the conductor. Figure 2-1 portrays the magnetic **field**

strength and figure 2-2 depicts the magnetic **energy density** distribution in space in the surroundings of a three-phase transmission line having three bundled conductors in each phase and loaded with symmetrical current. It is a snapshot taken when the phase B current peaks. The three upper diagrams to the left indicate the instantaneous phase currents.

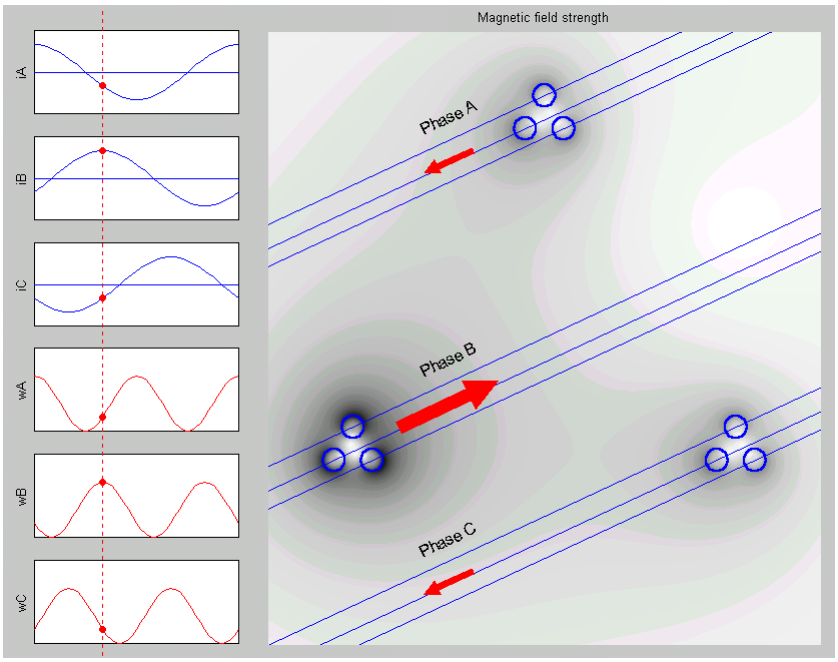

Figure 2-1 Magnetic field strength around a transmission line.

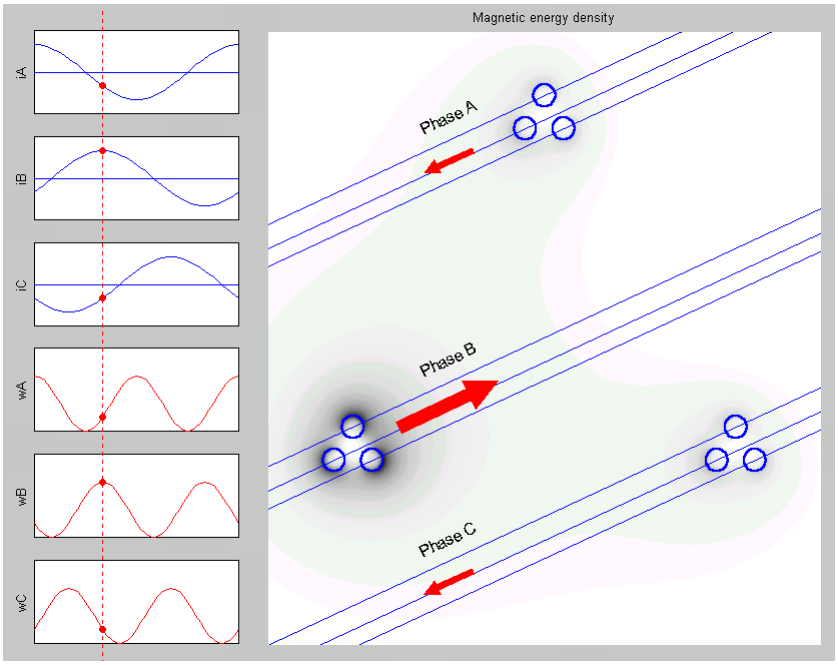

Figure 2-2 Magnetic energy density around the line.

The energy density is proportional to the square of the magnetic field strength and accordingly is even more concentrated around the conductors in each phase. We may conclude that the magnetic energy is more or less bound to the phase conductors. The three lower diagrams to the left in figure 2-2 show the energy associated with each phase in the line. The energy is proportional to the square of the instantaneous phase current. It can easily be confirmed that the total magnetic energy per unit length is constant in time at symmetrical load. However this constant total energy is being redistributed between the phases during each half cycle of the network frequency.

2.1.2 Redistribution of magnetic field energy in transmission lines

Consider a certain, e.g. 100 km long, segment of a transmission line. It contains three phase conductors running in parallel but separated from each other by only some tens of meters. Yet no bridges exist between the phase conductors where field energy bound to one phase may pass and bind to another phase. Thus no redistribution between the phases of magnetic field energy is possible within the considered segment. Accordingly, in order to perform the redistribution of the field energy between the phases, the whole field energy must be transported along the transmission line to a location, where such bridges are available. It may appear that bridges only exist at the line terminal(s) through the feeding source(s). Figure 2-3 illustrates this situation.

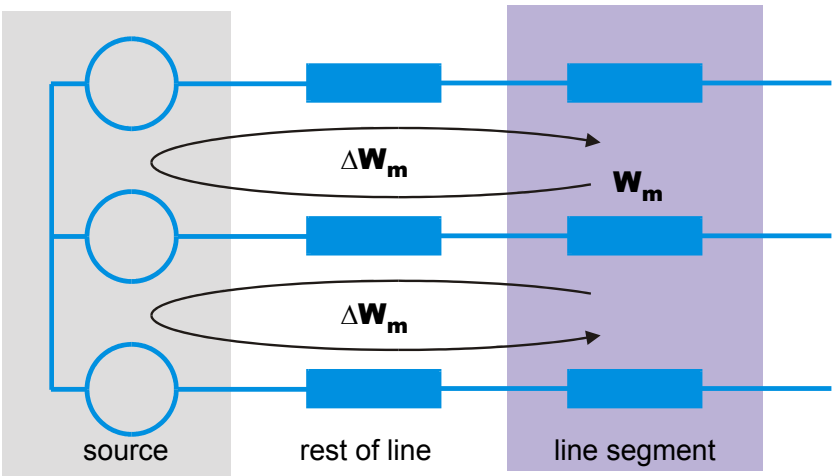

Figure 2-3 Redistribution of magnetic field energy.

In fact it can be concluded that in a long transmission line the field energy will have to be transported hundreds of kilometers in order to be redistributed to its neighbour phase conductor which runs some tens of meters away. And this transport is effectuated twice per cycle of the network frequency! When the line current is high and/or when the transmission line is long a large portion of the

driving source voltage is necessary to accomplish the redistribution of field energy and therefore a voltage drop occurs along the line.

The constant of nature μ_0=*1.26 mH/km* implies that each conductor in an overhead transmission line exhibits an inductance in the range of *1 mH/km*. The magnetic energy associated with each phase conductor illustrated in figure 2-2 then peaks at w_m=*2.2 kJ/km* when the line carries *1500 A rms*. This figure translates to a reactive power consumption in the line of $Q_L=3\omega_N w_m$=*2.1(2.5) Mvar/km* at *50 (60) Hz*. It appears that the reactive power consumption in the transmission line is considerable for lines having a length of some hundred kilometers. Further the reactive power consumption is proportional to the square of the load current, thereby limiting the practically useful line current rating to a few kiloamperes.

2.1.3 Reactive power compensation

The discussion above indicates that any means that substitutes the need for transport of field energy will improve the performance of the transmission system. There are two obvious principles, which can be applied to do this.

- The first principle, shunt compensation, is illustrated in figure 2-4. Bridges have been provided along the transmission line where field energy associated with different phases may be exchanged. Different kind of shunt compensators can be utilized. The energy may either be temporarily stored as electrostatic energy in shunt capacitors or it may be periodically redirected by means of power electronic devices like voltage source converters (VSC)

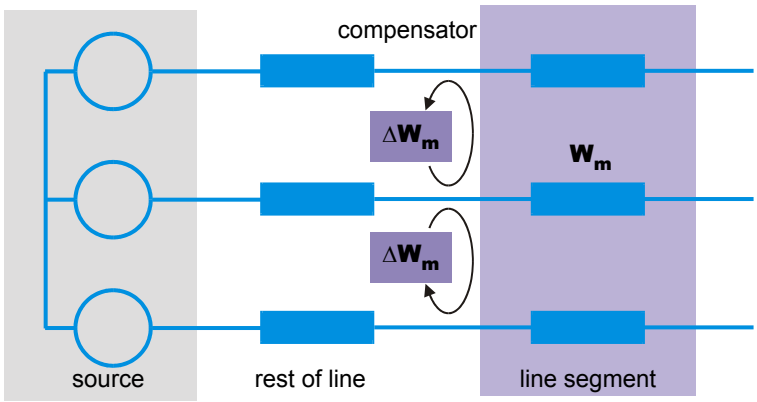

Figure 2-4 Principle of shunt compensation

- Figure 2-5 depicts the second principle, series compensation, where a storage device for the field energy has been provided in each phase. Instead of being transported the field energy is stored locally during the quarter cycle when the line current is low. Then it is returned during next quarter cycle, when the line current is high.

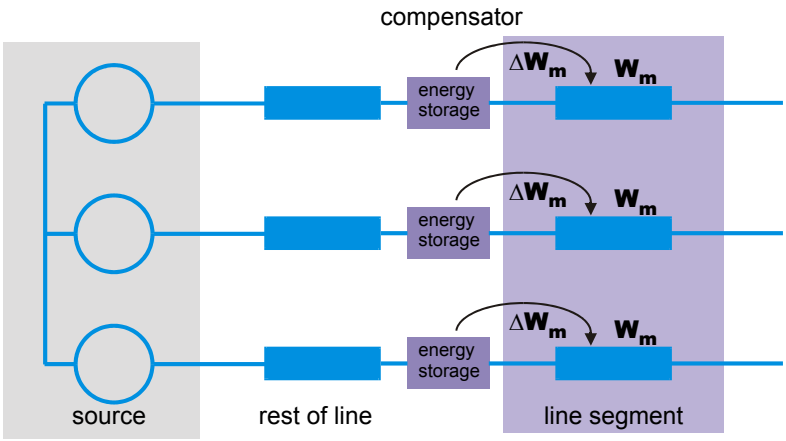

Figure 2-5 Principle of series compensation.

The energy storage devices in figure 2-5 may be implemented as passive capacitor banks as shown in figure 2-6.

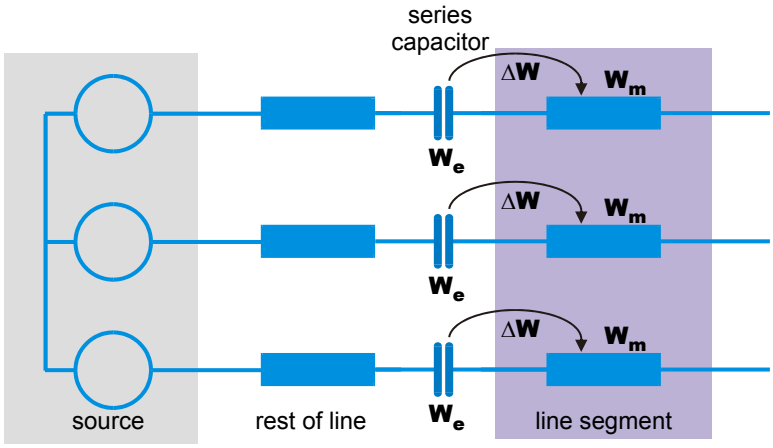

Figure 2-6 Passive capacitor bank as temporary energy storage.

The voltage across the capacitor opposes the movement of the magnetic energy along the transmission line, which reduces the voltage drop. Let the line current be sinusoidal

$$i(t) = \hat{I}_L \cos \omega_N t \tag{2-1}$$

Then the capacitor voltage is

$$u_C(t) = \hat{U}_C \sin \omega_N t$$
$$\hat{U}_C = \frac{\hat{I}_L}{\omega_N C} \tag{2-2}$$

The energies then become

$$w_m = \frac{L\hat{I}_L^2 \cos^2 \omega_N t}{2} = \frac{L\hat{I}_L^2}{4}\left(1 + \cos 2\omega_N t\right)$$
$$w_e = \frac{C\hat{U}_C^2 \sin^2 \omega_N t}{2} = \frac{C\hat{U}_C^2}{4}\left(1 - \cos 2\omega_N t\right) \quad (2\text{-}3)$$

The opposite signs of the time-varying term in the magnetic and electrostatic energies indicate that compensation really comes about. Further the proportionality between the line current amplitude and the capacitor voltage amplitude indicates that the compensation is self-regulating.

2.2 IMPACT OF SERIES COMPENSATION IN TRANSMISSION SYSTEMS

The power transmission system is a complex structure, which connects power generating plants and power consuming load areas, which are spread over huge, often nation-wide and sometimes even international, geographical areas. The ultimate objective of the control of such a system is to deliver voltage with constant frequency and amplitude to all customers irrespective of the operating conditions and in spite of the disturbances that will be imposed on the network due to lightning strokes and other faults. This goal can be accomplished only if it is possible to transport large amounts of power to almost any point in the network at any time. When the system becomes stressed due to high load and/or disturbed operating conditions the lines may be heavily loaded and the internal reactive power consumption in the lines may produce conditions that jeopardize continued operation due to phenomena like voltage collapse or loss of synchronism.

Having the discussion in the preceding section in mind makes one believe that the use of series compensation will relieve such problems to a great extent. It turns out that this guess is completely true and it will be illustrated below in two generic cases. The first case focuses on the improvement of voltage stability and the second case deals with the impact on the angular stability brought about by the use of series compensation.

2.2.1 Impact of series compensation on voltage stability

Some buses in the transmission system may lack reactive power support, i.e. there is no nearby generator that controls the voltage in the bus. The voltage in such a point depends very much on the actual power transfer on the line. In figure 2-7 it is assumed that only active power only is transported along a transmission line from the generating area *A* to the load area *B*. The voltage

characteristic in *B* versus the power transfer is depicted in figure 2-7. For obvious reasons such curve is called a "nose-curve". It indicates that at a certain maximum loading of the transmission line a voltage collapse situation occurs. No power can pass through a node with zero voltage. A situation, where one node voltage drops a lot or even collapses, may endanger the power transfer in the whole transmission system.

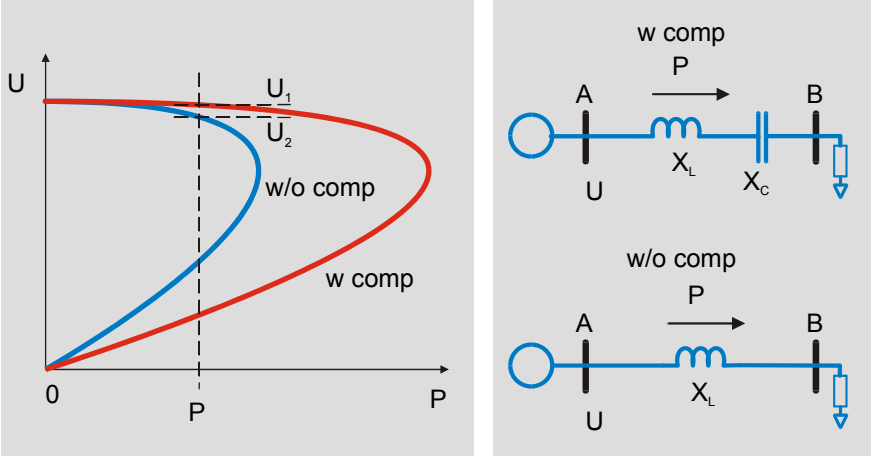

Figure 2-7 *Voltage vs power transfer to a passive node (B) lacking reactive power support.*

Insertion of a compensating series capacitor changes the nose-curve dramatically, pushing the voltage collapse to a much higher power loading. Also the voltage drop in the load point *B* at a certain load is reduced from $|U_N\text{-}U_2|$ to $|U_N\text{-}U_1|$ when series compensation is introduced.

2.2.2 Impact of series compensation on angular stability

A different situation is shown in figure 2-8. A line connects two buses *A* and *B*. Both buses have strong reactive support, i.e. nearby generators control the voltage amplitude in each line terminal. The current flowing in the line is determined by the difference between the terminal voltages. Both terminal voltages are close to their nominal value so the voltage across the line mainly is caused by the phase angle difference between the terminal voltages. The sending end voltage phasor is phase advanced relative the receiving end voltage. In order to push more active power through a line the phase angle difference must be increased and the higher the reactance in the line (i.e. the longer the line is) the bigger angle deviation is needed. When the angle difference is 90° the maximum power transfer is reached for the specific line. If part of the inductive reactance is compensated by an inserted series capacitor the total reactance becomes smaller and a smaller angle deviation is required to push a certain amount of power. Figure 2-8 illustrates the characteristics for power transfer versus angle separation δ between the terminal voltages of the line without and with series compensation.

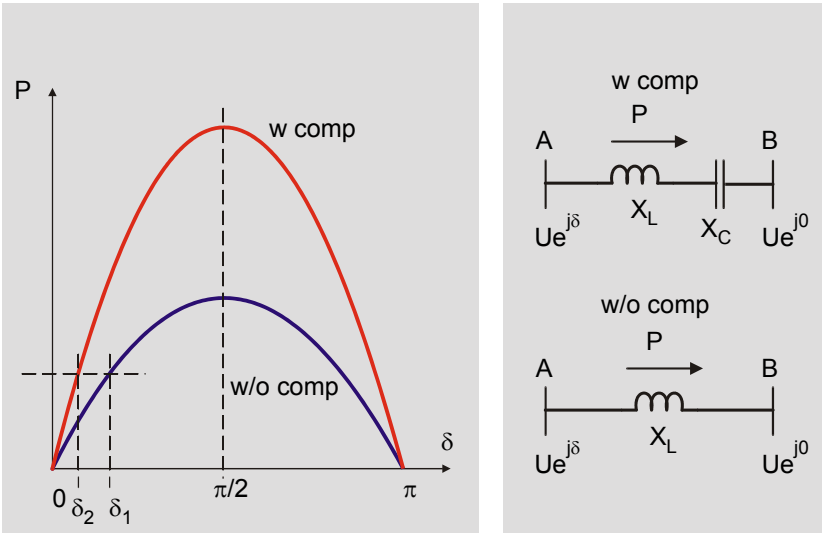

Figure 2-8 Power transfer vs terminal voltage angle separation for a line with rated voltage amplitude in both ends.

It is obvious from the figure that a significant increase of the maximum power transfer is obtained and also that the steady state operating angle deviation is reduced from δ_1 to δ_2. Both these effects contribute to improve the system's ability to remain in synchronous operation even after severe faults.

In practice the angle deviation between the end-point voltages of a line normally is kept below *30-40°* in order to preserve necessary stability margins. The power transfer capability of the line (without series compensation) then approximately reaches the so-called surge impedance load (SIL) of the line. The SIL is defined as

$$SIL = \frac{U_{N,l-l}^2}{Z_{SIL}}$$
$$Z_{SIL} = \sqrt{\frac{L}{C}} \qquad (2\text{-}4)$$

where $U_{N,l-l}$ is the rated line-line system voltage, L is the series inductance per km and C is the shunt capacitance per km of the line. L is somewhat smaller than $\mu_0 = 1.256\ mH/km$ and C is somewhat bigger than $\varepsilon_0 = 8.85\ nF/km$. Practical values of Z_{SIL} ranges from *200-400* Ω. The loadability of a *500 kV* line thus is the order of *800 MW*. The use of series compensation practically permits an increase of the line loadability almost to the double SIL thus reaching approximately *1500 MW*.

2.3 IMPLEMENTATION OF FIXED SERIES CAPACITORS

One way of explaining the improvements of transfer capability, which was reported in the preceding section, is to interpret the insertion of a compensating series capacitor as a virtual reduction of the length of the line. This was understood since a very long time and series compensation of transmission lines have been practiced since at least half a century. The first series-compensated 400 kV line was taken in service in Sweden in the 50'ies. Today it is in practical use in many countries, specifically where remote hydro-generation resources have been exploited to power load centres. Such power systems are found in e.g. Brazil, Argentina, USA, Canada, South Africa, China, Russia, Scandinavia and other countries. Today series compensators with a total accumulated rating exceeding *100 000 Mvars* of are in operation.

2.3.1 Single-line diagram

A fixed series capacitor installation, being inserted to compensate part of the inductive reactance of a transmission line, typically has a single line diagram as shown in figure 2-9.

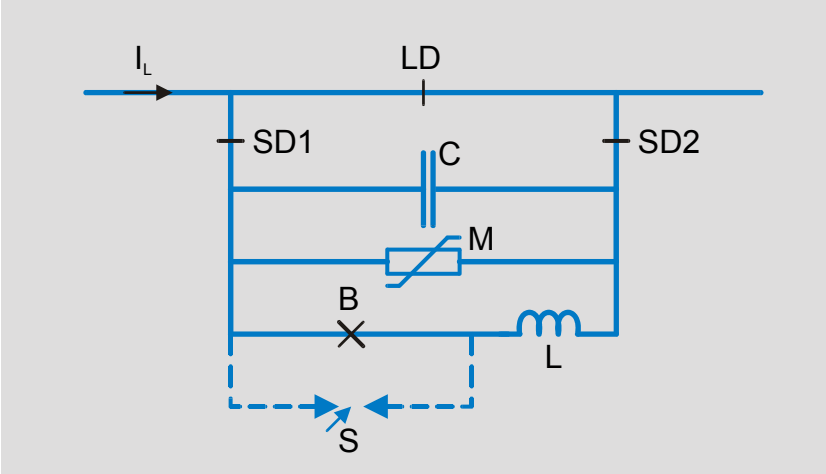

Figure 2-9 Single-line diagram of a series capacitor (SC) installation LD=line disconnector, SD1,SD2=Series capacitor disconnectors, C=capacitor bank, M=MOV varistor, B=bypass breaker, L=damping inductor, S=spark gap

The transmission line passes a disconnector arrangement *LD, SD1, SD2*. When *LD* is closed and *SD1* and *SD2* are open the series capacitor installation is isolated from the high-voltage line and is available for service or maintenance. The series capacitor *C* is inserted by closing *SD1* and *SD2*, opening *LD* (with *B*

closed) and finally opening *B*. A Metal Oxide Varistor *M* is provided across the capacitor bank in order to limit the capacitor voltage when fault currents flow in the line. The energy rating of the MOV is limited and for faults close to the SC installation the energy accumulated in the MOV is limited by firing of a triggered spark gap *S*. The inductor *L* only serves the purpose of limiting the discharge current from the capacitor bank when *B* is being closed.

2.3.2 Physical implementation

Figure 2-10 shows a photo of a series capacitor installation in a high voltage network. The equipment for each phase is located on a platform that is fully isolated towards ground and between the different phases. A typical insulation level is *1300 kV* for a *500 kV* system. The capacitor bank, the MOV, the damping inductor and the spark gap are the main components on the platform. The bypass breaker often is provided in a self-sustained structure. Typical ratings for SC installations are *100 Mvar* to *800 Mvar* for voltage levels in the range *230-800 kV*.

Figure 2-10 Series capacitor installation in a 400 kV system

2.3.3 Development of series compensation technology

During the fifty years since the first series capacitor was installed a continuous development of insulation materials has occurred. Improvements in materials and production technology has increased energy storage density and decreased losses in capacitors tremendously. In general the cost tend for capacitors is favourable and the space requirement for capacitor-based equipment has been remarkably reduced. Continuous improvement on the auxiliary equipment used in series compensators, like bypass circuit breakers, Metal Oxide Varistors and fast bypass equipment, also has taken place during the years. Finally digital systems have replaced the earlier analogue measuring and protection systems. E.g. are

optically powered current transducers used to perform measurement in the main circuit at high potential.

2.4 APPLICATIONS FOR CONTROLLED SERIES CAPACITORS (CSC)

The **active** power flow in the transmission line is inversely proportional to the total reactance of the compensated line. A change of the reactance of the inserted series capacitor thus **immediately** causes a change of the power flow in the line. The possibility to adjust the inserted series capacitor reactance therefore obviously can be utilized in two areas of application, namely for power flow control and for damping of power oscillations.

2.4.1 Power flow control using CSC

One problem in the operation of the transmission systems today is to route the power flow along certain desired transport facilities. The reason may be to avoid power flow bottlenecks, which limit the maximum power transfer in the system, or simply to comply with the commercial conditions that have been negotiated with neighbour utilities.

For this reason it may be of interest to vary the inserted reactance in certain lines in the system in order to manipulate the power flow pattern. This type of "reactance control" mainly can be used as a means to control the load-sharing between several parallel transmission facilities that transfer power between to power systems or subsystems. Figure 2-11 depicts such an application. Naturally the **total** power transfer between the areas depends only on the generation/load balance in the areas.

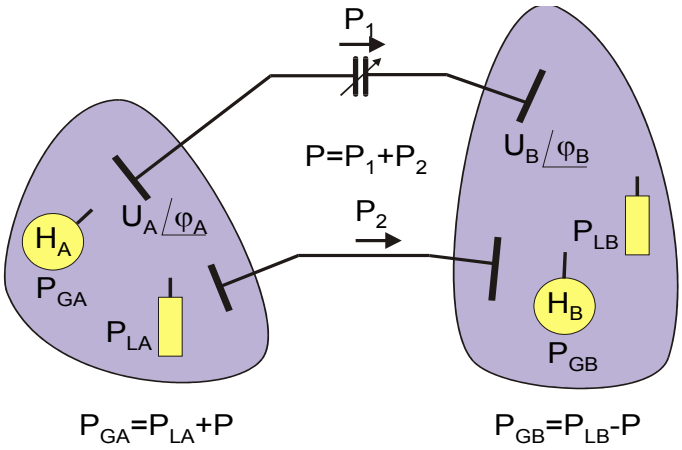

Figure 2-11 Power flow control using CSC.

In general power flow control in **meshed** power systems requires a device having the capability to achieve some phase-shifting action.

Power flow control applications seldom can benefit economically from the use of fast-acting controlling devices. Therefore equipment for this purpose most often would be based on mechanically switched apparatus, which are more cost-effective and cause less loss than semiconductor based equipment. Controllable series capacitors may be implemented as a series-connection of series capacitor sections equipped with individual bypass circuit-breakers.

2.4.2 Damping of power oscillations using TCSC

Events in the transmission system like line switching, line faults etc. disturb the equilibrium in speed and phase of the generators in the system. During the fault the sending end generators tend to speed up and phase advance while the receiving end generators speed down and phase retard. When the fault is cleared the generators must find a new equilibrium, where all run with the same speed and with phase angles that comply with the new steady state power flow pattern. Due to the inertia of the generators (and participating machines in the load) and the angle versus power characteristics this new equilibrium point will be reached via an oscillation known as "electro-mechanical power oscillation" or simply "power oscillation". The frequency of this oscillation falls in the range 0.2-2 Hz.

Figure 2-12 illustrates an interconnection of two power systems with an interconnecting transmission line having both fixed and controllable series capacitors.

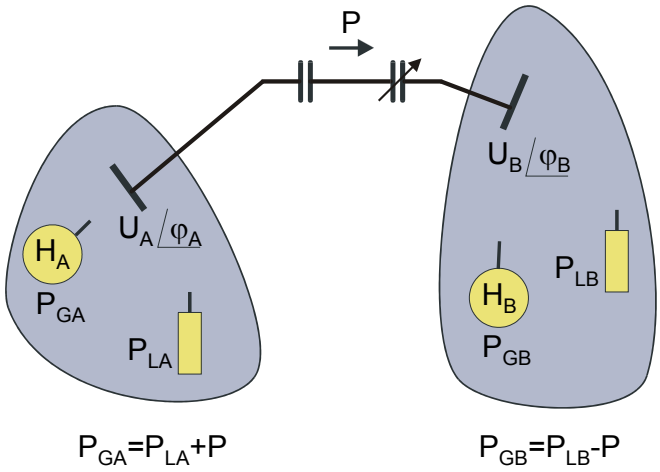

Figure 2-12 Series compensated interconnection between two power systems.

Indeed it was remarked in section 2.4.1 that insertion of the series capacitor in the interconnecting line does not impact on the power flow in steady state. However, during the transients following disturbances it is important that the power transfer capability in the interconnection is sufficiently strong, so that the

synchronism between the power systems is not at danger. This **first-swing stability** property is improved very much by the fixed series capacitor. However, essentially the fixed series capacitor does not provide substantial **damping** of the subsequent power oscillation. A controllable series capacitor therefore is installed in order to provide artificial damping of the power oscillations by active control of the inserted capacitive reactance. The use of controllable series compensation is a very efficient and robust method to achieve improved damping of power oscillations. Adequate equipment for power oscillation damping utilizes thyristor control of the inserted capacitive reactance.

2.5 IMPLEMENTATION OF THYRISTOR CONTROLLED SERIES CAPACITORS

2.5.1 Types of thyristor control

Thyristor control of series capacitors may be implemented in two versions

- Thyristor Switched Series Capacitor (TSSC)
- Thyristor Controlled Series Capacitor (TCSC)

The topology of the main circuit is identical for the two forms as illustrated in figure 2-13. The normal series capacitor bank has been equipped with a parallel thyristor controlled inductive branch.

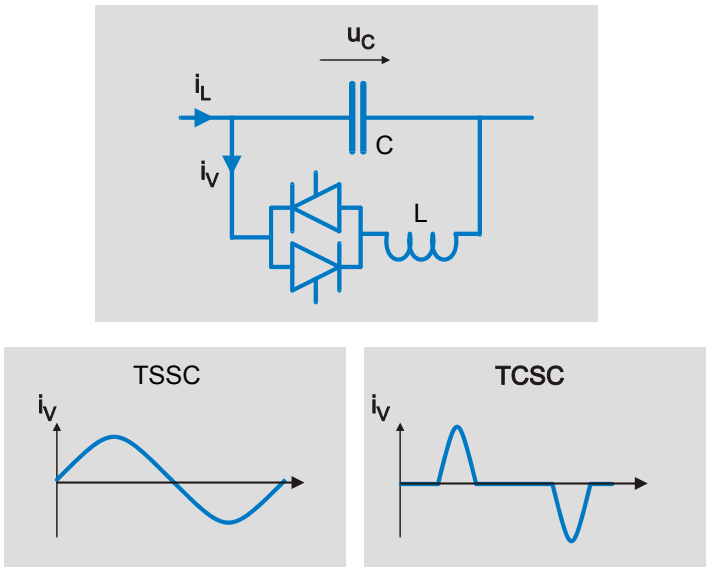

Figure 2-13 Main circuit and valve current waveform for TSSC and TCSC

In the TSSC the thyristor valve is utilized as a switch that inserts or bypasses the capacitor bank for any number of complete half-cycles of the network frequency. The inductance in TSSC can be small as the thyristor valve does not switch at

high valve voltages. Typically the reactance of the inductor is 2-5 % of the capacitor bank reactance at rated network frequency.

In the TCSC, on the other hand each thyristor is fired with phase angle control once per cycle. A bigger inductance is required; typically its reactance at network frequency is 5-20 % of the capacitor bank reactance.

2.5.2 TCSC and subsynchronous resonance (SSR)

When the line inductance is series compensated by a capacitor an electrical series resonance will be created. If the degree of compensation is below *100 %* then the resonance frequency will occur below the rated network frequency. Thermal power stations use turbine-generator sets with shaft systems that normally have mechanical torsional eigen-frequencies below rated frequency. Torsion oscillations modulate the generated voltage causing sidebands to *50* or *60 Hz* to show up. When the lower sideband at f_N-$f_{torsion}$ coincides with the electrical resonance frequency in the network subsynchronous resonance (SSR) is said to occur. It can be shown that at such conditions there is a risk that negative damping may appear, causing the torsional oscillations to increase in amplitude until shaft damage occurs if no protective action is taken.

The problems with SSR put restrictions on the useful degree of compensation that can be used in networks to which thermal power plants are being connected. Sometimes the restrictions limit the compensation degree to levels below what would have been desired from a strict power transmission point of view.

Use of thyristor control according to the TCSC approach has a major effect on the risk for SSR, as will be discussed in further detail in later chapters. For now it is sufficient to mention that the apparent impedance of the TCSC in the subsynchronous frequency range deviates completely from that of a passive capacitor bank. This fact can be utilized to enhance the degree of compensation using TCSC to levels beyond those that would be safe from a SSR standpoint using fixed, passive capacitor banks.

2.5.3 Existing installations

A test valve using the TSSC approach was installed for some years in:

- Kanawha River SC, USA: owned by AEP, built by ABB 1991 [I1, I2]

Five installations of the TCSC type so far have been built:

- Kayenta TCSC, USA: owned by WAPA, built by Siemens 1992 [I3, I4]
- Slatt TCSC, USA: owned by BPA, built by GE 1993 [I5, I6]
- Stöde TCSC, Sweden: owned by Svenska Kraftnät, built by ABB 1997 [I7]
- Imperatríz TCSC, Brazil: owned by Eletronorte, built by ABB 1999 [I8]
- Serra da Mesa TCSC, Brazil: owned by Furnas, built by Siemens 1999

Figure 2-14 shows a photo of the Imperatríz TCSC in Brazil. The capacitor bank is placed on the right-hand side of the platforms, the valve is located in the house on the left-hand side and the MOV arresters are placed in the middle of the platform. The bypass breaker is placed free-standing in the foreground to the left outside the platform. The TCSC inductor can be partly seen in the left-most side of the photo.

Figure 2-14 Photo of Imperatríz TCSC, Eletronorte, Brazil.

2.6 TCSC IN THE FACTS FAMILY

The TCSC is a member of the FACTS family, which consists of a number of power electronic based apparatus developed to improve the controllability of the AC transmission system. Beside the since long established members, like SVC and HVDC, TCSC seems to be one of the first new FACTS devices to find commercial applications. In the subclass of devices that insert voltage in series with the line the TCSC is competing with the

- Thyristor Controlled Phase Angle Regulator (TCPAR), a transformer based phase shifter with thyristor control
- Unified Power Flow Controller (UPFC), a back-back VSC configured as a phase shifter between a shunt transformer and a series boost transformer
- Static Synchronous Series Compensator (SSSC), a VSC based device injecting voltage via a boost transformer

The TCSC has the advantage of being directly implemented in the main circuit. No interfacing transformer is used, which brings about a big cost-advantage in high-voltage applications. Also losses are minimized when the interfacing equipment is not needed.

Comparing studies also have shown that the contribution to damping using a TCSC is as good as or better than TCPAR or UPFC of similar rating.

CHAPTER 3
TCSC IN STEADY STATE OPERATION

3.1 TOPOLOGY, PARAMETERS, NOTATION

In our analysis we shall first look at the waveforms in steady state operation. In this study we consider the simple main circuit according to figure 3-1.

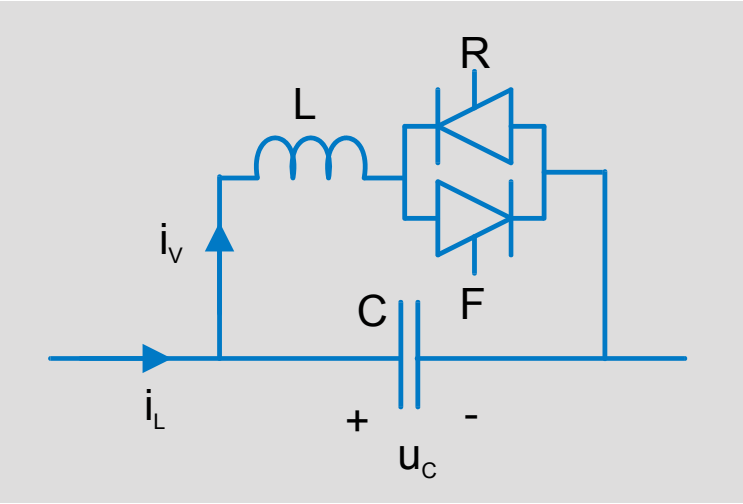

Figure 3-1 TCSC main circuit.

The reference directions of currents and capacitor voltage have been indicated in figure 3-1. These references are used throughout this thesis. The thyristor carrying conducting current in the positive direction is marked with an '*F*', for FORWARD direction. It can only be triggered when positive capacitor voltage exists. Correspondingly the *'R'* thyristor, the REVERSE thyristor, conducts current in the negative direction and can only be triggered, when the capacitor voltage is negative.

The capacitance of the bank in each phase is C and the inductance in the thyristor branch is L. These two branches together form an LC circuit with the resonance frequency ω_0

$$\omega_0 = \frac{1}{\sqrt{LC}} \tag{3-1}$$

The reactance in the capacitor bank and in the inductor have equal magnitude reactance X_0 at their common resonance frequency

$$X_0 = \omega_0 L = \frac{1}{\omega_0 C} = \sqrt{\frac{L}{C}} \tag{3-2}$$

For proper functioning of the TCSC it is necessary that $\omega_0 > \omega_N$, where ω_N is the network frequency. The quotient between the resonance frequency and the network frequency is a design parameter, which we will denote as λ in the analysis. Its definition is given in (3-3).

$$\lambda = \frac{\omega_0}{\omega_N} = \frac{\frac{1}{\omega_N C}}{X_0} = \frac{X_0}{\omega_N L} \tag{3-3}$$

Typical values of λ fall in the range *2 - 4*.

3.2 FORMULAS FOR STEADY STATE OPERATION

3.2.1 Assumptions, angle definitions

The normal operating mode of a TCSC is known as “capacitive boost mode”. The generic waveforms in steady state of this mode are shown in figure 3-2.

It is assumed that the line current i_L is sinusoidal; this assumption is justified by the fact that line current in high-voltage transmission systems normally is not very much polluted by harmonics. The waveform of the line current also is rather little influenced by any harmonic distortion in the series capacitor voltage due to the comparatively high impedance in the transmission line at higher frequencies.

Further the losses in the circuit have been neglected.

The thyristor is triggered when the capacitor voltage is approaching the zero line before zero-crossing occurs. If the line current is positive the capacitor voltage changes from negative to positive, so that the REVERSE thyristor will be forward biased before the zero-crossing. When it is triggered the valve current becomes negative and adds to the line current when it passes through the capacitor. Thus an extra charge will be pushed into the capacitor from the thyristor branch in addition to the charge provided by the line current. In this way an extra voltage, the boost voltage, will appear across the capacitor.

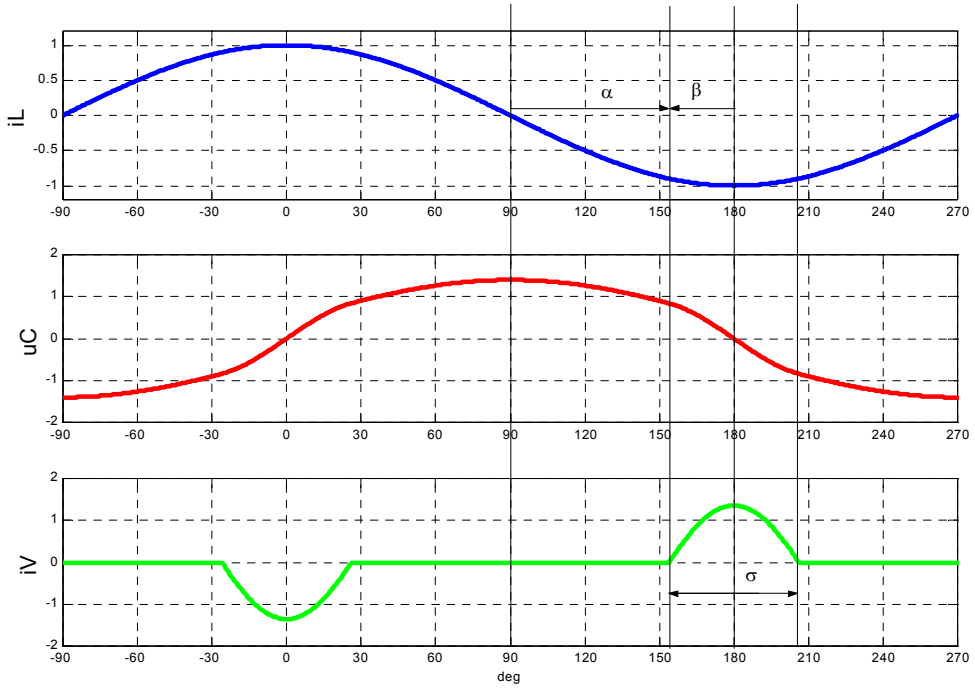

Figure 3-2 Generic waveforms for TCSC operating in capacitive boost mode.

In the study of steady state conditions the thyristor trigger angle α (shown in figure 3-2) can be used as the control parameter. Like in other line-commutated converters α is referred to the earliest instant when forward voltage appears across the thyristor. In capacitive mode operation the trigger angles is around 140-180°. Often it is more practical to use the control angle β (shown in figure 3-2). It is related to α by the expression

$$\alpha = \pi - \beta \tag{3-4}$$

Also the conduction angle σ (shown in figure 3-2) appears in formulas in the literature about TCSC. Obviously

$$\sigma = 2\beta \tag{3-5}$$

It should be noted that, although the definition of α was referred to the zero-crossing of the capacitor **voltage**, in practice the phase information to be used for synchronization is always derived from the line **current**, i.e. the angle used in practice is rather α-π/2, which is also shown in the figure.

3.2.2 Derivation of general formulas

The waveforms in steady state will be derived in the following. It is assumed that the TCSC circuit in figure 3-1 is powered by a stiff current source with current amplitude $\hat{I}_L$ and with frequency ω_N

$$i_L(t) = \hat{I}_L \cos\omega_N t \tag{3-6}$$

If the losses are negligible the thyristor conduction interval becomes symmetrical around the line current maximum. Let the conduction interval be

$$-\beta < \omega_N t < \beta \tag{3-7}$$

So far we have not determined which one of the thyristors (or both) that shall be conducting in the interval, we only have postulated that the valve is conductive. Among the solutions derived from this assumption we will sort out the different operating modes later.

- **Differential equations**

The following set of differential equations apply in the interval $-\beta<\omega_N t<\pi-\beta$ (solutions in other intervals are obvious)

$$\begin{aligned} L\dot{i}_V &= \begin{cases} u_C, & -\beta < \omega_N t < \beta \\ 0, & \beta < \omega_N t < \pi - \beta \end{cases} \\ C\dot{u}_C &= \begin{cases} \hat{I}_L \cos\omega_N t - i_V, & -\beta < \omega_N t < \beta \\ \hat{I}_L \cos\omega_N t, & \beta < \omega_N t < \pi - \beta \end{cases} \end{aligned} \tag{3-8}$$

- **Thyristor current and capacitor voltage as time functions**

The solution to the equations is given by

$$i_V(t)=\begin{cases}\dfrac{\lambda^2\hat{I}_L}{\lambda^2-1}\left(\cos\omega_N t-\dfrac{\cos\beta}{\cos\lambda\beta}\cos\lambda\omega_N t\right), & -\beta<\omega_N t<\beta\\ 0, & \beta<\omega_N t<\pi-\beta\end{cases} \tag{3-9}$$

and

$$u_C(t)=\begin{cases}\dfrac{\lambda X_0\hat{I}_L}{\lambda^2-1}\left(\dfrac{\lambda\cos\beta}{\cos\lambda\beta}\sin\lambda\omega_N t-\sin\omega_N t\right), & -\beta<\omega_N t<\beta\\ \lambda X_0\hat{I}_L\left[\sin\omega_N t-\dfrac{\lambda\cos\beta}{\lambda^2-1}\left(\lambda\tan\beta-\tan\lambda\beta\right)\right], & \beta<\omega_N t<\pi-\beta\end{cases} \tag{3-10}$$

As expected the limit value of equation (3-10), when β approaches zero, is

$$\lim_{\beta\to 0} u_C(t)=\lambda X_0\hat{I}_L\sin\omega_N t=\frac{\hat{I}_L}{\omega_N C}\sin\omega_N t \tag{3-11}$$

- **Asymptotic behavior**

Equations (3-9) and (3-10) both contain a factor $\cos\lambda\beta$ in the denominator. This factor equals zero for certain control angles, namely

$$\beta_n=\left(n+\frac{1}{2}\right)\frac{\pi}{\lambda},\quad n=0,1,\ldots,\mathrm{int}\left(\frac{\lambda-1}{2}\right) \tag{3-12}$$

For such control angles the capacitor voltage and the thyristor current tend towards infinity because the apparent inductive reactance at fundamental frequency of the thyristor-controlled inductor branch matches the capacitive reactance of the capacitor bank. When connected in parallel the apparent impedance of the combination at network frequency appears to be infinite. A very large voltage must be applied in order to force the line current to flow through the combination.

- **Thyristor peak current and capacitor peak and firing voltages**

The peak value of the valve current, $\hat{i}_V$, occurs at t=0 and we obtain from (3-9)

$$\boxed{\hat{i}_V = \hat{I}_L \frac{\lambda^2}{\lambda^2 - 1}\left(1 - \frac{\cos\beta}{\cos\lambda\beta}\right)} \tag{3-13}$$

Let the capacitor voltage at $\omega_N t = \pi/2$ be $\hat{u}_C$. Then (3-10) yields

$$\boxed{\begin{aligned} \hat{u}_C &= \hat{u}_{C0}\left[1 + \frac{\lambda}{\lambda^2 - 1}\left(\cos\beta\tan\lambda\beta - \lambda\sin\beta\right)\right] \\ \hat{u}_{C0} &= \frac{\hat{I}_L}{\omega_N C} = \lambda X_0 \hat{I}_L \end{aligned}} \tag{3-14}$$

The capacitor voltage at the beginning of the conduction interval also is interesting from valve design point of view. Name it $u_{CF} = u_C\left(-\frac{\beta}{\omega_N}\right)$. We obtain from (3-10)

$$\boxed{u_{CF} = \frac{\lambda X_0 \hat{I}_L}{\lambda^2 - 1}\left(\sin\beta - \lambda\cos\beta\tan\lambda\beta\right)} \tag{3-15}$$

- **Fourier analysis of thyristor current and capacitor voltage waveforms**

Thyristor current

The time function for the thyristor current in (3-9) can be expressed as a Fourier series of the following kind

$$i_V(t) = \sum_{\mu=1,3,5,\ldots} \hat{I}_{V\mu}\cos\mu\omega_N t \tag{3-16}$$

Calculation gives the Fourier coefficients for fundamental frequency ($\mu = 1$), and harmonics of order $\mu = 3, 5, 7, \ldots$

$$\begin{aligned} &\frac{\hat{I}_{V\mu}}{\hat{I}_L} = \\ &= \frac{2}{\pi}\frac{\lambda^2}{\lambda^2 - 1}\left\{\frac{\sin(1-\mu)\beta}{1-\mu} + \frac{\sin(1+\mu)\beta}{1+\mu} - \frac{\cos\beta}{\cos\lambda\beta}\left[\frac{\sin(\lambda-\mu)\beta}{\lambda-\mu} + \frac{\sin(\lambda+\mu)\beta}{\lambda+\mu}\right]\right\} \end{aligned} \tag{3-17}$$

In the formula some quotients may be replaced by the limit value

$$\lim_{x\to 0}\frac{\sin x\beta}{x}=\beta \tag{3-18}$$

This specifically applies to the fundamental frequency component

$$\boxed{\frac{\hat{I}_{V1}}{\hat{I}_L}=\frac{2}{\pi}\frac{\lambda^2}{\lambda^2-1}\left\{\beta+\frac{\sin 2\beta}{2}-\frac{2\cos^2\beta}{\lambda^2-1}\left(\lambda\tan\lambda\beta-\tan\beta\right)\right\}} \tag{3-19}$$

Capacitor voltage

The fundamental frequency component of the current passing through the capacitor is given by

$$\begin{aligned}&\frac{\hat{I}_{C1}}{\hat{I}_L}=\frac{\hat{I}_L-\hat{I}_{V1}}{\hat{I}_L}=\\&=1+\frac{2}{\pi}\frac{\lambda^2}{\lambda^2-1}\left\{\frac{2\cos^2\beta}{\lambda^2-1}\left(\lambda\tan\lambda\beta-\tan\beta\right)-\beta-\frac{\sin 2\beta}{2}\right\}\end{aligned} \tag{3-20}$$

Then fundamental frequency component of the capacitor voltage has frequency ω_N and the capacitor voltage then can be obtained through multiplication with the reactance $\frac{1}{j\omega_N C}=-j\lambda X_0$ (compare equation (3-3)). We get

$$\frac{\hat{U}_{C1}}{\hat{I}_L}=-j\lambda X_0\left\{1+\frac{2}{\pi}\frac{\lambda^2}{\lambda^2-1}\left[\frac{2\cos^2\beta}{\lambda^2-1}\left(\lambda\tan\lambda\beta-\tan\beta\right)-\beta-\frac{\sin 2\beta}{2}\right]\right\} \tag{3-21}$$

Finally the harmonic components of the capacitor voltage can be expressed as the product of the harmonic component in the negative valve current multiplied with the capacitor reactance $\frac{1}{j\mu\omega_N C}=-j\frac{\lambda X_0}{\mu}$. The following result is obtained

$$\boxed{\begin{aligned}\frac{\hat{U}_{C\mu}}{\hat{I}_L}=-j\frac{\lambda X_0}{\mu}\frac{2}{\pi}\frac{\lambda^2}{\lambda^2-1}\left\{\frac{\cos\beta}{\cos\lambda\beta}\left[\frac{\sin(\lambda-\mu)\beta}{\lambda-\mu}+\frac{\sin(\lambda+\mu)\beta}{\lambda+\mu}\right]-\right.\\\left.-\left[\frac{\sin(1-\mu)\beta}{1-\mu}+\frac{\sin(1+\mu)\beta}{1+\mu}\right]\right\}\end{aligned}} \tag{3-22}$$

These formulas will be illustrated in section 3.3 below.

Boost factor

The ratio between the capacitor voltage fundamental frequency component with and without thyristor action is of specific interest in TCSC applications. We will call it the **boost factor k_B**. The formula is obtained from (3-21)

$$k_B = \frac{\hat{U}_{C1}}{\frac{\hat{I}_L}{j\omega_N C}} = \frac{\hat{U}_{C1}}{-j\lambda X_0 \hat{I}_L} = \\ = 1 + \frac{2}{\pi}\frac{\lambda^2}{\lambda^2 - 1}\left[\frac{2\cos^2\beta}{\lambda^2 - 1}\left(\lambda\tan\lambda\beta - \tan\beta\right) - \beta - \frac{\sin 2\beta}{2}\right] \tag{3-23}$$

3.3 CHARACTERISTICS IN DIFFERENT OPERATING MODES

In this section the results of the mathematical analysis in section 3.2.2 will be evaluated and discussed. The different operating modes of the TCSC also will be explained.

3.3.1 Boost factor for varying conduction angles

The formula for the boost factor was given in (3-23).

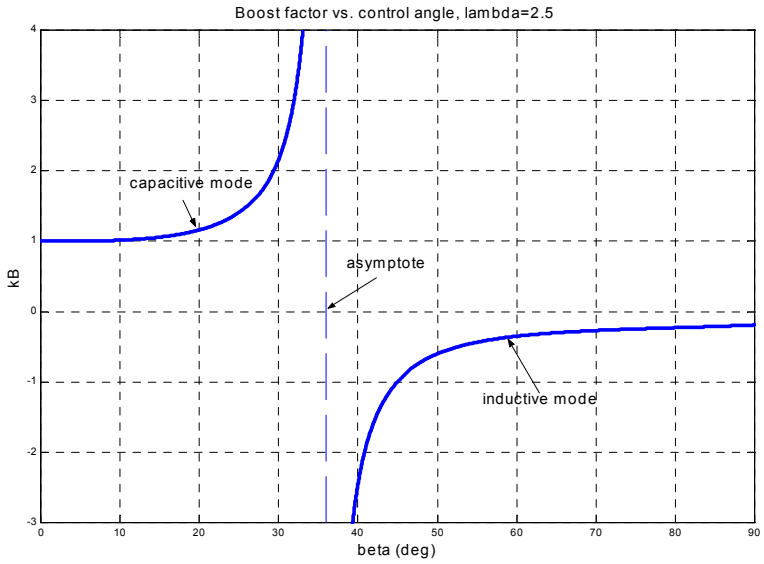

Figure 3-3: Boost factor vs. control angle, λ=2.5.

Figure 3-3 presents the curve for one case with main circuit parameter $\lambda = 2.5$. In this case the resonance frequency of the main circuit *LC* circuit is *125/150 Hz* in a *50/60 Hz* system respectively. The reactance of the inductor is $1/2.5^2 = 16\ \%$ of the capacitor bank reactance at fundamental frequency.

3.3.2 Capacitive boost mode

The boost factor commence at unity for $\beta=0$ and starts to increase at about $\beta=10°$ and it ascends along the asymptote at $\beta=90°\lambda=36°$. Figure 3-4 illustrates the waveforms of the capacitor voltage in this **capacitive boost mode.**

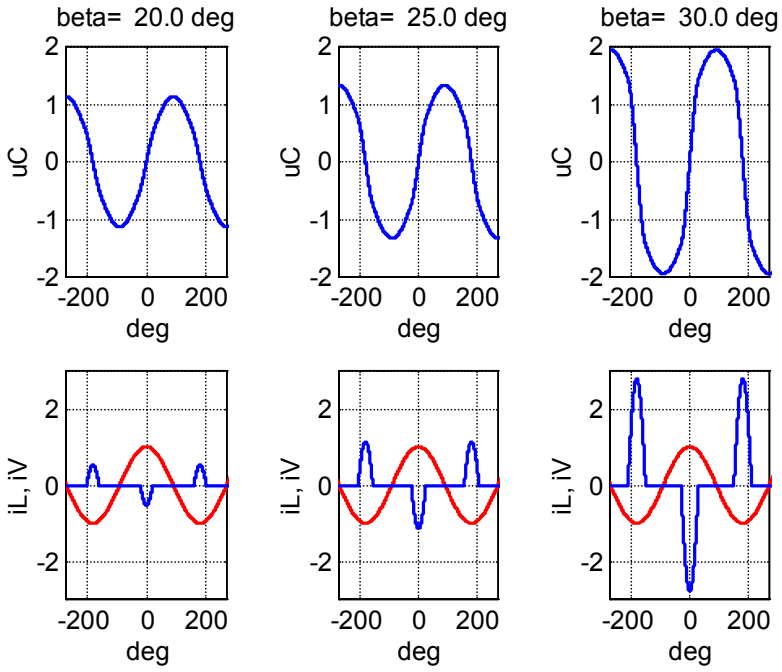

Figure 3-4 TCSC waveforms in capacitive boost mode for varying control angles with $\lambda=2.5$.

It should be noted that the boost factor characteristics is a most non-linear function of the conduction angle and thus of the trigger angle. At reasonably high boost factors even a small change in trigger angle results in a large change in the steady state boost.

The waveform of the capacitor voltage deteriorates when the boost factor increases. Figure 3-5 illustrates the relative harmonic voltage as a function of the boost factor in capacitive mode. The relative harmonic voltage is obtained by dividing (3-22) with (3-21).

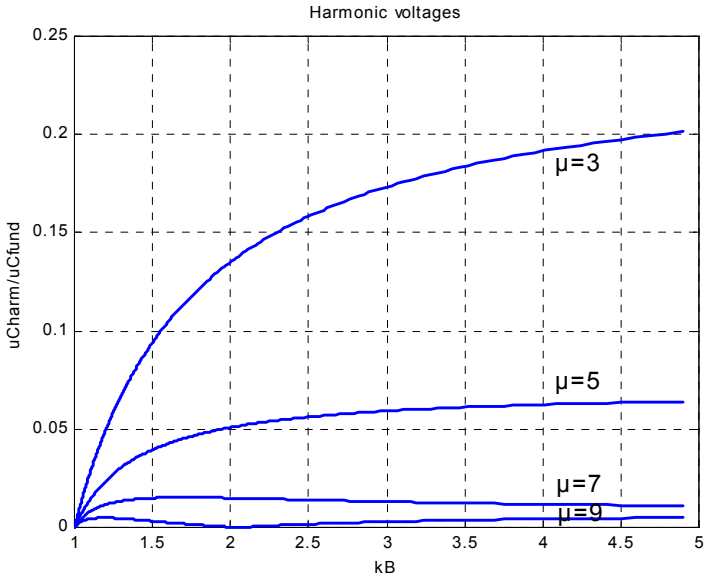

Figure 3-5 Relative harmonic voltage vs boost factor, λ=2.5.

3.3.3 Inductive boost mode

Figure 3-3 shows that the mathematical formula (3-23) for the boost factor generates a branch even for control angles exceeding the asymptotic angle 36°. The calculated corresponding waveforms are shown in figure 3-6.

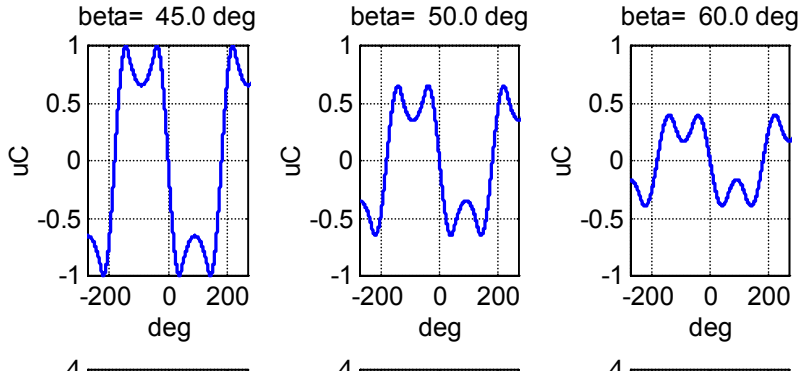

Figure 3.6 TCSC waveforms in inductive boost mode for varying conduction angles with λ=2.5.

The fundamental frequency component of the thyristor branch current now is **in phase** with the line current and its magnitude exceeds that of the line current. The fundamental frequency component of the **capacitor** current then opposes the line current as shown in figure 3-7.

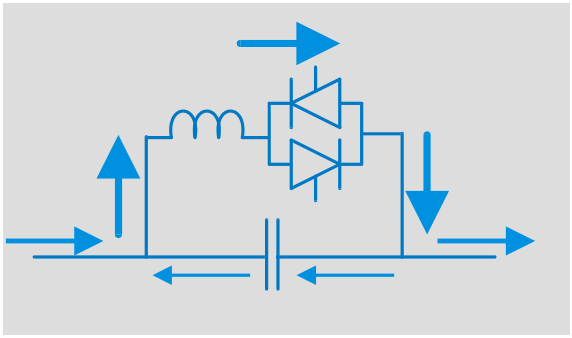

Figure 3-7 Currents in TCSC operating in inductive boost mode.

Accordingly the phase of the capacitor voltage, which is inserted in series with the line, appears to be inductive when referred to the line current direction. Therefore this mode of operation is called the **inductive boost mode**. In this mode of operation the thyristor current is very high.

The relative harmonic content in the capacitor voltage is depicted in figure 3-8.

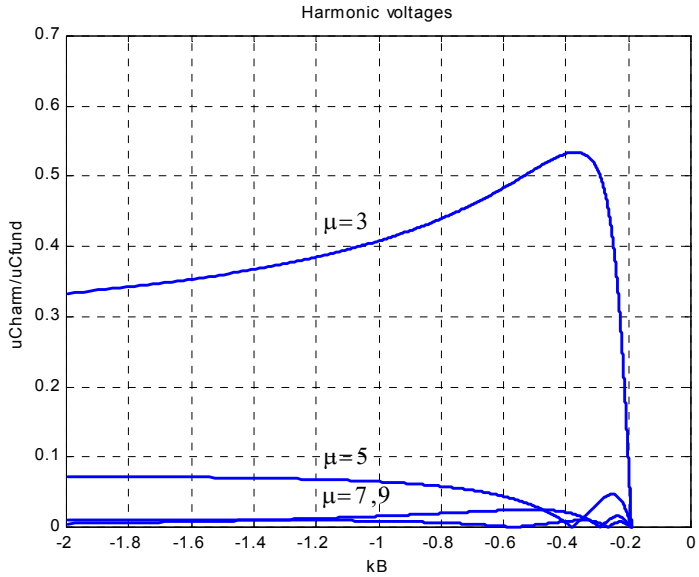

Figure 3.8 Relative harmonic voltage vs boost factor, λ=2.5.

The graph shows that the waveform is very much distorted even for small negative boost levels with absolute values close to *0.3*.

3.3.4 Impact of inductor size

As a second example we shall study the case that the inductor in the thyristor branch is smaller. We assume $\lambda = 3.5$, corresponding to a resonance frequency *175/210 Hz* in a *50/60 Hz* system respectively. The inductor reactance is about half the size of the preceding case i.e. *8.2 %* of the capacitor bank reactance.

Figure 3-9 shows the boost factor k_B versus the control angle β.

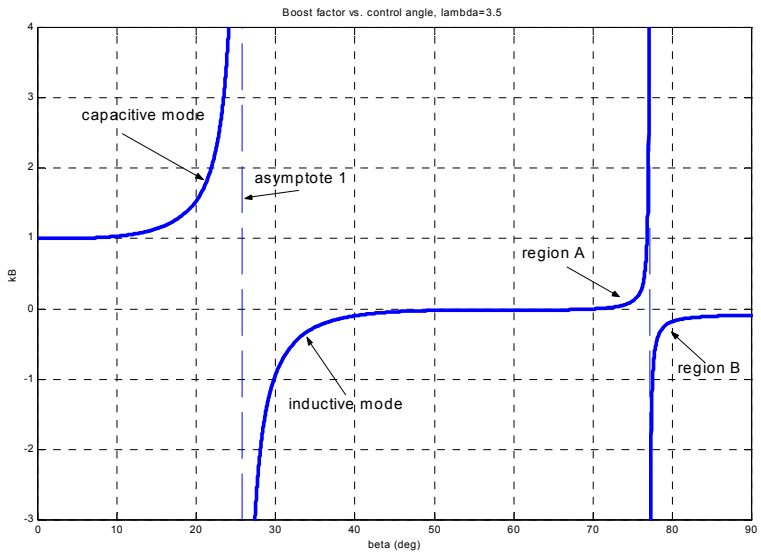

Figure 3-9 Boost factor versus conduction angle for TCSC with $\lambda = 3.5$.

The left part of the figure is similar to the curve in the preceding case (figure 3-3). The angle range for capacitive mode however is narrower and a second asymptote has entered from the right. It appears at β=77.14° according to equation (3-12).

Four different regions can be identified:

- capacitive boost mode region: 0<β<25.7°
- inductive boost mode region: 25.7°<β<approx. 55°
- region A: 55°<β<77.1° with capacitive boost
- region B: 77.1°<β<90°

Capacitive boost mode: The waveforms are similar to those in the preceding example. Figure 3-10 presents a comparison between the two main circuit designs when operating with identical boost factor. It shows the waveforms for the two different TCSC main circuits operating at the same boost factor $k_B=2.0$.

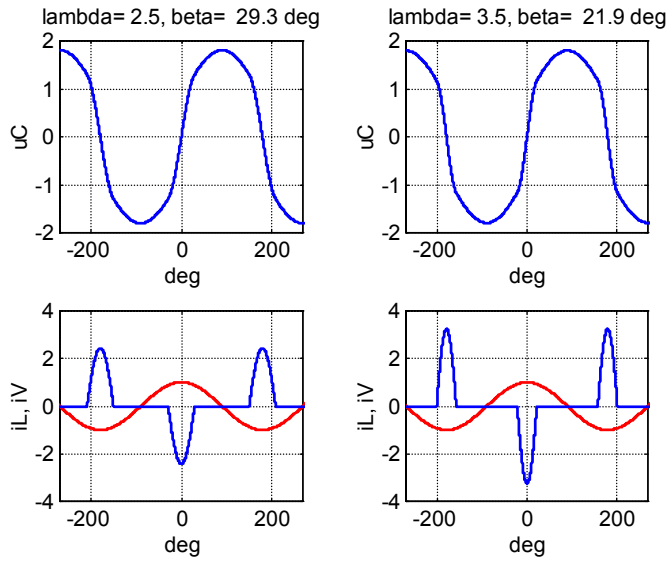

Figure 3-10 Waveforms at k_B=2.0 for TCSC with two different main circuits.

As expected the one using higher λ will have higher thyristor peak currents and somewhat more distorted waveform.

Remark: It appears in the figure that the capacitor peak voltage is lower than 2 pu even for a boost factor that equals 2 pu. The reason for this is that the thyristor current vanishes between the conduction intervals causing the corresponding added capacitor voltage to have some resemblance with a square-wave. It should be noted that the amplitude of the fundamental component of a square-wave having unity amplitude is $4/\pi \approx 1.27$.

Inductive boost mode: In figure 3-11 a similar comparison is made in the inductive boost mode region.

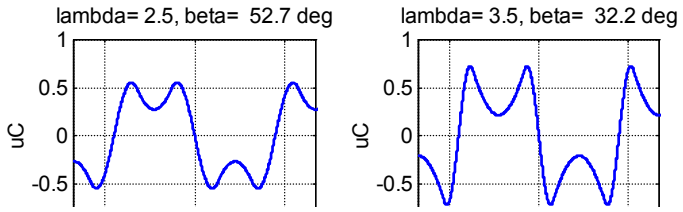

Figure 3-11 Waveforms k_B=-0.5 for two main different main circuits.

Obviously the harmonic content in these waveforms is high in general and the harmonic content worsens when λ gets high. In practice a rather low λ is required in order to make the operation possible. At low boost levels the harmonic composant in the capacitor voltage is higher than the peak value of the fundamental frequency component.

Behaviour close to the second asymptote

Region A: In figure 3-9 there is a narrow region close to the second asymptote in which the fundamental voltage is capacitive and has an absolute value below 1. The corresponding waveform is shown in left part of figure 3-12. This waveform results mathematically from the assumption made in the derivation of the boost factor formula, that the valve remains conducting during a certain angle interval, independent on the current direction. It appears in the calculated waveform that the valve current will flow alternatively in both directions during each conduction interval. In practice this kind of operation does not appear to be meaningful.

Region B: The right-hand side graphs in figure 3-12 show the waveforms when the conduction angle is in region B, i.e. a little bit to the right of the second asymptote in figure 3-9. This case also is a "pathological" case that results from the assumptions made for the mathematical derivation of formulas.

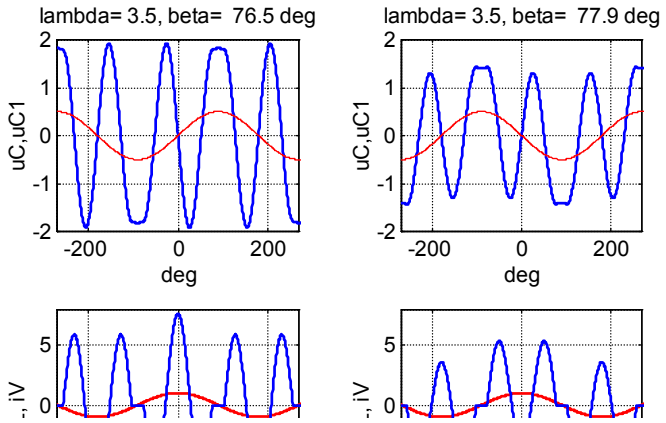

Figure 3-12 Waveforms close to the second asymptote in figure 3-9. Region A, capacitive boost (left), Region B, inductive boost (right).

3.3.5 Bypass mode

Assume that the TCSC inductor is selected so that $\lambda=2.5$ as in figure 3-8. When the control angle is 90° the valve becomes continuously conducting. In this condition the valve is said to operate in **bypass mode**. The resulting inserted reactance then tends towards the reactance of the capacitor and the inductor connected in parallel. The resulting boost factor is

$$k_{B,\beta=90^\circ} = \frac{1}{1-\lambda^2} \tag{3-24}$$

which in this case ($\lambda=2.5$) gives $k_B = -0.190$. It can be seen in figure 3-8 that no harmonics are generated in bypass mode. Note that the valve current in bypass mode exceeds the line current as the capacitor bank generates some current, which is added to the line current, when passing through the valve.

3.3.6 Blocking mode

When no triggering command at all is given to the thyristor valve the TCSC the fixed capacitor bank is inserted. The operating mode is called **blocking mode**.

CHAPTER 4
SYNCHRONOUS VOLTAGE REVERSAL

The waveforms for TCSC operating in steady state have been presented in the preceding chapter. Both capacitive and inductive boost modes of operation have been discussed. In this chapter the study will be continued in order to extend the description of the TCSC to facilitate also a discussion of the dynamics of the device.

For this purpose the concept of **equivalent, instantaneous capacitor voltage reversal** will be introduced in order to describe the impact of thyristor operation in the TCSC on the capacitor voltage. This concept will be introduced in section 4.1. The idea of describing the TCSC in terms of the equivalent, instantaneous voltage reversals is one of the major contributions in this thesis.

In section 4.3 the boost factor, k_B, will be redefined so that it can be used together with the new concept of the equivalent, instantaneous voltage reversals. The boost factor measures the apparent reactance of the TCSC at rated frequency as seen from the transmission system.

In section 4.4 the dynamics of the boost factor will be described using the instantaneous voltage reversal concept. An intuitive model of TCSC boost is derived which is used to outline a boost control system for the TCSC in section 4.5.

Section 4.6 describes how the principle of instantaneous voltage reversal can be applied to a real system where the reversal process takes finite time. An equation is derived which is used to determine the thyristor firing instant from measured values of capacitor voltage and line current and using the desired equivalent reversal instant of the capacitor voltage as reference. The solution of this equation in run-time results in a control system which we will call the Synchronous Voltage Reversal (SVR) scheme.

4.1 THE EQUIVALENT, INSTANTANEOUS CAPACITOR VOLTAGE REVERSAL

The TCSC main circuit is designed with respect to the stresses in the thyristor valve. Requirements on harmonic distortion of the capacitor voltage also may influence the main circuit selection. Usually the main circuit design parameter λ as defined in (3-3) will fall in the range *2 - 4*. Thus the thyristor conduction time is always shorter than the half cycle time at the rated network frequency; in normal designs it is considerably shorter. The thyristor conduction in the TCSC provides a “current pulse” or a “charge pulse” into the capacitor. In steady state the thyristor conduction intervals appear when the line current passes through its maximum positive or negative values. At these instances the derivative of the line current is low or zero and accordingly the variation of the line current within the thyristor conduction interval is very small. As a first approximation we may consider it to remain constant during the conduction interval.

Figures 4-1 and 4-2 demonstrate the capacitor voltage and the valve current. The behaviour immediately before, during and immediately after the thyristor conduction interval is shown. The main circuit design parameter λ varies between 2.5 and 10 and both capacitive (figure 4-1) and inductive (figure 4-2) boost mode operation is considered. The losses in the circuit have been neglected. With these assumptions the capacitor voltages at turn-on and turn-off, in the beginning and the end of the thyristor conduction interval, have equal magnitude but opposite signs. In other words **the result of the intervention of a thyristor in the TCSC is a capacitor voltage reversal**.

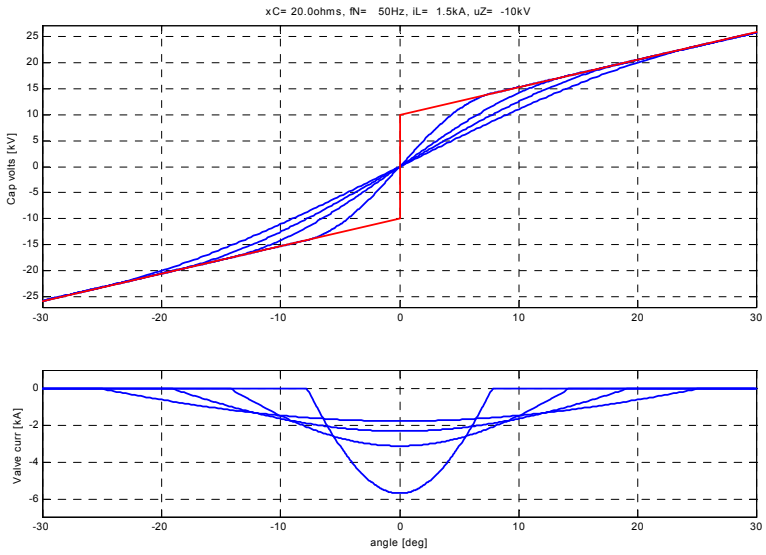

Figure 4-1 Voltage reversals in capacitive mode with k_B=1.424 and λ=2.5, 3.5, 5, 10, infinite.

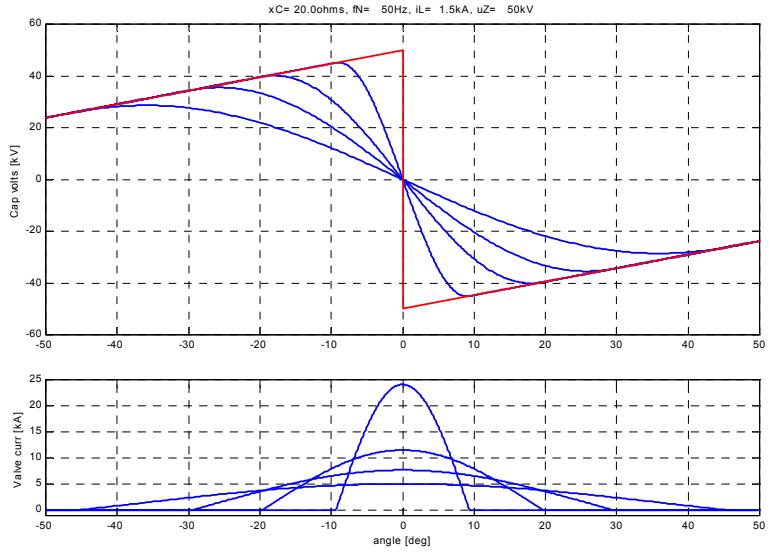

Figure 4-2 Voltage reversals in inductive mode with k_B=-1.122 and λ=2.5, 3.5, 5, 10, infinite.

Figures 4-1 and 4-2 show that if triggering is controlled so that the capacitor voltage zero-crossing instant remains unchanged, then all trajectories, irrespective of the main circuit design parameter λ, connect to the same post-reversal line. The latter has the same constant slope as the pre-reversal capacitor voltage line. The slope of both these lines is proportional to the line current which was assumed to be constant.

If no thyristor conduction occurs, i.e. if the thyristors are blocked, the pre- and the post-reversal lines coincide; the capacitor voltage just changes linearly due to the constant line current. Therefore it can be claimed that the effect of thyristor action in the TCSC is that it produces a parallel displacement of the pre- and post-reversal lines relative each other. The created vertical gap in this displacement is a measure of the strength of the thyristor action.

The trajectories in figures 4-1 and 4-2 represent various TCSC main circuits using inductors with different inductance. When the inductance decreases the thyristor conduction interval turns out to be shorter and the thyristor peak current becomes higher. When the thyristor current totally dominates relative the line current an almost instantaneous voltage reversal results. The capacitor voltage trajectory in the idealized case where the inductance is zero has been added in the figures.

Now let a real TCSC circuit having finite reversal time be fired at the angle $\omega_N t=-\beta$ in the figures. Assume that the line current can be approximated to be constant during the conduction interval. The capacitor voltage zero-crosses at angle $\omega_N t=0$ and simultaneously the thyristor current peaks. The same displacement between the pre- and post-reversal lines, i.e. same the boost action of the TCSC, would be obtained in a hypothetical circuit performing an

instantaneous capacitor voltage reversal at the angle $\omega_N t=0$. The hypothetical circuit then would perform an **equivalent, instantaneous capacitor voltage reversal**.

When the TCSC is connected in a transmission system the significant issue, from system point of view, is the boost action of the TCSC, i.e. the parallel displacement of the pre- and post-reversal voltage lines. The exact time function of the transfer between the lines is not very important. In the continued investigation of the TCSC therefore it is sufficient to deal with the equivalent, instantaneous voltage reversals in order to describe the TCSC dynamics.

4.2 THE ADDITIONAL CAPACITOR VOLTAGE CAUSED BY THYRISTOR ACTION

The interpretation of the parallel displacement of the pre- and post-reversal lines for the system can be made clear as follows. The capacitor voltage comprises two contributions. One originates from the line current and the other one from the current circulating through the thyristor branch and the series capacitor bank. The latter component represents the thyristor boost action. The corresponding additional capacitor voltage can be calculated by integration of the thyristor current and dividing the resulting charge with the bank capacitance. The thyristor branch does not carry any current during most of the time and then the additional capacitor voltage does not change. Therefore the additional voltage is square-wave-like. Curves showing the additional capacitor voltage for the cases in figures 4-1 and 4-2 are presented in figures 4-3 and 4-4.

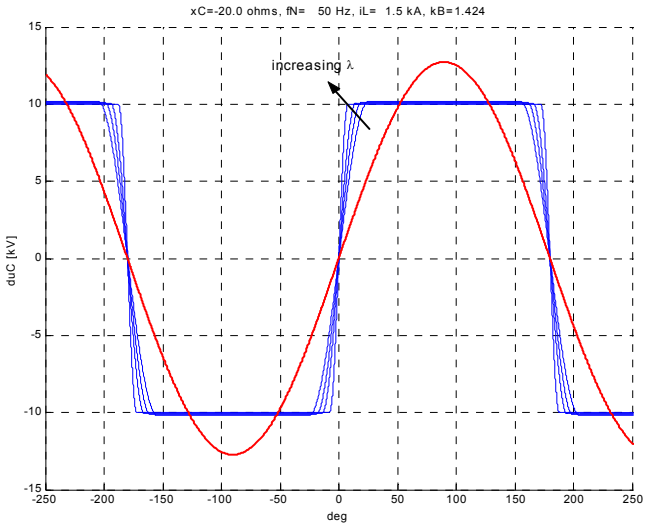

Figure 4-3 Additional capacitor voltage in capacitive mode with k_B=1.424 and λ=2.5, 3.5, 5, 10.

The waveforms have different main circuit design parameter λ but the fundamental frequency component is constant (the sinusoidal curve in the figures) and equals the fundamental component in a square-wave with 10 kV (capacitive mode with $k_B = 1.424$) and 50 kV (inductive mode with $k_B = -1.122$) respectively.

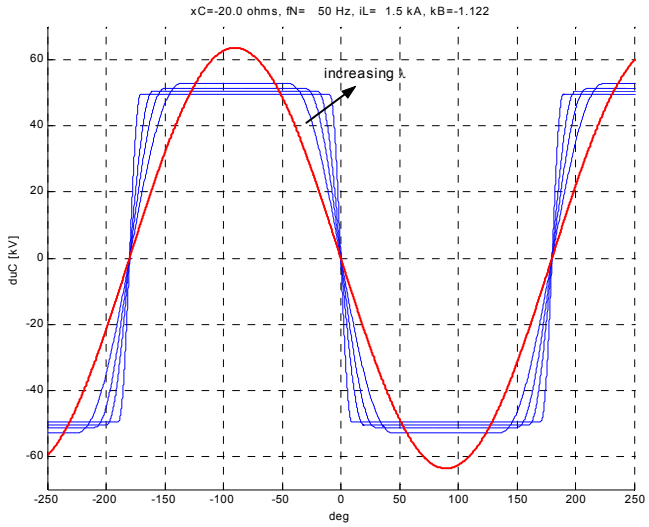

Figure 4-4 Additional capacitor voltage in inductive mode with k_B=-1.122 and λ=2.5, 3.5, 5, 10.

It can be seen that the amplitude of the additional voltage between the reversals, i.e. the difference between the pre- and post-reversal lines, for all cases are very close to each other. This applies specifically for capacitive mode of operation. The reason is of course that the waveforms for the capacitor voltage differ only for values close to the reversal point. The values of the capacitor voltage close to the zero-crossing contribute very little to the fundamental frequency component.

Remark 1: The equivalent, instantaneous capacitor voltage reversal describes the reversal in a hypothetical TCSC circuit with a very small inductor with a high Q-factor (low losses). The trajectories presented in figures 4-1 and 4-2 show that the thyristor current increases fast with increasing λ. The values shown for λ=10 in inductive mode of operation cannot be realized even for short-time operation, due to the very high di/dt that results from the combination of a small inductance in the circuit and a high turn-on voltage.

Remark 2: The assumption that the line current is constant during the whole thyristor conduction interval has the consequence that the thyristor current becomes symmetrical around the time instant when the capacitor voltage cuts the zero line. The deviation in a real circuit from the assumption of constant line current decreases with decreasing length of the conduction interval. Thus main circuits with high λ and operation in capacitive mode with low boost are better described by this approximation than low-λ circuits operating in inductive mode.

4.3 DEFINITION OF BOOST FACTOR

The boost factor k_B was introduced in section 3.2 dealing with the analysis of the TCSC operation in steady state. Equation (3-23) designates the formula for the boost factor versus the control angle β. In this thesis the boost factor k_B is used as a measure of the ratio of the apparent reactance of the TCSC as seen from the line and the physical reactance of the series capacitor bank. The reactance is evaluated at rated network frequency. Thus assume that a sinusoidal line current $\hat{I}_L$ with rated network frequency is injected into the TCSC and that it produces a sinusoidal voltage with amplitude $\hat{U}_{C0}$, when the thyristor valve is blocked. When the valve is deblocked and the control angle has been adjusted the fundamental frequency component of the capacitor voltage is changed to $\hat{U}_{C1}$. The boost factor then is defined as

$$k_B = \frac{\hat{U}_{C1}}{\hat{U}_{C0}} \tag{4-1}$$

In the formula the signed amplitude of $\hat{U}_{C1}$ is used, which means that the boost factor is positive for capacitive apparent reactance and negative for inductive apparent reactance. Figures 4-5 and 4-6 show the waveforms in capacitive and inductive mode of operation.

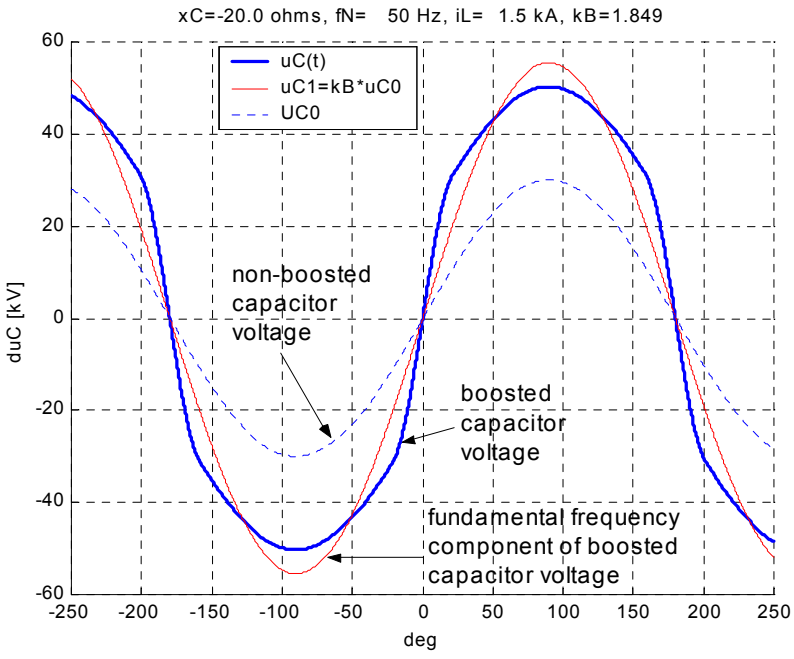

Figure 4-5 Illustration of boost factor in capacitive mode.

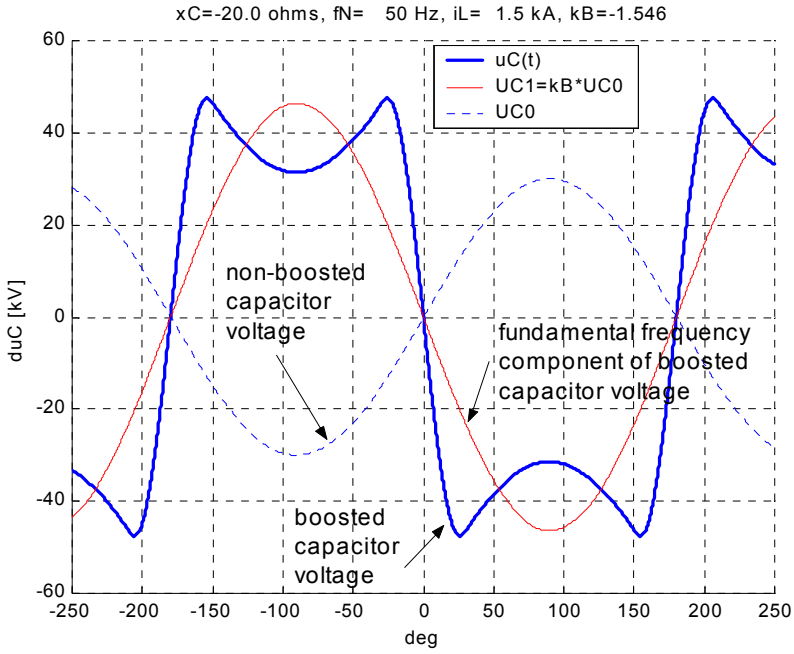

Figure 4-6 Illustration of boost factor in inductive mode.

In the following section of the thesis we will discuss the dynamics of the boost factor in the TCSC utilizing the idealized concept of equivalent, instantaneous capacitor voltage reversals. The additional voltage then becomes a square-wave.

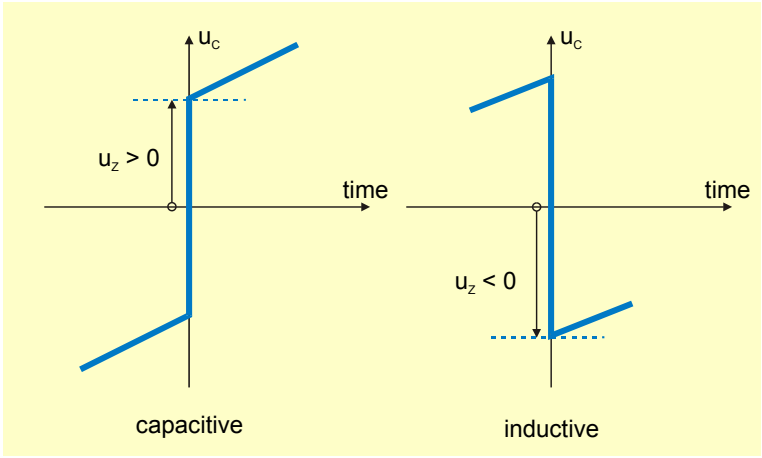

Figure 4-7 Definition of boost voltage.

The boost voltage u_Z is defined as the amplitude of the square-wave with sign according to figure 4-7. Positive sign indicates capacitive boost and negative sign inductive boost as shown in the figure. The fundamental frequency component of the additional capacitor voltage related to the equivalent, instantaneous capacitor voltage reversal is given by

$$\hat{U}_{add,1} = \frac{4}{\pi} u_Z \tag{4-2}$$

Accordingly the boost factor becomes

$$k_B = 1 + \frac{4}{\pi} \frac{u_Z}{\hat{U}_{C0}} \tag{4-3}$$

4.4 BOOST FACTOR DYNAMICS

In this section we shall demonstrate how simple the dynamics of the boost factor can be explained using the concept of equivalent, instantaneous capacitor voltage reversals. In this framework the TCSC capacitor voltage in steady-state operation appears as in figure 4-8. It is composed of pieces of sinusoidal curves joined by instantaneous reversals.

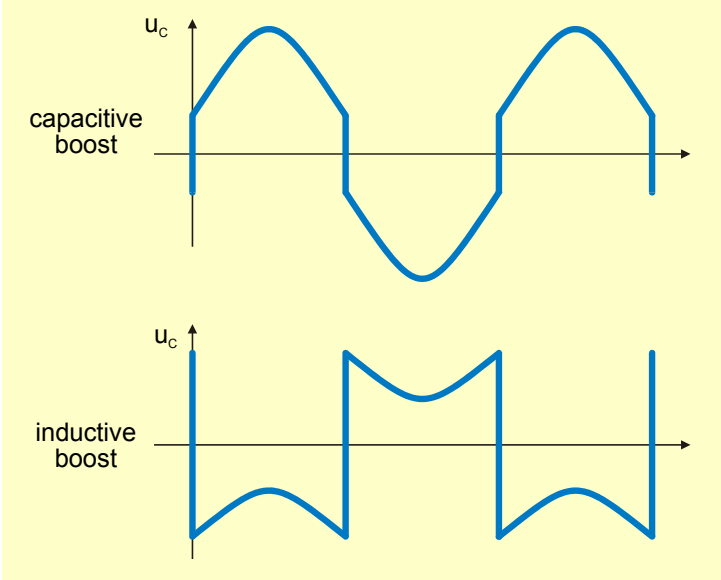

Figure 4-8 Idealized capacitor voltage waveforms in steady state.

The variation of the capacitor voltage in the meantime between consecutive reversals depends exclusively of the line current. In steady-state operation the capacitor voltage reversals occur equidistantly in the TCSC with a repetition rate that equals twice the frequency of the line current. The triggering of the reversals must appear with a particular phase relationship relative the line current if steady-state conditions shall prevail. The requirement simply is that the time integral of the line current between consecutive reversals must be zero. The

capacitor voltage immediately before an upcoming reversal equals the capacitor voltage immediately following the preceding reversal if this condition has been fulfilled. The boost voltage then remains constant in the successive reversals and the boost level remains constant and accordingly the TCSC operates in steady state. These equilibrium reversal positions coincide with the line current maximum and minimum values. Figure 4-9 illustrates the conditions just described.

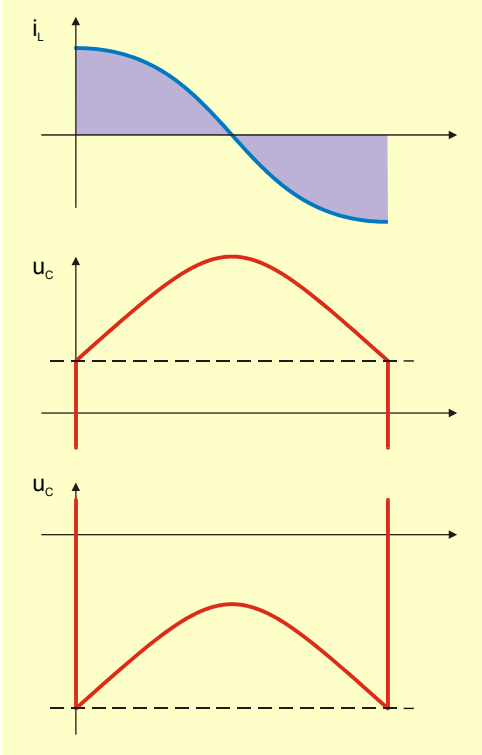

Figure 4-9 Steady-state boost in capacitive and inductive mode.

In figure 4-10 the voltage reversal has been phase advanced from the equilibrium position in figure 4-9. The displacement causes an increase of the boost voltage at the right-hand reversal because the capacitor bank is charged with more positive charge and it is discharged with less negative charge by the line current. The change in boost voltage at each reversal is proportional to the line current amplitude $\hat{I}_L$ and to the phase deviation $\Delta\varphi_C$ from the equilibrium position. There is a change of charge both at the beginning and at the end of the interval between the reversals so that

$$\Delta u_Z = \frac{2}{\omega_N C}\hat{I}_L \Delta\varphi_C \tag{4-4}$$

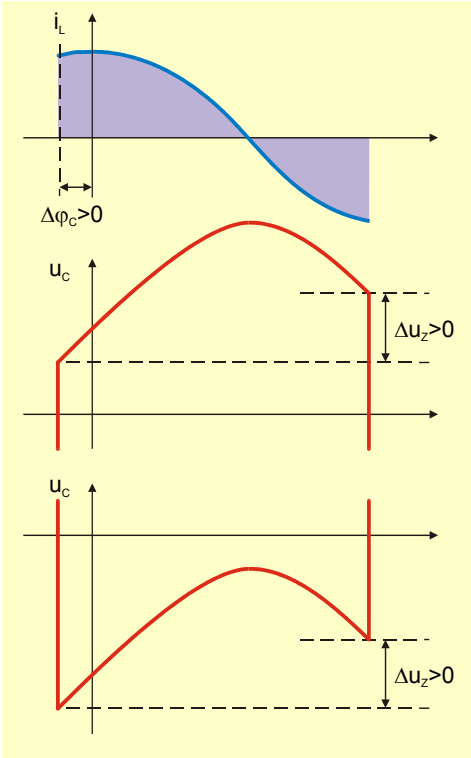

Figure 4-10 Increasing boost in capacitive and inductive mode.

As the steady-state non-boosted capacitor voltage is given by

$$\hat{U}_{C0} = \frac{\hat{I}_L}{\omega_N C} \tag{4-5}$$

the corresponding increase per reversal of the boost factor (defined in section 4.3) becomes

$$\Delta k_B = \frac{8}{\pi} \Delta\varphi_C \tag{4-6}$$

The reversal rate is the double network frequency so in average the rate of change of the boost factor is given by

$$\frac{d\Delta k_B}{dt} = \frac{16}{\pi} f_N \Delta\varphi_C \tag{4-7}$$

The boost factor continues to change with the speed given by (4-7) as long as the phase advancement $\Delta\varphi_C$ is present.

In a similar way the boost voltage decreases, as shown in figure 4-11, when the voltage reversals are being phase retarded relative their equilibrium positions.

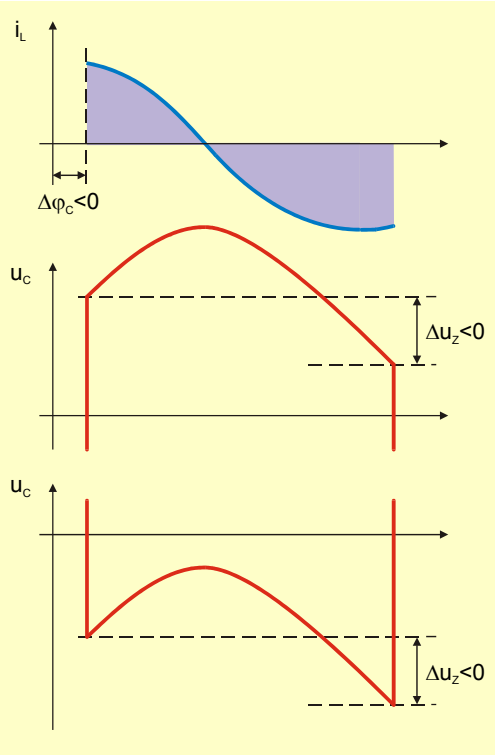

Figure 4-11 Decreasing boost in capacitive and inductive mode.

A net charge is taken from the capacitor bank by the line current due to the reduced amount of positive charge and the increased amount of negative charge. The boost factor keeps decreasing as long as the reversals remain retarded relative their equilibrium positions (i.e. $\Delta\varphi_C<0$). Of course the boost factor decrease ceases when the boost voltage becomes zero because the thyristor cannot conduct in its reverse direction.

It shall be observed that according to equation (4-7) the speed of change of the **boost factor** k_B is proportional to the displacement $\Delta\varphi_C$ of the reversal angle**.** The impact on the capacitor **voltage** is proportional to the actual line current. Accordingly the behaviour of the control system is critical when the line current is high. Any malfunction or imperfection then easily may cause hazardous voltage stress on the capacitor and the thyristor valve.

4.5 OUTLINE OF A BOOST CONTROL SYSTEM FOR TCSC

Equation (4-7) shows that the time derivative of the boost factor, $\frac{dk_B}{dt}$, depends on the angular displacement of the equivalent, instantaneous voltage reversals from their equilibrium position. If the timing of the equivalent, instantaneous capacitor voltage reversals can be adequately controlled by the TCSC's triggering system, then the design of the control system becomes easy and straightforward, because the TCSC boost then can be described simply as an integrating process as shown in figure 4-12.

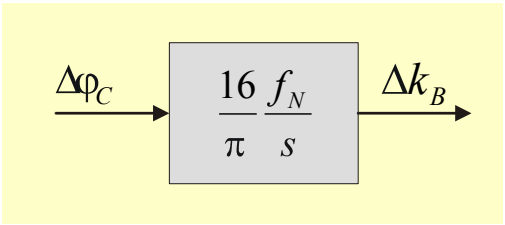

Figure 4-12 Model of the boost process.

In theory such a process can be controlled simply by proportional feedback; in practice a PI controller would be utilized. This is the simple solution to the boost factor control problem using the Synchronous Voltage Reversal (SVR) concept. To "control the timing of equivalent, instantaneous voltage reversals" translates in practice to "directly control the zero-crossing of the capacitor voltage".

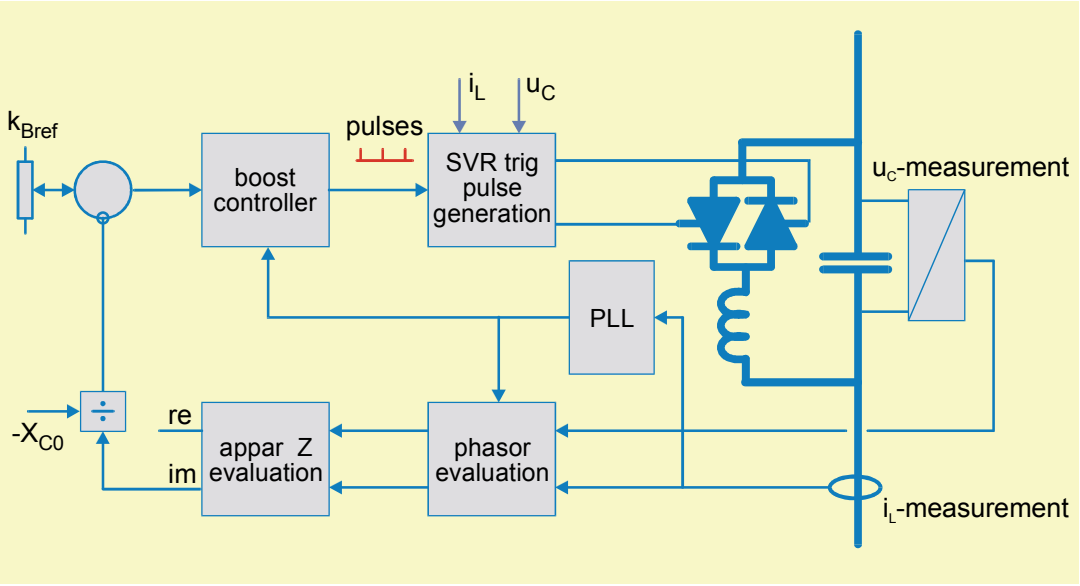

Figure 4-13 Outline of the boost control system.

In next section it will be explained how this control is obtained by a supplementary independent triggering control system. When given a time reference pulse this system selects the thyristor triggering instant such that the capacitor voltage zero-crossing instant occurs at a fixed delay time after the reference pulse. The boost control system now may be outlined according to figure 4-13. The line current and the capacitor voltage are measured and the fundamental frequency components are being extracted in the block marked "phasor evaluation". Then the complex quotient between the phasors is formed. Its imaginary part represents the measured apparent reactance of the TCSC. It is normalized with the capacitor bank's physical reactance to get the measured boost level. The boost response is compared with the actual reference value and the error is entered to the boost controller. A Phase Locked Loop (PLL) is arranged and supplies line current argument information to the boost controller. The output of the latter is a pulse train with timing reference pulses to a SVR trig pulse generator block. In this block the firing instant is being calculated and a trig pulse is generated and sent to the appropriate thyristor.

4.6 THE SYNCHRONOUS VOLTAGE REVERSAL EQUATION

The function of the block marked "SVR trig pulse generation" in figure 4-13 will be explained below with reference to figure 4-14.

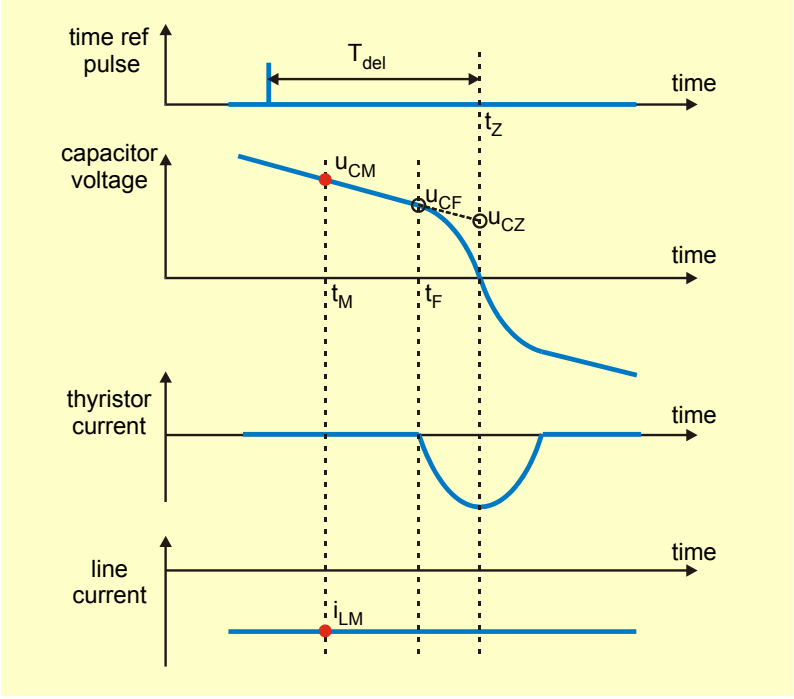

Figure 4-14 Waveforms and definitions for the SVR equation.

The time reference pulse defines the time t_Z, i.e. the time instant, when it is desired that the capacitor voltage shall become zero. It shall occur with a fixed, given delay T_{del} relative the reference pulse. Now measured values of the capacitor voltage and the line current are being collected. In the figure measured values are acquired at time t_M.

The thyristor triggering time-point t_F, which causes the capacitor voltage to zero-cross at t_Z is calculated based on the measured values of the capacitor voltage, the line current and the known main circuit design parameter λ. This calculation obviously involves some assumption about the variation of the line current in the interval between the measuring point t_M and the voltage zero-crossing instant t_Z at the midpoint of the thyristor conduction interval. In a simple approach the line current is extrapolated to remain constant keeping its latest measured value. Another more refined assumption may involve a sinusoidal line current waveform. Several calculations may be performed with newly updated measured values until triggering occurs.

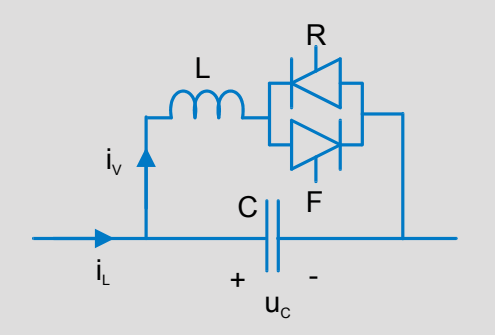

Figure 4-15 Main circuit and definition of direction.

Here the simplest assumption, i.e. the constant line current approximation, will be used. The previous figure 3-1 is reproduced once again as figure 4-15.

Let the measured line current at $t = t_M$ be i_{LM} and assume that it remains constant. The equations in the conduction interval are

$$\begin{aligned} \dot{i}_V &= \frac{1}{L} u_C \\ \dot{u}_C &= \frac{1}{C}\left(i_{LM} - i_V\right) \end{aligned} \tag{4-8}$$

Combining these two equation together with the definitions in (3-1) and (3-3) yields

$$\ddot{i}_V + \lambda^2 \omega_N^2 i_V = \lambda^2 \omega_N^2 i_{LM} \tag{4-9}$$

The solution, which has the initial value $i_V(t_F)=0$ is

$$i_V(t)=i_{LM}\left[1-\frac{\cos[\lambda\omega_N(t_Z-t)]}{\cos[\lambda\omega_N(t_Z-t_F)]}\right] \tag{4.10}$$

The capacitor voltage can be obtained according to (4-8) by differentiating the expression (4-10) for the valve current. Combining the result with the definition in (3-3) we get

$$u_{CF}=-X_0 i_{LM}\tan[\lambda\omega_N(t_Z-t_F)] \tag{4-11}$$

But we assumed that the line current is constant so we also get

$$\begin{aligned} u_{CZ}&=u_{CM}+\frac{i_{LM}}{C}(t_Z-t_M)=u_{CM}+X_0 i_{LM}\lambda\omega_N(t_Z-t_M)\\ u_{CZ}&=u_{CF}+\frac{i_{LM}}{C}(t_Z-t_F)=u_{CF}+X_0 i_{LM}\lambda\omega_N(t_Z-t_F)\end{aligned} \tag{4-12}$$

where we have again used (3-3). The upper equation in (4-12) makes it possible to calculate u_{CZ} every time a new measurement has been performed. Put

$$\beta=\omega_N(t_Z-t_F) \tag{4-13}$$

The latter equation in (4-12) together with (4-13) now forms a non-linear equation that determines the triggering time instant

$$u_{CZ}=X_0 i_{LM}[\lambda\beta-\tan(\lambda\beta)] \tag{4-14}$$

It is necessary to investigate under what circumstances a solution to (4-14) may be found and whether the solution is unambiguous. From its definition β is a positive quantity. Figure 4-16 shows the value of the function

$$y=x-\tan x \tag{4-15}$$

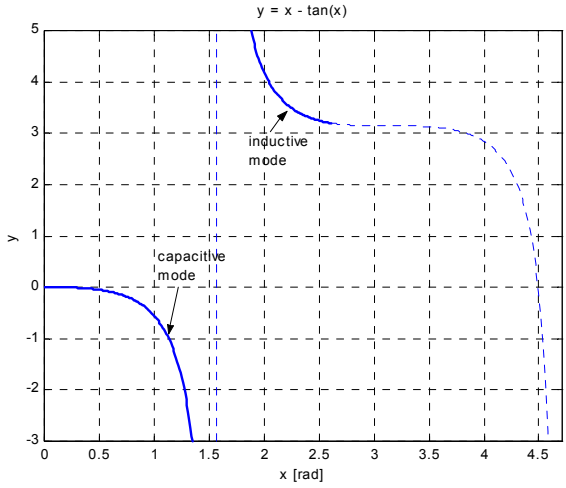

Figure 4-16 Function values of (4-15).

It can be seen in figure 4-14 that the boost voltage u_{CZ} is positive and the line current is negative in capacitive boost mode. Equation (4-14) then has a unique solution in the interval $0<\lambda\beta<\pi/2$ corresponding to the lower branch in figure 4-16.

Inductive boost mode also requires that the boost voltage u_{CZ} is positive. However also the line current is positive in this case. Figure 4-16 shows that a unique solution certainly exists in the interval $\pi/2<\lambda\beta<\pi$ if $u_{CZ} > \pi X_0 i_{LM}$.

We may summarize the SVR calculation scheme

$$\begin{array}{ll} u_{CZ}: & u_{CZ} = u_{CM} + X_0 i_{LM} \lambda\omega_N (t_Z - t_M) \\ \beta: & u_{CZ} = X_0 i_{LM} \left[\lambda\beta - \tan(\lambda\beta)\right] \\ t_F: & t_F = t_Z - \dfrac{\beta}{\omega_N} \end{array} \qquad (4\text{-}16)$$

Example 4-1

We shall illustrate the properties of the Synchronous Voltage Reversal equations by some simulation examples. First assume that the line current is sinusoidal with constant amplitude and frequency. Further assume that the losses are negligible and that the reference instants for the reversals appear at their ideal positions, i.e. they coincide with the line current maximum and minimum values. Under these conditions the circuit is expected to preserve a constant boost level. Figure 4-17 shows the result of such a simulation. The upper graph is the line current, the second from the top is the resulting capacitor voltage, the third from the top is the valve current and the bottom graph shows the calculated control angle β. The

trigger angle calculation is performed from the zero-crossing of the line current and it is repeated until triggering really occurs.

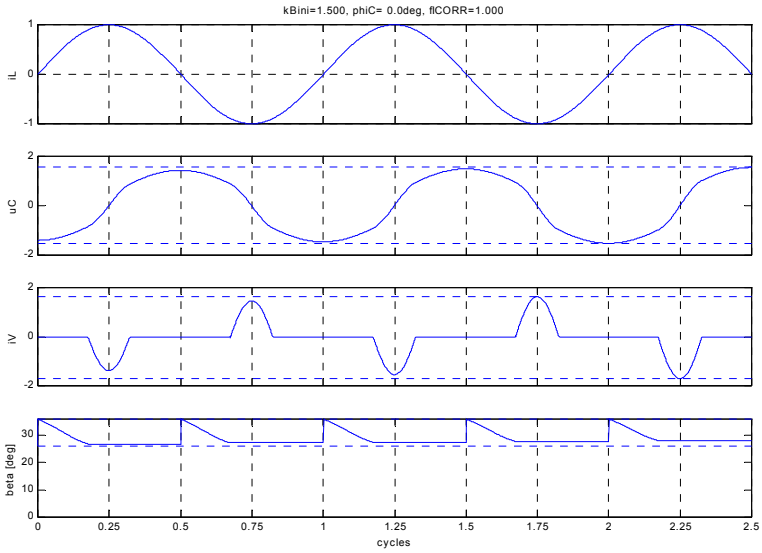

Figure 4-17 Simulation of SVR scheme operating without any corrections.

It can be seen that the calculated control angles decrease with time just before triggering. This depends on the approximation applied in the SVR equation that the line current will keep its measured value constant until the valve conduction interval has passed. This approximation improves when the calculation time gets closer to the line current peak. However, in reality the average line current in the conduction interval exceeds the measured value at triggering to some extent. Therefore the calculated control angle becomes a little bit too big. Accordingly the thyristor valve is triggered slightly too early so that the boost level slowly increases.

This drift in boost level easily is taken care of by the boost control regulator, but it might be of interest to investigate if a simple compensation can easily be applied in the triggering system. At least two approaches could be considered:

- apply a multiplicative factor on the measured line current value in order to compensate for the current increase during the conduction interval
- apply a fixed angle compensation of the commanded reversal instants.

Figure 4-18 presents some simulation results for these two approaches. The graphs show the ratio between consecutive half-cycle capacitor voltage peaks as function of the boost factor. The circuit design parameter is $\lambda=2.5$ and the main circuit losses have been neglected. The upper graph relates to line current compensation and the lower to angle compensation.

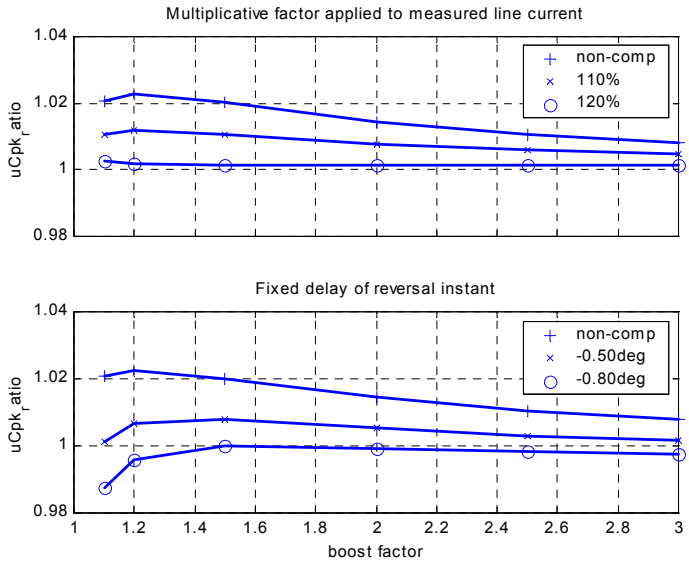

Figure 4-18 Compensation of the SVR equation. λ=2.5.

The graph shows that line current compensation provides excellent results. In this case *(λ=2.5)* a compensation factor $f_{ICORR} = 1.20$ is adequate.

Example 4-2

In the deduction of the SVR equations losses in the main circuit were not considered. In the context of equivalent instantaneous voltage reversals losses may be taken care of by a loss factor D_f indicating the absolute value of the ratio between the post reversal and the pre reversal capacitor voltages.

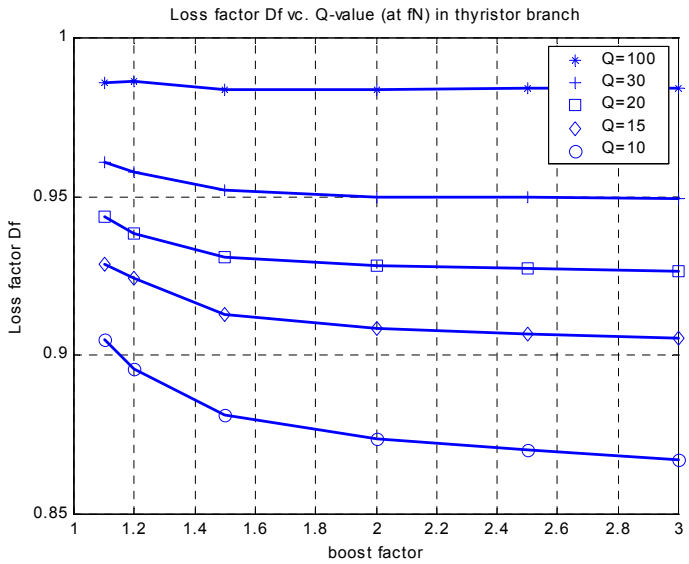

Figure 4-19 Loss factor D_f versus Q-factor (at f_N) for the inductor branch. (λ=2.5)

Simulations were performed in order to derive the relation between the loss factor D_f and the Q-value of the thyristor controlled inductive branch. Here the Q-value has been defined as the ratio between reactance and the resistance **at network frequency**. Please note that the loss factor is associated with the ratio of voltages before and after the reversal. It is not identical with the ratio between the capacitor peak voltages. In the simulations a current compensation factor $f_{ICORR} = 1.20$ was applied. The results obtained are shown in figure 4-19. The graphs indicate that $D_f = 0.95$ corresponds approximately to a Q-factor of *30*.

Example 4-3

The SVR approach inherently symmetrizes the capacitor voltage. As long as the reversal reference pulses are equidistant and the line current is symmetrical, a DC offset voltage will not be created. A varying control angle will create a varying boost factor, but the capacitor voltage will not contain any DC component.

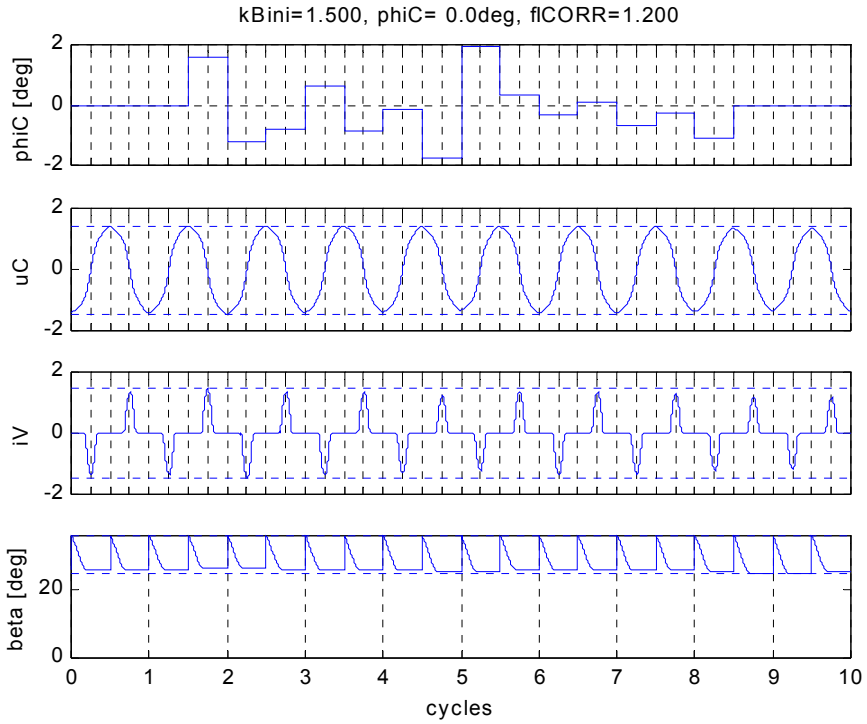

Figure 4-20 Simulation of TCSC with randomly varying reversal positions.

Figure 4-20 shows an example where the timing reference pulse train is being phase modulated by a random signal shown in the upper graph. The other graphs are in order from the top: capacitor voltage, thyristor current and control angle β. The figure shows that the voltage remains symmetric in spite of the randomly changing reversal instants. One can also detect the integrating property of the SVR algorithm, which means that the capacitor boost voltage depends on the integral of the applied deviation of the reversal angle.

CHAPTER 5
IDEAL APPARENT IMPEDANCE OF TCSC

5.1 INTRODUCTION

The preceding chapter dealt with the properties of TCSC control based on the Synchronous Voltage Reversal approach. It was assumed that the line current was stiff and sinusoidal. It was shown that the boost is controlled by the phase of the capacitor voltage zero-crossings with respect to the line current.

Another, most important, characteristic of the TCSC behaviour relates to how it reacts with respect to small changes in the line current. For frequencies not equal to the network rated frequency this property may be described in terms of "apparent impedance" as function of frequency. For the passive fixed series capacitor the reactance at subsynchronous frequency is capacitive with a magnitude, which is inversely proportional to the frequency. Thus, given the reactance at 50 or 60 Hz, the inserted reactance in the whole subsynchronous frequency range is determined. If a transmission line is compensated to a degree less than 100 %, an electrical resonance occurs at a subsynchronous frequency, where the magnitude of the capacitive reactance equals the total inductive reactance of the transmission line and the connected sources. The existence of the electrical resonance constitutes one of the prerequisites for establishing "subsynchronous resonance", SSR, in a power system. (SSR is an interaction between the electrical resonance in the transmission system and the mechanical torsional resonance in the turbine-generator shaft string in a thermal power station connected to the transmission system).

However, for a TCSC the apparent impedance for lower frequencies is not only determined by the inserted reactance at 50 or 60 Hz. On the contrary, the inner control of the TCSC has a substantial impact on the apparent impedance as will be seen in the following.

Figure 5-1 illustrates the basic difference between the fixed series capacitor and the TCSC at an angular frequency ω. Note that the voltage inserted in series with

the line is determined by the voltage across the capacitor, which is in its turn created by the current passing through the latter.

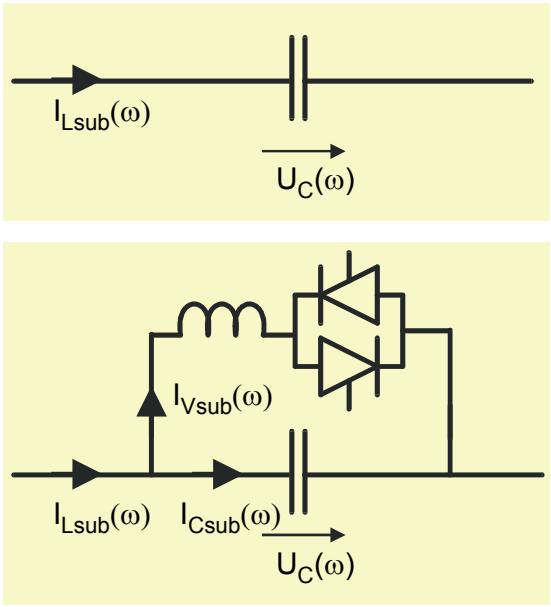

$$Z_{app}(\omega) = \frac{\bar{U}_C(\omega)}{\bar{I}_{Lsub}(\omega)} = -jX_C \frac{\omega_N}{\omega}$$

$$Z_{app}(\omega) = \frac{\bar{U}_C(\omega)}{\bar{I}_{Lsub}(\omega)} = -jX_C \frac{\omega_N}{\omega} \frac{\bar{I}_{Csub}(\omega)}{\bar{I}_{Lsub}(\omega)}$$

Figure 5-1 Apparent impedance for fixed series capacitor (upper) and for TCSC (lower)

In the fixed series capacitor any line current must pass through the capacitor and any subsynchronous current creates a subsynchronous voltage proportional to the capacitive reactance at that frequency. In the TCSC the subsynchronous current in the capacitor depends on the triggering system's reaction to any injected subsynchronous line current component. If the firing system is designed so that it prevents any subsynchronous current to pass through the thyristor controlled inductive branch, then the situation is just identical to that in the non-boosted series capacitor, i.e. the network sees a capacitive reactance with magnitude inversely proportional to frequency. On the other hand, if the whole subsynchronous current flows in the thyristor controlled inductive branch, then no subsynchronous current passes through the capacitor and no subsynchronous voltage will be created. Then the apparent impedance is zero. Due to the thyristor control also an amplified subsynchronous current may pass through the valve branch. Then the direction of the subsynchronous current passing **through the capacitor** must be phase opposed relative the subsynchronous line current. Then the reactance apparent to the network is inductive. Such behaviour is highly interesting with respect to the SSR problem, because in any frequency range where the TCSC apparent impedance is inductive, no electrical resonance can be created together with the inductance in the transmission system. Then one prerequisite for the existence of SSR is being set aside.

In this chapter we will consider how deviations in the line current impacts on the capacitor voltage in some cases. We want to isolate the impact of the line current and accordingly it is assumed that the control system does not react at all on the

deviations in the line current. The operation of the TCSC is governed by a pulse train with equidistant pulses, which provide timing reference for the voltage reversals.

5.2 DC CURRENT INJECTION

A first example is illustrated by figure 5-2. A TCSC is operating in steady state when a small DC current component is suddenly added to the line current passing through the TCSC. The control system continues to send out the pulse-train with equidistant pulses with constant phase relative the line current fundamental frequency component. The pulses indicate the desired instants for the voltage reversals (or rather voltage zero-crossings) and the firing of the thyristors is determined according to the SVR equation using the measured line current and capacitor voltage values. Current correction using the factor 1.20 was applied.

It can be seen that the TCSC, contrary to a fixed series capacitor, does not block a DC current component in the line. Instead according to the SVR algorithm the thyristors are fired so that the current pulses have different magnitude in the positive and the negative direction. The DC component in the line current therefore passes though the thyristor branch and does not cause any capacitor offset voltage.

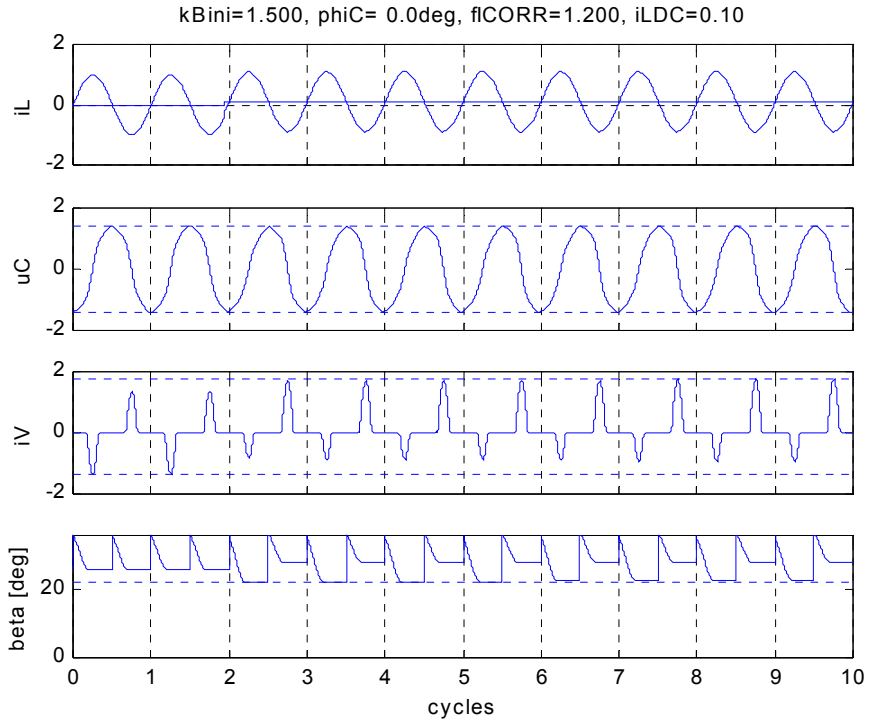

Figure 5-2 TCSC response to an added DC component in the line current.

Of course any TCSC control system must sooner or later bypass any sustained DC line current component in order to limit the voltage stress on the capacitor and the valve. However, it should be observed that in the SVR approach this function is automatically provided by the thyristor triggering control without any involvement of the system providing the reference pulse train. The lower graph (marked "beta") in figure 5-2 shows that different firing angles for the forward and the reverse thyristors will be obtained immediately at the onset of the DC current component.

It is very instructive to deal with this problem using the equivalent, instantaneous voltage reversals. Figure 5-3 shows such waveforms. At the start of this simulation the pulse train has been phase adjusted so that the TCSC circuit with loss factor $D_f = 0.95$ operates in steady state. During the first ten cycles of the simulation these conditions remain valid.

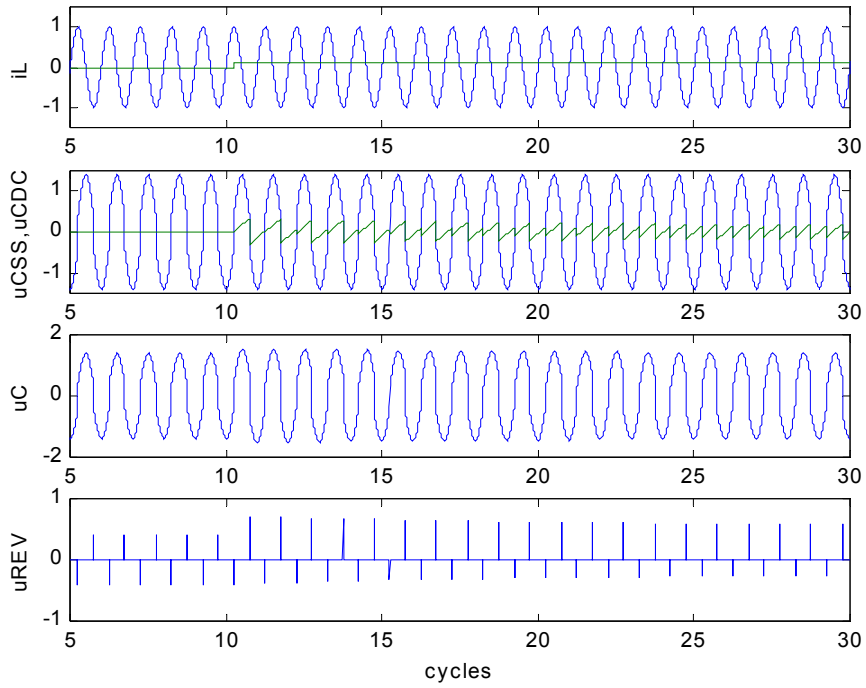

Figure 5-3 *Sudden DC component added to the steady state line current: AC current and DC (upper), steady state capacitor voltage and voltage caused by DC (second), total capacitor voltage (third), reversal voltage step height (bottom).*

The upper graph shows the line current components. In the second graph from the top the steady state capacitor voltage and the additional capacitor voltage caused by the DC current component are shown separate. The DC current component gets integrated in the series capacitor and reverses each half cycle as shown in the second graph in figure 5-3. The offset of the DC voltage curve depends on the phase at the onset of the DC component, but after some time the

initial component has decayed and only an almost symmetrical triangular wave remains. The total capacitor voltage is depicted in the third graph and finally the voltage steps at the reversals (i.e. the charge passing through the TCSC valve) are shown in the bottom graph. Note that the total capacitor voltage never contains any DC offset voltage, but the DC line current component causes a temporary change of the boost factor.

5.3 SUBSYNCHRONOUS SINUSOIDAL CURRENT INJECTION

We can repeat the procedure assuming that the added disturbance current is sinusoidal with a subsynchronous frequency. Figure 5-4 depicts the results of a simulation where a *10 Hz* current component has been added to the steady-state current.

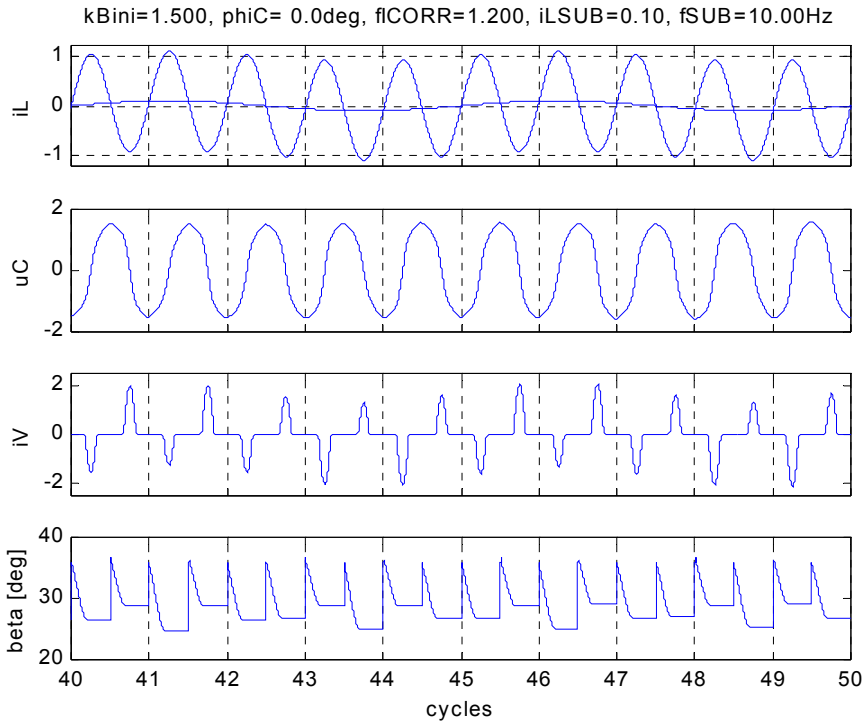

Figure 5-4 Sudden 10 Hz component added to the steady state line current: total line current, added component (upper), capacitor voltage (second), valve current (third), control angle (bottom).

The upper graph shows the total line current and the disturbance current. The second graph from the top shows the capacitor voltage. Very little deviation from the steady-state waveform can be noticed. The TCSC operates with a fixed pulse train that provides the time reference for the voltage zero-crossings. It shall be observed that the SVR block modulates the firing angle of the TCSC in order to

fulfil these requirements when the line current varies (join each second angle to see the subsynchronous variation). As a result the valve current is modulated with the subsynchronous frequency of the injected line current component.

5.4 VISUALIZING THE BEHAVIOUR OF SVR AT SUBSYNCHRONOUS FREQUENCY

We can anticipate the mathematical treatment to be presented in next section by showing some graphs, where the behaviour of the SVR-controlled TCSC will be illustrated using the equivalent, instantaneous voltage reversal model.

Assume that the capacitor bank in a TCSC has the reactance *20 Ω/phase* at *50 Hz*. In steady-state operation voltage reversals are performed each *10 ms*. Further assume that the line current contains a 10 Hz component with amplitude 100 A in addition to the 50 Hz component. We postulate that the boost control system providing the reference pulses for the reversals is not being influenced by the added line current component, but continues to command equidistant reversals each *10 ms*. Figure 5-5 depicts a simplified description of the TCSC behaviour according to the following statements

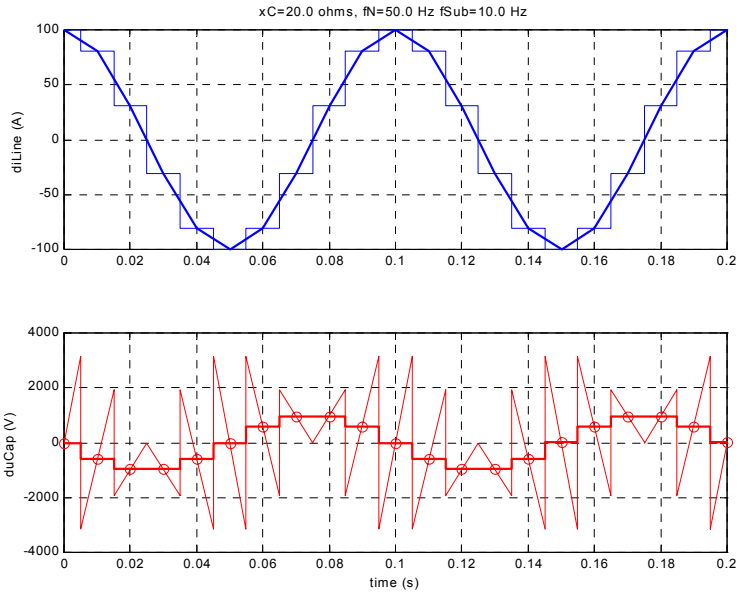

Figure 5-5 Illustration of apparent impedance of SVR-controlled TCSC.

- the additional line current component is represented by a constant current in each interval between consecutive reversals; this is shown by the staircase curve approximating the sinusoidal curve in the upper graph
- the additional current produces an additional capacitor voltage, which is shown in the lower graph; this voltage changes linearly within each interval

with a voltage slope that is proportional to the line current amplitude, i.e. to the height of the staircase line current curve

- at each reversal command the actual voltage reverses; in the model this occurs instantaneously
- the average capacitor voltage in each interval is represented by the value in the midpoint of the linear segments; these average values have been indicated by circles in the lower graph
- for a low frequency the capacitor voltage may be represented by its average value in the whole interval; this is indicated by the horizontal line segments in the lower graph

The figure shows that the average voltage line forms an approximation of a sinusoidal curve with *10 Hz* frequency. This curve is positive each time the line current has positive derivative, which is natural as the slope of the capacitor voltage in each consecutive interval is higher than in the preceding one and accordingly the average capacitor voltage gets higher in each consecutive interval. Similarly the average capacitor voltage is negative when the additional line current has a negative slope. The described behaviour with an average capacitor voltage, which is proportional to the line current derivative, however characterises an inductor. Thus the TCSC appears like an inductance for subsynchronous frequencies.

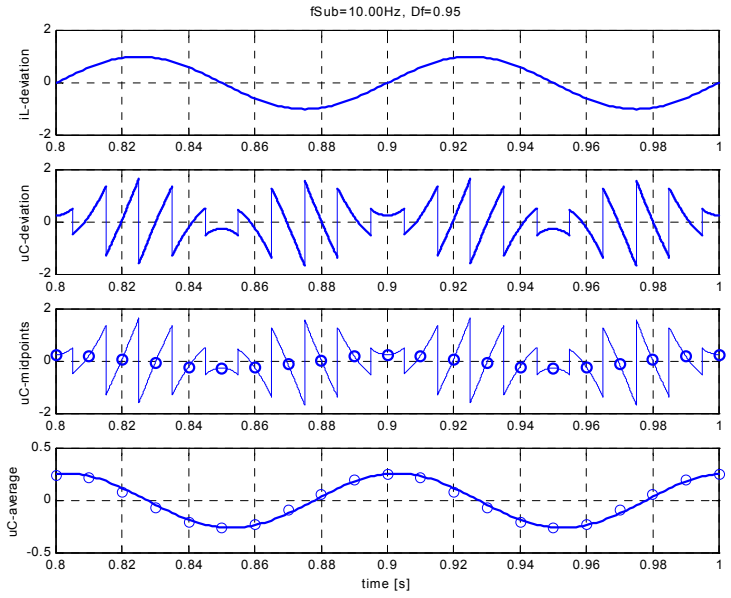

Figure 5-6 10 Hz component added to the steady state line current: line current deviation (upper), instantaneous capacitor deviation (second), capacitor voltage midpoints (third), capacitor average voltage (bottom)

Figure 5-6 shows a similar curve, where we have not used the staircase approximation of the line current, but rather integrated the sinusoidal input current. The graphs confirm that the main conclusion, that the apparent impedance of the TCSC is inductive, still holds. The upper graph shows the additional line current component, the second graph the capacitor voltage deviation caused by the disturbance current component in the line. In the third graph the midpoint of each curve segment has been marked and is considered to represent the average capacitor voltage for that segment. Finally, in the lower graph, all the midpoints have been joined by a continuous curve, which represents the average capacitor voltage at the subsynchronous frequency.

Figure 5-7 reveals curves similar to figure 5-5 for several different subsynchronous frequencies

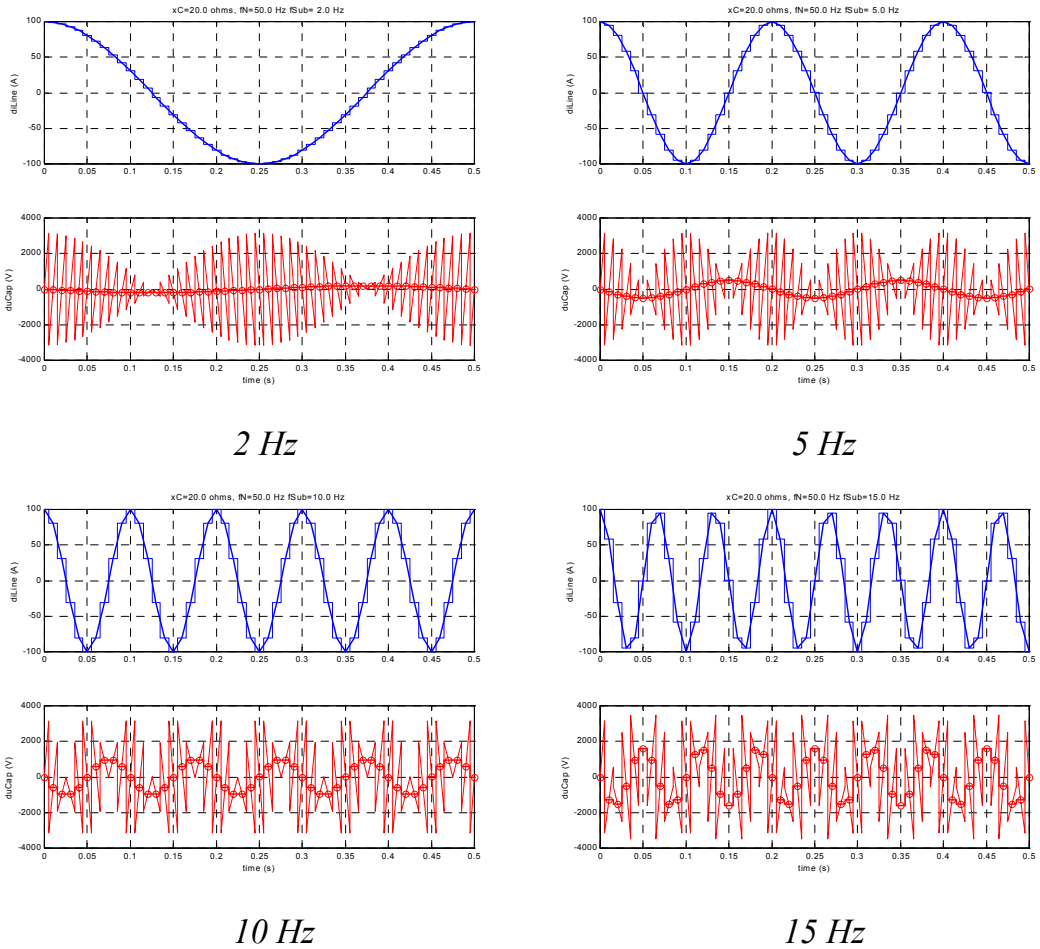

Figure 5-7 Impact of subsynchronous current at varying frequencies.

The graphs show that the voltage amplitude of the additional voltage increases with increasing frequency. This is in line with the result in section 5.2, where it has been shown that a DC line current component will be effectively bypassed by the TCSC without causing any DC voltage across the capacitor.

5.5 MATHEMATICAL FORMULATION

In this section we shall present a mathematical formulation of the discussion in the preceding section.

When the deviation of the line current from its steady state waveform only contains low frequency components a difference equation can be derived, which can be interpreted as a description of an equivalent circuit of the TCSC. It was shown in the preceding section that we may treat the deviation current quite separate from the steady state current. In principle the disturbance current gets integrated in the capacitor and then it is periodically reversed equidistantly with a repetition frequency of twice the network frequency.

5.5.1 Derivation of formula

Thus assume that the disturbance current is given by $\Delta i_L(t)$ and that the reversal instants occur at times

$$t_k = kh$$
$$h = \frac{\pi}{\omega_N} = \frac{1}{2f_N} \tag{5-1}$$

The deviation current can be approximated by one sampled value per interval between consecutive reversals if it does not contain components having frequencies exceeding the Nyquist frequency. Theoretically this means the whole subsynchronous frequency range.

The development of the capacitor voltage now can be calculated in three steps

- integrate the deviation line current from the first sample point to the reversal point in order to get the prereversal capacitor voltage
- perform the voltage reversal taking the applicable loss factor into account to obtain the postreversal capacitor voltage
- integrate the deviation line current from the reversal point to the second sample point to get the capacitor voltage in the second sampling point

The above calculations may be performed using the formal operator p to denote the differential operator d/dt. We will use the formula

$$\int_{t+a}^{t+b} f(\xi)d\xi = \int_{a}^{b} \left(e^{p\xi} f\right)(t)d\xi = \left(\frac{e^{pb} - e^{pa}}{p} f\right)(t) = \left(\frac{e^{p(b-a)} - 1}{p}\right)\left(e^{pa} f\right)(t) = \\ = (b-a)f(t+a) + \frac{(b-a)^2}{2!} f'(t+a) + \frac{(b-a)^3}{3!} f''(t+a) + \ldots \tag{5-2}$$

This formula is obtained by term-by-term integration of the Taylor expansion of the function *f(t)*. Accordingly it can be applied only in intervals where the Taylor expansion of the function exists and is convergent.

Then the calculation scheme yields the following equations

$$\Delta u_C(t_k - 0) = \Delta u_C\left(t_k - \frac{h}{2}\right) + \int_{t_k - \frac{h}{2}}^{t_k} \frac{\Delta i_L(\xi)}{C} d\xi = \Delta u_C\left(t_k - \frac{h}{2}\right) + \left(\frac{1 - e^{-\frac{hp}{2}}}{pC} \Delta i_L\right)(t_k)$$
$$\Delta u_C(t_k + 0) = -D_f \Delta u_C(t_k - 0) \tag{5-3}$$
$$\Delta u_C\left(t_k + \frac{h}{2}\right) = \Delta u_C(t_k + 0) + \int_{t_k}^{t_k + \frac{h}{2}} \frac{\Delta i_L(\xi)}{C} d\xi = \Delta u_C(t_k + 0) + \left(\frac{e^{\frac{hp}{2}} - 1}{pC} \Delta i_L\right)(t_k)$$

and reduction of the system gives

$$\Delta u_C\left(t_k + \frac{h}{2}\right) + D_f \Delta u_C\left(t_k - \frac{h}{2}\right) = \left(\frac{e^{\frac{hp}{2}} - 1 - D_f\left(1 - e^{-\frac{hp}{2}}\right)}{pC} \Delta i_L\right)(t_k) \tag{5-4}$$

Now we may regard the capacitor voltages in the interval midpoints to be sampled values of a continuous curve, the capacitor average voltage $\Delta u_{C,av}(t)$. We may express the capacitor voltage also using differential operators. Then

$$\Delta u_C\left(t + \frac{h}{2}\right) + D_f \Delta u_C\left(t - \frac{h}{2)}\right) = \left(\left(e^{\frac{hp}{2}} + D_f e^{-\frac{hp}{2}}\right) \Delta u_{C,av}\right)(t) \tag{5-5}$$

and we get the operator expression for the apparent impedance of the TCSC

$$Z_{app}(p)=\frac{\Delta u_{C,av}}{\Delta i_L}=\frac{e^{\frac{hp}{2}}-1-D_f\left(1-e^{-\frac{hp}{2}}\right)}{e^{\frac{hp}{2}}+D_f e^{-\frac{hp}{2}}}\frac{1}{pC} \tag{5-6}$$

5.5.2 Low-frequency approximation

Assume that the disturbance only changes slowly so that the operator p is small. Then we can approximate the impedance as follows

$$Z_{app}(p)\approx\frac{\left(e^{\frac{hp}{2}}-1\right)-D_f\left(1-e^{-\frac{hp}{2}}\right)}{\left(1+D_f\right)+\left(1-D_f\right)\frac{ph}{2}}\frac{1}{pC}\approx\frac{\frac{hp}{2}+\frac{h^2p^2}{8}-D_f\frac{hp}{2}+D_f\frac{h^2p^2}{8}}{\left(1+D_f\right)+\left(1-D_f\right)\frac{ph}{2}}\frac{1}{pC}\approx \tag{5-7}$$
$$\approx\frac{h}{2C}\left\{\frac{1-D_f}{1+D_f}+\left(\frac{1}{2}-\frac{\left(1-D_f\right)^2}{\left(1+D_f\right)^2}\right)\frac{h}{2}p\right\}$$

The loss factor normally is close to unity so we may neglect the last term. The remaining expression contains a constant term plus a term, which is proportional to the derivative operator p. The former represents an apparent resistance R_{TCSC} and the latter an apparent inductance L_{TCSC}. Using the expression for h in (5-1) we get the following approximation of the capacitor voltage caused by the low frequency deviation line current

$$\begin{aligned}
&\Delta u_{C,av}\approx\frac{\pi}{2\omega_N C}\frac{\left(1-D_f\right)}{\left(1+D_f\right)}\Delta i_L+\frac{\pi^2}{8\omega_N C}\frac{d\Delta i_L}{\omega_N dt}=R_{TCSC}\Delta i_L+L_{TCSC}\frac{d\Delta i_L}{dt}\\
&R_{TCSC}=\frac{\pi}{2}\frac{\left(1-D_f\right)}{\left(1+D_f\right)}\frac{1}{\omega_N C}\\
&X_{TCSC}(\omega_N)=\omega_N L_{TCSC}=\left(\frac{\pi^2}{8}\right)\frac{1}{\omega_N C}
\end{aligned} \tag{5-8}$$

The interpretation of equation (5-8) is that the average voltage across the TCSC for slow small deviation line currents corresponds to the voltage across an inductive-resistive circuit according to figure 5-8.

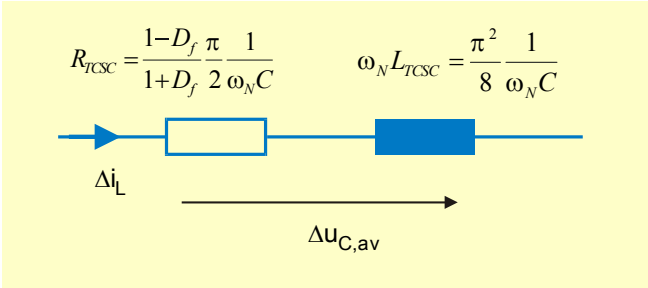

Figure 5-8 Low-frequency equivalent circuit of TCSC using SVR scheme.

When the losses are small is the equivalent resistance zero. The reactance of the equivalent series inductance at nominal network frequency corresponds to $\pi^2/8$ times that of the series capacitor bank.

5.5.3 Subsynchronous frequency function

The operator form (5-6) for the apparent impedance is close to the frequency function describing the apparent impedance. The latter can be obtained by replacing the operator p with the complex number $j\omega$, where ω is the frequency of the subsynchronous disturbance current. Thus

$$Z_{app}(j\omega)=\frac{e^{j\frac{\omega}{\omega_N}\frac{\pi}{2}}-1-D_f\left(1-e^{-j\frac{\omega}{\omega_N}\frac{\pi}{2}}\right)}{e^{j\frac{\omega}{\omega_N}\frac{\pi}{2}}+D_f e^{-j\frac{\omega}{\omega_N}\frac{\pi}{2}}}\frac{1}{j\omega C}= \tag{5-9}$$

$$=\frac{j}{\omega_N C}\frac{(1+D_f)\left[1-\cos\left(\frac{\omega}{\omega_N}\frac{\pi}{2}\right)\right]-j(1-D_f)\sin\left(\frac{\omega}{\omega_N}\frac{\pi}{2}\right)}{\frac{\omega}{\omega_N}\left[(1+D_f)\cos\left(\frac{\omega}{\omega_N}\frac{\pi}{2}\right)+j(1-D_f)\sin\left(\frac{\omega}{\omega_N}\frac{\pi}{2}\right)\right]}$$

Put

$$\zeta=\frac{\omega}{\omega_N}$$

$$Z_{app}(j\zeta\omega_N)=k_Z(\zeta)\frac{1}{\omega_N C} \tag{5-10}$$

$$k_Z(\zeta)=\frac{(1-D_f)\sin\left(\zeta\frac{\pi}{2}\right)+j(1+D_f)\left[1-\cos\left(\zeta\frac{\pi}{2}\right)\right]}{\zeta\left[(1+D_f)\cos\left(\zeta\frac{\pi}{2}\right)+j(1-D_f)\sin\left(\zeta\frac{\pi}{2}\right)\right]}$$

If the losses can be neglected the formula simplifies to

$$k_Z(\zeta) = j\frac{\left(1-\cos\frac{\zeta\pi}{2}\right)}{\zeta\cos\frac{\zeta\pi}{2}} \tag{5-11}$$

In this case obviously the apparent impedance is inductive in the whole subsynchronous frequency range. Figures 5-9 and 5-10 illustrate the frequency function derived above.

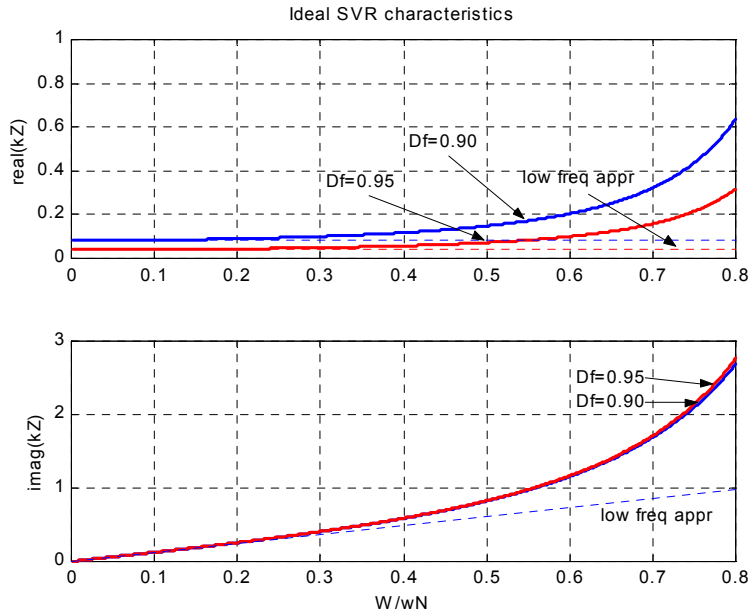

Figure 5-9 Ideal apparent impedance for TCSC using SVR scheme: apparent resistance factor (upper), apparent reactance factor (lower)

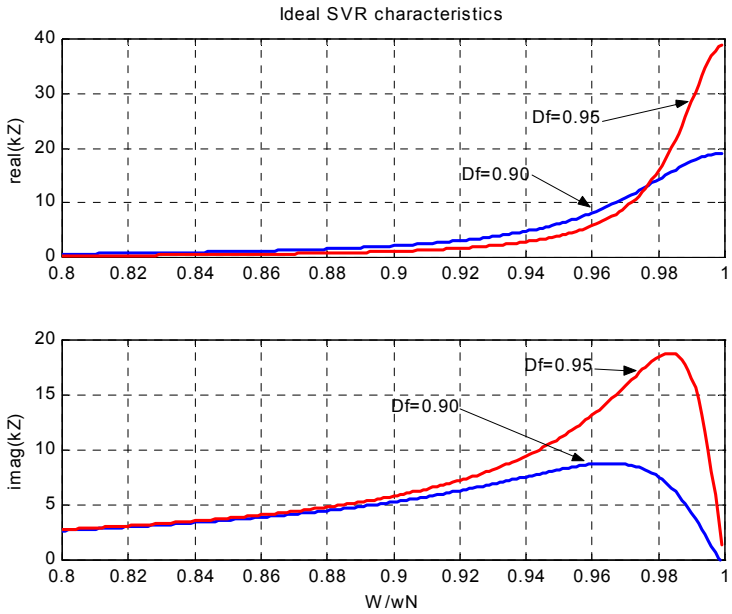

Figure 5-10 Ideal apparent impedance for TCSC using SVR scheme: apparent resistance factor (upper), apparent reactance factor (lower)

It can be seen from figure 5-10 that the low-frequency approximation according to equation (5-8) remains valid up to about one third of the nominal network frequency.

CHAPTER 6

REPRESENTATION OF THREE-PHASE POWER CONVERTERS

The dynamical model of the TCSC is a central item in this thesis. The idea of the Synchronous Voltage Reversal scheme has been presented in earlier chapters and the basic behaviour of the TCSC has already been presented.

So far the studies have considered each phase circuit of the TCSC separately. In a three-phase network, however, a strong interaction exists between the different phases. This is manifest by the fact that the current in the transmission line, where the TCSC is inserted, is mainly determined by the three-phase space vector representing the total inserted TCSC voltage. This space vector depends on the capacitor voltages in **all** phases and it is changed each time **any** thyristor is triggered in the TCSC.

Therefore we shall in the following work with a model in which the TCSC is treated as a three-phase power electronic converter. Such converters typically use internal control variables like ”control angle α”, “phase shift φ_C” or similar. These control variables are applied repeatedly to determine triggering of **each** thyristor in the converter. In this chapter we shall consider a formal procedure to deal with the interaction between such variables and the transmission network represented as a three-phase entity. In this formalism we will make use of a sequence of frames. We will call them “converter-oriented frames” in consistency with “rotor-fixed frames”, which are frequently applied in theory of electrical machines.

6.1 ROTATING COORDINATE SYSTEMS

Before introducing converter-oriented coordinate systems it might be constructive to consider the role of rotating coordinate systems in describing electrical machines. Electrical machines contain two sets of windings, one fixed in the stator and one movable in the rotor. From an electrical circuit analysis perspective this means that we have to analyse an electrical circuit having

variable topology, as the magnetic coupling between the stator and the rotor circuits changes depending on the angle of the rotor shaft in the fixed stator coordinate system. Due to the rotor inertia only continuous changes in the shaft angle may occur.

The analysis of machines is simplified by introduction of rotating coordinate systems, e.g. a rotor-fixed coordinate system. By transforming the stator variables into such a coordinate system they virtually operate on an electrical circuit with **fixed** topology.

6.2 COORDINATE SYSTEMS FOR THREE-PASE POWER ELECTRONIC CONVERTERS

Power electronic converters, just like machines, exhibit a time-variable electrical circuit topology. However, contrary to in rotating machinery, the topology changes are caused by switching operations, which occur at discrete time instants and theoretically are executed instantaneously. Therefore, any coordinate system adapted to reflect the converter state must be a sequence of frames rather than a continuously changing one.

In a three-phase power electronic converter the semiconductor valves are arranged symmetrically with respect to the three phases of the connected electric power network. Therefore, in steady state operation, the semiconductor valve quantities like valve current, valve voltage etc. are identical for all switches in the converter. It is desired that the analysis of the converter's behaviour could be performed in a single circuit with fixed topology. It is the purpose of the following discussion to outline an analysis method, which suggests such a description of power electronic converters. In this thesis we will deal with a TCSC, but it seems that similar principles may equally well be adapted on other comparable power electronic converters.

6.2.1 Outline of TCSC as a three-phase power electronic converter

The principal coupling between the electrical power network and the connected power electronic converter (TCSC) is demonstrated in figure 6-1. The transmission lines and the capacitor bank in the TCSC constitutes the "network", while the "power electronic converter" comprises the thyristor valves together with the branch inductors.

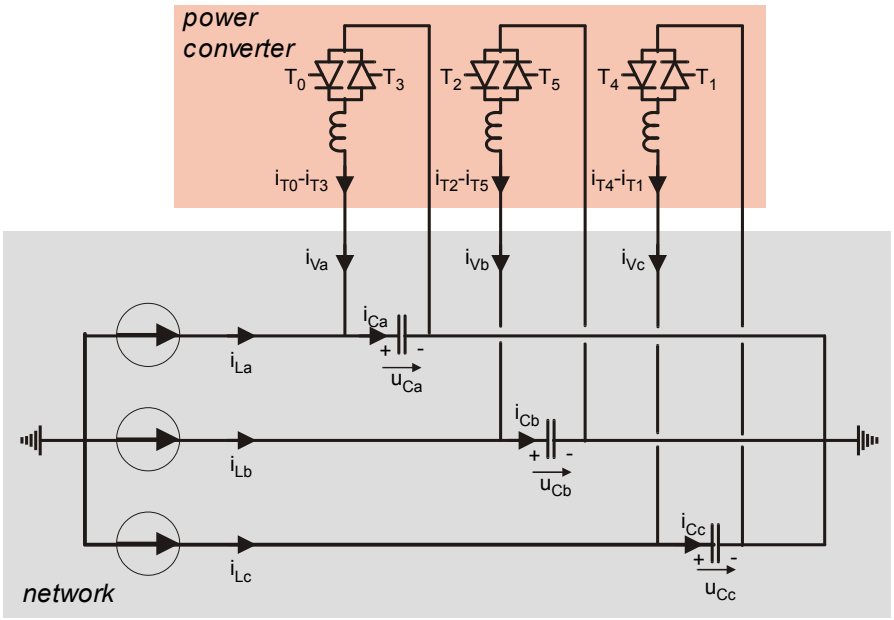

Figure 6-1 Interface between the power electronic converter (TCSC) and the network

6.2.2 Three-phase quantities in the network

The formalism for treating the quantities in the three-phase network is well established since almost hundred years. Here we shall consider the "space-vector" approach [B1], in which the phase quantities are described as projections of a complex vector, $\hat{s}(t)$, along the phase axes, $\left\{1, e^{j\frac{2\pi}{3}}, e^{-j\frac{2\pi}{3}}\right\}$, and in addition a scalar function, $s_\gamma(t)$, the homopolar component. Thus

$$\begin{aligned} s_a(t) &= \mathrm{Re}\{\hat{s}(t)\} + s_\gamma(t) \\ s_b(t) &= \mathrm{Re}\left\{\hat{s}(t)e^{-j\frac{2\pi}{3}}\right\} + s_\gamma(t) \\ s_c(t) &= \mathrm{Re}\left\{\hat{s}(t)e^{j\frac{2\pi}{3}}\right\} + s_\gamma(t) \end{aligned} \qquad (6\text{-}1)$$

Remark 1: This transformation keeps the magnitude of the phase quantities, i.e. the space vector length is identical with the phase quantity amplitude. The transformation is not "power" invariant.

Remark 2: Please note the distinction (in this thesis) between the two-dimensional vector $\bar{s}(t)$ and the three-dimensional vector $\vec{s}(t)$, which will be defined below.

The equation system (6-1) can be solved giving the result

$$\begin{aligned} \bar{s}(t) &= s_\alpha(t) + j s_\beta(t) = \frac{2}{3}\left\{ s_a(t) + e^{j\frac{2\pi}{3}} s_b(t) + e^{-j\frac{2\pi}{3}} s_c(t) \right\} \\ s_\gamma(t) &= \frac{1}{3}\{ s_a(t) + s_b(t) + s_c(t) \} \end{aligned} \tag{6-2}$$

It is common to denote the real and imaginary part of the complex vector function as the α- and β-components as has been done in (6-2). The vector function trajectories often are depicted in a complex plane. The homopolar component normally is ignored in the theory of electrical machines (often it is identically zero), but in the theory of TCSC it must be taken care of, so for that reason we would prefer to represent all components, including the homopolar component, as a vector in three dimensions. We denote the axes of this vector in R^3 as $\{\hat{e}_\alpha, \hat{e}_\beta, \hat{e}_\gamma\}$ and denote that system as the ***FIXED*** system. The transformation rules can be expressed in matrix form as

$$\begin{pmatrix} s_\alpha \\ s_\beta \\ s_\gamma \end{pmatrix} = \frac{1}{3}\begin{pmatrix} 2 & -1 & -1 \\ 0 & \sqrt{3} & -\sqrt{3} \\ 1 & 1 & 1 \end{pmatrix}\begin{pmatrix} s_a \\ s_b \\ s_c \end{pmatrix} \tag{6-3}$$

$$\begin{pmatrix} s_a \\ s_b \\ s_c \end{pmatrix} = \frac{1}{2}\begin{pmatrix} 2 & 0 & 2 \\ -1 & \sqrt{3} & 2 \\ -1 & -\sqrt{3} & 2 \end{pmatrix}\begin{pmatrix} s_\alpha \\ s_\beta \\ s_\gamma \end{pmatrix} \tag{6-4}$$

6.2.3 Rotating coordinate system

It is assumed that the undisturbed steady state line current in the TCSC is three-phase symmetrical with amplitude $\hat{I}_L$

$$\begin{aligned} \bar{I}_L(t) &= \hat{I}_L e^{j\omega_N t} \\ I_{L\gamma}(t) &= 0 \end{aligned} \tag{6-5}$$

We will use the coordinate system, which is synchronized with this undisturbed line current vector. This system is called the ***IL_SYNC*** system. Space vectors in the rotating coordinate system will be denoted with the superscript 'R'. Its components are called *d*- and *q*-components and the transformation rule is

$$\hat{s}^R(t) = s_d^R(t) + j s_q^R(t) = e^{-j\omega_N t}\hat{s}(t) \tag{6-6}$$

Let us denote the homopolar component of the *IL_SYNC* system as 's_0^R' and define it to be identical with the homopolar component in the *FIXED* coordinates. Then it translates to the matrix transformation

$$\bar{s}^R(t) = \begin{pmatrix} s_d^R(t) \\ s_q^R(t) \\ s_0^R(t) \end{pmatrix} = \begin{pmatrix} \cos\omega_N t & \sin\omega_N t & 0 \\ -\sin\omega_N t & \cos\omega_N t & 0 \\ 0 & 0 & 1 \end{pmatrix} \begin{pmatrix} s_\alpha(t) \\ s_\beta(t) \\ s_\gamma(t) \end{pmatrix} \tag{6-7}$$

6.2.4 Connecting individual thyristors to the network

When operating in steady state the thyristors in the TCSC are triggered with equidistant time delay in the sequence order as they have been numbered in figure 6-1. The total current contribution from all thyristor branches can be condensed into one quantity according to equation (6-2).

$$\begin{aligned} \hat{i}_V(t) &= i_{V\alpha}(t) + j i_{V\beta}(t) = \frac{2}{3}\left\{ i_{Va}(t) + e^{j\frac{2\pi}{3}} i_{Vb}(t) + e^{-j\frac{2\pi}{3}} i_{Vc}(t) \right\} \\ i_{V\gamma}(t) &= \frac{1}{3}\{ i_{Va}(t) + i s_{Vb}(t) + i_{Vc}(t) \} \end{aligned} \tag{6-8}$$

The current passing each one of the thyristors is associated with a certain phase current in the network. When inserted in (6-8) this phase current generates a contribution to the space vector $\hat{i}_V$ in a certain direction and to the homopolar current as indicated in Table 6-I.

Table 6-I Connection between thyristor / phase current / space vector and homopolar directions

thyristor	phase current	space vector direction	homopolar direction
T_0	$+i_{Va}$	0	+1
T_1	$-i_{Vc}$	$\pi/3$ (60°)	-1
T_2	$+i_{Vb}$	$2\pi/3$ (120°)	+1
T_3	$-i_{Va}$	-1 (180°)	-1
T_4	$+i_{Vc}$	$4\pi/3$ (240°)	+1
T_5	$-i_{Vb}$	$5\pi/3$ (300°)	-1

6.2.5 Streamlining calculations

As said above the thyristors are being triggered in the same order as they have been numbered. In studying the thyristor operation it is practical to transform the circuit as indicated by figure 6-2. In this figure a virtual three-phase network having phases *{u,v,w}* has been established to represent the thyristor part of the circuit in figure 6-1 in such a way that the latest triggered thyristor connects to phase *+u*, the preceding one to phase *–v*, etc. Table 6-II gives the details

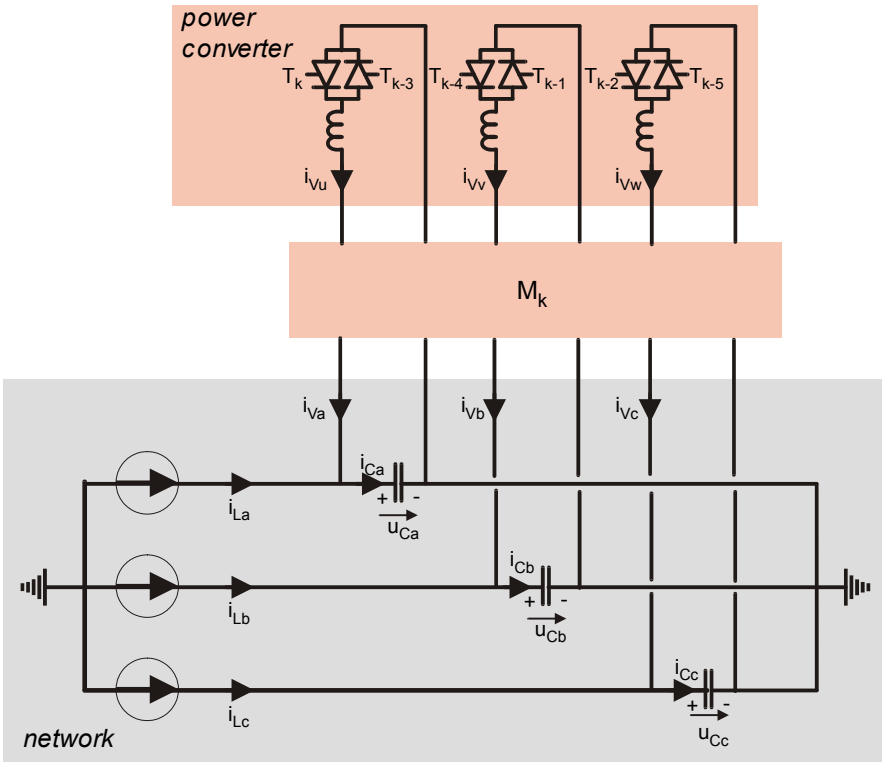

Figure 6-2 Transformation of the circuit in figure 6-1 in order to represent all thyristors by one single case

The connection to the real three-phase system is achieved through a switching network M_k. When the thyristor conduction intervals are shorter than $60°$ they do not overlap and then only one of the quantities i_{Vu}, i_{Vv}, i_{Vw} is non-zero. The idea is that switching takes place six times per cycle such that in practice only valve T_k will be conducting current, while the currents i_{Vv} and i_{Vw} will always be zero.

Table 6-II Connection between thyristors and phase currents in virtual network

thyristor	phase current
T_k	$+i_{Vu}$
T_{k-1}	$-i_{Vv}$
T_{k-2}	$+i_{Vw}$
T_{k-3}	$-i_{Vu}$
T_{k-4}	$+i_{Vv}$
T_{k-5}	$-i_{Vw}$

When the TCSC operates in capacitive boost mode and the line current is given by (6-5), the equivalent capacitor voltage reversals associated with conduction in thyristor k occurs at the time instant (compare figure 3-2 which shows capacitor voltage reversals in phase a occurring for $k=0$)

$$t_k = \frac{k\pi}{3\omega_N} \quad k = \ldots,-1,0,1,\ldots \tag{6-9}$$

We can study the transient related to this specific voltage reversal at time $t=t_k$ under the transformation

$$\begin{pmatrix} i_{Vu}^k(\varphi) \\ i_{Vv}^k(\varphi) \\ i_{Vw}^k(\varphi) \end{pmatrix} = M_{\mathrm{mod}(k,6)} \begin{pmatrix} i_{Va}\left(t_k + \dfrac{\varphi}{\omega_N}\right) \\ i_{Vb}\left(t_k + \dfrac{\varphi}{\omega_N}\right) \\ i_{Vc}\left(t_k + \dfrac{\varphi}{\omega_N}\right) \end{pmatrix} \tag{6-10}$$

$$M_0=\begin{pmatrix}1&0&0\\0&1&0\\0&0&1\end{pmatrix}\quad M_1=\begin{pmatrix}0&0&-1\\-1&0&0\\0&-1&0\end{pmatrix}\quad M_2=\begin{pmatrix}0&1&0\\0&0&1\\1&0&0\end{pmatrix}$$
$$M_3=\begin{pmatrix}-1&0&0\\0&-1&0\\0&0&-1\end{pmatrix}\quad M_4=\begin{pmatrix}0&0&1\\1&0&0\\0&1&0\end{pmatrix}\quad M_5=\begin{pmatrix}0&-1&0\\0&0&-1\\-1&0&0\end{pmatrix} \tag{6-11}$$

The inverse of each matrix is the transposed matrix, so

$$\begin{pmatrix}i_{Va}(t)\\i_{Vb}(t)\\i_{Vc}(t)\end{pmatrix}=M^{t}_{\mathrm{mod}(k,6)}\begin{pmatrix}i^{k}_{Vu}(\omega_N(t-t_k))\\i^{k}_{Vv}(\omega_N(t-t_k))\\i^{k}_{Vw}(\omega_N(t-t_k))\end{pmatrix} \tag{6-12}$$

In (6-10) and (6-12) we have replaced the time variable t with the angular deviation from the sampling time t_k. We will denote the system $\{uvw\}$ the "converter-oriented coordinate system" or the ***CONV_ORI*** system. By properly using a sequence of transformations as defined in (6-10) the behaviour of the TCSC circuit will be periodic with period $\pi/3$ (60°) in the converter-oriented sequence of frames.

Of course the behaviour of the three phase currents $\{i_{Vu}(\varphi), i_{Vv}(\varphi), i_{Vw}(\varphi)\}$ can be observed using space-vector/homopolar description as in (6-2), (6-3), (6-4) just as in the fixed system. We will denote this quantity with a numerical superscript 'k' indicating the index of the frame, and its components by the subscripts 'x', 'y', 'z'. Thus

$$\begin{aligned}\hat{i}^{k}_{V}(\varphi)&=i^{k}_{Vx}(\varphi)+ji^{k}_{Vy}(\varphi)=\frac{2}{3}\left\{i^{k}_{Vu}(\varphi)+e^{j\frac{2\pi}{3}}i^{\mathrm{k}}_{\mathrm{Vv}}(\varphi)+e^{-j\frac{2\pi}{3}}i^{\mathrm{k}}_{\mathrm{Vw}}(\varphi)\right\}\\ i^{k}_{Vz}(\varphi)&=\frac{1}{3}\left\{i^{k}_{Vu}(\varphi)+i^{\mathrm{k}}_{\mathrm{Vv}}(\varphi)+i^{\mathrm{k}}_{\mathrm{Vw}}(\varphi)\right\}\end{aligned} \tag{6-13}$$

with the inverse relation

$$
\begin{aligned}
i_{Vu}^{k}(\varphi) &= \mathrm{Re}\left\{\hat{i}_{V}^{k}(\varphi)\right\} + i_{Vz}^{k}(\varphi) \\
i_{Vv}^{k}(\varphi) &= \mathrm{Re}\left\{e^{-j\frac{2\pi}{3}}\hat{i}_{V}^{k}(\varphi)\right\} + i_{Vz}^{k}(\varphi) \\
i_{Vw}^{k}(\varphi) &= \mathrm{Re}\left\{e^{j\frac{2\pi}{3}}\hat{i}_{V}^{k}(\varphi)\right\} + i_{Vz}^{k}(\varphi)
\end{aligned}
\tag{6-14}
$$

Then it is found that the following relations, connecting variables in the *CONV_ORI* and *FIXED* systems, apply

$$
\begin{aligned}
\hat{i}_{V}^{k}(\varphi) &= e^{-j\frac{k\pi}{3}}\hat{i}_{V}\left(t_k + \frac{\varphi}{\omega_N}\right) \\
i_{Vz}^{k}(\varphi) &= (-1)^k i_{V\gamma}\left(t_k + \frac{\varphi}{\omega_N}\right)
\end{aligned}
\tag{6-15}
$$

Similarly the link between the *CONV_ORI* and *IL_SYNC* systems is

$$
\begin{aligned}
\hat{i}_{V}^{k}(\varphi) &= e^{j\varphi}\hat{i}_{V}^{R}\left(t_k + \frac{\varphi}{\omega_N}\right) \\
i_{Vz}^{k}(\varphi) &= (-1)^k i_{V0}^{R}\left(t_k + \frac{\varphi}{\omega_N}\right)
\end{aligned}
\tag{6-16}
$$

The matrix formulation of the above relations is

$$
\begin{aligned}
\bar{i}_{V}^{k}(\varphi) &= \begin{pmatrix} i_{Vx}^{k}(\varphi) \\ i_{Vy}^{k}(\varphi) \\ i_{Vz}^{k}(\varphi) \end{pmatrix} = \begin{pmatrix} \cos\frac{k\pi}{3} & \sin\frac{k\pi}{3} & 0 \\ -\sin\frac{k\pi}{3} & \cos\frac{k\pi}{3} & 0 \\ 0 & 0 & (-1)^k \end{pmatrix} \begin{pmatrix} i_{V\alpha}\left(t_k + \frac{\varphi}{\omega_N}\right) \\ i_{V\beta}\left(t_k + \frac{\varphi}{\omega_N}\right) \\ i_{V\gamma}\left(t_k + \frac{\varphi}{\omega_N}\right) \end{pmatrix} = \\
&= \begin{pmatrix} \cos\frac{k\pi}{3} & \sin\frac{k\pi}{3} & 0 \\ -\sin\frac{k\pi}{3} & \cos\frac{k\pi}{3} & 0 \\ 0 & 0 & (-1)^k \end{pmatrix} \bar{i}_{V}\left(t_k + \frac{\varphi}{\omega_N}\right)
\end{aligned}
\tag{6-17}
$$

$$\bar{i}_V^k(\varphi)=\begin{pmatrix} i_{Vx}^k(\varphi) \\ i_{Vy}^k(\varphi) \\ i_{Vz}^k(\varphi) \end{pmatrix}=\begin{pmatrix} \cos\varphi & -\sin\varphi & 0 \\ \sin\varphi & \cos\varphi & 0 \\ 0 & 0 & (-1)^k \end{pmatrix}\begin{pmatrix} i_{Vd}^R\left(t_k+\dfrac{\varphi}{\omega_N}\right) \\ i_{Vq}^R\left(t_k+\dfrac{\varphi}{\omega_N}\right) \\ i_{V0}^R\left(t_k+\dfrac{\varphi}{\omega_N}\right) \end{pmatrix}= \tag{6-18}$$

$$=\begin{pmatrix} \cos\varphi & -\sin\varphi & 0 \\ \sin\varphi & \cos\varphi & 0 \\ 0 & 0 & (-1)^k \end{pmatrix}\bar{i}_V^R\left(t_k+\frac{\varphi}{\omega_N}\right)$$

Inversely

$$\begin{aligned} \hat{i}_V(t)&=e^{j\frac{k\pi}{3}}\hat{i}_V^k(\omega_N(t-t_k)) \\ i_{V\gamma}(t)&=(-1)^k i_{Vz}^k(\omega_N(t-t_k)) \end{aligned} \tag{6-19}$$

and

$$\begin{aligned} \hat{i}_V^R(t)&=e^{-j\omega_N(t-t_k)}\hat{i}_V^k(\omega_N(t-t_k)) \\ i_{V0}^R(t)&=(-1)^k i_{Vz}^k(\omega_N(t-t_k)) \end{aligned} \tag{6-20}$$

The matrix relations are similar to (6-17) and (6-18) but use the transposed transformation matrices. Thus

$$\bar{i}_V\left(t_k+\frac{\varphi}{\omega_N}\right)=\begin{pmatrix} i_{V\alpha}\left(t_k+\dfrac{\varphi}{\omega_N}\right) \\ i_{V\beta}\left(t_k+\dfrac{\varphi}{\omega_N}\right) \\ i_{V\gamma}\left(t_k+\dfrac{\varphi}{\omega_N}\right) \end{pmatrix}=\begin{pmatrix} \cos\dfrac{k\pi}{3} & -\sin\dfrac{k\pi}{3} & 0 \\ \sin\dfrac{k\pi}{3} & \cos\dfrac{k\pi}{3} & 0 \\ 0 & 0 & (-1)^k \end{pmatrix}\begin{pmatrix} i_{Vx}^k(\varphi) \\ i_{Vy}^k(\varphi) \\ i_{Vz}^k(\varphi) \end{pmatrix}= \tag{6-21}$$

$$=\begin{pmatrix} \cos\dfrac{k\pi}{3} & -\sin\dfrac{k\pi}{3} & 0 \\ \sin\dfrac{k\pi}{3} & \cos\dfrac{k\pi}{3} & 0 \\ 0 & 0 & (-1)^k \end{pmatrix}\bar{i}_V^k(\varphi)$$

and

$$\bar{i}_V^R\left(t_k+\frac{\varphi}{\omega_N}\right)=\begin{pmatrix} i_{Vd}^R\left(t_k+\frac{\varphi}{\omega_N}\right) \\ i_{Vq}^R\left(t_k+\frac{\varphi}{\omega_N}\right) \\ i_{V0}^R\left(t_k+\frac{\varphi}{\omega_N}\right)\end{pmatrix}=\begin{pmatrix} \cos\varphi & \sin\varphi & 0 \\ -\sin\varphi & \cos\varphi & 0 \\ 0 & 0 & (-1)^k\end{pmatrix}\begin{pmatrix} i_{Vx}^k(\varphi) \\ i_{Vy}^k(\varphi) \\ i_{Vz}^k(\varphi)\end{pmatrix}= \tag{6-22}$$

$$=\begin{pmatrix} \cos\varphi & \sin\varphi & 0 \\ -\sin\varphi & \cos\varphi & 0 \\ 0 & 0 & (-1)^k\end{pmatrix}\bar{i}_V^k(\varphi)$$

Further from equation (6-15) we can also deduce the transformation rule between different members of the sequence of converter-oriented frames

$$\begin{aligned}\hat{i}_V^{k+1}\left(-\frac{\pi}{6}\right)&=e^{-j\frac{(k+1)\pi}{3}}\hat{i}_V\left(t_{k+1}-\frac{\pi}{6\omega_N}\right)=e^{-j\frac{\pi}{3}}\left\{e^{-j\frac{k\pi}{3}}\hat{i}_V\left(t_k+\frac{\pi}{3\omega_N}-\frac{\pi}{6\omega_N}\right)\right\}= \\ &=e^{-j\frac{\pi}{3}}\left\{e^{-j\frac{k\pi}{3}}\hat{i}_V\left(t_k+\frac{\pi}{6\omega_N}\right)\right\}=e^{-j\frac{\pi}{3}}\hat{i}_V^k\left(\frac{\pi}{6}\right) \\ i_{Vz}^{k+1}\left(-\frac{\pi}{6}\right)&=(-1)^{k+1}i_{V\gamma}\left(t_{k+1}-\frac{\pi}{6\omega_N}\right)=(-1)\left\{(-1)^k i_{Vz}^k\left(t_k+\frac{\pi}{3\omega_N}-\frac{\pi}{6\omega_N}\right)\right\}= \\ &=(-1)\left\{(-1)^k i_{Vz}^k\left(t_k+\frac{\pi}{6\omega_N}\right)\right\}=-i_{V\gamma}^k\left(\frac{\pi}{6}\right)\end{aligned} \tag{6-23}$$

The matrix formulation of this important relation is

$$\bar{i}_V^{k+1}\left(-\frac{\pi}{6}\right)=\begin{pmatrix} i_{Vx}^{k+1}\left(-\frac{\pi}{6}\right) \\ i_{Vy}^{k+1}\left(-\frac{\pi}{6}\right) \\ i_{Vz}^{k+1}\left(-\frac{\pi}{6}\right)\end{pmatrix}=P_{next}\begin{pmatrix} i_{Vx}^{k}\left(\frac{\pi}{6}\right) \\ i_{Vy}^{k}\left(\frac{\pi}{6}\right) \\ i_{Vz}^{k}\left(\frac{\pi}{6}\right)\end{pmatrix}=P_{next}\bar{i}_V^k\left(\frac{\pi}{6}\right) \tag{6-24}$$

$$P_{next}=\begin{pmatrix} \frac{1}{2} & \frac{\sqrt{3}}{2} & 0 \\ -\frac{\sqrt{3}}{2} & \frac{1}{2} & 0 \\ 0 & 0 & -1\end{pmatrix}$$

Normally the space vector function is being studied in the interval

$$-\frac{\pi}{6} < \varphi < \frac{\pi}{6} \tag{6-25}$$

in each member frame. Equation (6-24) shows that at each change of frame a rotation in negative direction occurs with the angle $\pi/3$ *(60°)*.

The discussion about different coordinate systems above has been applied to valve currents only. However, it is clear that the same transformations can be applied also to the valve voltages and other quantities.

Example 6-1

Assume that the TCSC is operating in steady state with fixed boost factor. We further assume that the line current is three-phase symmetrical and with no zero-sequence current. The line current space vector is given by (6-5) and the transformation into the converter-oriented coordinate system delivers a space-vector trajectory, which is a *60°* long arc passing from *-30°* to *+30°* with constant angular speed in a sixth of a cycle at mains frequency.

The time function for the capacitor voltage was derived in equation (3-10) in chapter 3 discussing steady-state conditions. The following equation was obtained

$$u_{Ca}(t) = \begin{cases} = \dfrac{\lambda X_0 \hat{I}_L}{\lambda^2 - 1}\left(\dfrac{\lambda\cos\beta}{\cos\lambda\beta}\sin\lambda\omega_N t - \sin\omega_N t\right), & -\beta < \omega_N t < \beta \\ = \lambda X_0 \hat{I}_L\left[\sin\omega_N t - \dfrac{\lambda\cos\beta}{\lambda^2 - 1}\left(\lambda\tan\beta - \tan\lambda\beta\right)\right], & \beta < \omega_N t < \pi - \beta \\ = -u_{Ca}\left(t - \dfrac{\pi}{\omega_N}\right), & \pi - \beta < \omega_N t \\ = -u_{Ca}\left(t + \dfrac{\pi}{\omega_N}\right), & \omega_N t < -\beta \end{cases} \tag{6-26}$$

The capacitor voltages in the other phases can be obtained from

$$u_{Cb}(t) = u_{Ca}\left(t - \frac{2\pi}{3\omega_N}\right)$$
$$u_{Cc}(t) = u_{Ca}\left(t + \frac{2\pi}{3\omega_N}\right) \tag{6-27}$$

The capacitor voltages have been depicted together with the line currents and the valve currents as functions of the angle $\omega_N t$ in figure 6-3

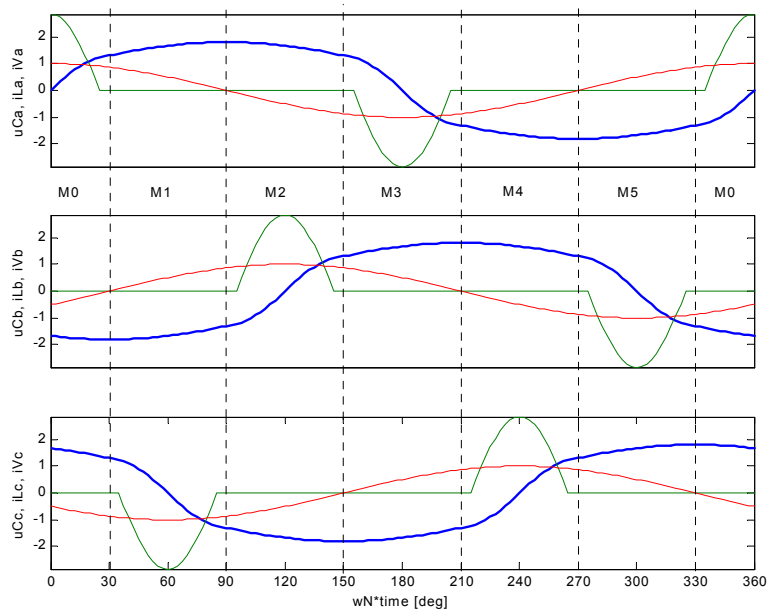

Figure 6-3 Phase quantities in the TCSC; boost factor k_B = 2.0, design factor λ=3.0

Inserting the phase voltages in (6-8) yields a vector function in the $\alpha\beta\gamma$-space. The trajectory of the vector is depicted in figure 6-4.

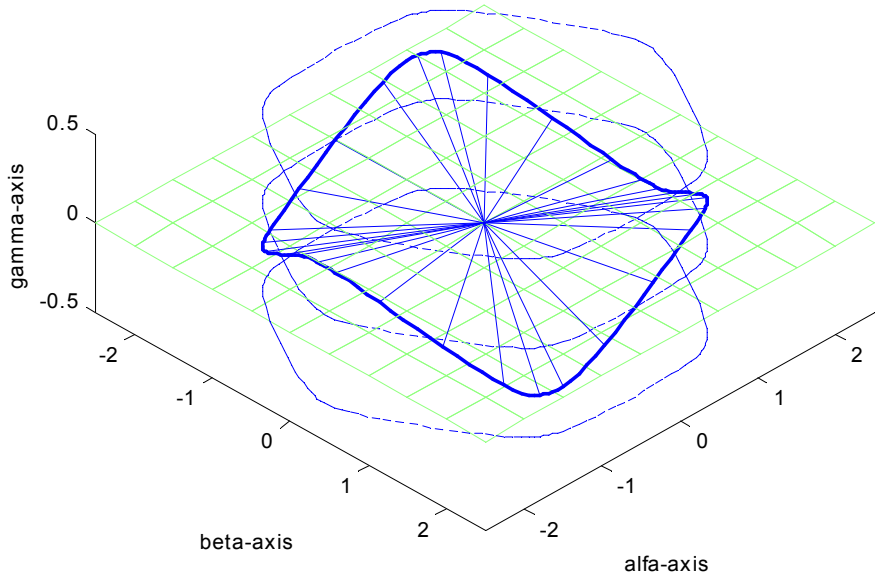

Figure 6-4 Trajectory in the αβγ-space of the capacitor voltage function at boostfactor k_B=2.0 and design factor λ=3.0.

The projection in the *αβ*-plane, i.e. the so-called "space vector", and the homopolar component are shown in figure 6-5.

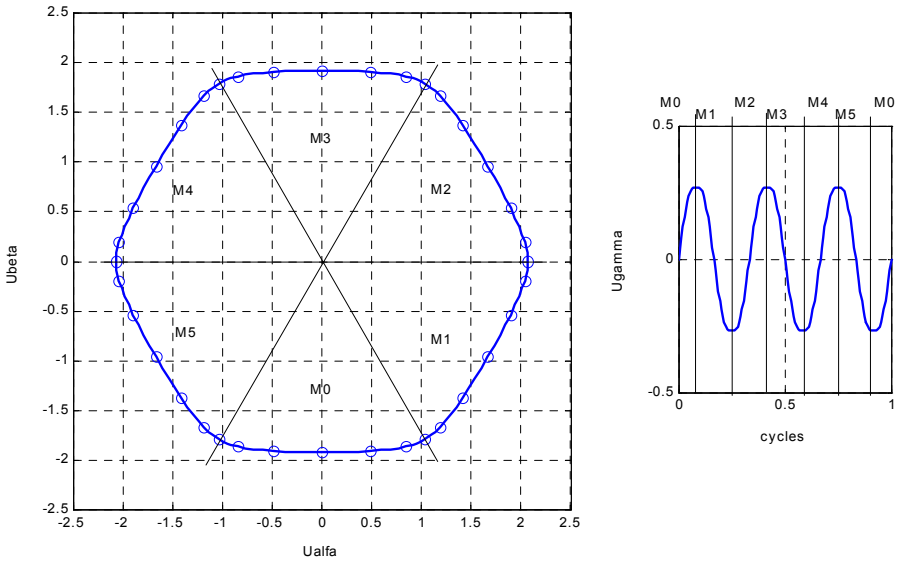

Figure 6-5 Trajectory projection in the αβ-plane and the homopolar γ-component.

When the $\alpha\beta$-vector is transformed by (6-6) into the rotating coordinate system *IL_SYNC* an almost constant vector along the negative imaginary axis results. Due to the harmonics, however, the tip of the vector encircles a small closed loop as shown in figure 6-6. The loop is encircled in negative direction six times per cycle of the network frequency.

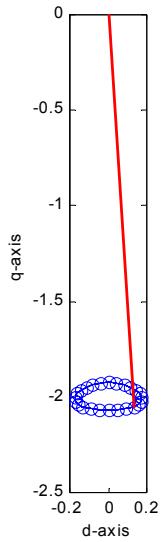

Figure 6-6 Capacitor voltage in dq-plane (k_B=2.0, λ=3.0)

If we instead transform into the converter-oriented sequence of frames according to (6-15) the result is as shown in figure 6-7, which illustrates the trajectory in the *xyz*-space.

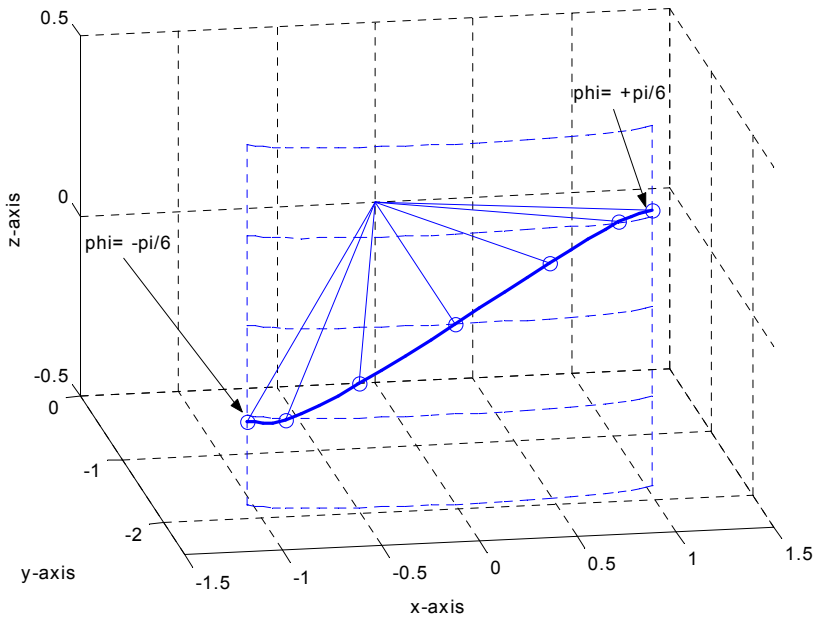

Figure 6-7 Capacitor voltage trajectory in converter-oriented frame (k_B=2.0, λ=3.0).

The trajectory in figure 6-7 is being repeated during each sixth of the period at network frequency. Each time the curve has passed through from left to right a transformation to a new frame occurs. The transformation rule is as in (6-24) and the curve starts again to the left in the new frame. Figure 6-8 demonstrates the component time functions in each converter-oriented frame.

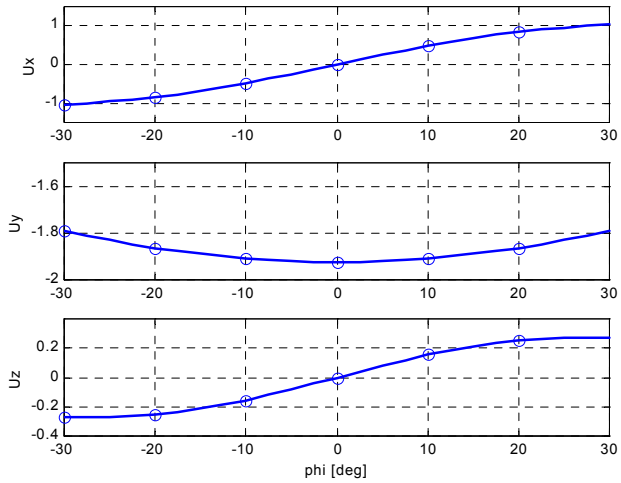

Figure 6-8 Component time functions of the capacitor voltage in each converter-oriented frame (k_B=2.0, λ=3.0).

Finally figure 6-9 shows how the functions are repeated for each 60° interval.

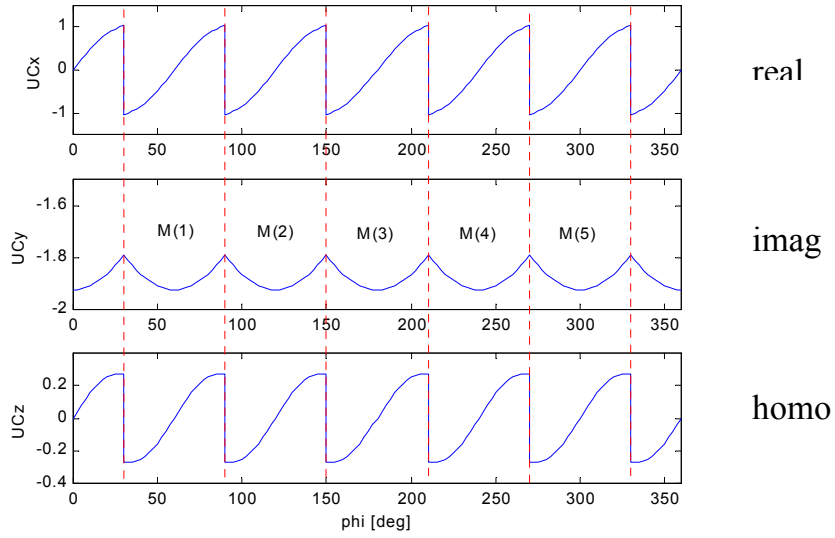

Figure 6-9 Component time functions of the capacitor voltage in the sequence of converter-oriented frames (k_B=2.0, λ=3.0).

6.3 HARMONIC SPECTRUM IN STEADY-STATE

Figure 6-6 shows that the capacitor voltage in the rotating coordinates system *IL_SYNC* is periodic with frequency $6\omega_N$. This means that it can be expanded in a Fourier series

$$\begin{aligned} \hat{u}_C^R(t) &= \sum_{m=-\infty}^{+\infty} \hat{u}_{Cm} e^{j6m\omega_N t} \\ \hat{u}_{Cm} &= \frac{3}{\pi} \int_{-\frac{\pi}{6}}^{\frac{\pi}{6}} e^{-j6m\omega_N \xi} \hat{u}_C^R(\xi) d\xi \end{aligned} \tag{6-28}$$

Equation (6-6) then shows that the capacitor voltage in the fixed coordinate system is given by

$$\hat{u}_C(t) = e^{j\omega_N t} \sum_{m=-\infty}^{+\infty} \hat{u}_{Cm} e^{j6m\omega_N t} = \sum_{m=-\infty}^{+\infty} \hat{u}_{Cm} e^{j(6m+1)\omega_N t} \tag{6-29}$$

The formula shows that the capacitor voltage space vector in three phase symmetrical, steady state operation can be split in its positive and negative sequence components. The former have frequencies $+\omega_N$, $+7\omega_N$, $+13\omega_N$, ... while the latter ones have frequencies $-5\omega_N$, $-11\omega_N$, ...

CHAPTER 7
DYNAMICAL MODEL OF TCSC

This chapter deals with a three-phase model of the TCSC using the Synchronous Voltage Reversal scheme. The dynamical model is intended to extend the qualitative description from chapter 4 with an accurate quantitative model of the dynamics of the TCSC. The model is intended for detailed analysis of the control and protection systems for the TCSC. Another objective, equally important, is to be used as a module in power system stability programs.

7.1 AVAILABLE MODELS IN THE LITERATURE

Several models have been described earlier in literature. Early papers only considered the steady-state relations [M1,M2]. In [M3] different periodic solutions of the mathematical equation representing the TCSC were investigated. The conditions causing "harmonic instability" were discussed. In a paper [M4] dynamical models based on Poincaré map theory were introduced and the behavior of the Kayenta TCSC was analyzed. In a further paper [M5] a model of the TCSC for use together with available stability programs was presented. In this paper a discrete-time model the TCSC circuit was obtained by representing the thyristor valve by an equivalent current source. By introducing an internal state variable to keep track of the capacitor voltage a discrete-time equation for the current in this equivalent source is formulated. The paper [M6] introduces a linearized discrete-time difference equation for the capacitor voltage. It is proposed that the model is then converted into a continuous differential equation, which can be used as a module in any stability program. A model considering TCSC using strictly line current synchronization has been published in [M7]. In [M8] a simplified dynamical model of the TCSC based on constant conduction angle is used to investigate the impact of the TCSC with respect to damping of SSR. Further models have been derived using a general averaging theory for converter switching circuits. These models are based on forming dynamical equations, which describe the development of the essential Fourier components

that characterize the operation of the TCSC. Such models have been described by [M9].

7.2 MOTIVATION FOR THE MODEL IN THE THESIS

Most if not all models in the literature have been derived from considering a single phase of the TCSC. The discrete-time models then uses a sampling time of a half cycle of the network frequency. Accordingly the bandwidth of the model is restricted to mains frequency. In this thesis the bandwidth of the model will be further expanded by using a shorter sampling interval. This means that the interaction between the different phases in the three-phase system must be represented in the model. A natural step then is to consider a sampling interval which is one sixth of the network fundamental frequency.

Some motivations for the increased sampling rate are the following:

- the TCSC has six thyristors, which each can be fired once per cycle of the fundamental frequency; thus the natural maximum sampling rate of the apparatus is six times the network's frequency
- accordingly the bandwidth of the model in principle equals the bandwidth of the main circuit
- the model can be used to investigate the limitations of speed of response caused by constraints imposed by the TCSC main circuit
- the model can be used to investigate the impact of transmission system data on the dynamics of the total system. The transmission system may have different parameters for positive, negative and zero-sequence components
- phenomena like SSR have three-phase character by nature as they involve generation of electrical torque in three-phase generators
- the higher sampling rate permits the conversion from the discrete time model into an equivalent continuous model with substantial bandwidth

In all models presented in the literature it is assumed that controller output is the turnon angle of the thyristor valve. It has been demonstrated in the preceding chapters that the dynamical behaviour of the TCSC can be much easier explained in terms of the timing of the equivalent, instantaneous capacitor voltage reversals. The new model takes advantage of this fact. This means that the command signal obtained from the boost controller primarily is a reference for the timing of the equivalent reversals rather than the turnon angle itself. Given the reference for the equivalent reversal instants a subsystem calculates the exact thyristor firing time depending on the instantaneous capacitor voltage and line current as described in section 4.5. The benefits of this approach are:

- the very non-linear gain related to the control angle versus capacitor voltage (figure 3-3) will not be seen by the controller

- the controller can dynamically utilize angles that are "forbidden" from a steady-state point of view in order to force the dynamical response at high boost levels; the maximum voltage limitation will be taken care of by the sub-system controlling the trigger pulses

7.3 GENERAL ASSUMPTIONS FOR THE NEW MODEL

In the derivation of the model it is assumed that an undisturbed steady-state operating point is defined. The model describes the dynamics of deviations from this state. The steady-state operation makes it possible to define a synchronously rotating coordinate system by selecting a system, which is aligned with the undisturbed line current space-vector. This rotating coordinate system is referred to as the *IL_SYNC* system throughout this thesis. Space vector functions given in the *IL_SYNC* frame are notified by the superscript 'R'.

The control of the TCSC in all practical implementations use an internal synchronizing system, generally in the form of a Phase Locked Loop (PLL), which is locked to the line current or some other periodic quantity measured in the power system. The TCSC control system uses this angle as an internal angle reference. The synchronizing system can be thought of as a means to derive, in real-time, the synchronously rotating coordinate system *IL_SYNC*, which has been utilized in the derivation of the difference equation representing the TCSC.

The TCSC model assumes that two signals are provided to displace the reversals from their steady-state positions. One emerges from the boost control system and the other from the synchronizing system. Both exhibit some dynamics, when the TCSC is connected to a power system and its input signals vary.

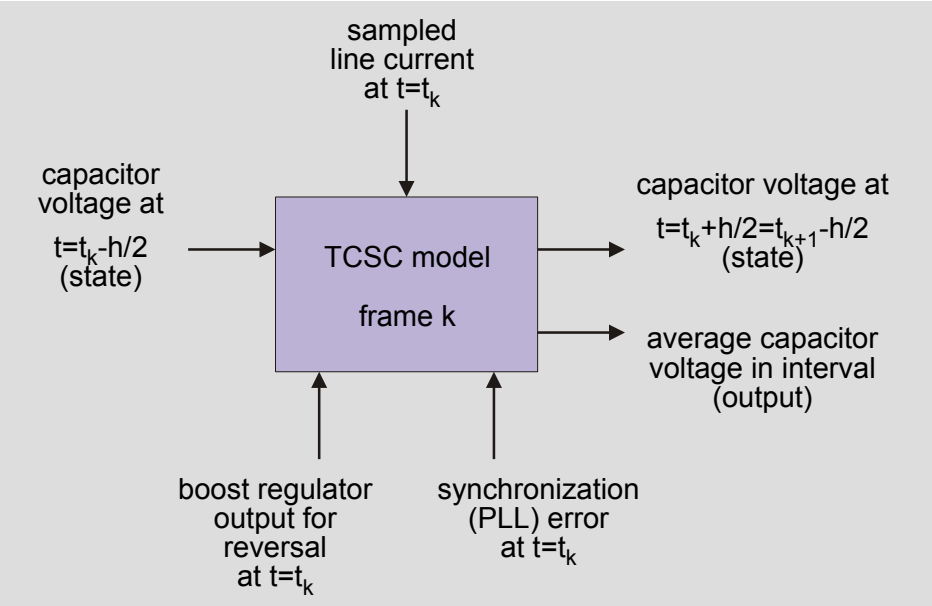

Figure 7-1 Overview of the TCSC model.

The general appearance of the TCSC model is depicted in figure 7-1. It is a discrete-time model for a sampling interval, the length of which is one sixth of the cycle at the network frequency. The intervals are selected so that equivalent, instantaneous capacitor voltage reversals occur in the middle of the interval in steady state operation.

The discrete model calculates the change of the state variables between consecutive sampling instants taking into account

- the line current in the sampling interval
- the boost controller's and the synchronization system's output angles, which have been used to determine control the voltage reversal occurring between the sampling instants

The mentioned angles are being represented by angles acting on the equivalent, instantaneous capacitor voltage reversal occurring inside the sampling interval. Further the model delivers an average of the TCSC capacitor voltage in the synchronously rotating coordinate system within the sampling interval as an output signal.

The states of the model are defined in a sequence of fixed frames, which is here given the name "converter-oriented", *CONV_ORI,* coordinate system, and which has been described in the preceding chapter.

7.4 EFFECT OF INSTANTANEOUS CAPACITOR VOLTAGE REVERSAL IN TCSC

The Synchronous Voltage Reversal (SVR) scheme utilizes the approximation that the conduction time of the thyristors is very short and can be neglected. Even if this is a rough approximation it simplifies the derivation of the model tremendously and we will see that the results produced with this approximation are quite satisfactory.

We start by deriving an equation that describes the effect of an instantaneous thyristor intervention with respect to the capacitor voltages represented in the converter-oriented frame. This equation can easily be derived as follows.

The reversal that occurs close to the steady-state reversal instant at $t=t_k$ is studied. It is assumed that the conduction time is short, so only one thyristor conducts in each time frame in the converter-oriented sequence. Accordingly all thyristors in figure 6-3 are blocked except T_k, which is connected to the *'+u'* phase and which conducts for a very short interval at $t=t_k$. Figure 7-2 illustrates the conditions in the interval.

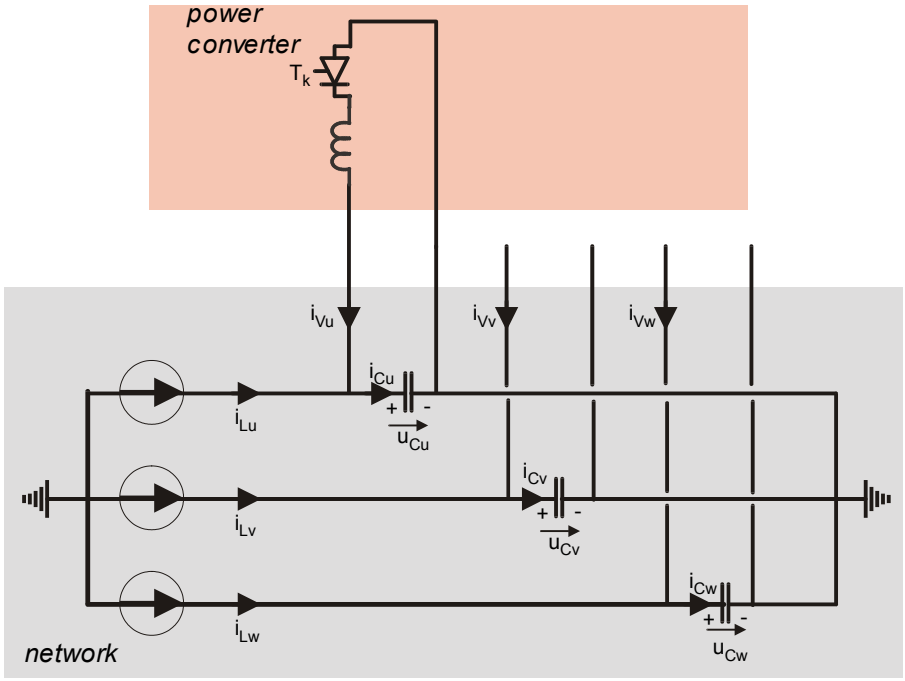

Figure 7-2 Conditions in the converter-oriented frame.

It can immediately be concluded from the figure that the capacitor in the *u*-phase performs a voltage reversal, when the thyristor T_k is triggered, while the other capacitors do not change their voltages during the (infinitely) short conduction time. Now the phase quantities are given by a formula similar to (6-14)

$$u_{Cu}^{k} = \mathrm{Re}\left\{\hat{u}_{C}^{k}\right\} + u_{Cz}^{k} \tag{7-1}$$

Therefore we can express the condition that the capacitor voltage in the *u*-phase reverses with a loss factor D_f as follows

$$\mathrm{Re}\left(\hat{u}_{C}^{k}\right)_{post} + \left(u_{Cz}^{k}\right)_{post} = -D_f \left\{\mathrm{Re}\left(\hat{u}_{C}^{k}\right)_{pre} + \left(u_{Cz}^{k}\right)_{pre}\right\} \tag{7-2}$$

The loss factor D_f, is somewhat smaller than unity and is intended to represent the losses related to the capacitor voltage reversal.

Let the charge passing through the thyristor be q_T^k. The associated current only flows in phase *u*. Looking at equation (6-13) it can then be seen that this current causes the following contributions (Dirac-pulses) to the capacitor current

$$\Delta\hat{i}_C^k = \frac{2}{3} q_T^k \delta(t_k)$$
$$\Delta i_{Cz}^k = \frac{1}{3} q_T^k \delta(t_k) \tag{7-3}$$

Thus the voltage change caused by the thyristor current at $t=t_k$ in space vector $\hat{u}_C^k$ is real and two times the voltage change in the homopolar component u_{Cz}^k. This yields

$$\mathrm{Re}\left(\hat{u}_C^k\right)_{post} - \mathrm{Re}\left(\hat{u}_C^k\right)_{pre} = 2\left\{\left(u_{Cz}^k\right)_{post} - \left(u_{Cz}^k\right)_{pre}\right\} \tag{7-4}$$

The imaginary part of the capacitor voltage remains unchanged during the reversal.

Using this and equations (7-2) and (7-4) we obtain the connection between components *x* and *y* of the space-vectors and the homopolar components before and after the capacitor reversal. We introduce the name A_{rev} for the matrix and get

$$\bar{u}_{C,post}^k = \begin{pmatrix} u_{Cx}^k \\ u_{Cy}^k \\ u_{Cz}^k \end{pmatrix}_{post} = A_{rev} \begin{pmatrix} u_{Cx}^k \\ u_{Cy}^k \\ u_{Cz}^k \end{pmatrix}_{pre} = A_{rev} \bar{u}_{C,pre}^k$$
$$A_{rev} = \begin{pmatrix} -\frac{2D_f - 1}{3} & 0 & -\frac{2(1+D_f)}{3} \\ 0 & 1 & 0 \\ -\frac{1+D_f}{3} & 0 & \frac{2-D_f}{3} \end{pmatrix} \tag{7.5}$$

Note that the '***x,post***' component depends on both the '***x,pre***' and the '***z,pre***' components. Thus, unlike the situation for many other power electronic converters, the homopolar component cannot be neglected!

For the ideal case where the reversals occur without losses we obtain

$$A_{rev} = \begin{pmatrix} -\frac{1}{3} & 0 & -\frac{4}{3} \\ 0 & 1 & 0 \\ -\frac{2}{3} & 0 & \frac{1}{3} \end{pmatrix} \tag{7-6}$$

7.5 CAPACITOR VOLTAGE DEVIATIONS WITHIN THE SAMPLING INTERVAL

In the following we shall consider **deviations** from the steady state capacitor voltage waveform due to a small variation in the line current and a small displacement of the reversal time. Specifically our goal is to derive a difference equation, which describes the change of the capacitor voltage during a sampling interval from t_k-$h/2$ to t_k+$h/2$. The change caused by the reversal has already been discussed in the preceding section. As input the pre-reversal voltage deviation is required. It depends both on the line current deviation and on the displacement of the reversal instant from its steady state equilibrium instant, the latter deviation being directed by the control system. Finally the capacitor voltage in the upcoming sampling point similarly depends on the line current deviation and the timing of the reversal.

7.5.1 The capacitor voltage trajectory in steady state

The capacitor voltage trajectory in the converter-oriented *CONV_ORI* coordinate system has been depicted in figure 6-6. Now we will consider instantaneous reversals, and the trajectory then becomes as shown in figure 7-3.

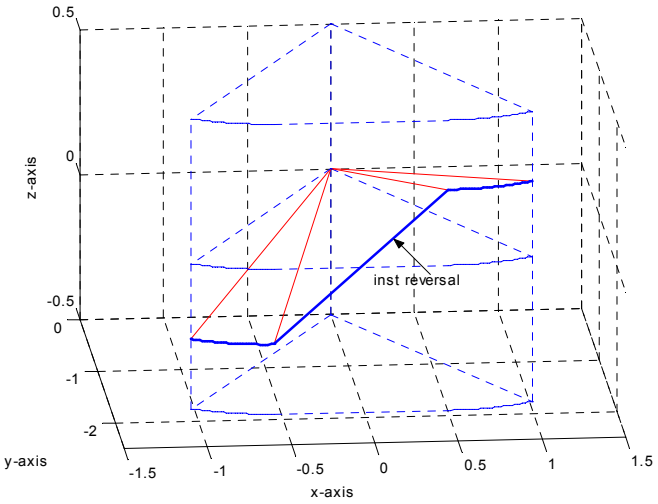

Figure 7-3 Trajectory of the capacitor voltage in CONV_ORI system (k_B=1.95)

The trajectory is traversed from the left to the right six times during each cycle of the network frequency. At the instantaneous capacitor voltage reversal an instantaneous movement along the inclined line segment occurs. The corresponding trajectories of each component have been depicted in figure 7-4.

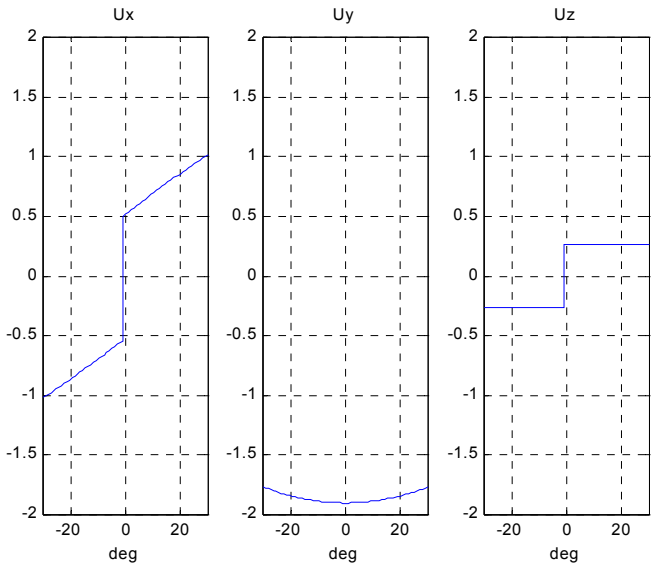

Figure 7-4 Capacitor voltage components in the CONV_ORI system (k_B≈1.95)
{uC_dev1.m}

It can be seen that, due to the circuit losses in the circuit, the reversals occur somewhat before $\varphi=0$. The loss factor was assumed to be $D_f = 0.95$. Further notice that the step in the x-component is two times that in the zero-sequence component.

7.5.2 Effect of displacement of reversal

Let us first consider the case that the steady state **line current** is not disturbed. If the voltage reversal occurs at the same time as in steady state operation the conditions are trivial as shown in figure 7-5. No change of the **capacitor voltage** deviation in addition to the voltage reversal then takes place inside the sampling interval. The pre-reversal capacitor voltage deviation equals the value at the start of the sampling interval and the capacitor voltage deviation at the end of the sampling interval equals the post-reversal voltage. The change of the capacitor voltage deviation only depends on the reversal equation (7-5) in this case.

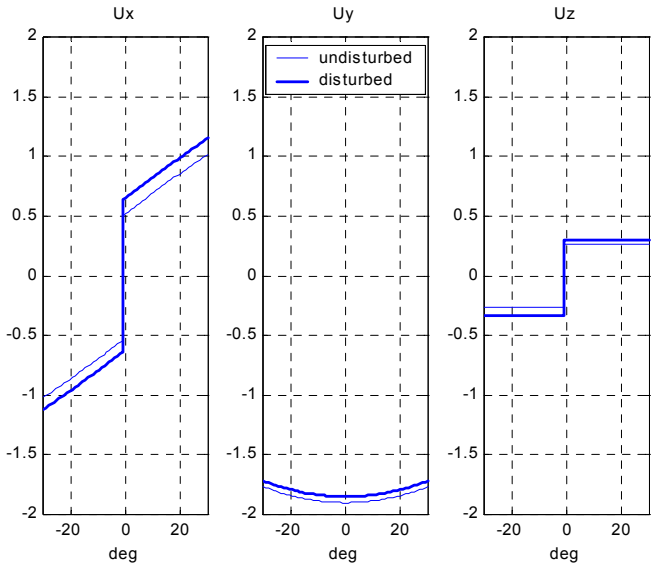

Figure7-.5 Capacitor voltage components in CONV_ORI frame; no reversal instant displacement.

However, the reversal instants do not always occur at their steady state time instants, because the reversal instant is directed by the control system, which comprises a boost controller and a synchronization system. Let the reversal instant be phase advanced by the angle $\Delta\theta$ before the steady state reversal at $t=t_k$ due to actions of the boost controller $(\Delta\theta_{reg})$ and due to deviation in the synchronization signal $(\Delta\theta_{PLL})$ from the PLL system. Thus

$$\Delta\theta_k = \Delta\theta_{reg,k} + \Delta\theta_{PLL,k} \tag{7-7}$$

The capacitor voltage time derivative is proportional to the line current

$$\frac{d\bar{u}_C^k(\varphi)}{d\varphi} = \frac{1}{\omega_N}\frac{d\bar{u}_C^k(\varphi)}{dt} = \frac{1}{\omega_N}\frac{\bar{i}_L^k(\varphi)}{C} = \lambda X_0 \bar{i}_L^k(\varphi) \tag{7-8}$$

As the angle $\Delta\theta_k$ represents a phase advance from the steady state reversal instant and as further the undisturbed line current is $\bar{i}_L^k(0) = \begin{pmatrix} \hat{I}_L \\ 0 \\ 0 \end{pmatrix}$ at $t=t_k$, the deviation of the pre-reversal voltage caused by $\Delta\theta_k$ becomes

$$\begin{aligned}\Delta\overline{u}_{C,pre}^{k} &= \Delta\overline{u}_{C}^{k}\left(-\frac{\pi}{6}\right)-\lambda X_0\begin{pmatrix}\hat{I}_L\\0\\0\end{pmatrix}\Delta\theta_k\\ \Delta\overline{u}_{C}^{k}\left(\frac{\pi}{6}\right) &= \Delta\overline{u}_{C,post}^{k}+\lambda X_0\begin{pmatrix}\hat{I}_L\\0\\0\end{pmatrix}\Delta\theta_k\end{aligned} \tag{7-9}$$

Define

$$P_{100}=\begin{pmatrix}1\\0\\0\end{pmatrix} \tag{7-10}$$

Then

$$\boxed{\begin{aligned}\Delta\overline{u}_{C,pre}^{k} &= \Delta\overline{u}_{C}^{k}\left(-\frac{\pi}{6}\right)-\lambda X_0 P_{100}\hat{I}_L\Delta\theta_k\\ \Delta\overline{u}_{C}^{k}\left(\frac{\pi}{6}\right) &= \Delta\overline{u}_{C,post}^{k}+\lambda X_0 P_{100}\hat{I}_L\Delta\theta_k\end{aligned}} \tag{7-11}$$

Figure 7-6 shows the capacitor voltage components.

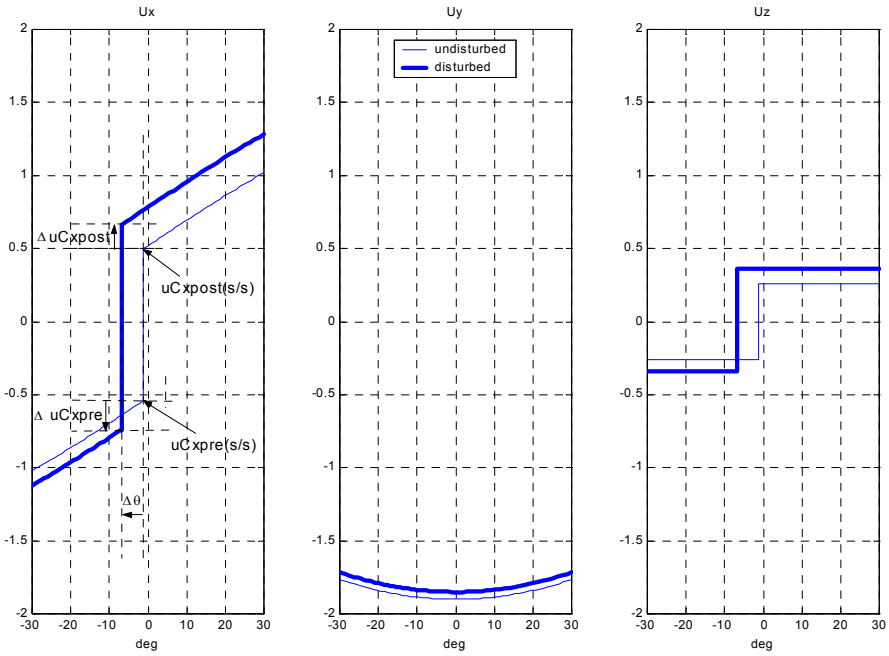

Figure 7-6 Capacitor voltage components in CONV_ORI at displacement of the reversal instant.

It can be clearly seen that the displacement of the reversal point only impacts on the pre-reversal voltage in the x-component.

7.5.3 Effect of line current deviation

Line current deviations cause additional changes in the pre-reversal voltage. The alteration is governed by the differential equation (7-8). For small angle deviations $\Delta\theta_k$ the linearized variation of the capacitor voltage due to the line current deviation is given by

$$\Delta\bar{u}_{C,pre}^{k} = \Delta\bar{u}_{C}^{k}(0-) = \Delta\bar{u}_{C}^{k}\left(-\frac{\pi}{6}\right) + \lambda X_0 \int_{-\frac{\pi}{6}}^{0} \Delta\bar{i}_{L}^{k}(\eta)\,d\eta \tag{7-12}$$

Similarly the linear variation of the capacitor voltage versus the line current deviation in the interval $<t_k+0, t_k+h/2>$ after the reversal is given by

$$\Delta\bar{u}_{C}^{k}\left(\frac{\pi}{6}\right) = \Delta\bar{u}_{C}^{k}(0+) + \lambda X_0 \int_{0}^{\frac{\pi}{6}} \Delta\bar{i}_{L}^{k}(\eta)\,d\eta = \Delta\bar{u}_{C,post}^{k} + \lambda X_0 \int_{0}^{\frac{\pi}{6}} \Delta\bar{i}_{L}^{k}(\eta)\,d\eta \tag{7-13}$$

The model outlined in figure 7-1 is a **discrete, sampled** model. The capacitor voltage is sampled at the midpoints, $t=t_k+h/2$, of the intervals between consecutive reversals in steady state operation. In such a discrete, sampled system it is adequate that only **one** current deviation sample will be used per interval. This value is sampled at the instant of the undisturbed steady state reversal, $t=t_k$, and it is used in the whole sampling interval both before and after the voltage reversal.

The sampled line current deviation in an interval is a triple of values representing the components of the line current.

$$\Delta\bar{i}_L^k(0)=\begin{pmatrix}\Delta i_{Lx}^k(0)\\ \Delta i_{Ly}^k(0)\\ \Delta i_{Lz}^k(0)\end{pmatrix} \tag{7-14}$$

We are going to use these values to calculate the integrals in (7-12) and (7-13). For that purpose we have to determine how the instantaneous values of the line current deviation shall be calculated from the sampled value at any time instant in the interval between the samplings.

It appears that the homopolar current component is lacking any naturally preferred approximation beside the trivial assumption that it is constant throughout the interval. If the sampled values of the zero-sequence component in the *CONV_ORI* remains constant, $\Delta i_{Lz}^k = const \quad \forall k$, this means that that the zero-sequence current in the *FIXED* coordinate system is a third harmonic square wave current.

For the *x*- and *y*-components several interpretations are possible. They may be considered to be approximately piecewise constant around the sampling point of the capacitor voltage components. However, such piecewise constant representations may be adopted in various coordinate systems:

- in the *FIXED* coordinate system
- in a rotating coordinate system synchronous with the steady state line current vector, the *IL_SYNC* system
- in a coordinate system rotating with arbitrarily chosen frequency, $\xi\omega_N$ with constant ξ, relative the stator coordinate system

- ***FIXED*, stator coordinate system**

The *abc*-frame, or *FIXED* coordinate system, is used for line current deviations which mainly contain low frequency components in the phase quantities. Figure 7-6 shows the approximation of sinusoidal current deviations for different frequencies. It can be used for deviations with electrical frequencies below 20 Hz.

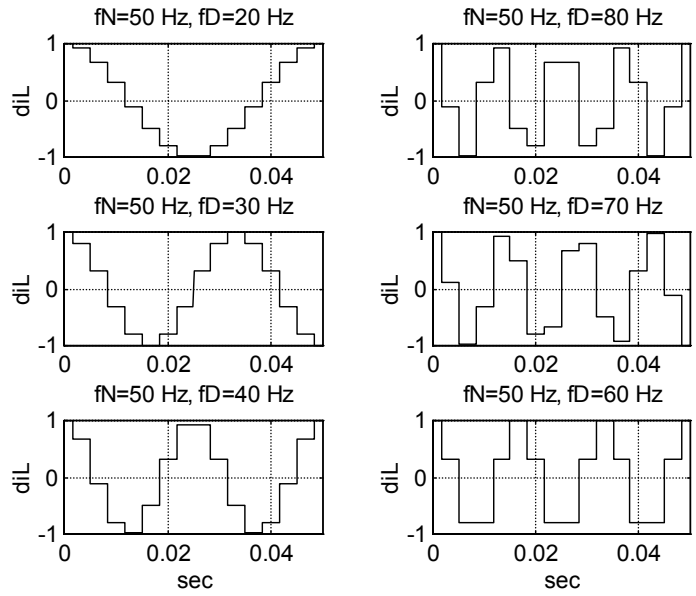

Figure 7-6 Approximation of the line current deviations as piecewise constant functions in FIXED system; frequencies 50±30 Hz, 50±20 Hz and 50±10 Hz

- ***IL_SYNC, s*teady state rotating coordinate system**

The two-dimensional space vector $\Delta\hat{i}_L^k(\varphi) = \Delta i_{Lx}^k(\varphi) + j\Delta i_{Ly}^k(\varphi)$ in the *CONV_ORI* system as defined by equation (6-10) and (6-13) represents the line current deviation. If it varies only slowly relative the rotating coordinate system *IL_SYNC* defined according to equation (6-7) it is beneficial to approximate the line current deviation within the sampling interval as a constant **in the latter coordinate system**. Specifically this appears to be adequate when electromechanical transients in the network should be investigated. Also for current and voltage deviations in the subsynchronous frequency range corresponding to mechanical frequencies below 30 Hz (electrical frequency 20-80 Hz) this approximation seems appropriate. Some examples are shown in figure 7-7.

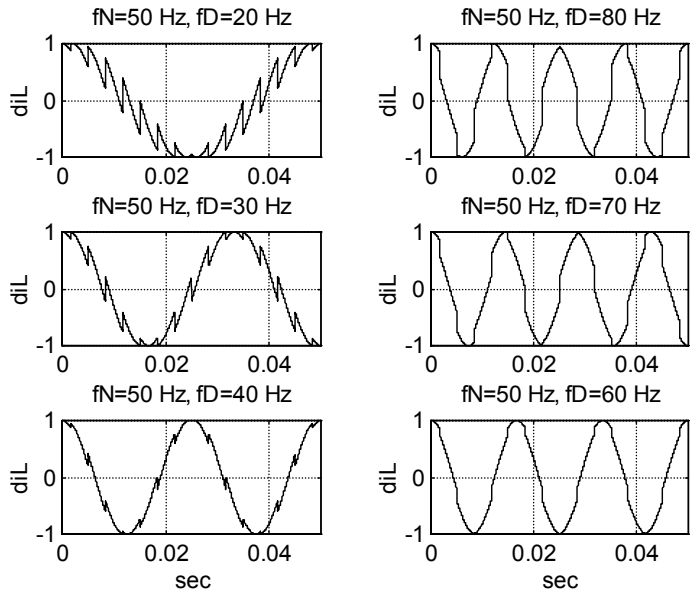

Figure 7-7 Line current deviation in the FIXED (abc) system approximated as a piecewise constant function in IL_SYNC system; frequencies 50±30 Hz, 50±20 Hz and 50±10 Hz

This approach seems to be the best one for deriving general-purpose time-domain linear models.

- **Rotating coordinate system with other rotational speed**

If the deviation current is a positive sequence current having a narrow frequency spectrum around the centre frequency $\xi\omega_N$, it is a good idea to approximate the current deviation to be piece-wise constant in a coordinate system that rotates with frequency $\xi\omega_N$. This method can specifically be used to calculate the frequency domain transfer function as calculation of the transfer function value at a specific frequency assumes that the TCSC circuit will be excited with this single frequency component only. In the frame that rotates with the specific speed the approximation of the current deviation as piecewise constant will be perfect and without error.

- **General approach**

The two earlier mentioned alternatives can be looked upon as special cases

  - the stator-fixed coordinate system, *FIXED,* is generated if $\xi = 0$
  - the synchronously rotating coordinate system, *IL_SYNC,* is obtained if $\xi = 1$

Accordingly put

$$\Delta\bar{i}_L^k(\varphi)=\begin{pmatrix}\Delta i_{Lx}^k(\varphi)\\ \Delta i_{Ly}^k(\varphi)\\ \Delta i_{Lz}^k(\varphi)\end{pmatrix} \tag{7-15}$$

with

$$\begin{aligned}\Delta i_{Lx}^k(\varphi)&=\mathrm{Re}\left\{\left[\Delta i_{Lx}^k(0)+j\Delta i_{Ly}^k(0)\right]e^{j\xi\varphi}\right\}=\Delta i_{Lx}^k(0)\cos\xi\varphi-\Delta i_{Ly}^k(0)\sin\xi\varphi\\ \Delta i_{Ly}^k(\varphi)&=\mathrm{Im}\left\{\left[\Delta i_{Lx}^k(0)+j\Delta i_{Ly}^k(0)\right]e^{j\xi\varphi}\right\}=\Delta i_{Lx}^k(0)\sin\xi\varphi+\Delta i_{Ly}^k(0)\cos\xi\varphi\\ \Delta i_{Lz}^k(\varphi)&=\Delta i_{Lz}^k(0)\end{aligned} \tag{7-16}$$

Inserting these expressions in the formulas (7-12) and (7-13) yields after integration the following result, which also includes the contribution to the voltage deviation according to equation (7-11)

$$\boxed{\begin{aligned}\Delta\bar{u}_{C,pre}^k&=\Delta\bar{u}_C^k\left(-\frac{\pi}{6}\right)+\lambda X_0 B_P\Delta\bar{i}_L^k(0)-\lambda X_0\hat{I}_L P_{100}\Delta\theta_k\\ \Delta\bar{u}_C^k\left(\frac{\pi}{6}\right)&=\Delta\bar{u}_{C,post}^k+\lambda X_0 B_P^t\Delta\bar{i}_L^k(0)+\lambda X_0\hat{I}_L P_{100}\Delta\theta_k\end{aligned}} \tag{7-17}$$

$$B_P=\begin{pmatrix}\dfrac{\sin\left(\frac{\xi\pi}{6}\right)}{\xi} & \dfrac{1-\cos\left(\frac{\xi\pi}{6}\right)}{\xi} & 0\\ -\dfrac{1-\cos\left(\frac{\xi\pi}{6}\right)}{\xi} & \dfrac{\sin\left(\frac{\xi\pi}{6}\right)}{\xi} & 0\\ 0 & 0 & \dfrac{\pi}{6}\end{pmatrix} \tag{7-18}$$

7.6 NORMALIZATION OF THE EQUATIONS

It may be observed that the equation (7-17) contains capacitor voltage components and terms that include the product $\lambda X_0\hat{I}_L$. Going back to the definition (3-3) this product can be identified as

$$\lambda X_0 \hat{I}_L = \frac{\hat{I}_L}{\omega_N C} \tag{7-19}$$

which is the capacitive reactive voltage drop across the capacitor bank in the TCSC at line current $\hat{I}_L$ without any boost, i.e. at $k_B = 1.0$. It is advantageous to normalize the equation with this quantity. We will do this and work with the **relative** line current and capacitor voltage deviations defined in equation (7-20) and (7-21)

$$\Delta\tilde{\bar{i}}_L^k = \begin{pmatrix} \Delta\tilde{i}_{Lx}^k \\ \Delta\tilde{i}_{Ly}^k \\ \Delta\tilde{i}_{Lz}^k \end{pmatrix} = \frac{\Delta\bar{i}_L^k}{\hat{I}_L} = \frac{1}{\hat{I}_L}\begin{pmatrix} \Delta i_{Lx}^k \\ \Delta i_{Ly}^k \\ \Delta i_{Lz}^k \end{pmatrix} \tag{7-20}$$

$$\Delta\tilde{\bar{u}}_C^k = \begin{pmatrix} \Delta\tilde{u}_{Cx}^k \\ \Delta\tilde{u}_{Cy}^k \\ \Delta\tilde{u}_{Cz}^k \end{pmatrix} = \frac{\Delta\bar{u}_C^k}{\lambda X_0 \hat{I}_L} = \frac{1}{\lambda X_0 \hat{I}_L}\begin{pmatrix} \Delta u_{Cx}^k \\ \Delta u_{Cy}^k \\ \Delta u_{Cz}^k \end{pmatrix} \tag{7-21}$$

Introducing the variables above in (7-17) yields

$$\boxed{\begin{aligned} \Delta\tilde{\bar{u}}_{C,pre}^k &= \Delta\tilde{\bar{u}}_C^k\left(-\frac{\pi}{6}\right) + B_P\Delta\tilde{\bar{i}}_L^k(0) - P_{100}\Delta\theta_k \\ \Delta\tilde{\bar{u}}_C^k\left(\frac{\pi}{6}\right) &= \Delta\tilde{\bar{u}}_{C,post}^k + B_P^t\Delta\tilde{\bar{i}}_L^k(0) + P_{100}\Delta\theta_k \end{aligned}} \tag{7-22}$$

The same normalization also is applied to equation (7-5) giving the result

$$\boxed{\tilde{\bar{u}}_{C,post}^k = A_{rev}\tilde{\bar{u}}_{C,pre}^k} \tag{7-23}$$

7.7 DIFFERENCE EQUATION DESCRIBING THE DISCRETE SYSTEM.

Combining the above equations (7-22) and (7-23) provides a difference equation that associates the state variable, i.e. the capacitor voltage deviation, at the end of the sampling interval with

- its value at the start of the sample interval
- the line current deviation within the sample interval
- the deviation of the reversal time instant due to control system intervention

We get

$$\Delta\widetilde{\overline{u}}_C^{\,k}\left(\frac{\pi}{6}\right) = A_{rev}\Delta\widetilde{\overline{u}}_C^{\,k}\left(-\frac{\pi}{6}\right) + \left(A_{rev}B_P + B_P^t\right)\Delta\widetilde{\overline{i}}_L^{\,k}(0) + \left(I - A_{rev}\right)P_{100}\Delta\theta_k \tag{7-24}$$

Finally formulas like (6-24) provides the formula for connecting quantities in consecutive members of the sequence of frames in the *CONV_ORI* system

$$\Delta\widetilde{\overline{u}}_C^{\,k+1}\left(-\frac{\pi}{6}\right) = P_{next}\Delta\widetilde{\overline{u}}_C^{\,k}\left(\frac{\pi}{6}\right) \tag{7-25}$$

When this formula is applied to (7-24) the desired state equation for the discrete, sampled model results

$$\boxed{\begin{aligned}&\Delta\widetilde{\overline{u}}_C^{\,k+1}\left(-\frac{\pi}{6}\right) = \\ &= P_{next}A_{rev}\Delta\widetilde{\overline{u}}_C^{\,k}\left(-\frac{\pi}{6}\right) + P_{next}\left(A_{rev}B_P + B_P^t\right)\Delta\widetilde{\overline{i}}_L^{\,k}(0) + P_{next}\left(I - A_{rev}\right)P_{100}\Delta\theta_k\end{aligned}} \tag{7-26}$$

7.8 OUTPUT FROM THE DISCRETE SYSTEM

Equation (7-26) is a state recursion equation for the discrete system describing the TCSC. The relative capacitor voltage deviation at the beginning of the sampling interval is the state, and the sampled relative line current deviation in the sample interval midpoint and the displacement of the reversal instant are the input variables.

Three states are required to represent the TCSC circuit, e.g. the capacitor voltage in the *CONV_ORI (x,y,z)* frame as in (7-26). The **homopolar** (=zero-sequence) capacitor voltage interacts strongly with the other capacitor voltage components why it **cannot be disregarded**. However, in the transmission network the impedance level for the zero-sequence components is generally higher than for the positive- and negative-sequence components and the dominating homopolar component of the TCSC voltage is the third harmonic component. Therefore the zero-sequence component of the **line current** will be small and can in general be neglected. In the following we will only consider the non-zero-sequence

components of the relative line current deviation as input signals. Accordingly the capacitor voltage components, which mainly interact with the transmission system, are the two non-zero-sequence components and they are required as output signals from the TCSC model. They may be extracted from the model as **sampled** values of the relative deviation of the capacitor voltage or, alternatively, as values obtained by **averaging** during the whole sample interval. In the latter case the output signals correspond to Fourier coefficients for the fundamental frequency components of the inserted voltage.

7.8.1 Sampled output

The state (relative capacitor voltage deviation) is sampled in the *CONV_ORI* system at time t_k-*h/2*. A better output signal is the voltage vector in the *IL_SYNC* system. According to the transformation rules in (6-20) we get

$$\Delta\widetilde{\widetilde{u}}_C^R\left(t_k-\frac{h}{2}\right)=e^{j\frac{\pi}{6}}\widetilde{\widetilde{u}}_C^k\left(-\frac{\pi}{6}\right) \tag{7-27}$$

The matrix formulation can be obtained from (6-22)

$$\begin{pmatrix}\Delta\widetilde{u}_{Cd}^R\left(t_k-\frac{h}{2}\right)\\ \Delta\widetilde{u}_{Cq}^R\left(t_k-\frac{h}{2}\right)\end{pmatrix}=P_{x2d}\begin{pmatrix}\Delta\widetilde{u}_{Cx}^k\left(-\frac{\pi}{6}\right)\\ \Delta\widetilde{u}_{Cy}^k\left(-\frac{\pi}{6}\right)\\ \Delta\widetilde{u}_{Cz}^k\left(-\frac{\pi}{6}\right)\end{pmatrix}=P_{x2d}\Delta\widetilde{\widetilde{u}}_C^k\left(-\frac{\pi}{6}\right) \tag{7-28}$$

$$P_{x2d}=\begin{pmatrix}\cos\frac{\pi}{6} & -\sin\frac{\pi}{6} & 0\\ \sin\frac{\pi}{6} & \cos\frac{\pi}{6} & 0\end{pmatrix}=\frac{1}{2}\begin{pmatrix}\sqrt{3} & -1 & 0\\ 1 & \sqrt{3} & 0\end{pmatrix}$$

7.8.2 Averaged output

When the variation of the line current deviation inside the sampling interval (the factor *'ξ'* in (7-16)) and the loss factor D_f has been selected, the capacitor voltage deviation inside the sampling interval is completely determined. Then it becomes possible to calculate the average of the relative capacitor voltage deviation's *d*- and *q*-components, defined by (6-6), in the *IL_SYNC* rotating coordinate system. Let

$$\Delta\widetilde{\bar{u}}^{R}_{C,av}(t_k)=\Delta\widetilde{u}^{R}_{Cd,av}(t_k)+j\Delta\widetilde{u}^{R}_{Cq,av}(t_k)=\frac{3}{\pi}\int_{-\frac{\pi}{6}}^{\frac{\pi}{6}}e^{-j\varphi}\Delta\widetilde{\bar{u}}^{k}_{C}(\varphi)d\varphi \tag{7-29}$$

In steady state these average values represent the components of the fundamental frequency Fourier components of the relative capacitor voltage deviation. Evaluation of the formula (7-29) as described in Appendix A yields the result

$$\begin{aligned}\begin{pmatrix}\Delta\widetilde{u}^{R}_{Cd,av}(t_k)\\ \Delta\widetilde{u}^{R}_{Cq,av}(t_k)\end{pmatrix}&=\left(F_{beg}+F_{end}A_{rev}\right)\Delta\widetilde{\bar{u}}^{k}_{C}\left(-\frac{\pi}{6}\right)+\\&+\left\{F_{end}\left(A_{rev}B_P+B'_P\right)P_{spv}+G_{IL}\right\}\begin{pmatrix}\Delta\widetilde{i}^{R}_{Ld}(t_k)\\ \Delta\widetilde{i}^{R}_{Lq}(t_k)\end{pmatrix}+\\&+\left\{F_{end}\left(I-A_{rev}\right)P_{100}+G_\theta P_{10}\right\}\Delta\theta_k\end{aligned} \tag{7-30}$$

where

$$\begin{aligned}F_{beg}&=\frac{3}{2\pi}\begin{pmatrix}1 & \sqrt{3}-2 & 0\\ 2-\sqrt{3} & 1 & 0\end{pmatrix}\\F_{end}&=\frac{3}{2\pi}\begin{pmatrix}1 & 2-\sqrt{3} & 0\\ \sqrt{3}-2 & 1 & 0\end{pmatrix}\\G_{IL}&=\begin{pmatrix}0 & -g_{IL}\\ g_{IL} & 0\end{pmatrix}\qquad g_{IL}=\frac{\sin\frac{\xi\pi}{6}}{\frac{\xi\pi}{6}}-\frac{\sin\frac{(1-\xi)\pi}{6}}{\frac{(1-\xi)\pi}{6}}\\G_\theta&=k_B-1\\P_{spv}&=\begin{pmatrix}1 & 0\\ 0 & 1\\ 0 & 0\end{pmatrix}\end{aligned} \tag{7-31}$$

7.8.3 Boost factor

The *d*-axis in the rotating coordinate system is in this thesis aligned with the steady state line current vector. The steady state capacitor voltage therefore is aligned with the negative imaginary axis, i.e. the negative *q*-axis in the *IL_SYNC* system. The components in (7-30) extracts the fundamental frequency components of the relative capacitor voltage deviations steady. The *q*-axis component equals the negative deviation of the boost factor from its steady state value. Thus we obtain the expressions

$$\begin{aligned}\Delta k_B\left(t_k-\frac{h}{2}\right)&=-\Delta\tilde{u}_{Cq}^{R}\left(t_k-\frac{h}{2}\right)\\ \Delta k_B\left(t_k\right)&=-\Delta\tilde{u}_{Cq,av}^{R}\left(t_k\right)\end{aligned} \tag{7-32}$$

for the sampled and the averaged output respectively.

CHAPTER 8
TCSC MODEL DYNAMICS

In this chapter the characteristics of the TCSC model, which has been derived in the preceding chapters, is investigated in order to clarify the nature of the TCSC.

It is common practice among control system engineers and researchers to separate the design problem in a "servo" and a "regulator" problem. In the former focus is on the possibility to change the output, in this case the boost factor or the controlled reactance, by manipulating the input control signal, i.e. the timing command for the reversals. The latter design problem deals with the question of how external disturbances, e.g. changes in the line current amplitude and phase, impact on the output signal. In this chapter we will look at the transfer functions of the TCSC, which are of interest for the control system design in both these respects.

Another objective of the study is to compare the different outputs, i.e. the sampled and the averaged outputs given in (7-26) and (7-28)-(7-30).

8.1 TCSC SERVO CHARACTERISTICS

The transfer function from displacement of the reference angle for the equivalent voltage reversal, $\Delta\theta_k$, to the resulting deviation in boost factor, Δk_B, is governed by the discrete recursive state equation

$$\begin{aligned}
&\Delta\widetilde{\bar{u}}_C^{k+1}\left(-\frac{\pi}{6}\right) = A\Delta\widetilde{\bar{u}}_C^{k}\left(-\frac{\pi}{6}\right) + B_1\Delta\theta_k \\
&A = P_{next}A_{rev} \\
&B_1 = P_{next}\left(I - A_{rev}\right)P_{100}
\end{aligned} \tag{8-1}$$

This equation is obtained from (7-26) with no line current deviation.

8.1.1 Sampled state variable as output

Equations (7-28) and (7-32) in the preceding chapter yield a first output signal representing the boost factor

$$\begin{aligned}\Delta k_B\left(t_k-\frac{h}{2}\right)&=C_1\Delta\tilde{\tilde{u}}_C^k\left(-\frac{\pi}{6}\right)\\ C_1&=\begin{pmatrix}0 & -1\end{pmatrix}P_{x2d}=\frac{1}{2}\begin{pmatrix}-1 & -\sqrt{3} & 0\end{pmatrix}\end{aligned}\tag{8-2}$$

Let the time shift operator q be defined by

$$qf(k)=f(k+1)\tag{8-3}$$

Set the loss factor to $D_f=0.95$. Then the following transfer function is obtained in operator form

$$H_{\theta 1}(q)_1=\frac{\Delta k_B\left(t_k-\frac{h}{2}\right)}{\Delta\theta_k}=C_1(qI-A)^{-1}B_1=\frac{0.65q^2+1.30q+0.65}{q^3-0.95}\tag{8-4}$$

The transfer function poles appear at

$$\begin{aligned}p_1&=\sqrt[3]{D_f}=0.9830\\ p_2&=\sqrt[3]{D_f}e^{j\frac{2\pi}{3}}=-0.4915+j0.8513\\ p_3&=\sqrt[3]{D_f}e^{-j\frac{2\pi}{3}}=-0.4915-j0.8513\end{aligned}\tag{8-5}$$

corresponding to the exponential damping coefficients and frequencies given by

$$\begin{aligned}\sigma_1+j\Omega_1&=\frac{\log p_1}{h}=-5.129\quad\left(s^{-1}\right)\\ \sigma_2+j\Omega_2&=\frac{\log p_2}{h}=-5.129+j628.32\quad\left(s^{-1},rad/s\right)\\ \sigma_3+j\Omega_3&=\frac{\log p_3}{h}=-5.129-j628.32\quad\left(s^{-1},rad/s\right)\end{aligned}\tag{8-6}$$

The results are summarized in table 8-I below

Table 8-I Poles in transfer function $\Delta\theta$ -> Δk_B

pole	time constant [s]	frequency [Hz]
p_1=0.9830	0.195	0
$p_{2,3}$=-0.4915±j0.8513	0.195	±100

8.1.2 Fourier component as output

In another capacitor voltage model the average voltage component in a synchronously revolving coordinate system *IL_SYNC* is being calculated. Neglecting the line current deviations we obtain in this case from (7-30), (7-31) and (7-32)

$$\begin{aligned}
&\Delta k_B(t_k) = C_2 \Delta \widetilde{\bar{u}}_C^k\left(-\frac{\pi}{6}\right) + D_2 \Delta\theta_k \\
&C_2 = \begin{pmatrix} 0 & -1 \end{pmatrix}\left(F_{beg} + F_{end} A_{rev}\right) \\
&D_2 = \begin{pmatrix} 0 & -1 \end{pmatrix}\left[F_{end}\left(I - A_{rev}\right)P_{100} + G_\theta P_{10}\right]
\end{aligned} \tag{8-7}$$

We select the parameter $\xi=1$ and evaluate the matrices (which are independent of k_B). The recursive state difference equation then becomes

$$\begin{aligned}
&H_{\theta 2}(q) = \frac{\Delta k_B(t_k)}{\Delta\theta(t_k)} = C_2\left(qI - A\right)^{-1} B_2 + D_2 = \\
&= \frac{0.166317q^3 + 1.075091q^2 + 1.075091q + 0.166317}{q^3 - 0.95}
\end{aligned} \tag{8-8}$$

The poles in the transfer function poles are the same as before, but the numerator has been changed somewhat.

8.1.3 Time domain response

The linear response to a unit step in the control angle is shown in figure 8-1 for both output functions. The lower graph simply is a zoomed part of the upper curve. It appears from figure 8-1 that there is not any significant discrepancy between the two output signals except at their steady-state gains. The step response after half a second differs about 5 %.

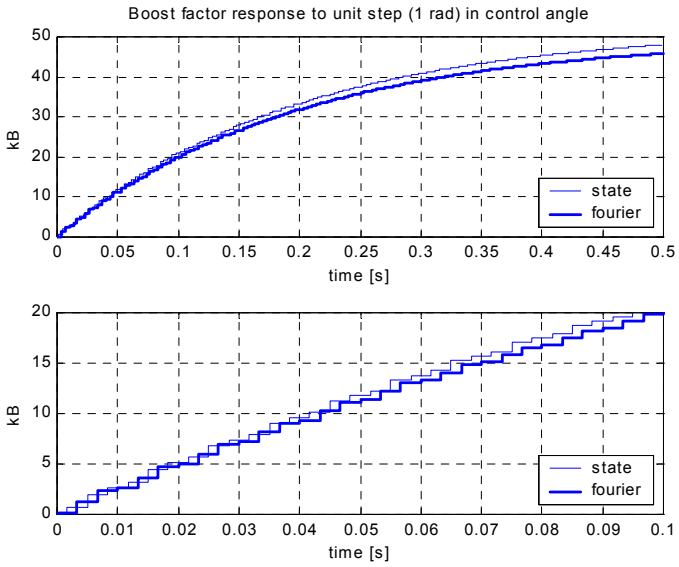

Figure 8-1 Control angle step response.

8.1.4 Frequency domain response

For sinusoidally varying signals with frequency Ω and with $|\Omega|<3\omega$ (i.e. below the Nyquist frequency) the following transfer functions is obtained from equation (8-4)

$$H_{\theta 1}(j\Omega)=\frac{\Delta k_B(t_k)}{\Delta\theta_k}=\frac{e^{j\frac{\Omega h}{2}}\Delta k_B\left(t_k-\frac{h}{2}\right)}{\Delta\theta_k}=e^{j\frac{\Omega h}{2}}\frac{0.65e^{j2\Omega h}+1.30e^{j\Omega h}+0.65}{e^{j3\Omega h}-0.95} \tag{8-8}$$

and from equation (8-8)

$$H_{\theta 2}(j\Omega)=\frac{\Delta k_B(t_k)}{\Delta\theta_k}= =\frac{0.166317e^{j3\Omega h}+1.075091e^{j2\Omega h}+1.075091e^{j\Omega h}e^{j\Omega h}+0.166317}{e^{j3\Omega h}-0.95} \tag{8-9}$$

These transfer functions have been illustrated in figure 8-2. Basically identical plots are obtained for the two models. At the assumed loss factor the system is integrating from a few Hz. At lower losses the transition frequency, where the system changes from proportional to integrating characteristics, decreases. The integrating character remains up to approximately the network frequency. A resonance peak then occurs at the double network frequency, i.e. at *100* or *120*

Hz and then the gain drops very fast at frequencies exceeding the resonance frequency.

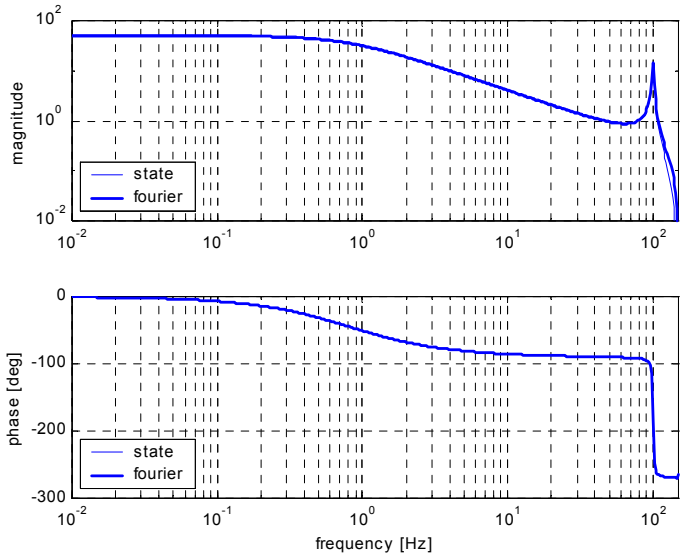

Figure 8-2 Frequency domain response for transfer function from control angle to boost factor

8.2 TCSC REGULATOR CHARACTERISTICS

It has been shown earlier in section 4-4 that it is the deviation of the reversal instants from their steady state equilibrium position that causes changes of the boost level in the TCSC. Therefore a phase shift in the line current is almost equivalent to a control angle shift and it has a big impact on the output. Also line current amplitude change influence on the TCSC boost, but with less strength.

Formally the difference from preceding section dealing with transfer functions due to changes in the control angle is that other *B* and *D* matrices will be used in the system description.

8.2.1 Phase shift in line current

We use the relative line current change as input variable to the state equation (7-26). A sudden small-signal step change of the quadrature component of the line current is identical to a phase shift.

$$\Delta\left(\arg I_L\right) = \frac{\Delta i_{Lq}^R}{\hat{I}_L} = \Delta\tilde{i}_{Lq}^R \tag{8-10}$$

Assuming no changes in the control angle we get from (7-26)

$$\Delta\widetilde{\overline{u}}_C^{k+1}\left(-\frac{\pi}{6}\right)=A\Delta\widetilde{\overline{u}}_C^{k}\left(-\frac{\pi}{6}\right)+B_2\Delta\widetilde{i}_{Lq}^{R}(t_k)$$
$$A=P_{next}A_{rev} \tag{8-11}$$
$$B_2=P_{next}\left(A_{rev}B_P+B_P^t\right)\begin{pmatrix}0\\1\\0\end{pmatrix}$$

- **Sampled output**

In the first output alternative, using the sampled state variable, we can use (8-2) again. Using the loss factor $D_f=0.95$ as before we get the transfer function

$$H_{ILq1}(q)=\frac{\Delta k_B\left(t_k-\frac{h}{2}\right)}{\Delta\widetilde{i}_{Lq}^{R}(t_k)}=-\frac{0.9531q^2+0.7371q+0.9098}{q^3-0.95} \tag{8-12}$$

The transfer function has the same poles as before. The transfer function has zeros as specified in Table 8-II.

Table 8-II Zeros in transfer function $\Delta\widetilde{i}_{Lq}^{R}\rightarrow\Delta k_B$, sampled output

zero	time constant [s]	frequency [Hz]
$z_{1,2}$=-0.3867±j0.8972	0.143	94.43

- **Fourier component as output**

The Fourier components also can be used for output. In this case we obtain from (7-30), (7-31) and (7-32)

$$\Delta k_B(t_k)=C_3\Delta\widetilde{\overline{u}}_C^{k}\left(-\frac{\pi}{6}\right)+D_3\Delta\widetilde{i}_{Lq}^{R}$$
$$C_3=\begin{pmatrix}0 & -1\end{pmatrix}\left(F_{beg}+F_{end}A_{rev}\right)$$
$$D_3=\begin{pmatrix}0 & -1\end{pmatrix}\left\{F_{end}\left(A_{rev}B_P+B_P^t\right)P_{spv}+G_{IL}\right\}\begin{pmatrix}0\\1\end{pmatrix}= \tag{8-13}$$
$$=\begin{pmatrix}0 & -1\end{pmatrix}F_{end}\left(A_{rev}B_P+B_P^t\right)\begin{pmatrix}0\\1\\0\end{pmatrix}$$

The transfer function now becomes

$$H_{ILq2} = \frac{\Delta k_B(t_k)}{\Delta \tilde{i}_{Lq}^{R}(t_k)} = -\frac{0.4997q^3 + 0.7655q^2 + 0.7417q + 0.4759}{q^3 - 0.95} \tag{8-14}$$

The transfer function has the same poles as before and zeros as specified in Table 8-III.

Table 8-III Zeros in transfer function $\Delta \tilde{i}_{Lq}^{R} \rightarrow \Delta k_B$, Fourier component output

	time constant [s]	frequency [Hz]
z_1=-1.000		$f_{Nyquist}$
$z_{2,3}$=-0.2659±j0.9389	0.136	88.18

- **Time domain step response**

The response to a 1 rad phase shift in line current (in the linearized model) is shown in figure 8-3 for both output functions. The lower curve is simply a zoomed part of the upper curve. The difference between the two approaches seems not to be very significant.

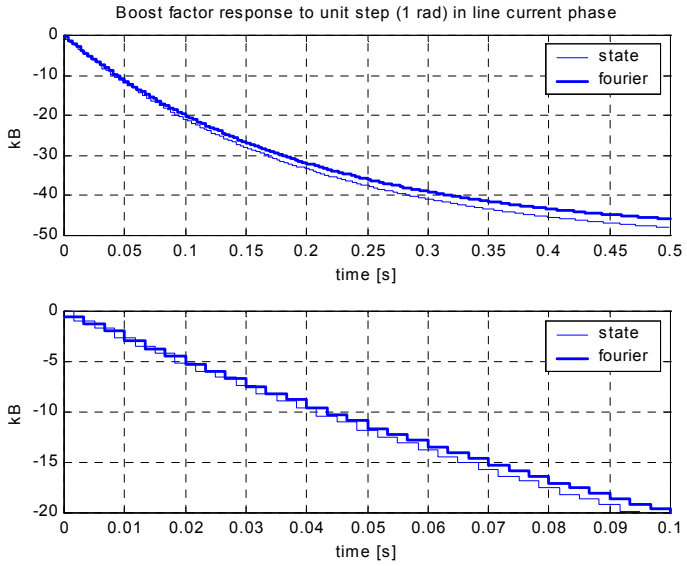

Figure 8-3 Response to line current phase shift.

- **Frequency domain response**

The frequency response of the two output signals is depicted in figure 8-4. For frequencies exceeding approximately 30 Hz a certain discrepancy can be detected between the two alternative output signals. The gain in the averaged output drops much faster at frequencies approaching 100 Hz, than the sampled output.

It should be noted that none of the transfer functions dealt with so far depends on the steady state boost factor.

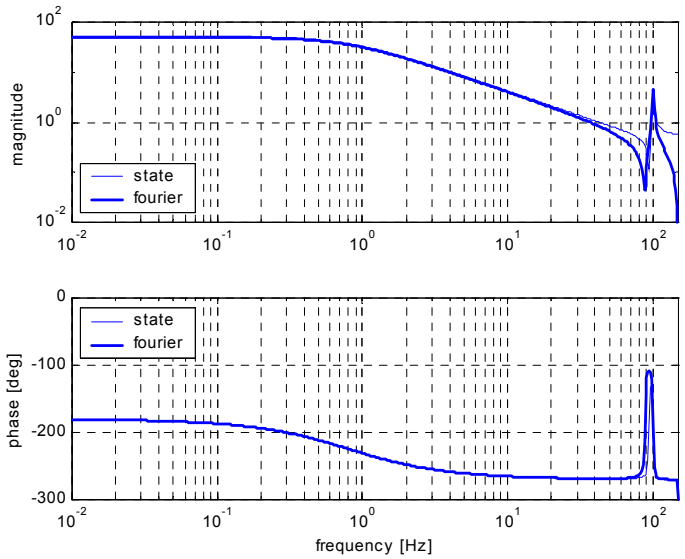

Figure 8-4 Frequency domain response in boost factor from line current phase shift.

8.2.2 Line current amplitude changes

We shall also look at the dynamics of a sudden change in line current amplitude. The procedure is similar to the one used before. The only change is that the relative line current's *d*-component is being used rather than its *q*-component. The state recursion equation in this case is similar to (8-11) but using the other line current component. Thus

$$\Delta\widetilde{\bar{u}}_C^{k+1}\left(-\frac{\pi}{6}\right) = A\Delta\widetilde{\bar{u}}_C^{k}\left(-\frac{\pi}{6}\right) + B_3\Delta\widetilde{i}_{Ld}^{R}(t_k)$$
$$A = P_{next}A_{rev} \qquad (8\text{-}15)$$
$$B_3 = P_{next}\left(A_{rev}B_P + B_P^t\right)\begin{pmatrix}1\\0\\0\end{pmatrix}$$

- **Sampled output**

In this case equation (8-2) still applies and we get the transfer function

$$H_{ILd1}(q) = \frac{\Delta k_B\left(t_k - \frac{h}{2}\right)}{\Delta \widetilde{i}_{Ld}^{\,R}(t_k)} = \frac{0.175q^2 + 0.025q - 0.015}{q^3 - 0.95} \tag{8-16}$$

The transfer function has the same poles as before and zeros as specified in Table 8-IV.

Table 8-IV Zeros in transfer function $\Delta \widetilde{i}_{Ld}^{\,R} \rightarrow \Delta k_B$, sampled output

	time constant [s]	frequency [Hz]
z_1=-1.000		$f_{Nyquist}$
z_2=0.8571	0.022	0

- **Fourier component as output**

The Fourier components also can be used for output. In this case we obtain from (7-30), (7-31) and (7-32)

$$\begin{aligned} \Delta k_B(t_k) &= C_4 \Delta \widetilde{\overline{u}}_C^{\,k}\left(-\frac{\pi}{6}\right) + D_4 \Delta \widetilde{i}_{Ld}^{\,R} \\ C_4 &= \begin{pmatrix} 0 & -1 \end{pmatrix}\left(F_{beg} + F_{end} A_{rev}\right) \\ D_4 &= \begin{pmatrix} 0 & -1 \end{pmatrix}\left\{F_{end}\left(A_{rev} B_P + B_P^t\right) P_{spv} + G_{IL}\right\}\begin{pmatrix} 1 \\ 0 \end{pmatrix} \end{aligned} \tag{8-17}$$

The transfer function now becomes

$$H_{ILq2} = \frac{\Delta k_B(t_k)}{\Delta \widetilde{i}_{Lq}^{\,R}(t_k)} = \frac{0.0898q^3 + 0.2063q^2 - 0.1649q - 0.0812}{q^3 - 0.95} \tag{8-18}$$

The poles in the transfer function are the same as before and zeros as given in Table 8-V.

Table 8-V Zeros in transfer function $\Delta\tilde{i}_{Ld}^{R} \rightarrow \Delta k_B$, Fourier component output

	time constant [s]	frequency [Hz]
z_1=0.8930	0.029	0.00
z_2=-0.3574	0.003	$f_{Nyquist}$
z_3=-2.8316	-0.003	$f_{Nyquist}$

- **Time domain response**

These transfer functions have been illustrated in figure 8-5 below. It can be recognized that the strength of the influence on the boost factor is more than one order of magnitude weaker than the impact due to changes in the control signal or in the line current phase. In fact the transfer function must have unity gain in steady state as the system equations only involve relative capacitor voltage and relative line current. A unity step in the relative line current amplitude means that the line current doubles. In steady state then also the capacitor voltage doubles as the control signals remain unchanged. That means that the change of the relative capacitor voltage also becomes unity.

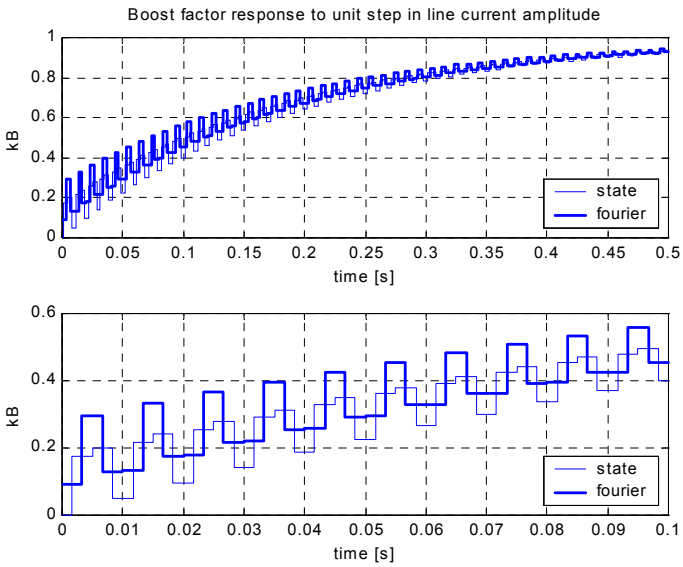

Figure 8-5 Response to line current amplitude change.

- **Frequency domain response**

Figure 8-6 shows the frequency response of the output functions derived from state variable and from the Fourier coefficient. The response is relatively weak in the range 10 - 40 Hz. A peak occurs at 100 Hz.

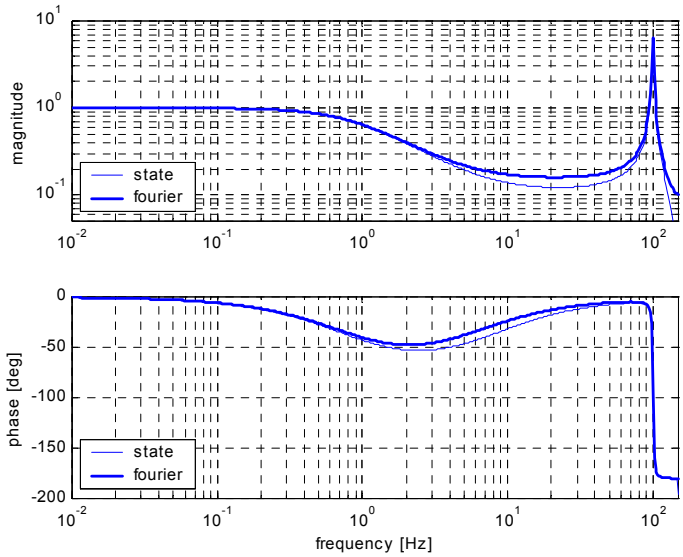

Figure 8-6 Frequency response to line current amplitude changes.

CHAPTER 9
CONTROL ARCHITECTURE FOR TCSC

9.1 MOTIVATION FOR FEEDBACK CONTROL

So far we have dealt with different aspects of modelling the dynamics of the TCSC itself. If the TCSC main circuit would be perfectly stable and insensitive to disturbances it would be possible to operate it with an open loop control, providing triggering at the steady state positions relative the line current. However, the operation conditions in a power transmission system do not provide such a stable environment, and the main circuit of the TCSC is highly dynamical and, if left uncontrolled, it can easily reach boost levels that would jeopardized the operation of the transmission network and that would be destructive for the TCSC main circuit components. We shall only remind the reader that the TCSC shall work within a wide range of current levels that varies more than one order of magnitude. Energizing of transformers and switching of transmission lines, loads and other apparatus occurs during normal operation. Further the TCSC control system must handle a lot of situations related to short-circuits in the power system. Such events require a protection system, which operates with sequences of mode changing, start, restart, bypass, limiting operation on capacitor voltage and inserted reactance etc. All these operations require that a fast-acting control system is implemented and in service. Furthermore, in the power oscillation damping applications, the reason for installing the TCSC is to actively vary the inserted reactance of the TCSC, in order to provide artificial damping of power oscillations.

Feedback control of the TCSC is required to cope with all the uncertainties that exist during its operation. We assume that an inner loop, which incorporates a "boost regulator", is used to control the inserted reactance or, equivalently, the boost factor of the TCSC. The regulator requires a measured response of the actual boost factor, which can be compared with the given boost reference.

9.2 CONTROL SYSTEM OUTLINE

The principal control system outline was discussed briefly already in chapter 4 (figure 4-13). It is a very conventional, straight-forward approach. The actual boost value is measured and compared with the boost reference. The error drives the boost regulator, which modifies the reference for the reversals by adding deviations to a synchronization signal. The latter is derived from the line current. Finally a SVR-block determines the triggering instants taking into account the reversal reference and the actual capacitor voltage and line current.

9.2.1 Dynamics of the measuring systems

It should be noted that it is not trivial to implement the measuring systems, neither to detect the actual boost level, nor to derive synchronization signals from the relatively volatile line current signal. In fact, the dynamics of these systems are as important as those of the main circuit! Therefore we shall address the problem of representing these systems in the next chapter.

9.2.2 Role of synchronization

In power electronic control a synchronization system is often implemented without further motivation. In analysis of the control system sometimes the dynamics in the synchronization system is not discussed in depth. However, it should be stressed that in reality the dynamics of the synchronization system has a great impact on the system performance.

When a synchronization system is implemented, the question arises how the device shall be tuned? Shall the synchronization system be tuned to be fast or slow relative the regulator?

One way to explain the role of the synchronization system can be described as follows:

- let the TCSC be running in steady-state
- assume that the regulator provides a train with equidistant pulses that provide timing reference for the reversals in the TCSC
- assume that the boost regulator has an integrating member which impacts on the phase of the pulse train
- the regulator then finds a suitable phase with respect to the line current where the measured boost coincides with the boost reference

Obviously no synchronization system is required for establishing the correct phase of the pulse train. The approach is identical with the simplest current regulator in DC-motor drives, where the integral part in the current regulator reflects the speed of the motor.

Now the servo performance of the TCSC can be improved by tuning the boost regulator. The synchronization system still is not required.

When the optimal tuning with respect to servo performance has been obtained we can test the TCSC with respect to its sensitivity to line current disturbances. As we know already from the study of the transfer functions, the TCSC is as sensitive to line current phase shifts as it is to control angle deviations. In order to suppress the sensitivity of the TCSC to line current phase shifts the synchronization system is introduced. The purpose is to implement a measuring device dedicated to discover phase shifts in the line current and to introduce the measured phase signal as a **feed-forward** signal into the TCSC control. Naturally the speed of the synchronization system must be at least as fast as the tuned boost control system if the feed-forward signal shall provide any improvement to the regulator performance of the TCSC.

We will follow the described approach in this thesis.

CHAPTER 10
PHASOR ESTIMATION

10.1 INTRODUCTION

Most high power electronic apparatus used in power transmission systems aim for controlling the fundamental frequency component at power frequency of current or voltage or a combination of both. In the TCSC case the controlled quantity is the boost factor, which basically is the scaled quotient between the fundamental components of capacitor voltage and line current.

It was mentioned in the preceding chapter that a synchronizing system may be implemented to detect the phase of the line current in real-time. This phase angle is used for synchronizing the capacitor voltage reversals, controlled by the boost regulator. This objective can be met by a phase locked loop (PLL).

In both cases pointed out above there is a need for real-time extraction of the fundamental frequency component of measured quantities like AC currents and voltages. Any analysis of the TCSC performance requires that the dynamics of the measuring system and the synchronization system is known and well defined. The measuring system limits the permitted gain in the feedback loop and thereby determines the attainable performance. Due to the importance of the measuring system we will devote this chapter exclusively to discussing the phasor extraction issue.

The description of the dynamics for the measuring system and the synchronization system boils down to the following problem:

- given a coordinate system, which rotates with fundamental frequency of the network. The coordinate system may be aligned e.g with the steady state line current space vector
- given a measured signal of e.g. line current or capacitor voltage; the measured signal may be a phase quantity (scalar) or a space vector (complex) representing the zero-sequence-free part of a three-phase quantity

- find a phasor, i.e. a complex function of time that is fixed or only slowly moving in the given coordinate system, which can be used to represent the fundamental frequency component of the measured quantity

This problem is closely related to linear estimation and algorithms like Recursive Least Square (RLS) estimation. We shall discuss a certain class of algorithms, which we will name "Phasor Estimators" or PE. They may operate on three-phase complex space vector signals or on single-phase scalar signals. This discussion is found in section 10.2.

Once the phasor estimation algorithm has been defined a corresponding PLL can easily be defined and its dynamics can be derived. This is dealt with in chapter 11.

10.2 PHASOR ESTIMATION FORMULAS

10.2.1 Derivation

Assume that a rotating coordinate system has been defined by a given angle time function $\theta_{CS}(t)$ which determines the angle of its real axis in the fixed coordinate system. The corresponding rotation frequency of the frame is

$$\omega_{CS}(t) = \dot{\theta}_{CS}(t) \tag{10-1}$$

First assume that the instantaneous values of the phase quantities of a certain three-phase current or voltage are being measured. Application of the transformation in (6-2) yields a space vector function $\hat{s}(t)$, which represents the zero-sequence-free part of the three-phase quantities. We shall presume that each phase quantity predominantly contains a sinusoidal component with the network frequency and a constant DC offset. The space vector function then has the form

$$\hat{s}(t) = \vec{S}^{av}(t) + \vec{S}^{p}(t)e^{j\theta_{CS}(t)} + \vec{S}^{n*}(t)e^{-j\theta_{CS}(t)} \tag{10-2}$$

where $\vec{S}^{av}(t), \vec{S}^{p}(t), \vec{S}^{n}(t)$ are complex phasors, which are ideally constants and which represent in order the average, the positive sequence and the negative sequence components respectively. A straight-forward engineering approach to extract the "constants" in (10-2) is to rearrange the equations so that the "constants" become isolated and to apply lowpass filtering on the resulting expressions. This process yields the following algorithm to obtain the phasor estimates $\tilde{\vec{S}}^{av}(t), \tilde{\vec{S}}^{p}(t), \tilde{\vec{S}}^{n}(t)$.

$$\begin{aligned}
\tilde{\tilde{S}}^{av}(t) &= H_{av}(p)\left\{\hat{s}(t) - \tilde{\tilde{S}}^{p}(t)e^{j\theta_{CS}(t)} - \tilde{\tilde{S}}^{n*}(t)e^{-j\theta_{CS}(t)}\right\} \\
\tilde{\tilde{S}}^{p}(t) &= H_{p}(p)\left\{e^{-j\theta_{CS}(t)}\left[\hat{s}(t) - \tilde{\tilde{S}}^{av}(t) - \tilde{\tilde{S}}^{n*}(t)e^{-j\theta_{CS}(t)}\right]\right\} \\
\tilde{\tilde{S}}^{n*}(t) &= H_{n}(p)\left\{e^{j\theta_{CS}(t)}\left[\hat{s}(t) - \tilde{\tilde{S}}^{av}(t) - \tilde{\tilde{S}}^{p}(t)e^{j\theta_{CS}(t)}\right]\right\}
\end{aligned} \tag{10-3}$$

The operators $H_{av}(p)$, $H_p(p)$, $H_n(p)$ represent low pass linear transfer functions of the operator $p = \frac{d}{dt}$. Equation (10-3) defines a dynamical system where $\tilde{\tilde{S}}^{av}(t), \tilde{\tilde{S}}^{p}(t), \tilde{\tilde{S}}^{n*}(t)$ are states and $\hat{s}(t), \theta_{CS}(t)$ inputs. It is advantageous to transform the states according to equation (10-4)

$$\begin{aligned}
\hat{w}^{av}(t) &= \tilde{\tilde{S}}^{av}(t) \\
\hat{w}^{p}(t) &= \tilde{\tilde{S}}^{p}(t)e^{j\theta_{CS}(t)} \\
\hat{w}^{n*}(t) &= \tilde{\tilde{S}}^{n*}(t)e^{-j\theta_{CS}(t)}
\end{aligned} \tag{10-4}$$

because the transfer functions from input signal $\hat{s}(t)$ to the new states, $\hat{w}^{av}(t), \hat{w}^{p}(t), \hat{w}^{n*}(t)$, are linear time-invariant (LTI) filters, i.e. they have constant **time-independent** coefficients. The details are given in Appendix B, where the models of the filters are given in both the time and the frequency domain. Figure 10-1 outlines the Phasor Estimator.

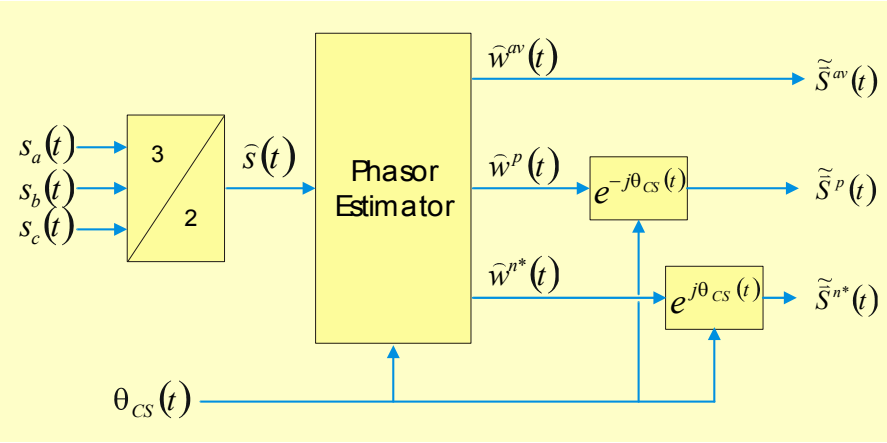

Figure 10-1 Outline of the Phasor Estimator

Further mathematical aspects related to similar filters are given in [S1].

10.2.2 Transformation to *IL_SYNC* coordinates

The connection between the TCSC main circuit model and the transmission system and the control system is described by equation (7-30). The electrical quantities in the transmission system then are defined in *IL_SYNC* coordinates. Accordingly, in our analysis, the Phasor Estimators will operate in the *IL_SYNC* environment and it appears to be adequate to transform the PE models also to this frame. The following input and outputs then are used

$$\hat{s}^R(t) = \hat{s}(t)e^{-j\omega_N t} = \vec{S}^{av}(t)e^{-j\omega_N t} + \vec{S}^{p}(t) + \vec{S}^{n*}(t)e^{-j2\omega_N t} \tag{10-5}$$

and

$$\begin{aligned}
\hat{v}^{av}(t) &= \tilde{\tilde{S}}^{av}(t)e^{-j\omega_N t} \\
\hat{v}^{p}(t) &= \tilde{\tilde{S}}^{p}(t) \\
\hat{v}^{n*}(t) &= \tilde{\tilde{S}}^{n*}(t)e^{-j2\omega_N t}
\end{aligned} \tag{10-6}$$

Figure 10-2 shows the modifications necessary and Appendix C gives the modified models in frequency and time domains.

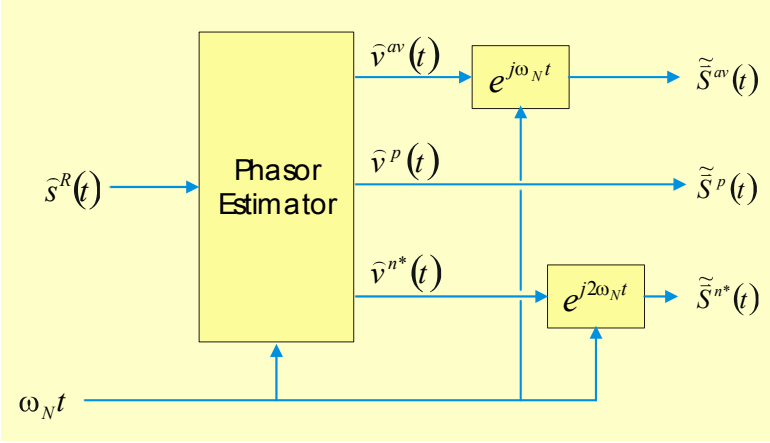

Figure 10-2 Outline of the Phasor Estimator operating in IL_SYNC coordinates

Example 10-1

A phasor estimator for 50 Hz is equipped with lowpass filters of first order. It has

- average filter with 3 dB bandwidth at 10 Hz
- positive sequence filter with 3 dB bandwidth at 20 Hz

- negative sequence filter with 3 dB bandwidth at 5 Hz

Thus

$$H_{av}(p)=\frac{1}{1+\frac{p}{2\pi 10}} \qquad H_{p}(p)=\frac{1}{1+\frac{p}{2\pi 20}} \qquad H_{n}(p)=\frac{1}{1+\frac{p}{2\pi 5}} \tag{10-7}$$

The frequency domain characteristics of the phasor estimator filter in the *IL_SYNC* coordinates are depicted in figure 10-3.

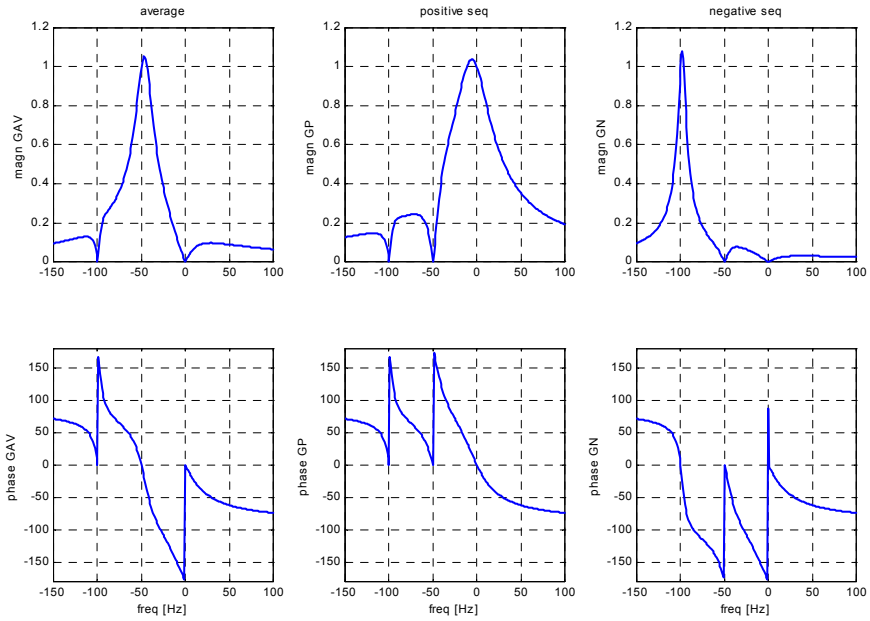

Figure 10-3 Frequency domain characteristics of Phasor Estimator operating in IL_SYNC coordinates.

It is worth noting that each output of the phasor estimator has unity gain and zero phase shift at pure constant, positive sequence or negative sequence input signals respectively. The bandwidth of the lowpass filters for the different output signals is reflected in the graphs.

In figure 10-4 the time-domain responses to a sudden constant input signal in the *IL_SYNC* system is shown. This input signal corresponds to a suddenly applied three-phase signal having only a positive sequence component. It can be seen that the steady-state response appears in the $\hat{v}_p$ signal. The rise time constant for this signal is approximately *10 ms*. The settling time for each component is inversely proportional to the bandwidth of its associated filter.

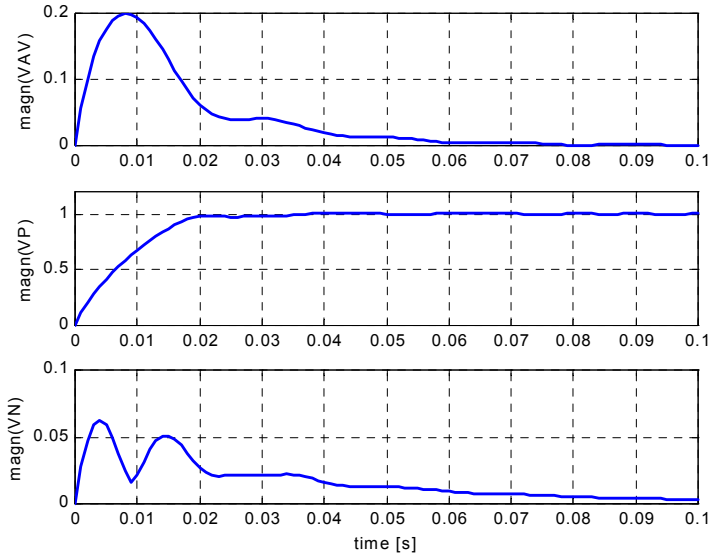

Figure 10-4 Time domain response to step in IL_SYNC input signal.

- **Transfer functions from component to component**

In figure 10-2 the Phasor Estimator has a complex vector input signal and complex vector output signals. In the TCSC control system we are primarily interested in the positive sequence phasor output signal. The model of the TCSC, however, is formulated with the components of the line current as inputs and the components of the positive sequence components as outputs. For this reason we would like to adapt the transfer functions from complex input to complex output into transfer functions from either vector component in the input signal to either component in the output signal. Figure 10-5 depicts these desired arrangement.

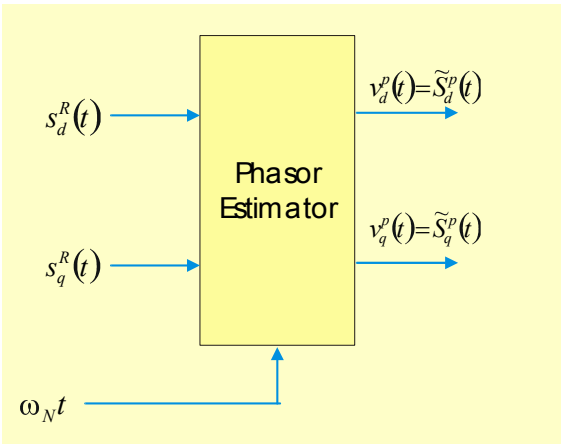

Figure 10-5 Phasor Estimator using real components as input and output signals.

The complex-to-complex transfer function $G_p^R(j\Omega)$ is given in (C-8) in Appendix C. There it also shown that the following rules apply

$$
\begin{aligned}
G_{PE}^{R,d->d}(j\Omega) &= \frac{\widetilde{S}_d^{\,p}(j\Omega)}{s_d^R(j\Omega)} = \frac{G_p^R(j\Omega)+\left[G_p^R(-j\Omega)\right]^*}{2} \\
G_{PE}^{R,d->q}(j\Omega) &= \frac{\widetilde{S}_q^{\,p}(j\Omega)}{s_d^R(j\Omega)} = \frac{G_p^R(j\Omega)-\left[G_p^R(-j\Omega)\right]^*}{2j} \\
G_{PE}^{R,q->d}(j\Omega) &= \frac{\widetilde{S}_d^{\,p}(j\Omega)}{s_q^R(j\Omega)} = -\frac{G_p^R(j\Omega)-\left[G_p^R(-j\Omega)\right]^*}{2j} \\
G_{PE}^{R,q->q}(j\Omega) &= \frac{\widetilde{S}_q^{\,p}(j\Omega)}{s_q^R(j\Omega)} = \frac{G_p^R(j\Omega)+\left[G_p^R(-j\Omega)\right]^*}{2}
\end{aligned}
\tag{10-8}
$$

Example 10-2

Figure 10-6 shows the transfer functions from component to component of the Phasor Estimator described in example 10-1.

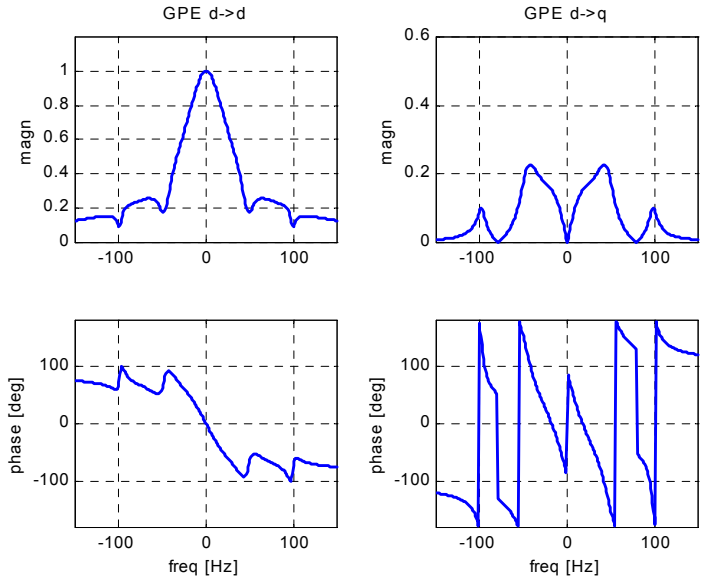

Figure 10-6 Transfer functions between the components in input and output vectors.

The amplitude curve of course becomes symmetrical along the frequency axis as we are dealing with transfer functions between real functions.

10.2.3 Single-phase vs three-phase measurements

- **General discussion**

So far it has been assumed that the input signal to the Phasor Estimator is a complex space vector representing a three-phase quantity. However in practical implementation of a TCSC there are good reasons to utilize a control system, which regulates the inserted reactance on a phase-by-phase basis. In transmission systems the line current is not necessarily three-phase symmetrical. The phase current magnitudes may differ both due to single-phase loads and because of use of long non-transposed transmission lines. The same reasons also may cause differences in the mutual phase displacement. Finally, the TCSC control system must be able to operate adequately, when single-line to ground faults occur and cause large asymmetry in the loading.

A TCSC single-phase control system obviously requires single-phase measuring and synchronization systems. So how can single-phase phasor estimation be achieved within the concept described in the preceding sections?

Any phasor estimation requires that a rotating coordinate system, where the phasor can reside, has been defined. Let us assume that the earlier used coordinate system, defined by (10-1), has been selected. Further assume that a scalar input signal, *s(t)*, comprises an offset component and a sinusoidal contribution as stated in equation (10-9)

$$s(t) = S^{av} + \mathrm{Re}\left[\vec{S}^{ph} e^{j\theta_{CS}(t)}\right] = S^{av} + \frac{\vec{S}^{ph}}{2} e^{j\theta_{CS}(t)} + \frac{\vec{S}^{ph*}}{2} e^{-j\theta_{CS}(t)} \qquad (10\text{-}9)$$

We would like to focus on determining the phasor $\vec{S}^{ph}(t)$, which should be a complex constant or a complex function that varies slowly with time.

It is might be anticipated that estimation of three-phase signals inherently can be made faster than single-phase measurements. However, we will see below that this belief is not true.

It is obvious that the magnitude and phase of a scalar measured quantity, e.g. a phase current in a transmission line, cannot be determined if we are given only one instantaneous measured value. This applies even if the signal does not contain any harmonic distortion. Measuring all three phase quantities certainly defines a definite value of the space vector, but it is not possible to separate the positive and negative sequence components. This is valid even if one knows that the constant offset average component is zero.

Next it shall be shown that it actually takes approximately the same time to determine a phasor independent of whether a single-phase or a three-phase approach has been selected.

- **Single phase phasor estimation**

Figure 10-1 shows a Phasor Estimator, which takes an input signal $\hat{s}(t)$ formed by the three phase quantities and which accordingly normally is complex-valued. The PE block has three outputs $\hat{w}^{av}(t), \hat{w}^{p}(t), \hat{w}^{n*}(t)$. The input-output relations are governed by linear time-invariant (LTI) transfer functions. These are explicitly defined by formulas (B-6) and (B-7) in Appendix B.

We may think of entering a real-valued input signal, e.g. a measured phase quantity, to the phasor estimator. If it contains a DC offset signal plus a sinusoidal function of $\theta_{CS}(t)$ it will have the form given in equation (10-9). The transfer functions from the real-valued input, i.e. $s(t)$, to the real-values of the output signals, i.e. to $y_{av}(t) = \mathrm{Re}\left[\hat{w}^{av}(t)\right]$, $y_{p}(y) = \mathrm{Re}\left[\hat{w}^{p}(t)\right]$ and $y_{n}(t) = \mathrm{Re}\left[\hat{w}^{n*}(t)\right]$, still are given by the earlier mentioned formulas in Appendix B.

However, we may consider the real-valued input signal to be generated by the phasor $\vec{S}^{ph}$, which we want to extract. A natural approach then is to multiply the complex output function $\hat{w}^{p}(t)$ by the exponential $e^{-j\theta_{CS}(t)}$ as indicated in figure 10-1. Then the phasor $\frac{\vec{S}^{ph}}{2}$ is obtained as output signal in steady state. In order to estimate the desired phasor $\vec{S}^{ph}$ a gain factor 2 must be applied as shown in figure 10-7.

When the input signal is real-valued it can be considered to be a superposition of a positive and a negative sequence component with the same magnitude. Then there are no good reasons to utilize different characteristics for the lowpass filters for positive and negative sequence output signals. Accordingly we postulate that the filters are equal

$$H_{p}(p) = H_{n}(p) = H_{ph}(p) \tag{10-10}$$

Inspection of the algorithm in (10-3) and (10-4) indicates that the output signal $\tilde{\vec{S}}^{av}(t)$ then becomes real and the output signals $\hat{w}^{p}(t), \hat{w}^{n*}(t)$ form a conjugate pair. The negative sequence phasor output thus gives redundant information.

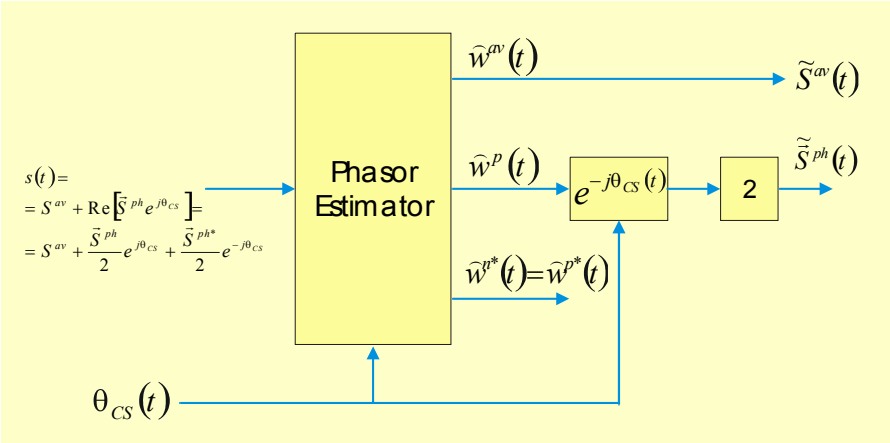

Figure 10-7 Real-valued signal entering the Phasor Estimator.

- **Comparison between single-phase and three-phase estimation**

From the above it can be concluded that the single-phase measuring system can be modelled with the **same linear, time-invariant model** as in the three-phase case. The difference is that in the single-phase case the **input signal contains both positive and negative sequence components** of equal magnitude. Thus the following outputs will be obtained when we assume that

$$\theta_{CS}(t) = \omega_{CS} t \tag{10-11}$$

Three-phase Phasor Estimation

input signal: $Ae^{j\omega t}$

estimated phasor output signal: $AG_p(j\omega)e^{j(\omega-\omega_{CS})t}$

Single-phase Phasor Estimation

input signal: $\mathrm{Re}\left[Ae^{j\omega t}\right]$

estimated phasor output signal: $AG_p(j\omega)e^{j(\omega-\omega_{CS})t} + A^*G_p(-j\omega)e^{-j(\omega+\omega_{CS})t}$

It can be seen that an additional term is obtained in the single-phase case as compared to the three-phase case. The low-pass characteristics of the filters in the Phasor Estimator cause the transfer function $G_p(j\omega)$ to mainly transfer frequencies ω close to frequency $+\omega_{CS}$ and to suppress all other frequencies. It has a zero at frequency $-\omega_{CS}$. Accordingly the contribution of the additional term is very small. The suppression becomes more effective when the bandwidth in the phasor filters is lowered, but at the same time the speed of response of the phasor estimation slows down.

To conclude:

- the main contribution to the estimated phasor output is identical for the single-phase and the three-phase cases
- the single-phase Phasor Estimator output contains an additional, small, undesired disturbance term.

The formulas related to the single-phase Phasor Estimator are given in Appendix D.

Example 10-3

Let the Phasor Estimator operate to extract a 50 Hz fundamental frequency component from a scalar input signal. The filters are second order filters with damping ζ=0.866 and with 3 dB bandwidths at 10 Hz and 15 Hz for the average and phasor outputs respectively. The filter transfer functions then are

$$H_{av}(p)=\frac{1}{\left(\frac{s}{79.92}\right)^2+1.732\left(\frac{s}{79.92}\right)+1}$$
$$H_{ph}(p)=\frac{1}{\left(\frac{s}{119.89}\right)^2+1.732\left(\frac{s}{119.89}\right)+1} \qquad (10\text{-}12)$$

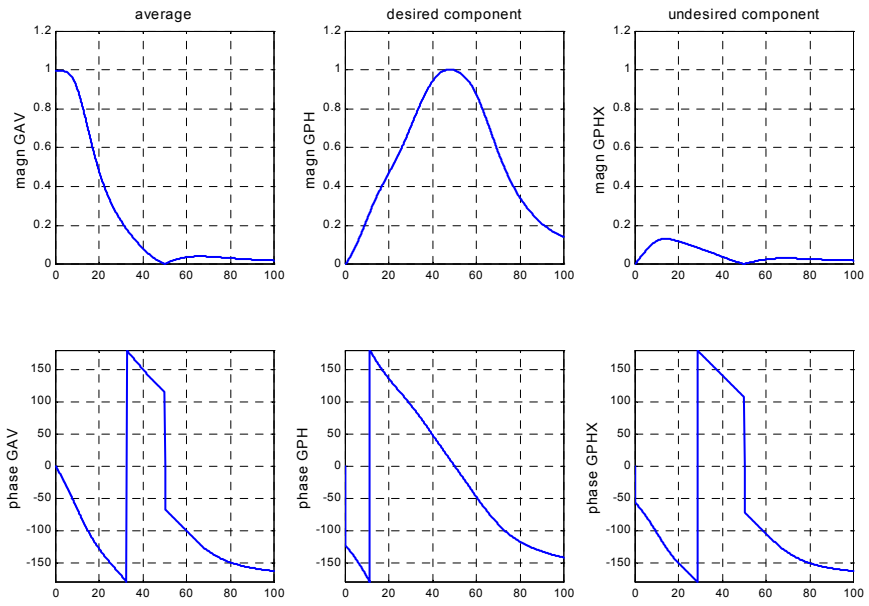

Figure 10-8 Transfer functions of a single-phase Phasor Estimator.

The transfer functions in the frequency domain of this Phasor Estimator are depicted in figure 10-8. For scalar input signals only positive frequency is of interest.

It can be seen that the output signal extracts the generating phasor in a band centred around 50 Hz and with 3 dB damping at about ±15 Hz. The phase shift in the filter is very linear (Bessel filter). Offset signals in the input do not contribute to the output signal neither in the desired nor in the undesired component. The undesired output signal has low gain around the centre frequency and at harmonic frequencies.

In Appendix D formulas have been derived for the time domain model of the single-phase Phasor Estimator. We will assume that the same filter arrangement is used as above. The step responses in the phasor output following a sudden application of cosine and sine input signals having the coordinate system rotation frequency are shown in figure 10-9. The response for a three-phase Phasor Estimator having an exponential positive sequence input signal also has been included for comparison

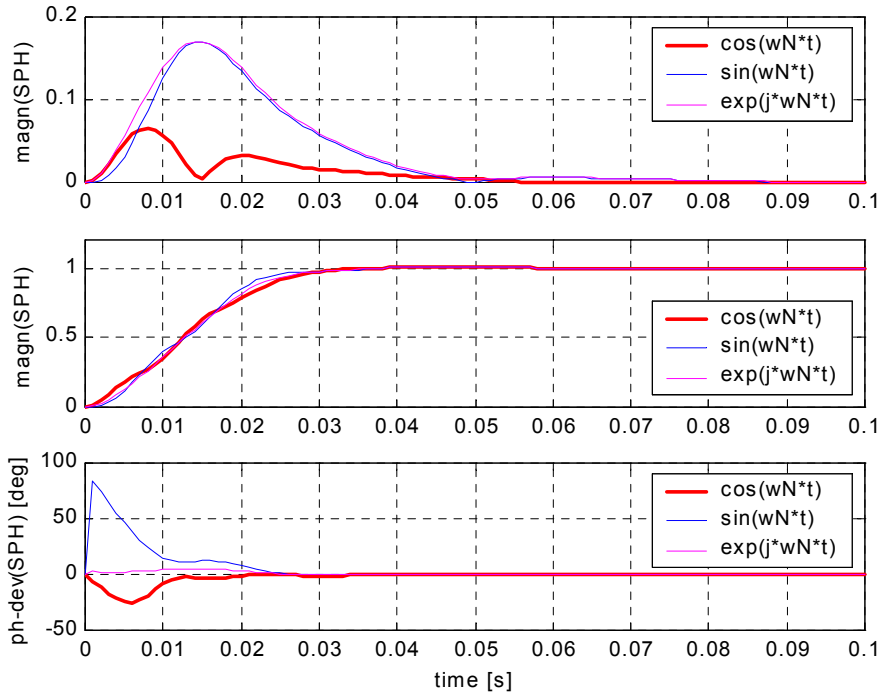

Figure 10-9 Time domain response to suddenly applied scalar input signal (reponse to exponential input in 3-ph PE included for comparison)

The graph shows that the amplitude response is very similar in all cases. The angle information depends on the phase of the applied scalar input signal. After about half the output signal rise time the phase error is rather small.

- **Model used in the simulation of TCSC**

It has been shown that the transfer functions characterising the Phasor Estimators for single- and three-phase input signals are identical in the frequency domain. Further the undesired contribution to the phasor output signal that appears in the single-phase case is suppressed by the filters to a large extent. Due to this reason it appears adequate to utilize the three-phase model of the Phasor Estimator, which takes the complex vector time function as input signal. For practical reasons we use the formulation in the *IL_SYNC* coordinate system.

10.2.4 Phasor Estimation and RLS algorithms

The phasor estimation problem also can be formulated as an estimation problem, which can be attacked by the Recursive Least Square (RLS) method. In the case that the input signal is scalar as defined in (10-9) we can write

$$s(t) = S^{av} + \mathrm{Re}\left[\vec{S}^{ph} e^{j\theta_{CS}(t)}\right] = S^{av} + S_d^{ph}\cos\theta_{CS}(t) - S_q^{ph}\sin\theta_{CS}(t) \tag{10-13}$$

A number of measurements are being collected at time instants $\{t_k\}$. At these time instants the regressors $\varphi(t_k)$ and the measured values $s(t_k)$ are known. The regressors are given by

$$\varphi^t(t_k) = \begin{pmatrix} 1 & \cos\theta_{CS}(t_k) & -\sin\theta_{CS}(t_k) \end{pmatrix} \tag{10-14}$$

The parameter vector

$$\Theta = \begin{pmatrix} S^{av} & S_d^{ph} & S_q^{ph} \end{pmatrix}^t \tag{10-15}$$

shall be estimated such that

$$\left\| s(t_k) - \varphi_k(t_k)\Theta \right\| = \min \tag{10-16}$$

The RLS algorithm, which solves this problem, is described in almost any textbook dealing with linear estimation, e.g. in [B2]. The modified version, which includes a forgetting factor, permits adjustment of the bandwidth of the estimator. The solution in the RLS algorithm has the same form as the solution to the Kalman problem. The correspondence is discussed in [B3]. In the continuous case this means that the derivative of the estimate is given by the product of the

Kalman gain and the "innovation", i.e. error between the measured and the estimated signal.

$$\frac{d\Theta}{dt} = K(t)\left[s(t) - \varphi^t(t)\Theta\right] \tag{10-17}$$

The components in the Kalman gain vector converge rather fast towards a constant for the average component and towards sinusoidal functions of time with the coordinate system rotation frequency. The periodic, steady state solution corresponds to a linear time-invariant filter given in Appendix E. The system matrix of this filter has some resemblance of the filters that has been discussed in Appendix D. The filter performance also is quite similar, when looked upon in frequency or time domain.

In an interesting further development of the measuring technique following this track it should be possible to utilize not only the steady state solution of the RLS algorithm, but rather the complete solution. The process, from which the input signals are extracted, then is monitored and when extraordinary events occur the RLS algorithm is resetted, with suitable initializations of the Kalman gain factors. A similar idea has been applied in a measuring system described in [S2].

CHAPTER 11

BOOST MEASUREMENT AND SYNCHRONIZATION

The study approach selected in this thesis is to treat the TCSC as a three-phase device operating in a three-phase network. The TCSC model described in the previous chapters also has been adapted to that objective. In this chapter dynamical models for the boost measuring and synchronization systems shall be derived. In order to fit these models to the main circuit representation it is preferred to use a Phasor Estimator model that takes a complex-valued input that represents a space-vector in the *IL_SYNC* coordinate system. In real installations the Phasor Estimators used may be implemented as single-phase devices, but we have shown in the preceding chapter that the use of a vector-based three-phase representation does not introduce any significant error. This conclusion applies at least as long as the cut-off frequencies in the low-pass filters in the Phasor Estimators are less than about one third of the rated network frequency.

11.1 BOOST FACTOR MEASURING SYSTEM

The model of the TCSC operates in the *IL_SYNC* system. Accordingly the line current vector in steady state is real, $\hat{I}_L$. Let the steady state boost factor be k_B so that the capacitor voltage vector is negative imaginary, $\hat{U}_C = \frac{k_B \hat{I}_L}{j\omega_N C}$. The fundamental frequency components of the line current and the capacitor voltage are measured by identical Phasor Estimators utilizing the **same** rotating coordinate system. The measuring system creates the complex quotient between the estimated capacitor voltage and the line current phasors and extracts the imaginary part of the result. Figure 11-1 outlines the boost measuring system. In the model we utilize the relative quantities as defined in (7-20) and (7-21). The measured boost factor then becomes

$$k_B + \Delta k_{B,m} = -\mathrm{Im}\left\{ \frac{PE\left[e^{j\Delta\theta}\left(-jk_B + \Delta\tilde{u}^R_{Cd,av} + j\Delta\tilde{u}^R_{Cq,av}\right)\right]}{PE\left[e^{j\Delta\theta}\left(1 + \Delta\tilde{i}^R_{Ld} + j\Delta\tilde{i}^R_{Lq}\right)\right]} \right\} \tag{11-1}$$

where PE signify the Phasor Estimation procedure and $\Delta\theta$ represents the phase error between the undisturbed line current vector and the coordinate system used by the Phasor Estimators. The quotient is independent of the coordinate system, if the Phasor Estimator is linear and the dynamics in $\Delta\theta$ can be neglected, i.e. if the synchronizing PLL is slow. Linearisation of the expression in (11-1) then proceeds as follows

$$\begin{aligned} k_B + \Delta k_{B,m} &= -\mathrm{Im}\left\{ \frac{PE\left(-jk_B + \Delta\tilde{u}^R_{Cd,av} + j\Delta\tilde{u}^R_{Cq,av}\right)}{PE\left(1 + \Delta\tilde{i}^R_{Ld} + j\Delta\tilde{i}^R_{Lq}\right)} \right\} \approx \\ &\approx -\mathrm{Im}\left\{ PE\left(-jk_B + \Delta\tilde{u}^R_{Cd,av} + j\Delta\tilde{u}^R_{Cq,av}\right) * PE\left(1 - \Delta\tilde{i}^R_{Ld} - j\Delta\tilde{i}^R_{Lq}\right) \right\} \approx \\ &\approx k_B - G^{R,d->q}_{PE}\Delta\tilde{u}^R_{Cd,av} - G^{R,q->q}_{PE}\Delta\tilde{u}^R_{Cq,av} - k_B G^{R,d->d}_{PE}\Delta\tilde{i}^R_{Ld} - k_B G^{R,q->d}_{PE}\Delta\tilde{i}^R_{Lq} \end{aligned} \tag{11-2}$$

Here the transfer functions for the Phasor Estimators used have been denoted with the lower index *'PE'*. Using the symmetry properties of the component transfer functions, i.e. $G^{R,d->d}_p = G^{R,q->q}_p$, $G^{R,d->q}_p = -G^{R,q->d}_p$, we get

$$\boxed{\Delta k_{B,m} = -G^{R,q->q}_{PE}\left(\Delta\tilde{u}^R_{Cq,av} + k_B\Delta\tilde{i}^R_{Ld}\right) - G^{R,d->q}_{PE}\left(\Delta\tilde{u}^R_{Cd,av} - k_B\Delta\tilde{i}^R_{Lq}\right)} \tag{11-3}$$

The Phasor Estimator transfer functions to be utilized are given in (10-8).

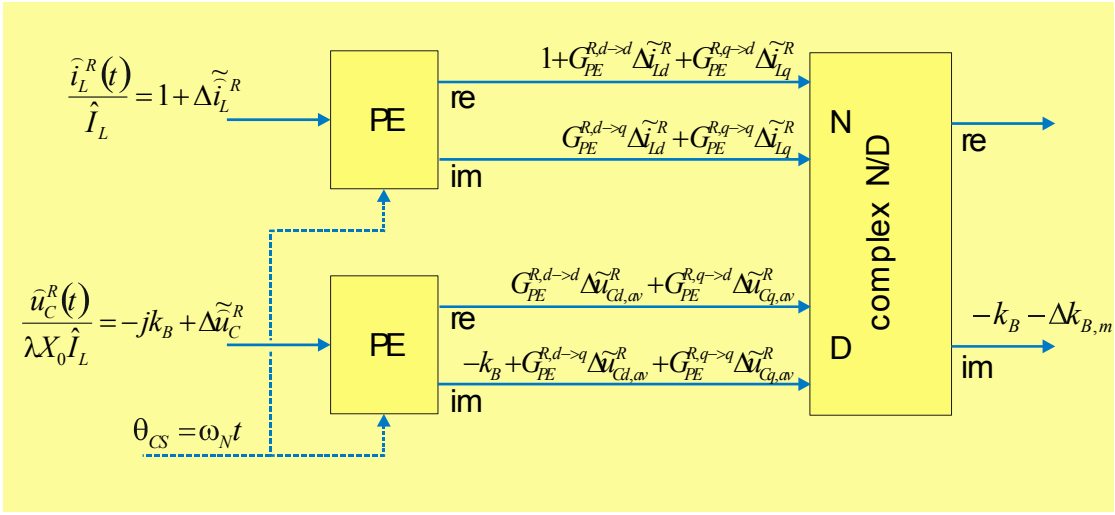

Figure 11-1 Outline of the boost measuring system.

Example 11-1

Figure 11-2 shows an example where the measured capacitor voltage and the line current are both complex exponentials, which abruptly *(t=0.010 s)* change their amplitude and phase *(Δu_{Crel}=-0.03-j0.06, Δi_{Lrel}=0.025+j0.02)*. In the three graphs Phasor Estimators with varying bandwidth have been used. In the upper graph the 3 dB bandwidth is 15 Hz in the middle 20 Hz and in the lower graph it is 25 Hz. It appears reasonable to select the lower bandwidth of 15 Hz. The rise time is about 15 ms and the overswing is in the range of 15-20%. A certain static error occurs in the linearized model due to the approximation of the complex division formula.

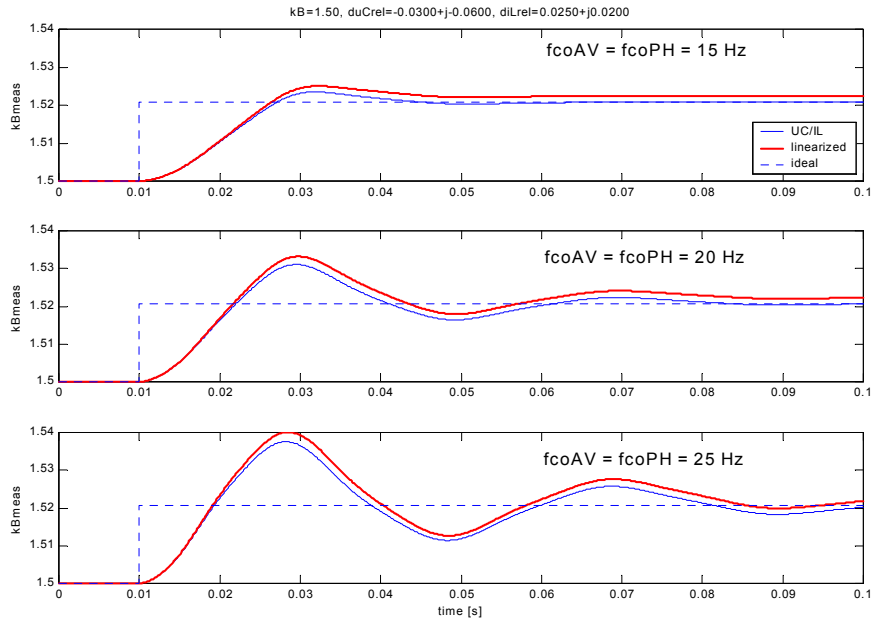

Figure 11-2 Step response in boost factor measurement. Phasor Estimators with varying bandwidth.

An important feature in applications related to series capacitors is the impact of offset voltages appearing across the capacitor.

Figure 11-3 presents the result of a simulation where *0.1 pu* DC offset voltage step is suddenly *(t=0.010 s)* added to the capacitor voltage. The figure shows that the disturbance causes a drop in the boost factor response signal with about *0.02 pu* during approximately *20-25 ms* if the cutoff frequency is *15 Hz*.

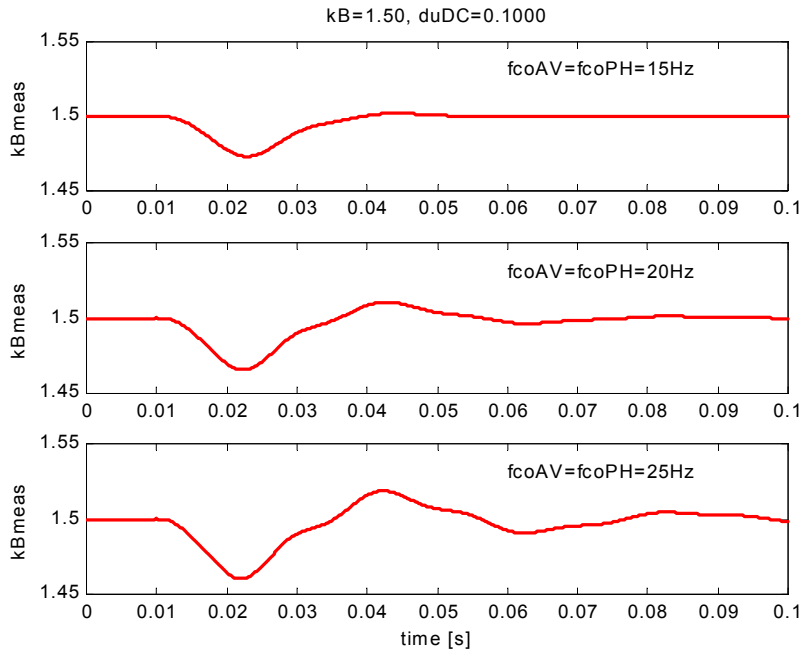

Figure 11-3 Response in measured boost factor to DC offset step in capacitor voltage. Phasor Estimators with different bandwidth.

11.2 PHASE-LOCKED LOOP (PLL)

It is natural to look at the TCSC to be a device into which a line current is being injected and which generates and inserts a voltage in series with the line. Therefore, when the control system needs some synchronization with the network, the phase will be related to the phase of the **line current**. The capacitor voltage is a most volatile signal, which cannot be used to provide a stable and robust phase reference signal for the control system.

The control system architecture already has been discussed in chapter 9. It was pointed out that the role of the synchronization system, from a boost factor control perspective, is to provide a feed-forward signal, which makes the TCSC less sensitive to line current phase shifts.

The objective of extracting the argument of the line current of course is closely associated with the phasor estimation problem.

11.2.1 Getting the line current phase directly from a PE

As a first approach one may consider to simply provide the measured line current signal to a Phasor Estimator and detect the phase of the extracted phasor. Figure 11-4 illustrates this approach.

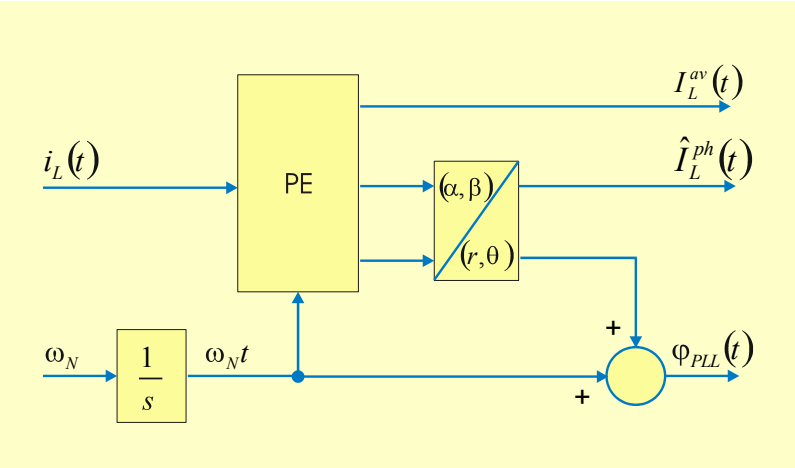

Figure 11-4 Direct derivation of synchronization angle from PE.

In steady state the relative line current is unity. Therefore the transfer function from phase shift in the line current in the *IL_SYNC* coordinate system to change in PLL angle is given by the transfer function $G_{PE}^{R,q->q}(j\Omega)$ in (10-8). Likewise, the transfer function from change in relative line current amplitude to change in the PLL angle is $G_{PE}^{R,d->q}(j\Omega)$. In these formulas the frequency Ω is the frequency of the line current components in the *IL_SYNC* coordinate system.

Example 11-2

Figure 11-5 shows results of time domain simulations using the approach shown in figure 11-4. A sudden phase shift of *0.1 rad* was applied to a sinusoidal single phase signal.

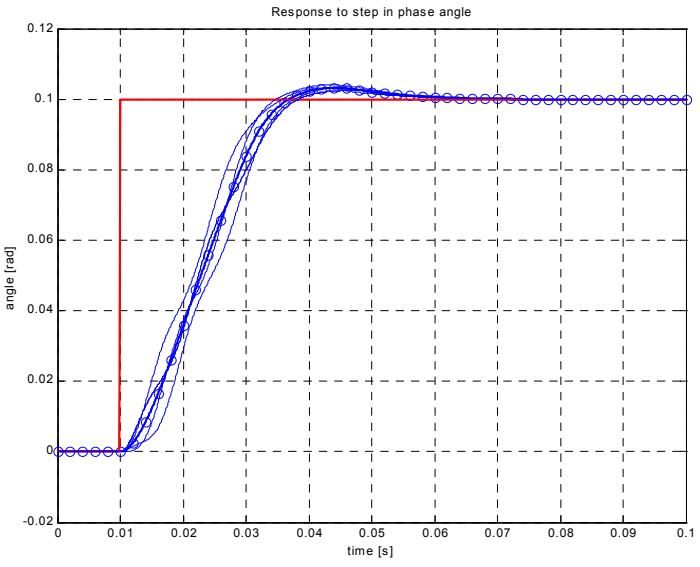

Figure 11-5 Response to phase angle shift.

The phase step inception was initiated at varying point-of-wave during a half cycle of the input wave. Second order Bessel filters with *3 dB* cutoff frequency at *15 Hz* were utilized. Corresponding results for the case that a complex-valued input signal was used also are shown. They are marked by small circles in the graph.

The result indicates that the rise time varies in the range *15-25* ms and that the overshoot is below *5 %* in this case.

The frequency domain transfer function of the Phasor Estimator used above is shown in figure 11-6. The transfer function $G_{PE}^{R,d->q}(j\Omega)$ is marked '*DiLd->phase'* and the transfer function $G_{PE}^{R,q->q}(j\Omega)$ '*DiLq->phase'*. The angle measuring system has a bandwidth *(–3dB)* of approximately *20 Hz*.

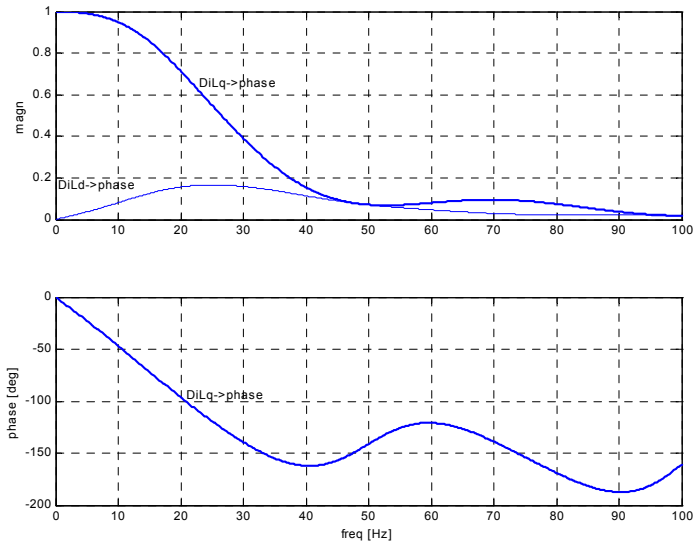

Figure 11-6 Frequency domain characteristics of the Phasor Estimator.

11.2.2 PLL with frequency regulator

Another more conventional approach is shown in figure 11-7. In this case the coordinate transformation angle is being generated by integration of a frequency signal delivered by a frequency controller. The latter is a proportional-integrating (PI) regulator having the argument of the estimated line current phasor as its input signal. The frequency regulator keeps integrating until the estimated phasor argument equals zero.

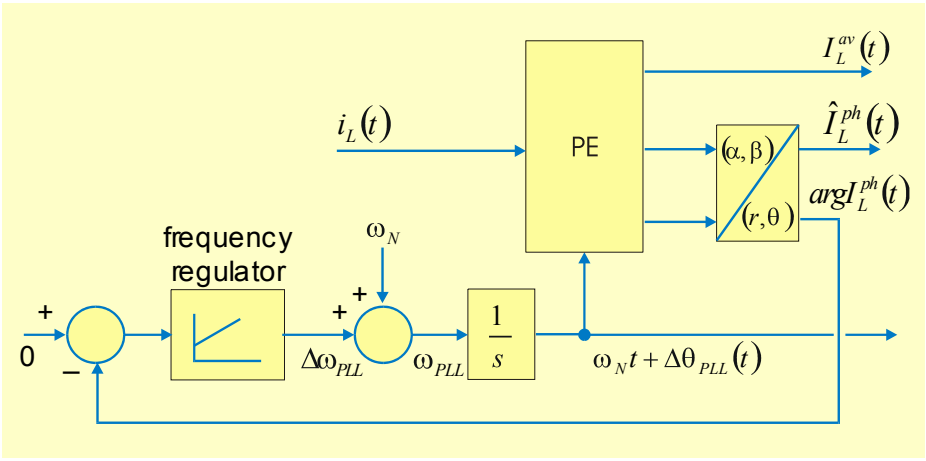

Figure 11-7 PLL with frequency regulator.

For modeling purposes let us introduce the PLL deviation angle $\Delta\theta_{PLL}(t)$, which denotes the deviation between the estimated line current argument, as delivered by the PLL, and the angle of the undisturbed line current space vector. Naturally the deviation angle $\Delta\theta_{PLL}(t)$ can not be measured in a real application as it refers to the coordinate system associated with the **undisturbed** line current phasor, which is an artificial quantity not available in an installation. The rotating coordinate system of the real-life Phasor Estimator therefore utilizes the estimated line current argument from the PLL. The input signal to the frequency regulator then becomes

$$\Delta\varphi_{PLL}(t) = \arg\left\{\left(1+\Delta\tilde{\bar{i}}_L^{\,R}\right)e^{j\omega_N t}\left[e^{-j(\omega_N t+\Delta\theta_{PLL})}\right]\right\} \approx -\Delta\theta_{PLL}(t) + \Delta\tilde{i}_{Lq}^{\,R}(t) \qquad (11\text{-}4)$$

The block diagram in figure 11-8 illustrates the dynamical model of the PLL.

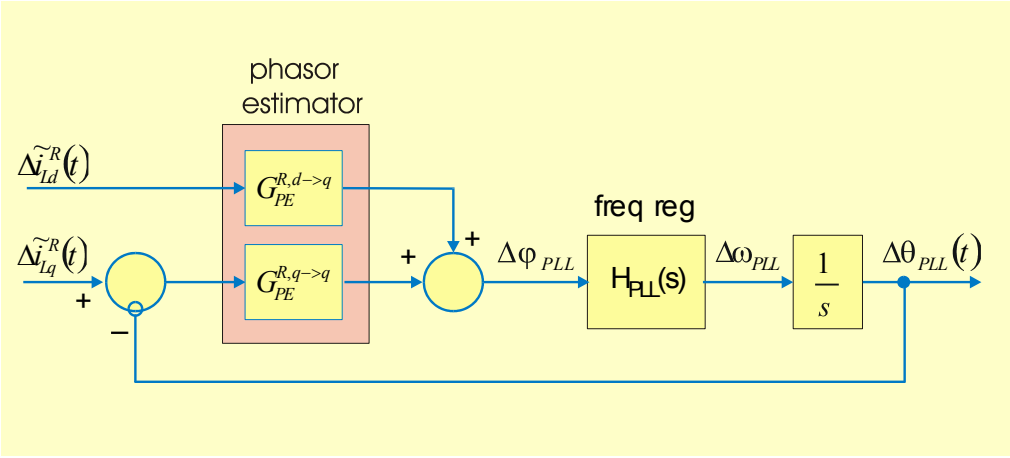

Figure 11-8 Dynamical model of PLL .

The transfer function of the frequency regulator has been denoted $H_{PLL}(s)$. Most often it would contain a PI link as its dominating constituent, but sometimes also other links also may be inserted in order to adjust the phase shift of the transfer function.

The closed loop frequency domain transfer functions become

$$H_{PLLd}^{cl}(s) = \frac{\Delta\theta_{PLL}}{\Delta\tilde{i}_{Ld}^{R}} = \frac{G_{PE}^{R,d->q}(s)H_{PLL}(s)}{s + G_{PE}^{R,q->q}(s)H_{PLL}(s)}$$
$$H_{PLLq}^{cl}(s) = \frac{\Delta\theta_{PLL}}{\Delta\tilde{i}_{Lq}^{R}} = \frac{G_{PE}^{R,q->q}(s)H_{PLL}(s)}{s + G_{PE}^{R,q->q}(s)H_{PLL}(s)} \quad (11\text{-}5)$$

The PLL can be represented in the time-domain by a linear time-invariant state space model.

$$\dot{x}_{PLL} = A_{PLL}x_{PLL} + B_{PLL}\begin{pmatrix}\Delta\tilde{i}_{Ld}^{R}\\ \Delta\tilde{i}_{Lq}^{R}\end{pmatrix}$$
$$\Delta\theta_{PLL} = C_{PLL}x_{PLL} \quad (11\text{-}6)$$

The derivation of this model is described in Appendix F.

Example 11-3

Let us assume that the frequency regulator is of the proportional-integrating type with the transfer function

$$H_{PLL}(s) = 2\pi\, k_{PLL}\frac{1 + sT_{PLL}}{sT_{PLL}} \quad (11\text{-}7)$$

The parameters were selected to $k_{PLL} = 3.0$ *Hz/rad*, $T_{PLL} = 0.3$ *s*. The Phasor Estimator parameters equal those used for figure 11-5.

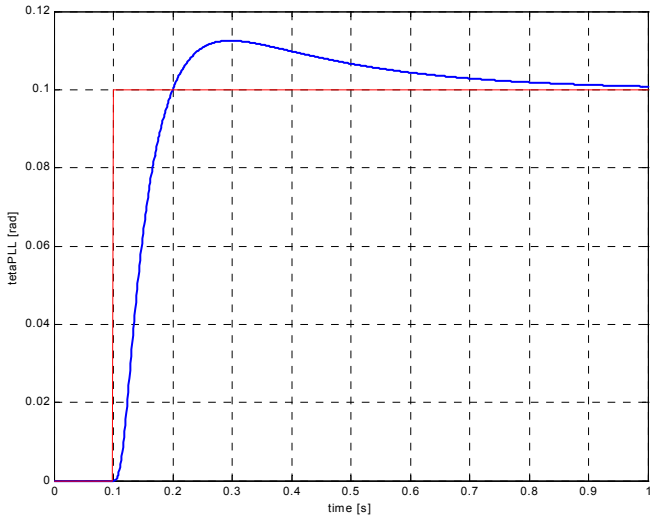

Figure 11-9 PLL step response .

With this conservative tuning of the PLL only a slow response can be obtained. The corresponding closed loop transfer curves in the frequency domain are presented in figure 11-10.

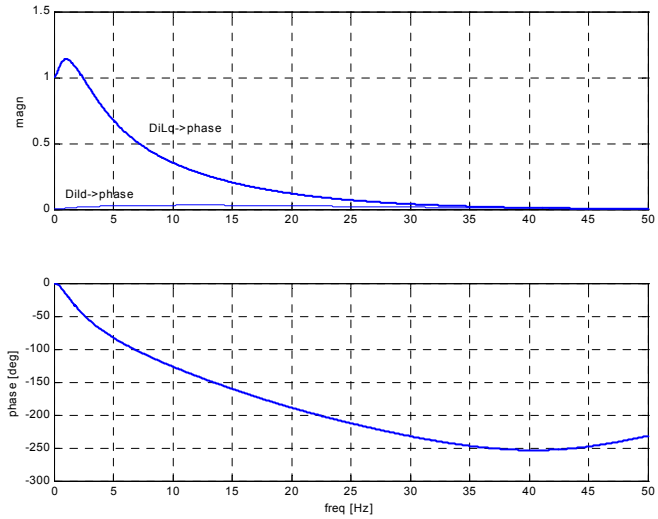

Figure 11-10 Frequency domain closed-loop transfer function.

First it should be noted that signal amplitude changes have a very small impact on the measured angle. This is visualized by the curve close to the bottom (marked *'DiLd→phase'*) in the upper graph in figure 11-10. The other curve in the same graph (marked *'Dilq→phase'*) shows the closed loop transfer function from actual phase in the input signal to the measured value. The figure shows that the angle measuring system in this case has a bandwidth of only *4 Hz*.

Example 11-4

It is possible to make the frequency controlled PLL much faster. E.g. one can utilize a PID regulator and incorporate some additional phase compensating links.

As an example the following arrangement can be used:

- Phasor Estimator average filter: 1st order, *15 Hz* cutoff frequency *(3 dB)*
- Phasor Estimator phasor filter: 2nd order Bessel, *25 Hz* cutoff frequency *(3 dB)*
- PID-controller $H_{PID}(s) = k_P\left(sT_d + \frac{sT_I + 1}{sT_I}\right)$ with

  $k_P = 250$ (rad/s)/rad, $T_I = 0.04$ s, $T_D = 0.005$ s
- Complex lead-lag filter

$$H_{CMPLX}(s) = \frac{\omega_n}{\omega_d}\frac{\left(\frac{s}{\omega_n}\right)^2 + 2\zeta_n\left(\frac{s}{\omega_n}\right) + 1}{\left(\frac{s}{\omega_d}\right)^2 + 2\zeta_d\left(\frac{s}{\omega_d}\right) + 1}$$

$$\omega_n = \frac{\omega_{center}}{\sqrt{k_\omega}} \quad \omega_d = \omega_{center}\sqrt{k_\omega}$$

$$\zeta_n = \frac{\zeta_{center}}{\sqrt{k_\zeta}} \quad \zeta_d = \zeta_{center}\sqrt{k_\zeta}$$

where $\omega_{center} = 300$ rad/s, $k_\omega = 2.5$, $\zeta_{center} = 0.5$, $k_\zeta = 1$

The Nichols' chart for this PLL is shown in figure 11-11. It visualizes the total open loop frequency curve $L(j\Omega)$ for the Phasor Estimator and the regulator links as a function of frequency Ω (markers indicate rad/s) in a graph, where the magnitude of the open loop gain (in dB) is drawn vertically and the phase shift of the open loop is drawn horizontally. For closed loop stability it is required that the frequency curve does not enclose the *(-180°, 0 dB)* point.

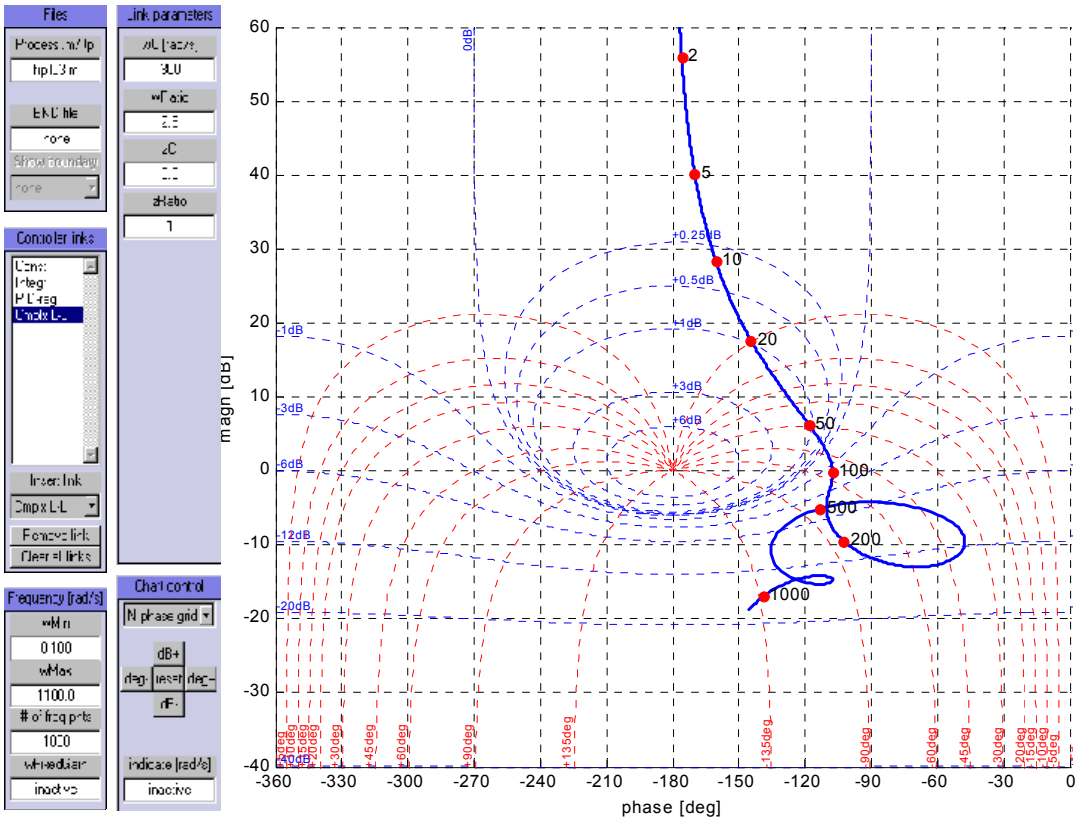

Figure 11-11 Nichols chart for the frequency controlled PLL.

The grid in the chart indicates locus curves for amplitude and phase of the closed loop transfer function $G_{ClosedLoop}(j\Omega)=\frac{L(j\Omega)}{1+L(j\Omega)}$. It can be used to judge the closed loop behaviour of the system. E.g. the figure shows that maximum closed loop gain will be approximately *2 dB* at about *30 rad/s* and that the phase shift in the closed loop at *100 rad/s (15.9 Hz)* is almost *-45 °*.

Figure 11-12 shows the phase step response of the PLL. Note that the time scale is different from that in figure 11-10! In figure 11-13 the corresponding closed loop transfer function in frequency domain is presented. The *3 dB* magnitude bandwidth has been increased to about *20 Hz* at the expense of a higher sensitivity towards amplitude changes.

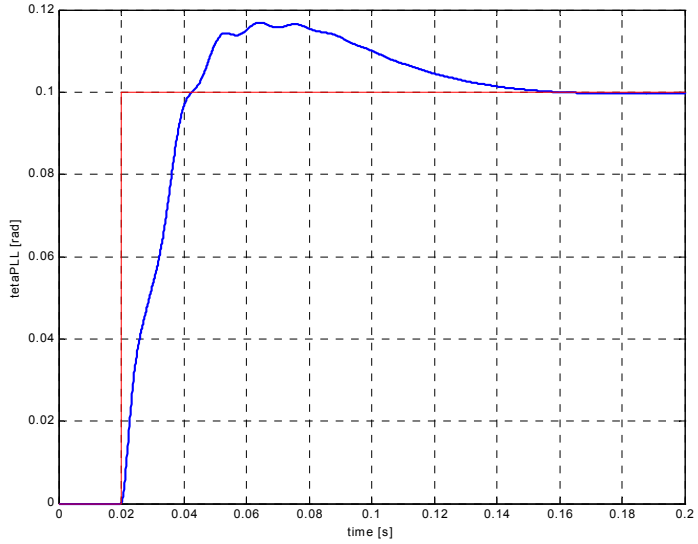

Figure 11-12 Step response, frequency controlled PLL.

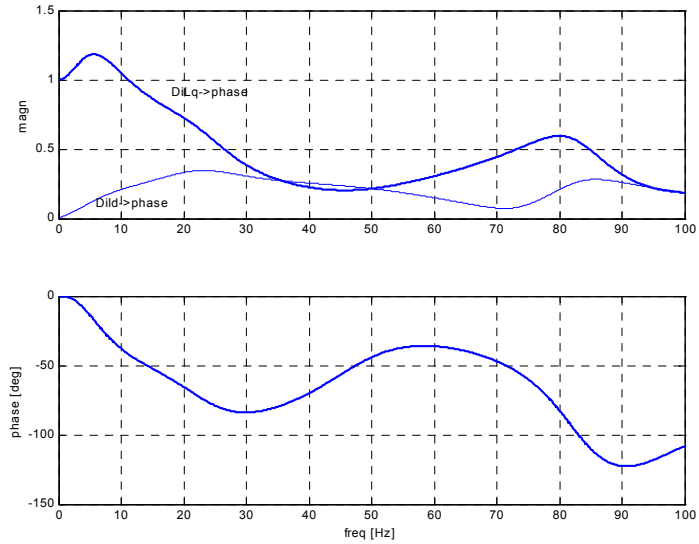

Figure 11-13 Closed loop transfer function for the frequency-controlled PLL.

CHAPTER 12
BOOST CONTROL, STIFF LINE CURRENT

12.1 INTRODUCTION

The themes in this thesis so far have concentrated on

- describing the SVR concept
- creating a dynamical model of the TCSC using the idealised description using equivalent, instantaneous capacitor voltage reversals
- describing how the fundamental component of capacitor voltage and line current may be extracted using the Phasor Estimator
- investigating the dynamics of the Phasor Estimator, the boost measuring system and the PLL

In this chapter things will be put together in order to arrive at a dynamical model of the boost-controlled TCSC, as it appears in a real power system.

The objectives of the boost controller are twofold

- to control the inserted reactance of the TCSC in accordance with the given reference k_{Bref}; the capability of the TCSC in this respect is characterized by its "servo performance"
- to maintain the inserted reactance of the TCSC at the reference value k_{Bref} suppressing the impact of external disturbances in the line current; the capability of the TCSC in this regard is distinguished as its "regulator performance"

Within the Synchronous Voltage Reversal (SVR) scheme the TCSC operation is described by equivalent, instantaneous voltage reversals rather than in terms of the thyristor turn-on angle. The TCSC boost regulator generates the timing references, which define the desired capacitor voltage zero-crossing instants. A secondary thyristor trigger pulse system then turns on the thyristor in question at the correct time instant taking into account the given timing reference, the instantaneous values of the capacitor voltage and the line current.

Thus, in this thesis the "boost regulator" refers to the regulator that generates the timing references for the **reversals**. These references interface the TCSC model, which has been described in chapter 7.

At this point a few words about the continuous/discrete character of the models presented so far are required. The TCSC model represents a discrete, sampled system. The output signal from the model is the average relative voltage across the TCSC capacitor. The sampling frequency is 300 or 360 Hz, when the rated network frequency is 50 or 60 Hz respectively. Thus the Nyquist frequency is 150/180 Hz (942/1131 rad/s) respectively. We expect that the regulators involved in the control will have a far lower bandwidth and accordingly the model used can be interpreted as representing a continuous system.

In this chapter we shall consider the design and tuning of the boost regulator. In a first stage the servo performance will be considered. Then only the main circuit model, the boost measurement system and the boost regulator are involved. Once the servo performance has been investigated focus will be changed towards the regulator behaviour and we shall investigate the sensitivity to disturbances in the line current. It will be shown that the suppression of such disturbances can be improved by introduction of a PLL. In fact the improvement of the regulator performance is the main motivation for the use of the PLL in the control system.

In the design procedure we will use the methodology established in the Quantitative Feedback Theory (QFT) [B4]. This method permits control system design that meets specifications in time-domain for servo performance (reference step response) and sensitivity (disturbance step response) with specified uncertainties in the process parameters. It is important to emphasize that it is the **process uncertainties** and the **unknown disturbances** that determine the need for feedback; if the plant were deterministic and not exposed to disturbances there would not be any need for the feedback control!

QFT utilizes the traditional frequency domain design methods according to Bode/Nyquist/Nichols. The Nichols' chart, visualising logarithmic gain versus phase displacement of the total (i.e. including both the process and the regulator) open-loop transfer function is extensively used during the design procedure. In fact the core of the design method deals with frequency shaping of the regulator transfer function G so that the total nominal transfer frequency curve for each frequency resides outside a given area, defined for that frequency, within the Nichol's chart. This area has a border known as the "Horowitz bound". It is determined by the performance requirements and the process uncertainties. There is one such bound for each frequency, but in practice the designer selects a few critical frequencies to be used during the design.

As stated above it is anticipated in the QFT method that a time-domain specification for the system closed-loop performance exists. However, often in development work no such specification can be defined upfront, but one rather wants the performance to be "as good as possible". This means that one must set up a provisional specification and try to meet it with a suitable design. Then the

specification must be refined according to the outcome of the design in an iterative process.

The design work is split in two parts in this thesis. In the first one it is assumed that the line current is stiff. Then it is assumed that the line current change caused by variation of the TCSC inserted reactance is negligible. In the second part, reported in chapter 13, we will consider the TCSC response, when it has been inserted in a (possibly series compensated) line.

12.2 STIFF LINE CURRENT CONDITIONS

Assume that the TCSC is inserted in a line with stiff line current. The TCSC operation is governed by a regulator, which controls the generated train of equidistant pulses serving as time references for the capacitor voltage reversals. The regulator controls the phase shift of the pulse train relative the line current fundamental component as has been described earlier in chapter 4. Further suppose that the boost factor is being measured and that a feedback regulator with transfer function G compensates the deviations Δk_{Bref} from the boost reference. The output from the regulator is an angle $\Delta\theta_{Breg}$, which represents the phase deviation of the pulse train from its undisturbed position. It is anticipated that the transfer function G includes at least one integrating member. Then, in steady state, the regulator will establish a phase shift (if the system is stable) such that the boost level remains constant at its reference level k_{Bref} even though a specific synchronizing system (PLL) is not included in the scheme. Accordingly $\Delta\theta_{Breg}$ remains at zero in undisturbed conditions. The arrangement is depicted in figure 12-1.

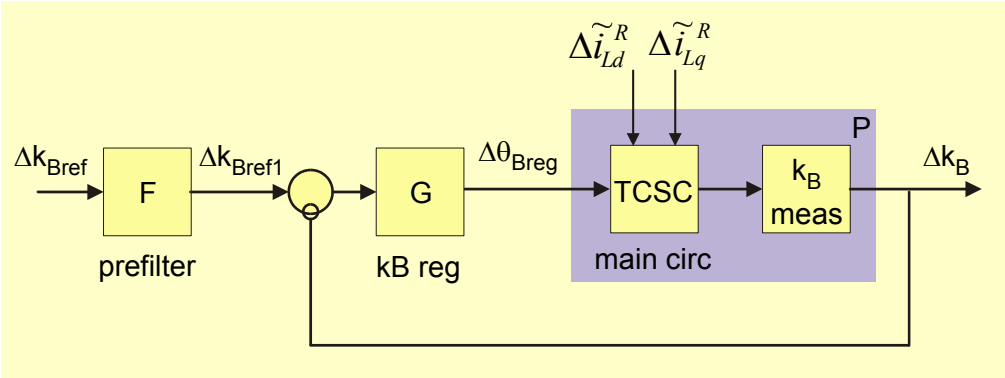

Figure 12-1 Simple boost control system for the TCSC.

The blocks incorporated within the shaded area, i.e. the TCSC main circuit and the boost measuring system, constitute the "plant" to be controlled by the regulator with the transfer function G and the prefilter F.

12.3 SERVO PERFORMANCE

Let us we first consider the servo problem, i.e. the capability of the TCSC to follow changes Δk_{Bref} in the reference**.** This objective is fully met by the control system shown in figure 12-1. As the line current is assumed to be stiff, no disturbances will effect the TCSC. The closed-loop transfer function, the so-called complementary sensitivity function, is given by

$$G_{servo} = \frac{\Delta k_B}{\Delta k_{Bref}} = F \frac{GP}{1+GP} \tag{12-1}$$

12.3.1 Uncertainties

Even if we are considering the case that line current is stiff there are some uncertainties, which must be taken into account in the controller design. The following contributions have been identified:

- the loss factor D_f in the TCSC main circuit model is estimated to lie in the range *[0.95 ... 1.00]*
- in the idealised model instantaneous voltage reversals are being considered. This means that, in the model, any control order changes appearing just before a reversal will be executed immediately in the upcoming reversal. In a real circuit the reversal takes finite time and control values obtained after thyristor firing will not be executed until next reversal occurs. An uncertain delay τ was introduced at the input of the TCSC module to reflect this delay. It also shall cover the program execution time in the control computer. The uncertain delay time was specified to be *[1 ... 3]* ms.
- the design shall be valid for all operating boost factors k_B . The maximum variation range was assumed to be *[1.0 ... 3.0]*.

A set of "nominal" parameters were selected to be $D_f = 0.98$, $\tau = 1\ ms$ and $k_B = 1.5$.

12.3.2 Modelling

The models of the TCSC and the boost reference measuring system have been discussed earlier and will not be repeated here. Additionally the following other parameters have been selected:

- line frequency *50 Hz*
- second order Bessel filter *(ζ=0.866)* with cutoff frequency *15 Hz* were selected for the average and phasor filters in the Phasor Estimator

In the simulation **one** Phasor Estimator using **one** complex-valued input signal, which represents the whole three-phase capacitor voltage vector, has been implemented. Similarly **one** boost controller providing **one** control angle for the

TCSC is utilized in the simulation. It has been shown earlier that the response of the Phasor Estimator using single-phase input signal is very close to the response of the device using a complex input signal, and this means that the result obtained from the simulations are also applicable to the case that Phasor Estimator and the regulators have been implemented phase-wise in the TCSC.

Figure 12-2 shows Bode plots of the open-loop transfer function for the plant. The nominal parameters generate the curve marked by the circles and the surrounding solid lines indicate the envelop of the transfer functions produced by **all** combinations of the uncertain parameters.

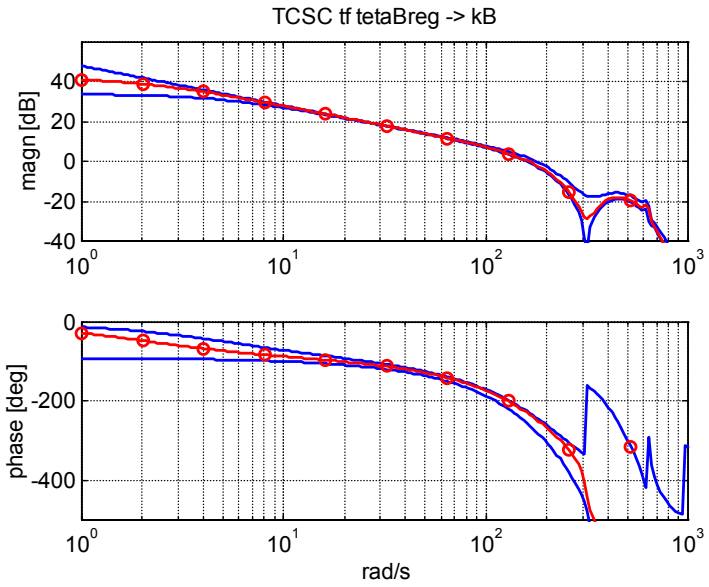

Figure 12-2 Bode plots of nominal and envelops of open-loop transfer function for the TCSC.

It appears that the biggest spread in the transfer functions occur at low frequency (due to the uncertainty in loss factor) and at high frequencies (due to spread in time delay)

Figure 12-3 demonstrates another way to visualize the uncertainties. The nominal plant open-loop transfer function is shown in a Nichols' chart. In addition, for a number of frequencies the transfer function has been calculated and depicted in the plot for the whole ensemble of parameter combinations. Using QFT vocabulary this plot illustrates the "templates".

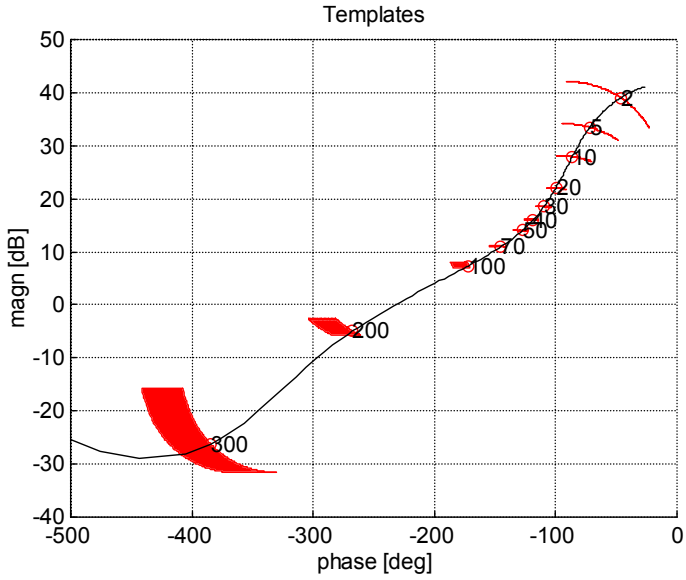

Figure 12-3 Nominal open-loop plant transfer function with templates showing the uncertainty at certain frequencies (marks in curve in rad/s).

12.3.3 Specification

In QFT the specification normally will be expressed in terms of speed and accuracy of the response to step changes in the reference. The following criteria are used here:

- rise time to 90 % shorter than 50 ms
- settling time to less than 5 % error shorter than 150 ms
- overshoot less than 10 %

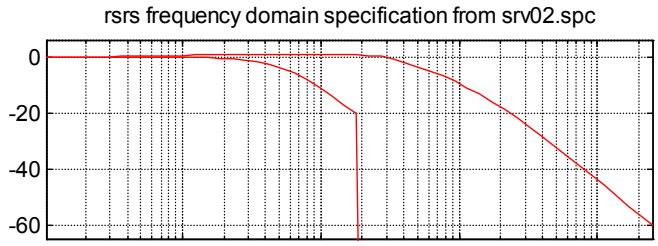

Figure 12-4 Frequency- and time-domain servo specifications.

The closed-loop time-domain specification is showed in the lower diagram in figure 12-4. It is converted by an approximate transformation into a closed loop specification in the frequency domain. This is shown in the upper diagram in figure 12-4.

12.3.4 Feedback regulator design

In the QFT approach enough feedback is being introduced in order to **reduce the uncertainty gap** at each frequency in the closed loop transfer function to less than the width between the curves in the upper diagram of figure 12-4. When the width is sufficiently small the closed loop gain is corrected by a prefilter, which acts on the regulator input signal.

From the acceptable uncertainty gap in the frequency-domain specification and the templates defined by the plant uncertainties the “Horowitz bounds” in figure 12-5 have been calculated for a number of selected frequencies. The value of the nominal open-loop transfer function at the respective frequency must reside above or to the right of the corresponding bound.

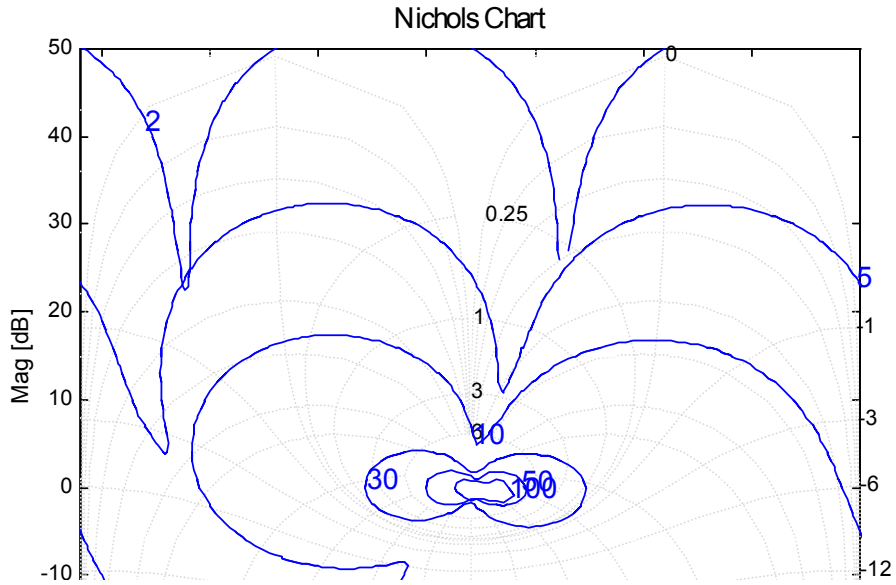

Figure 12-5 Horowitz bounds for 2, 5, 10, 30, 50 and 100 rad/s for the servo specification and the specified process uncertainties

The control system designer now must construct a transfer function for the regulator that fulfils these requirements. In practice this is done by implementing

the regulator as a number of simple blocks like PI-regulators, lead-lag links etc. connected in cascade. In the actual case a PI controller was selected having the transfer function

$$G_{Breg}(s) = P_{Breg}\frac{1+sT_{Breg}}{sT_{Breg}} \tag{12-2}$$

with the parameters $P_{Breg} = 0.15$ *rad/pu,* $T_{Breg} = 50$ *ms.*

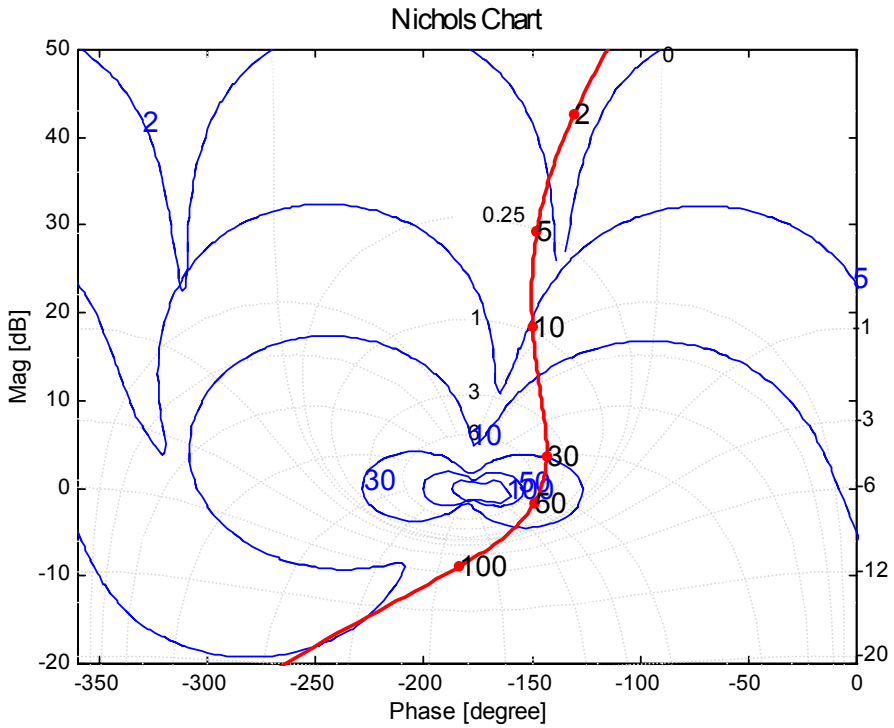

Figure 12-6 Open-loop transfer curve together with some Horowitz bounds.

Figure 12-6 shows the selected total frequency transfer function and the Horowitz bounds. The nominal transfer function trajectory is located well above the corresponding bounds at *2, 5* and *10 rad/s*. At *30 rad/s* it passes just at the limit of the corresponding bound and for *50* and *100 rad/s* it passes to the right and below the corresponding Horowitz bound.

This feedback reduces the width of the closed loop transfer function to the same level as required in the specification. This is visualized in figure 12-7, where nominal closed loop function (thin solid line) is shown together with the maximum and minimum values of the closed loop gain (circles) at the selected frequencies. In addition the frequency-domain specification (thick solid lines) has been drawn in the same graph.

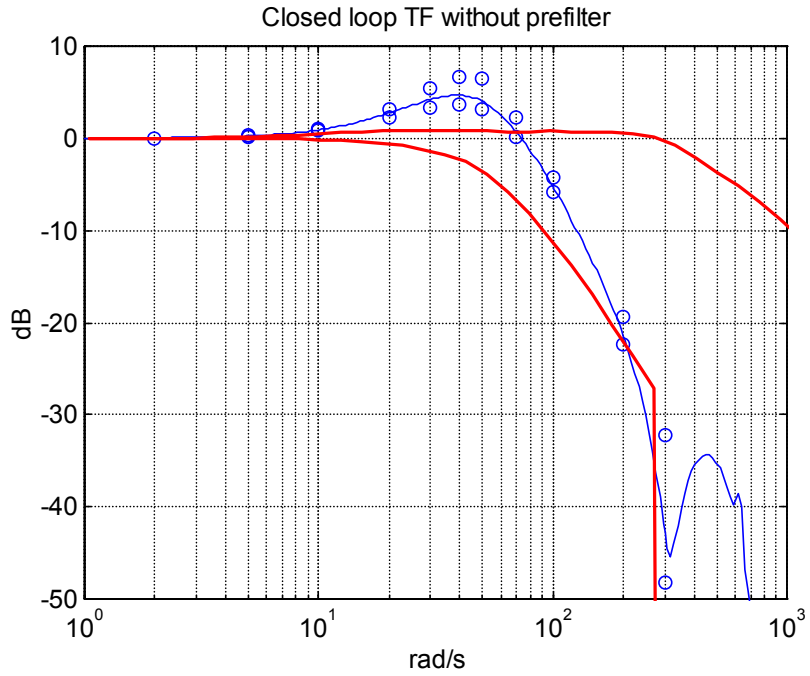

Figure 12-7 Close-loop transfer function; specification and calculated without prefilter.

It can be seen that due to the introduction of feedback the variation of the closed loop transfer function (the vertical distances between the circles) has been reduced to a value that is equal to or smaller than the difference between the specification curves. The closed loop gain however peaks at about 40 rad/s, which indicates that an overshoot exists in the step response.

Time domain simulations are presented in figure 12-8.

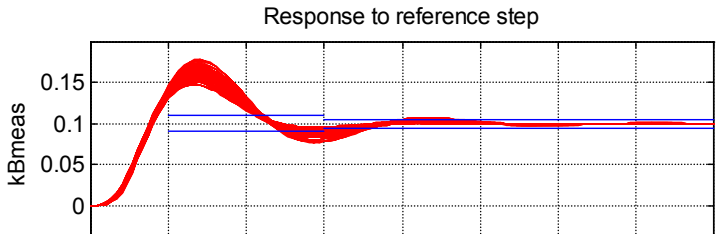

Figure 12-8 Step response and controller output without prefilter

The upper graph shows the measured boost response while the lower one depicts the regulator output during the transient. Note that a certain change of the steady-state control angle is required in order to obtain the new boost level. The necessary change of the angle varies due to the different loss factor within the ensemble of uncertain systems.

12.3.5 Prefilter design

The overshoot exceeds the specification a lot. A prefilter *F* (figure 12-1) can be used to improve this situation. This is shown in figure 12-9, which depicts the same step response when a prefilter is used. The time domain step response now is quite close to the specification.

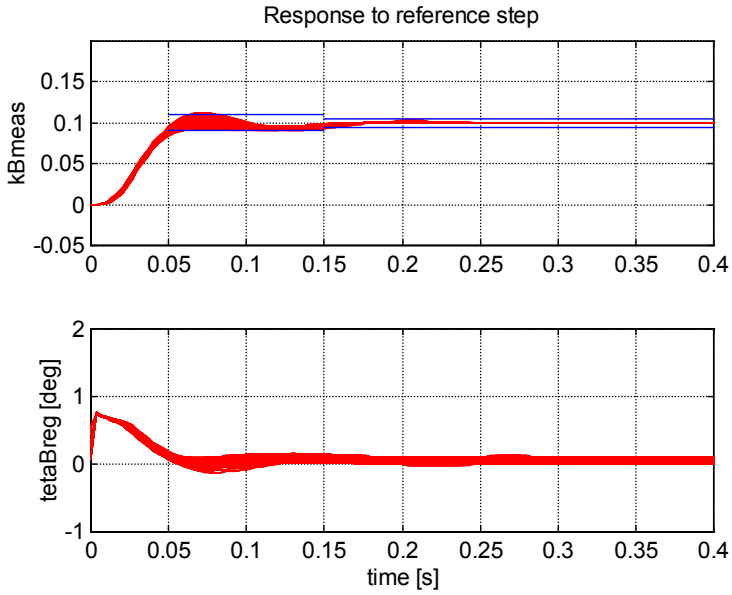

Figure 12-9 Step response and controller output for regulator with prefilter.

The transfer function of the prefilter is given by

$$F(s)=\frac{\left(\frac{s}{\omega_n}\right)^2+2\zeta_n\frac{s}{\omega_n}+1}{\left(\frac{s}{\omega_d}\right)^2+2\zeta_d\frac{s}{\omega_d}+1} \qquad (12\text{-}3)$$

using the parameters ω_n=41.0 rad/s, ζ_n=0.594, ω_d=38.9 rad /s, ζ_d=1.217.

The corresponding closed loop characteristics (with prefilter inserted) is shown in figure 12-10. It shows that closed loop 3 dB bandwidth of the TCSC controller is at least 40 rad/s.

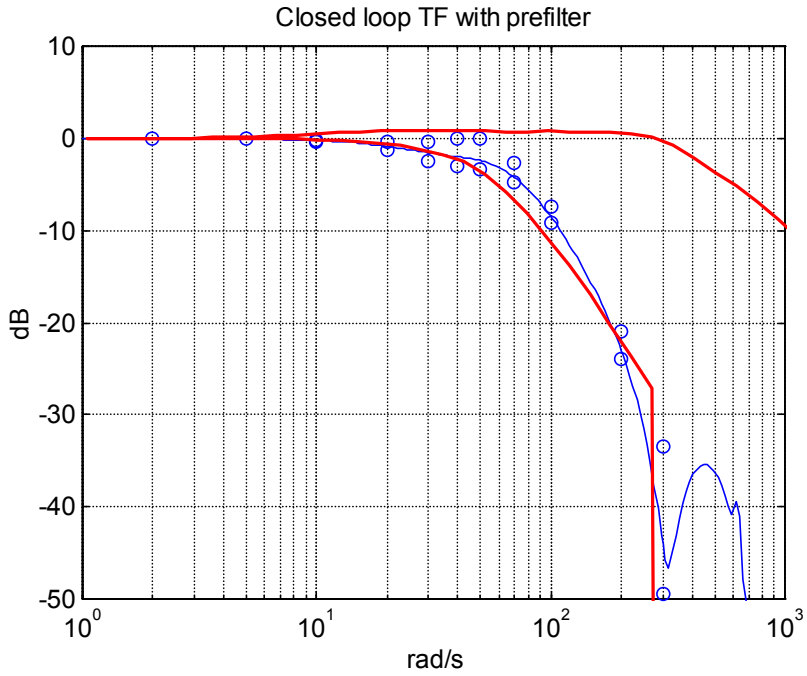

Figure 12-10 Specification and calculated close-loop transfer function calculated with prefilter.

12.3.6 Comparison with detailed model of TCSC

The results obtained so far are all based on the description of the TCSC in terms of instantaneous voltage reversals. How does the results agree with a TCSC having a real main circuit, where the capacitor voltage reversals are not instantaneous but have a finite duration? The line current is still assumed to be stiff. In order to investigate this question a MATLAB model was used, which simulates the TCSC main circuit and control. The following parameters were used:

- network frequency *50 Hz*
- LC resonance frequency in the main circuit *125 Hz*, i.e. $\lambda=2.5$
- quality factor $Q=30$ for the valve circuit (inductor plus valve); this corresponds approximately to loss factor $D_f=0.95$ according to the results in figure 4-19

The TCSC model comprises three phases. In each phase the capacitor voltage and line current phasors are extracted and used to get the boost factor response from that specific phase. Each phase further has an individual boost controller using the phasors extracted in that phase.

In addition the space vectors representing the three-phase capacitor voltage and line current are created from the phase quantities. They are then fed into phasor estimators accepting complex input functions. These estimators generate phasors that represent the whole three-phase system. The apparent impedance is formed by dividing the capacitor voltage phasor with the line current phasor. Finally the

imaginary part of the quotient, normalized with the capacitor reactance at network frequency, delivers the boost factor response.

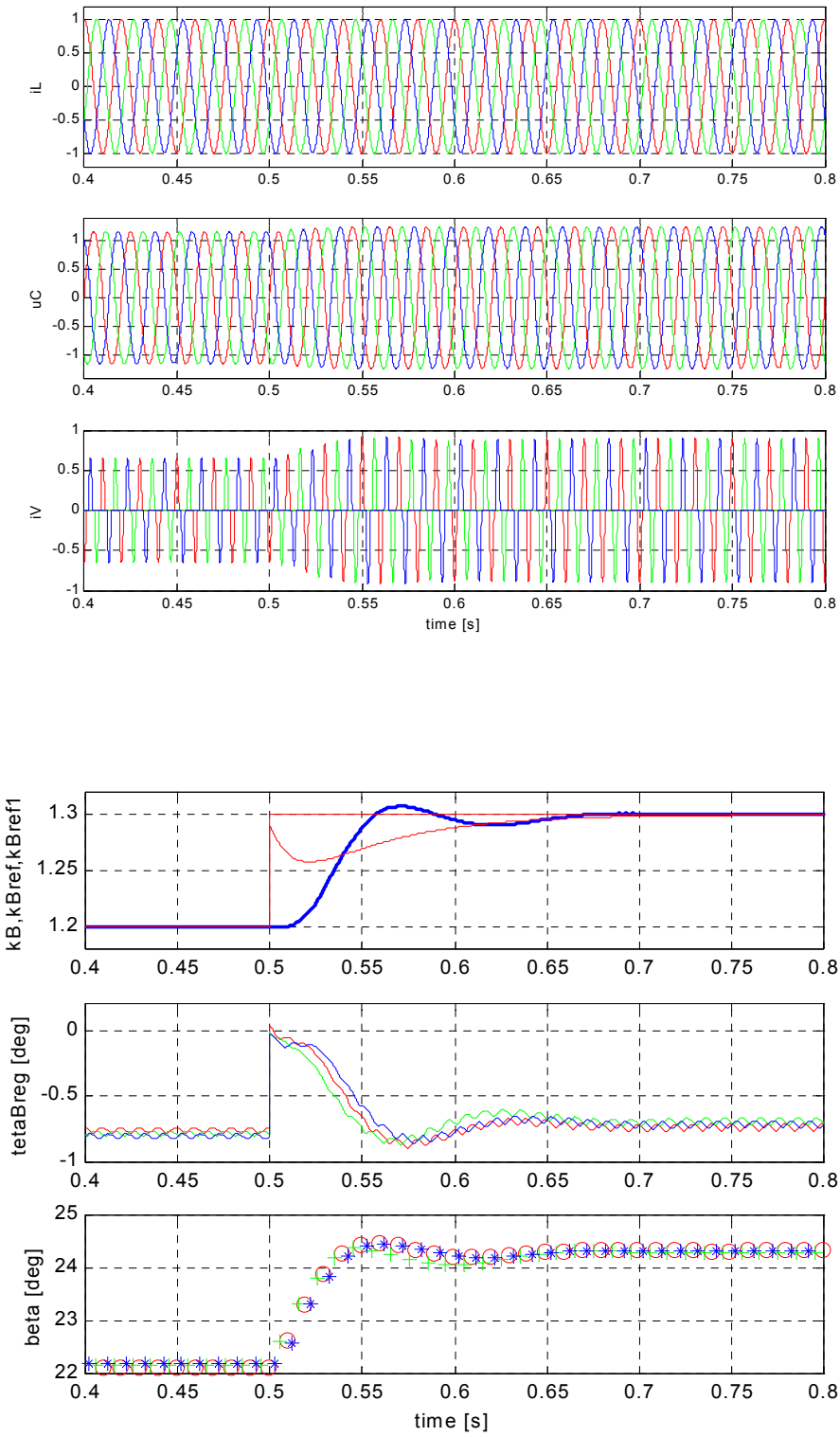

Figure 12-11 Simulation results for fully implemented TCSC model.

Figure 12-11 presents some results from such a simulation, where the boost factor reference is increased by 0.1 per unit from a steady-state level of $k_B=1.2$.

The graphs verify the very good agreement between the results obtained from the simplified model using instantaneous voltage reversals and from the model using detailed representation of the TCSC main circuit.

An interesting feature with the control system approach based on SVR is that the servo dynamical performance is inherently independent of the boost level. This is in contrast to systems, which directly generate the control angle, where the strong non-linear relation between the control angle and the inserted reactance (shown in figure 3-3) must be considered. This fact is illustrated by the graphs in figure 12-12, which depicts the response of the detailed TCSC model at a 0.1 pu reference step at a higher initial steady state boost factor ($k_{Bref} = 2.5$). Specifically it should be noticed that the change in the control angle β, which signifies the displacement of the turn-on instant of the thyristors, differs about one magnitude of order, when the steady-state boost level changes from $k_B=1.2$ to $k_B=2.5$. This gain adaptation results from the action of the subsystem denoted as "SVR trig pulse generation" in figure 4-13.

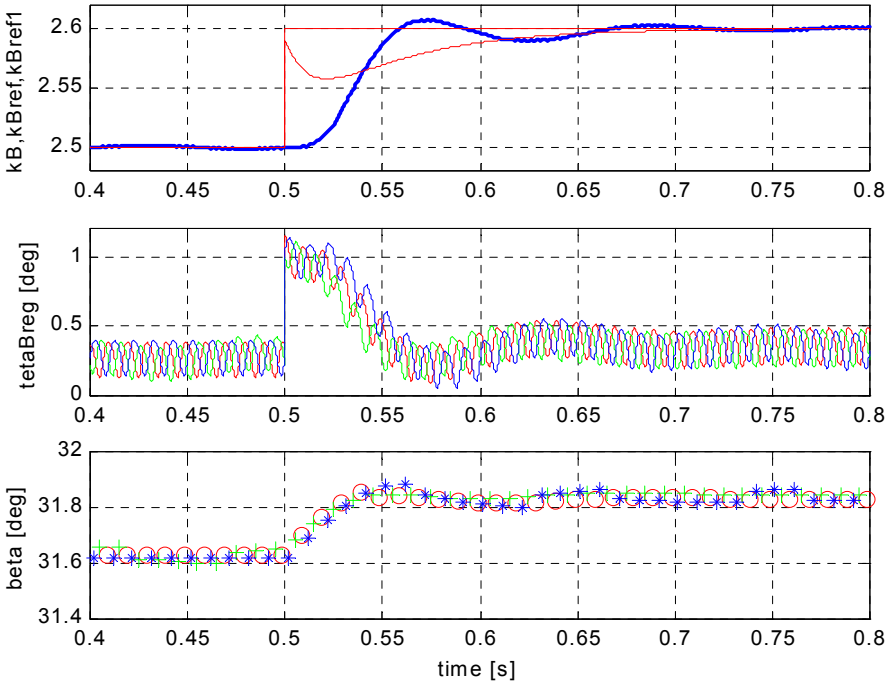

Figure 12-12 Simulation results with higher boost factor.

The servo performance agrees with that in figure 12-11, but the ripple in the control signals is higher and the steady state control angle θ_{Breg} has increased somewhat. These features result from the increased harmonic content in the capacitor voltage and the higher losses at elevated boost levels.

12.4 REGULATOR PERFORMANCE

We are again considering the situation that the line current is stiff. The block diagram shown in figure 12-1 still is applicable. Now we shall investigate how line current changes impacts on the boost factor, i.e. on the reactance that the TCSC inserts in series with the line. Certainly the QFT method can be applied to tune the regulator according to a given sensitivity specification and existing uncertainties. However, we want to reduce the sensitivity of the TCSC with respect to line current changes as much as possible. Therefore stability considerations will establish the limits for the performance. The situation is very much the same in the servo case and accordingly we will use the boost regulator parameters from the preceding section in the simulations that follow. This means that the regulator is of PI type with gain $P_{Breg}=0.15$ *rad/pu* and integrating time constant $T_{Breg}=50$ *ms* (transfer function in (12-2)).

12.4.1 Line current amplitude change, idealized model

Figure 12-13 exemplifies the simulation results produced by the idealized model using instantaneous voltage reversals for the case when line current amplitude is suddenly increased by 10 %. The step response has been calculated for the whole ensemble of systems defined by the uncertainties given in section 12.3.1.

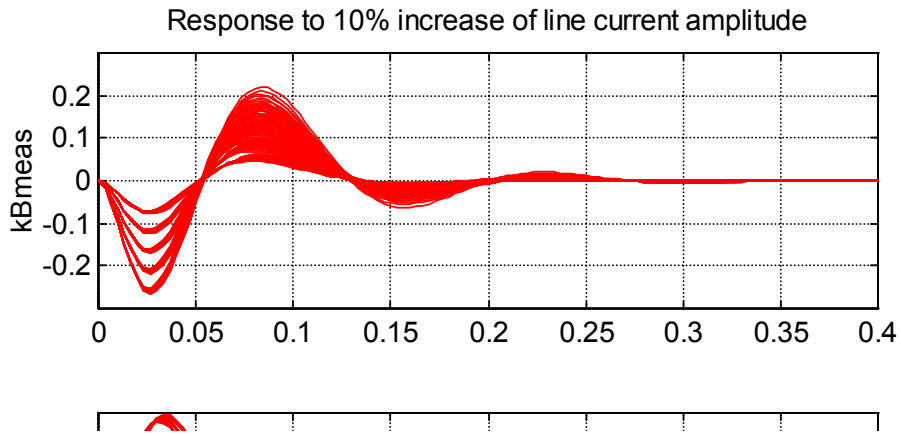

Figure 12-13 Response to 10% amplitude increase in line current.

In the step response five different bands can be identified. They are associated with the different boost factors k_B=*1.0, 1.5, 2.0, 2.5, 3.0.* The sensitivity for line current changes namely depends on the steady-state boost level, contrary to the servo performance. The highest impact naturally occurs when the boost level is high. The disturbance manifests the inherent property of the SVR control to keep the capacitor voltage constant irrespective of the line current changes.

12.4.2 Line current amplitude change, detailed model

As before the results are compared with those obtained from the detailed model of the TCSC. Such simulation results are presented in figure 12-14 for low and in figure 12-15 for high steady state boost level.

The upper three graphs show from top to bottom

- instantaneous line current
- instantaneous capacitor voltage
- instantaneous valve current

The lower three graphs show

- boost factor evaluated from positive sequence components of the space vectors representing capacitor voltage and line current
- output (timing reference for capacitor voltage zero-crossing) from the three boost regulators in the individual phases
- control angles β for the three phases, as determined by the SVR trig pulse block

It can be noted that in each case the boost individual regulator outputs have different magnitude. The lowest amplitude occurs in the phase where the line current is peaking, when the amplitude step occurs. The maximum magnitude of the boost regulators agrees with the value produced by the idealized model using instantaneous voltage reversals.

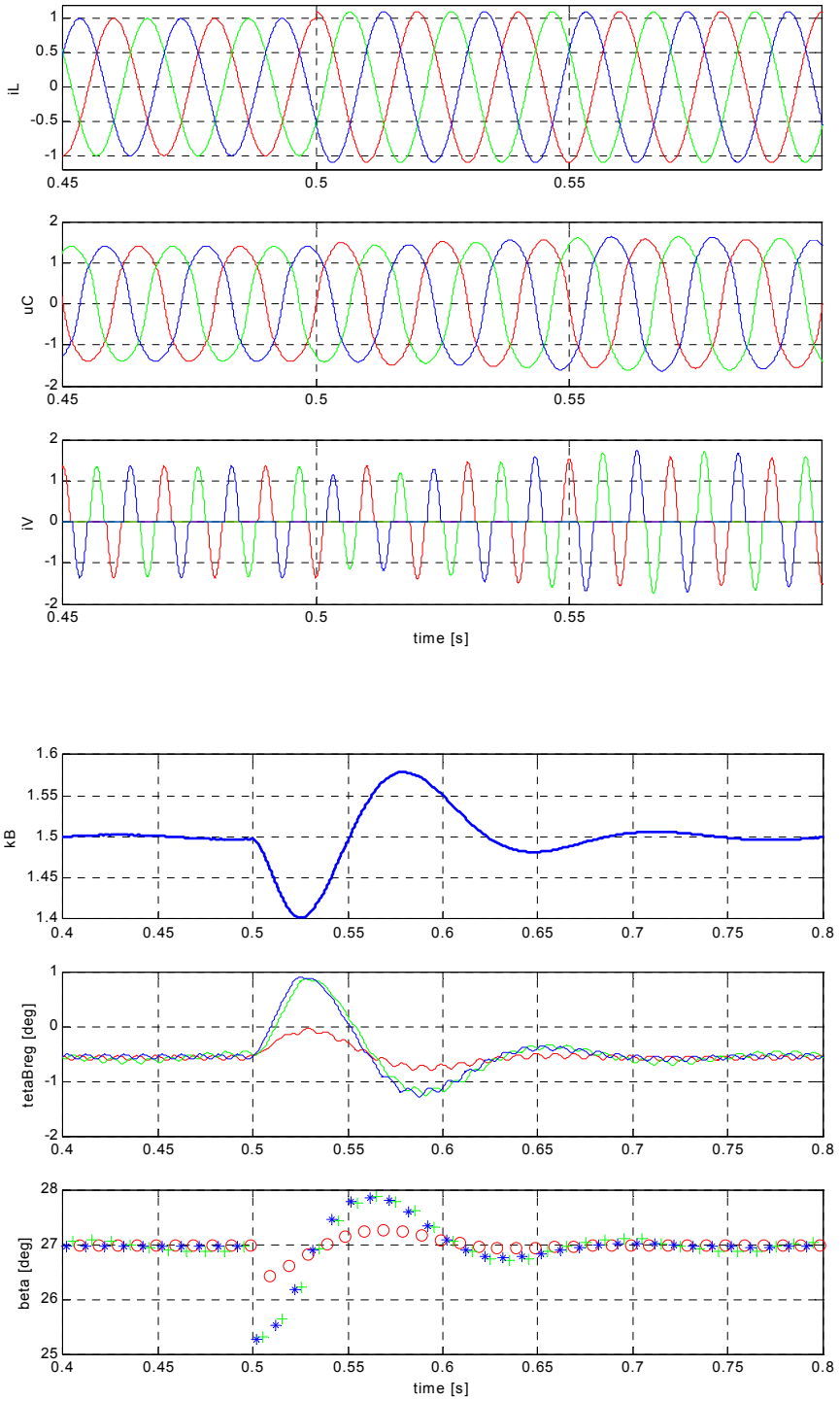

Figure 12-14 Response to 10% amplitude in line current at boost k_B =1.5.

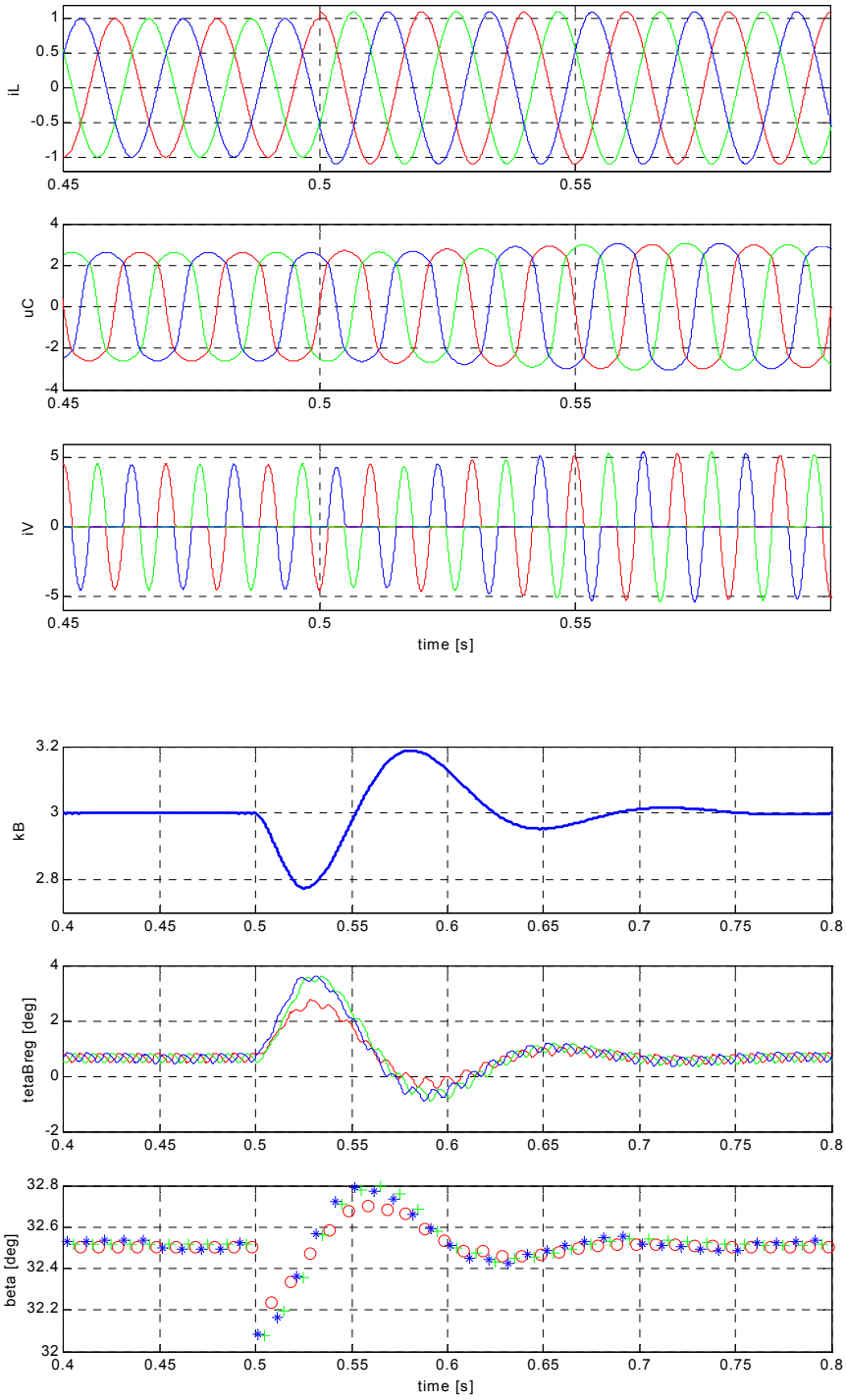

Figure 12-14 Response to 10% amplitude in line current at boost k_B=3.0.

12.4.3 Line current phase shift, idealized model

A line current deviation in the quadrature direction in the *IL_SYNC* coordinate system represents a phase shift. A change of the relative current by 0.1 pu corresponds to a phase advance of approximately *0.1 rad (5.7°)*. Such small

phase shifts frequently occurs in transmission systems e.g. due to switching operations in the network or tripping of generators or other equipment. Figure 12-15 depicts the simulation results from the idealized model derived in this thesis.

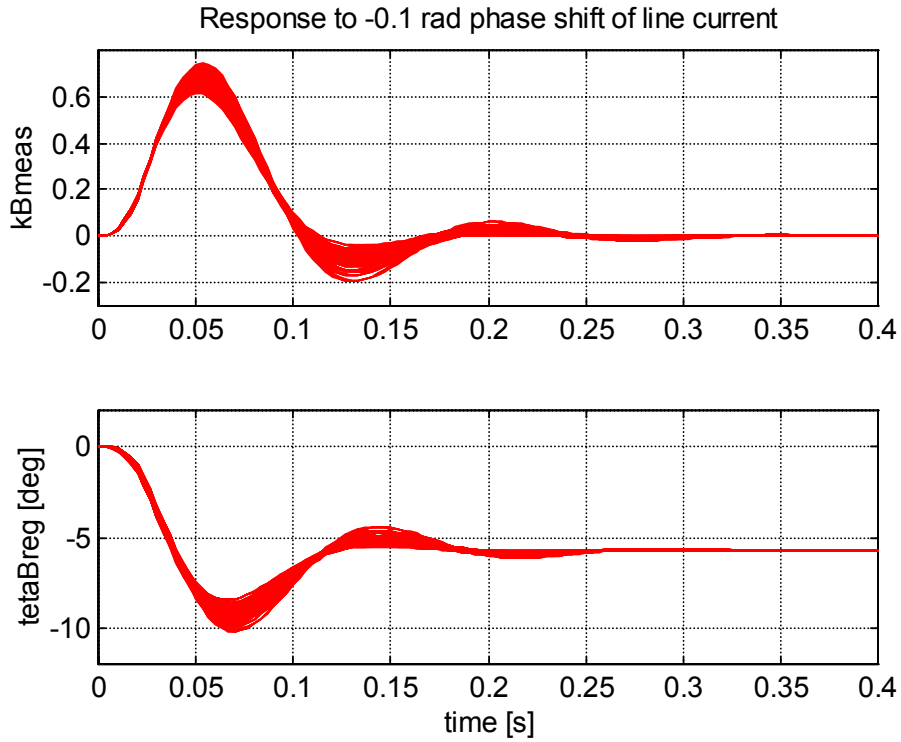

Figure 12-15 Response to –0.1 rad phase shift of line current.

In this graphs the whole ensemble of systems defined by the uncertainties have been investigated. It appears that only minor variation is obtained in the result. We conclude that the boost factor deviation only marginally depends on the steady-state boost level. The diagrams show that the TCSC with this regulator setup is far more sensitive to line current **phase shifts** than to **amplitude changes**. The difference is substantial and reaches almost one order of magnitude at low steady state boost levels.

It is not very surprising that the TCSC exhibits such high sensitivity to phase shifts in the line current. We have explained already in chapter 4 (figures 4-9 to 4-11) that the phase of capacitor voltage reversals relative to the line current is the determining factor for whether the boost level in the TCSC shall increase or decrease. This phase shift also is the variable acted on by the boost regulator itself in order to follow the given boost reference.

12.4.4 Line current phase shift, detailed model

Figure 12-16 shows the results from a simulation using the detailed TCSC model. The shown graphs are the same as in section 12.4.2. The agreement between the results from the two models is very good.

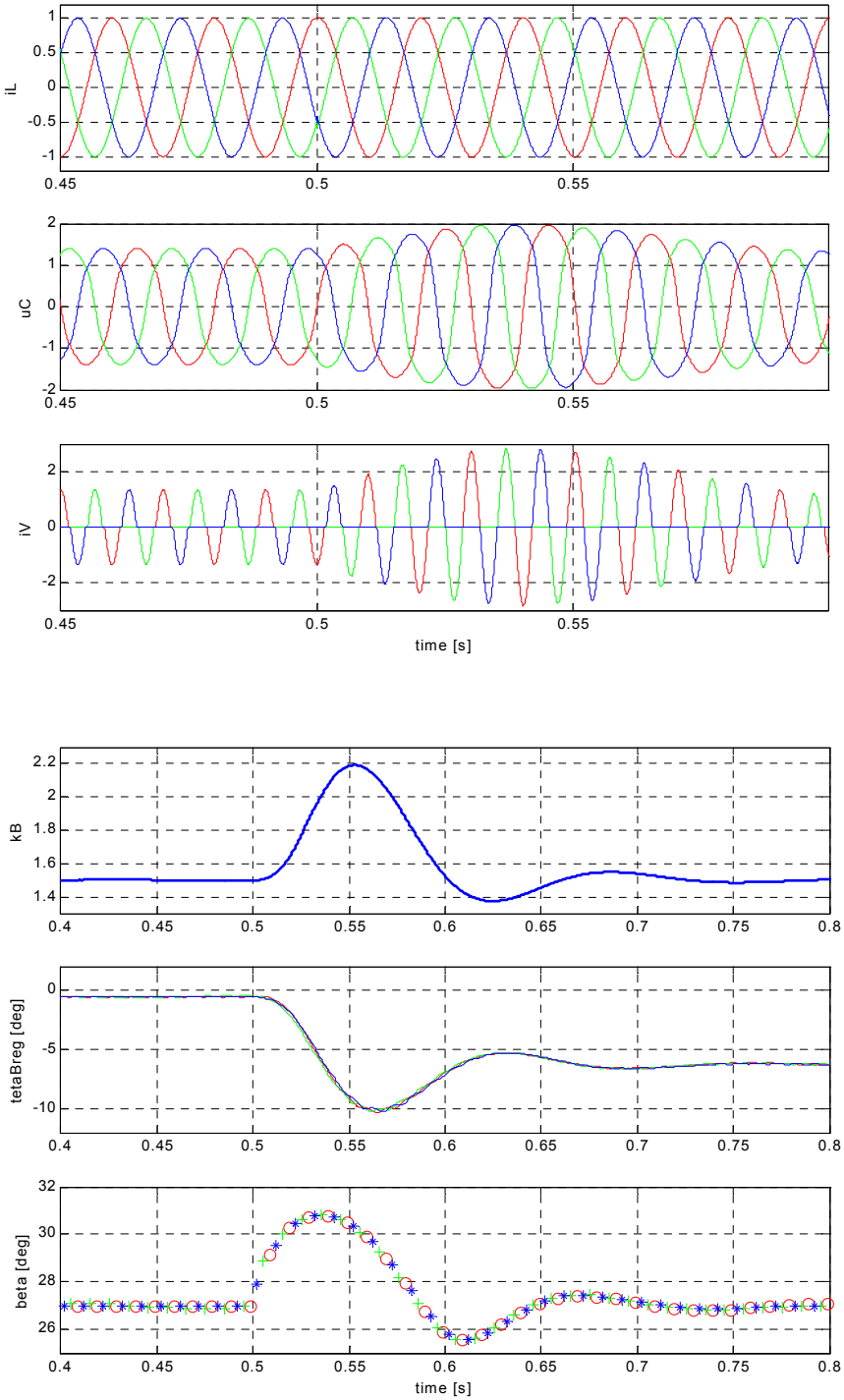

Figure 12-16 Response to –0.1 rad phase shift in line current at boost k_B =1.5.

Very similar results were obtained from simulation at high boost level. The only difference is that the control angle β variation is much smaller at the high boost.

12.5 ADDITION OF A SYNCHRONIZING SYSTEM (PLL)

12.5.1 Motivation and purpose

Up to this point we have investigated the servo and the regulator performance of the TCSC using a simple PI-type boost regulator. It was found that the servo performance is adequate and that the sensitivity towards line current amplitude is reasonable but that the TCSC is very sensitive to line current phase shifts.

The reason of course is that the line current phase shift directly impacts on the boost changing mechanism in the TCSC. In steady-state the phase error will be taken care of by the integral part of the output signal from the boost regulator. However, in order to change the integral part of the output signal, a boost factor change must first occur, then pass through the measuring system and finally get integrated by the boost regulator. This takes a certain time and a substantial deviation from the boost factor reference will be obtained during that period.

Under these circumstances it appears to be a bright idea to design a device that is dedicated to observe the line current phase and to adjust the boost regulator output immediately, when a phase shift occurs, without awaiting that any boost error develops. Such a device is the Phase Locked Loop (PLL) operating on the line current. The phase changes detected by the PLL are directly added to the boost regulator output as a feed forward signal. The arrangement simply is a "synchronizing system" for the TCSC.

It appears to the author that the feed-forward interpretation of the synchronizing system is the correct description of its role in the over-all control. It should be noted that the phase reference for the AC quantity that drives the main circuit, i.e. the line current for the TCSC, the bus voltage for the SVC etc., must always be created from locally measured quantities. The dynamics of the system that provides the phase information, like the PLL in the case of TCSC, has an essential impact on the control performance.

Occasionally the question is raised about what is the adequate principle for tuning the control system of power electronic equipment. Two alternatives then normally will be examined:

- fast synchronisation system (PLL) and slow regulator
- slow synchronization system (PLL) and fast regulator

From the discussion above the answer would be that one would first consider a fast acting regulator because it will provide both good **servo performance** and **regulator performance**. If the system remains too sensitive to phase shifts in the AC quantity driving the main circuit, a PLL can be added to provide a feed-

forward control link. It can contribute to improved performance only if its response time is faster than the closed loop response time of the regulator. If the regulator performance is much more important than the servo performance it might be reasonable that PLL speed is increased as a trade-off of reduced regulator speed.

There may of course be reasons to implement a slow-acting PLL for other reasons than control performance. As an example it may be needed in order to simplify startup sequences etc.

12.5.2 Line current phase shift, idealized model including PLL

Figure 12-17 presents the time-domain simulation results obtained with the idealized TCSC model when the PLL described in example 11-4 in section 11.2.2 is used. The PLL has a phase-correcting filter in the frequency regulator so that it can operate with a high gain in order to be fast-acting (figure 11-12). The disturbance is the same line current phase shift as in figure 12-15.

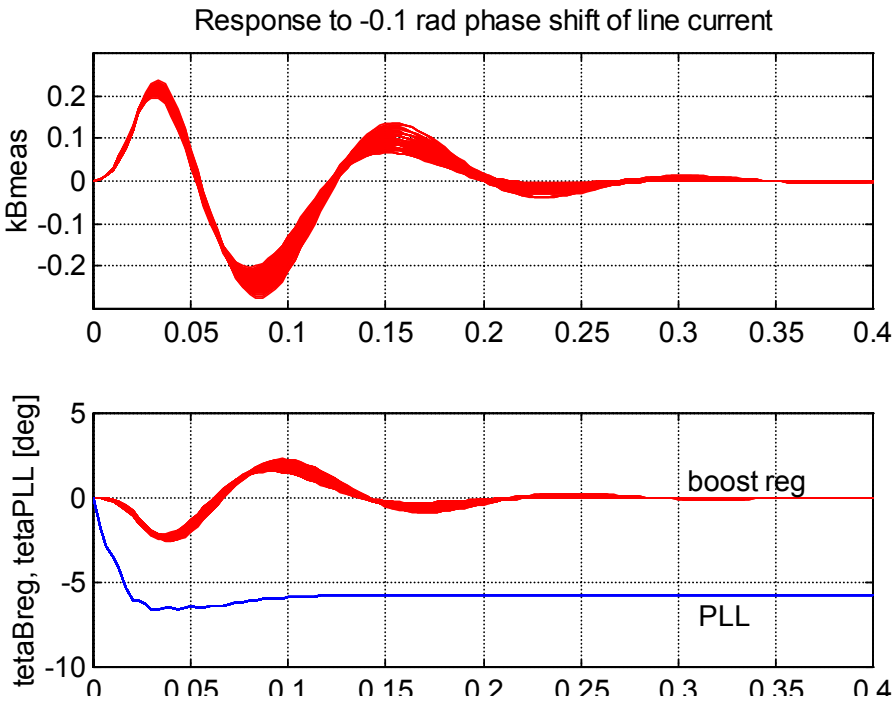

Figure 12-17 Response to –0.1 rad phase shift of line current with PLL.

A comparison between figure 12-17 and figure 12-15 shows that the sensitivity for line current phase shift has been reduced to about one third of its original value. The response probably can be further improved by retuning the boost regulator and the PLL simultaneously.

12.5.3 Line current phase shift, detailed model including PLL

Finally simulation results results obtained for the detailed TCSC model are presented in figure 12-18. Inspection shows that the idealized model reproduces the transient at the line current disturbance with very good accuracy.

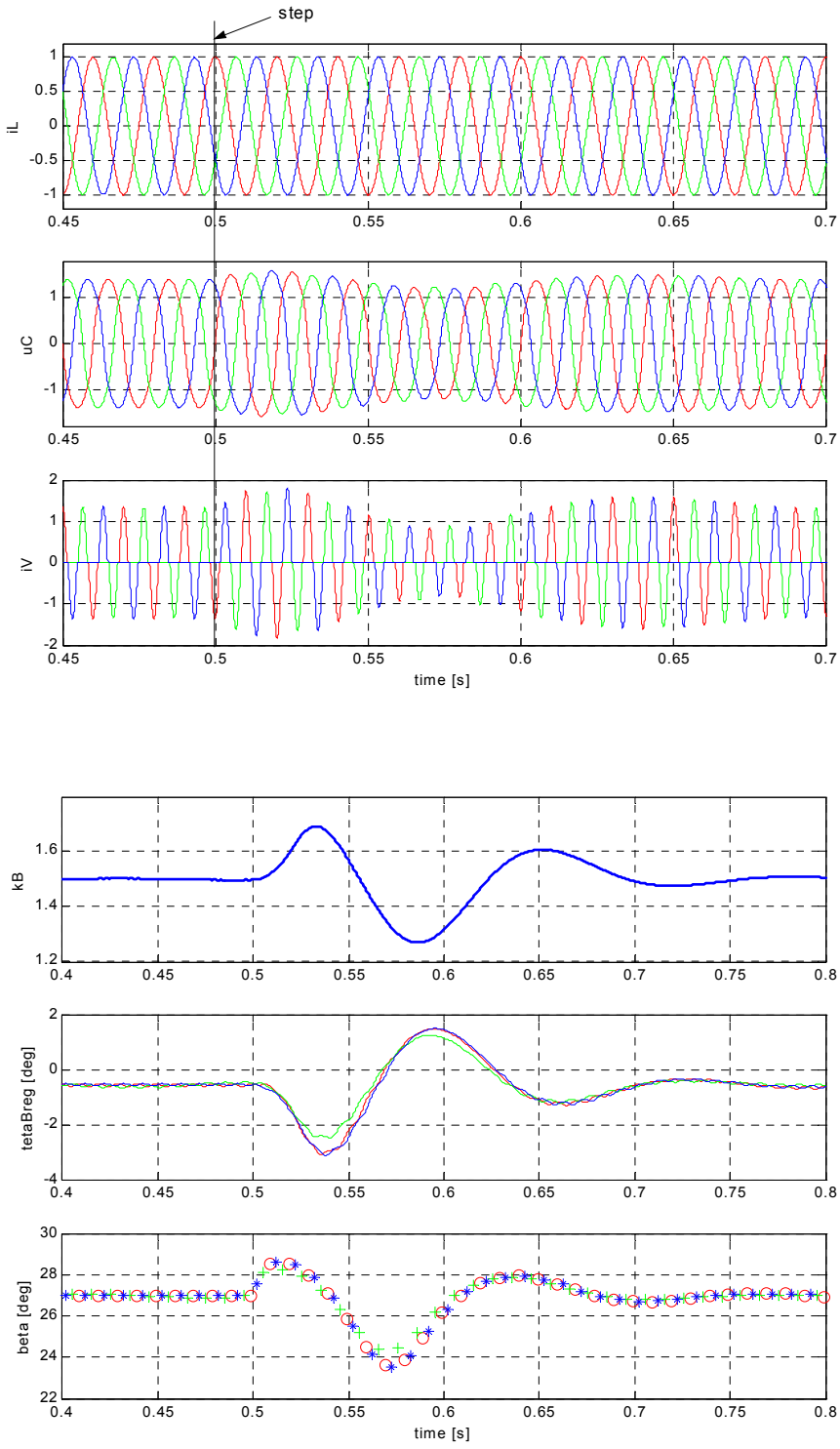

Figure 12-18 Response to –0.1 rad phase shift of line current at k_{Bref}=1.5. Detailed model including PLL .

CHAPTER 13
BOOST CONTROL, TCSC IN THE SYSTEM

13.1 OBJECTIVES

In the preceding sections we have investigated the boost control problem of the TCSC assuming that the line current is unaffected by the TCSC voltage. Such studies have the benefit of simplifying investigations of the regulator performance and to find out the basic limits for speed of control, stability etc. However, from a practical viewpoint the restriction to stiff line current of course does not make sense. If the TCSC does not have any impact on the line current there is no reason to install it at all!

A natural next step is to look at the TCSC when it is inserted in a transmission line with given voltages on the line terminal buses. In this study we will use a simple resistive-inductive line model. We will also have the possibility to include a fixed series capacitor bank.

We shall investigate the boost control design problem (tuning) of the boost controller in view of the uncertainties that are related to the varying parameters and the unknown short circuit strength at the line terminal buses.

The idealized TCSC model using instantaneous voltage reversals is used.

13.2 SYSTEM MODEL

The system model according to the description above is depicted in figure 13-1. We may consider the line terminal voltages to be given external quantities that are independent of the TCSC. Of course only the line terminal voltage **difference** has any impact on the current, so one terminal voltage may be considered to be stiff. The boost control system uses locally measurable quantities as its feedback signals; they are derived from the line current and capacitor voltage. Certainly the TCSC generates some zero-sequence third harmonic voltages. However, due

to the high zero-sequence impedance, this zero-sequence current in the line can be neglected.

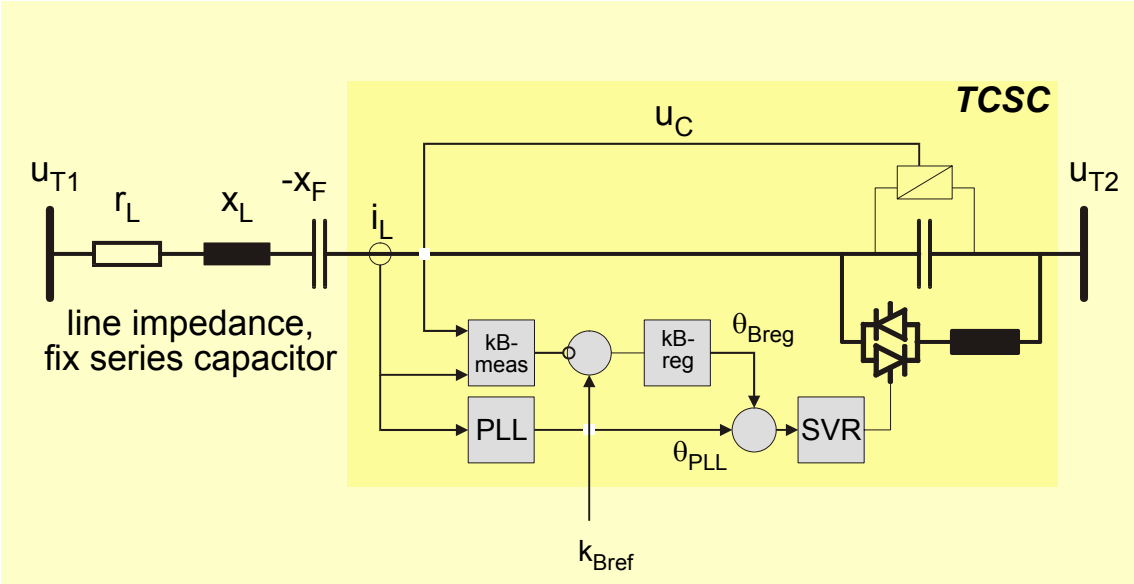

Figure 13-1 TCSC inserted in the transmission line.

In this study a small-signal linearized model shall be developed using the TCSC blocks that have been derived earlier. Figure 13-2 depicts how the quantities associated with the TCSC interact with the system.

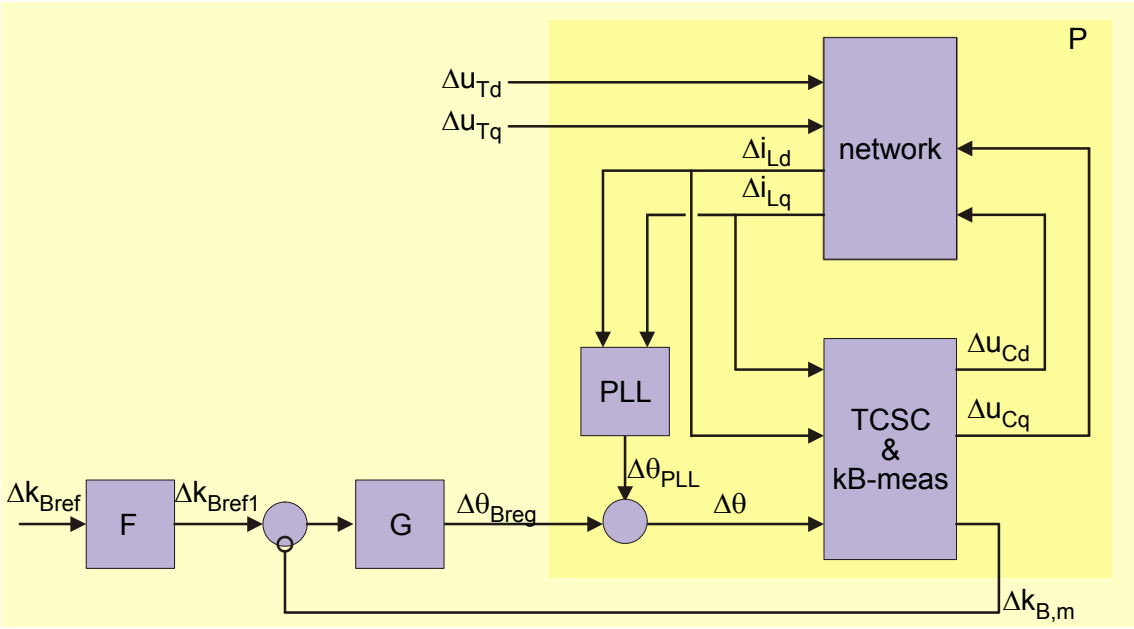

Figure 13-2 Quantities interacting between the TCSC, the control system and the transmission system.

Considering the boost control system its servo performance will be impacted by the line current change, which is caused by the change of the inserted reactance. The external disturbances will be represented by changes in the line terminal voltages. These disturbances may involve a voltage component in phase with the line current. This component here is denoted Δu_{Td} while the voltage component in quadrature direction relative the line current has been designated Δu_{Tq}.

Here we shall pursue an exercise with the aim to tune the boost regulator for servo performance. Such tuning may e.g. be requested in a Power Oscillation Damping (POD) application, where the TCSC is installed in order to provide damping of electromechanical oscillations in the 0.1-2 Hz frequency range.

The blocks inside the shaded area of figure 13-2 constitute the "plant" which shall be controlled by the boost regulator. The boost regulator's output, i.e. the angle $\Delta\theta_{Breg}$, is connected to the plant's control input and the output from the plant is the boost factor response from the Phasor Estimation unit. The PLL also is included in the plant. Disturbances enter the control system from changes in the line terminal voltages.

As the plant encloses the boost factor measurement system and the synchronizing system (PLL) it is necessary to establish the parameters of those systems in order to define its open loop transfer function. A high gain in the PLL is required in order to reduce the sensitivity for line current disturbances. As it has been demonstrated in chapter 11.2.2 high gain can be used in the PLL if its frequency regulator contains a complex lead-lag link in addition to the standard PI link.

The phasor estimators for the boost measuring system and for the PLL utilize 1st order LP filters with -3 dB bandwidth 15 Hz for the average and 25 Hz for the phasor components. The frequency regulator is equipped with two cascaded links

- PI-link with transfer function $G_1(s) = k_{PLL}\dfrac{1+sT_{PLL}}{sT_{PLL}}$ with k_{PLL}=*150 (rad/s)/rad* and T_{PLL} = *0.100 s*
- complex lead-lag filter with transfer function $G_2(s) = \dfrac{\frac{s^2}{\omega_n} + 2\zeta_n s + \omega_n}{\frac{s^2}{\omega_d} + 2\zeta_d s + \omega_d}$ with ω_n=*170 rad/s,* ω_d=*240 rad/s* and $\zeta_n = \zeta_d$ = *0.4*

Step response to a phase shift of 0.1 rad of the input signal has been depicted in figure 13-3

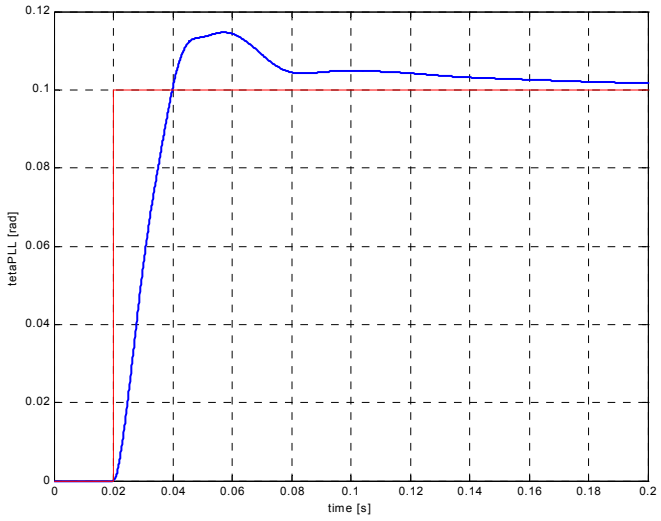

Figure 13-3 Step response of the PLL included in the plant.

The system equations can be derived from figure 13-1. We are interested in small deviations from a steady state operation with line current amplitude $\hat{I}_L$ and we may normalize the line current with its steady-state value as base. Further let the physical reactance (at network frequency) of the TCSC capacitor constitute the impedance base. When all quantities are represented in the rotating steady-state coordinate system *IL_SYNC* we get the following equations for the line and the fixed series capacitor

$$\begin{aligned}
&\frac{x_L}{\omega_N}\Delta\dot{\tilde{\tilde{i}}}_L^R + jx_L\Delta\tilde{\tilde{i}}_L^R = \Delta\tilde{\tilde{u}}_T^R - r_L\Delta\tilde{\tilde{i}}_T^R - \Delta\tilde{\tilde{u}}_F^R - \Delta\tilde{\tilde{u}}_C^R \\
&\frac{1}{\omega_N}\Delta\dot{\tilde{\tilde{u}}}_F^R + j\Delta\tilde{\tilde{u}}_F^R = x_F\Delta\tilde{\tilde{i}}_L^R \\
&\tilde{\tilde{u}}_T^R = \tilde{\tilde{u}}_{T1}^R - \tilde{\tilde{u}}_{T2}^R
\end{aligned} \qquad (13\text{-}1)$$

The corresponding state-space system is obtained by resolving the vector functions in their real and imaginary parts. This yields the equations (13-2), which interface the equations describing the dynamics of the TCSC, and which have been discussed in the preceding chapters.

$$\frac{d}{dt}\begin{pmatrix}\Delta\widetilde{i}_{Ld}^{R}\\ \Delta\widetilde{i}_{Lq}^{R}\\ \Delta\widetilde{u}_{Fd}^{R}\\ \Delta\widetilde{u}_{Fq}^{R}\end{pmatrix}=\begin{pmatrix}-\frac{\omega_N r_L}{x_L} & \omega_N & -\frac{\omega_N}{x_L} & 0\\ -\omega_N & -\frac{\omega_N r_L}{x_L} & 0 & -\frac{\omega_N}{x_L}\\ \omega_N x_F & 0 & 0 & \omega_N\\ 0 & \omega_N x_F & -\omega_N & 0\end{pmatrix}\begin{pmatrix}\Delta\widetilde{i}_{Ld}^{R}\\ \Delta\widetilde{i}_{Lq}^{R}\\ \Delta\widetilde{u}_{Fd}^{R}\\ \Delta\widetilde{u}_{Fq}^{R}\end{pmatrix}+$$
$$+\begin{pmatrix}\frac{\omega_N}{x_L} & 0 & -\frac{\omega_N}{x_L} & 0\\ 0 & \frac{\omega_N}{x_L} & 0 & -\frac{\omega_N}{x_L}\\ 0 & 0 & 0 & 0\\ 0 & 0 & 0 & 0\end{pmatrix}\begin{pmatrix}\Delta\widetilde{u}_{Td}^{R}\\ \Delta\widetilde{u}_{Tq}^{R}\\ \Delta\widetilde{u}_{Cd}^{R}\\ \Delta\widetilde{u}_{Cq}^{R}\end{pmatrix} \tag{13-2}$$

In order to derive the transfer functions for the combined TCSC and transmission line system we may introduce transfer function notation in order to formulate the following linear equation system:

$$\begin{aligned}
\Delta\widetilde{u}_{Cd}^{R} &= G_{TCSC}^{R,d->d}\Delta\widetilde{i}_{Ld}^{R}+G_{TCSC}^{R,q->d}\Delta\widetilde{i}_{Lq}^{R}+G_{TCSC}^{R,\theta->d}\left(\Delta\theta_{Breg}+\Delta\theta_{PLL}\right)\\
\Delta\widetilde{u}_{Cq}^{R} &= G_{TCSC}^{R,d->q}\Delta\widetilde{i}_{Ld}^{R}+G_{TCSC}^{R,q->q}\Delta\widetilde{i}_{Lq}^{R}+G_{TCSC}^{R,\theta->q}\left(\Delta\theta_{Breg}+\Delta\theta_{PLL}\right)\\
\Delta\widetilde{i}_{Ld}^{R} &= G_{TL}^{R,Td->d}\Delta\widetilde{u}_{Td}^{R}+G_{TL}^{R,Tq->d}\Delta\widetilde{u}_{Tq}^{R}+G_{TL}^{R,Cd->d}\Delta\widetilde{u}_{Cd}^{R}+G_{TL}^{R,Cq->d}\Delta\widetilde{u}_{Cq}^{R}\\
\Delta\widetilde{i}_{Lq}^{R} &= G_{TL}^{R,Td->q}\Delta\widetilde{u}_{Td}^{R}+G_{TL}^{R,Tq->q}\Delta\widetilde{u}_{Tq}^{R}+G_{TL}^{R,Cd->q}\Delta\widetilde{u}_{Cd}^{R}+G_{TL}^{R,Cq->q}\Delta\widetilde{u}_{Cq}^{R}\\
\Delta\theta_{PLL} &= G_{PLL}^{R,d->\theta}\Delta\widetilde{i}_{Ld}^{R}+G_{PLL}^{R,q->\theta}\Delta\widetilde{i}_{Lq}^{R}
\end{aligned} \tag{13-3}$$

The transfer functions $G_{TCSC}^{R,d->d}, G_{TCSC}^{R,q->d}, G_{TCSC}^{R,\theta->d}, G_{TCSC}^{R,d->q}, G_{TCSC}^{R,q->q}, G_{TCSC}^{R,\theta->q}$ represent equations (7-26) and (7-30) describing the TCSC dynamics. They have been transformed from the discrete state space form in the time domain, where they are represented by the matrix quadruple *[A,B,C,D]*, to the frequency domain using the standard transformation rule $G(j\Omega)=C\left(I\,e^{j\Omega h}-A\right)^{-1}B+D$, where h is the sampling time.

The transfer functions $G_{TL}^{R,Td->d}, G_{TL}^{R,Tq->d}, G_{TL}^{R,Cd->d}, G_{TL}^{R,Cq->d}, G_{TL}^{R,Td->q}, G_{TL}^{R,Tq->q}, G_{TL}^{R,Cd->q}, G_{TL}^{R,Cq->q}$ represent the transmission line, and its interaction with the fixed series capacitor and the TCSC. These transfer functions can be obtained from (13-2) using the standard formula $G(s)=C(sI-A)^{-1}B+D$ applicable for any linear time-invariant state space systems represented by the quadruple of matrices *[A,BC,D]*.

The transfer functions $G_{PLL}^{R,d->q}, G_{PLL}^{R,q->q}$ describe the PLL and can be obtained from (11-5).

Finally we can use the formula (11-3) to get the measured boost factor response as

$$k_{B.m} = -G_{PE}^{R,q->q}\left(\Delta\widetilde{u}_{Cq,av}^{R} + k_B\Delta\widetilde{i}_{Ld}^{R}\right) - G_{PE}^{R,d->q}\left(\Delta\widetilde{u}_{Cd,av}^{R} - k_B\Delta\widetilde{i}_{Ld}^{R}\right) \tag{13-4}$$

In order to solve the transfer functions we rewrite the linear system as

$$\begin{pmatrix} 1 & 0 & -G_{TCSC}^{R,d->d} & -G_{TCSC}^{R,q->d} & -G_{TCSC}^{R,\theta->d} \\ 0 & 1 & -G_{TCSC}^{R,d->q} & -G_{TCSC}^{R,q->q} & -G_{TCSC}^{R,\theta->q} \\ -G_{TL}^{R,Cd->d} & -G_{TL}^{R,Cq->d} & 1 & 0 & 0 \\ -G_{TL}^{R,Cd->q} & -G_{TL}^{R,Cq->q} & 0 & 1 & 0 \\ 0 & 0 & -G_{PLL}^{R,d->\theta} & -G_{PLL}^{R,q->\theta} & 1 \end{pmatrix} \begin{pmatrix} \Delta\widetilde{u}_{Cd}^{R} \\ \Delta\widetilde{u}_{Cq}^{R} \\ \Delta\widetilde{i}_{Ld}^{R} \\ \Delta\widetilde{i}_{Lq}^{R} \\ \Delta\theta_{PLL} \end{pmatrix} =$$
$$= \begin{pmatrix} 0 & 0 & G_{TCSC}^{R,\theta->d} \\ 0 & 0 & G_{TCSC}^{R,\theta->q} \\ G_{TL}^{R,Td->d} & G_{TL}^{R,Tq->d} & 0 \\ G_{TL}^{R,Td->q} & G_{TL}^{R,Tq->q} & 0 \\ 0 & 0 & 0 \end{pmatrix} \begin{pmatrix} \Delta\widetilde{u}_{Td}^{R} \\ \Delta\widetilde{u}_{Tq}^{R} \\ \Delta\theta_{Breg} \end{pmatrix} \tag{13-5}$$

$$\Delta k_{B,m} = \begin{pmatrix} -G_{PE}^{R,d->q} & -G_{PE}^{R,q->q} & -k_B G_{PE}^{R,d->d} & -k_B G_{PE}^{R,q->d} & 0 \end{pmatrix} \begin{pmatrix} \Delta\widetilde{u}_{Cd}^{R} \\ \Delta\widetilde{u}_{Cq}^{R} \\ \Delta\widetilde{i}_{Ld}^{R} \\ \Delta\widetilde{i}_{Lq}^{R} \\ \Delta\theta_{PLL} \end{pmatrix} \tag{13-6}$$

13.3 SYSTEM UNCERTAINTIES

Next we shall investigate a simple, but despite that representative, example. Assume the following line data and conditions

- system voltage *500 kV, 50 Hz*
- line length *400 km*
- line impedance *0.025 + j*0.25 Ω/km*, thus total line impedance is *10 + j*100 Ω/phase*
- resistance deviation due to temperature variation *-25 %* to *+30 %*
- short circuit current capacity in each line terminal is nominally *8 kA* but it may vary between *3* and *15 kA* due to changing network conditions; each

source reactance thus is nominally *36 Ω/phase* but varies between *19* and *96 Ω/phase*

- short circuit sources have nominal X/R ratio *8* with a variation in the range between *5* and *10*; the corresponding resistance is nominally *36/8 = 4.5 Ω/phase* with variation in the range *[19/10 ...96/5] = [1.9 ... 19.2] Ω/phase*
- fixed series compensation degree is *50 %* of the line reactance, thus *50 Ω/phase*
- TCSC capacitor bank physical reactance *15 Ω/phase*
- TCSC boost level varies in the range *1.0* to *1.5*, nominal *1.2*

Using the TCSC capacitor bank reactance *(15 Ω/phase)* as a base the following parameters are obtained:

- line reactance (including sources)
  nominal: $x_L = 100 + 2\times36 = 172\ \Omega/phase = 11.47\ pu$
  minimum: $x_L = 100 + 2\times 19 = 138\ \Omega/phase = 9.2\ pu$
  maximum: $x_L = 100 + 2\times 96 = 292\ \Omega/phase = 19.47\ pu$
- line resistance (including sources)
  nominal: $r_L = 10 + 2\times4.5 = 19\ \Omega/phase = 1.27\ pu$
  minimum: $r_L = 0.70\times10 + 2\times 1.9 = 10.8\ \Omega/phase = 0.72\ pu$
  maximum: $r_L = 1.25\times10 + 2\times19.2 = 50.9\ \Omega/phase = 3.39\ pu$
- fixed series capacitor: $x_F = 50\ \Omega/phase = 3.33\ pu$

We further assume that the TCSC operates with a steady state boost factor in the range

- k_B *= [1…1.5], nominal value 1.2*
- and from the discussion in the preceding chapter we inherit the main circuit uncertainties for the loss factor and the control time delay
- D_f *=[0.95…1.0], nominal value 0.98*
- τ_{delay} *= [0…3ms], nominal value 1 ms*

13.4 PLANT TRANSFER FUNCTION

We can now apply the idealized model. The envelops enclosing the open-loop plant transfer functions, i.e. the transfer function from control angle θ_{Breg} to the measured boost factor $k_{B,m}$ for the whole ensemble of parameter combinations have been depicted in figure 13-4. The transfer function for the nominal plant (marked by circles) also has been included in the drawing.

The transfer function for the system with stiff line current has been shown earlier in figure 12-2. Comparison with the new curves in figure 13-4 shows that the TCSC uncertainties dominate at low frequency but that new uncertainty has been added in the frequency range *30-200 rad/s*. The series-compensated transmission

line has a resonance somewhere in this frequency range and this causes a gain increase. The resonance frequency is uncertain due to the uncertainty in the source inductance and the resonance gain due to the variation in both line and source resistance.

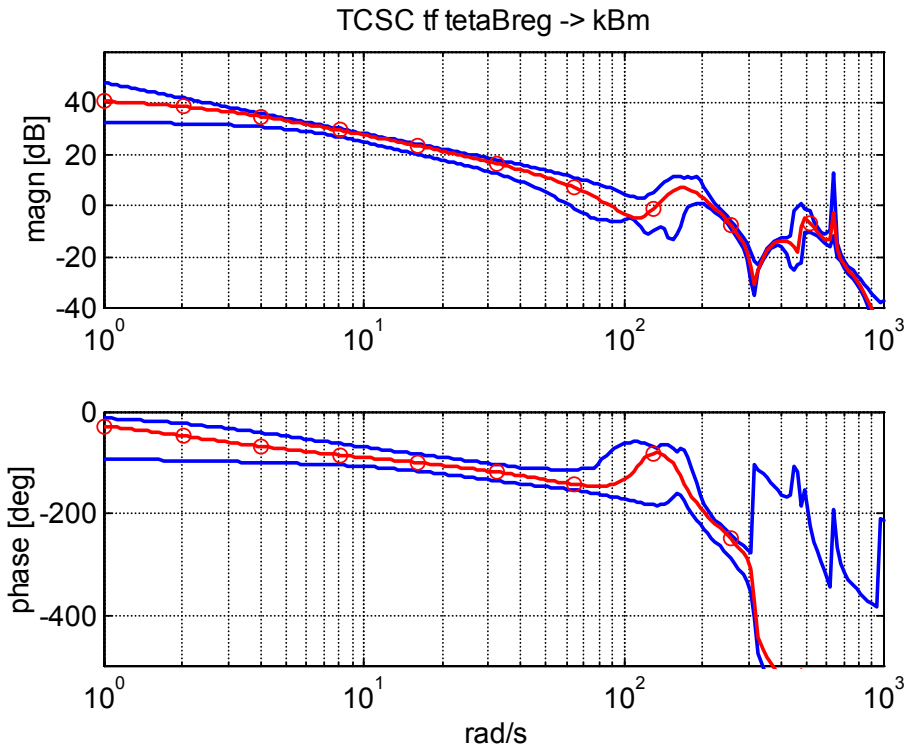

Figure 13-4 *Open loop transfer function from control angle to boost factor response for the plant.*

In figure 13-5 the **nominal** plant transfer function is depicted together with its variation at certain frequencies in a Nichols chart. These areas are known as 'templates' in the QFT vocabulary. The figure clearly shows that the biggest uncertainty occurs at *125 - 150 rad/s*. At these frequencies the gain and phase variation exceeds 20 dB and 100 deg respectively.

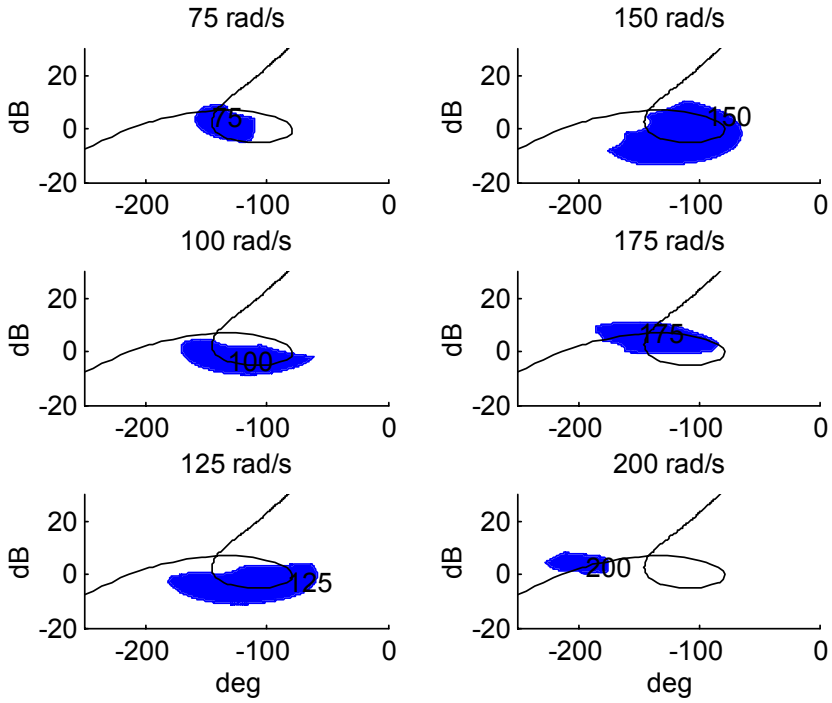

Figure 13-5 Templates for plant transfer function at specific frequencies.

13.5 SERVO SPECIFICATION AND REGULATOR DESIGN

For the system with the uncertainties described above we may specify the following for the measured boost factor response signal at a sudden reference step, namely

- rise time from 0 to 90 % of its final value in less than 100 ms
- settling time to ±5 % of its final value within 200 ms
- overshoot less than 10 %

The corresponding Horowitz bounds may then be calculated. Each such bound, valid for a specific frequency, define an area in the Nichol's chart, where the total nominal open loop transfer function must not reside at that frequency. It is the task for the control system engineer to find suitable regulator links that fulfils this requirement. It is advantageous to use as low feedback gain as possible as this will minimize the noise injection to the system.

Figure 13-6 shows the final nominal open loop gain in the feedback loop together with the Horowitz bounds for some interesting frequencies.

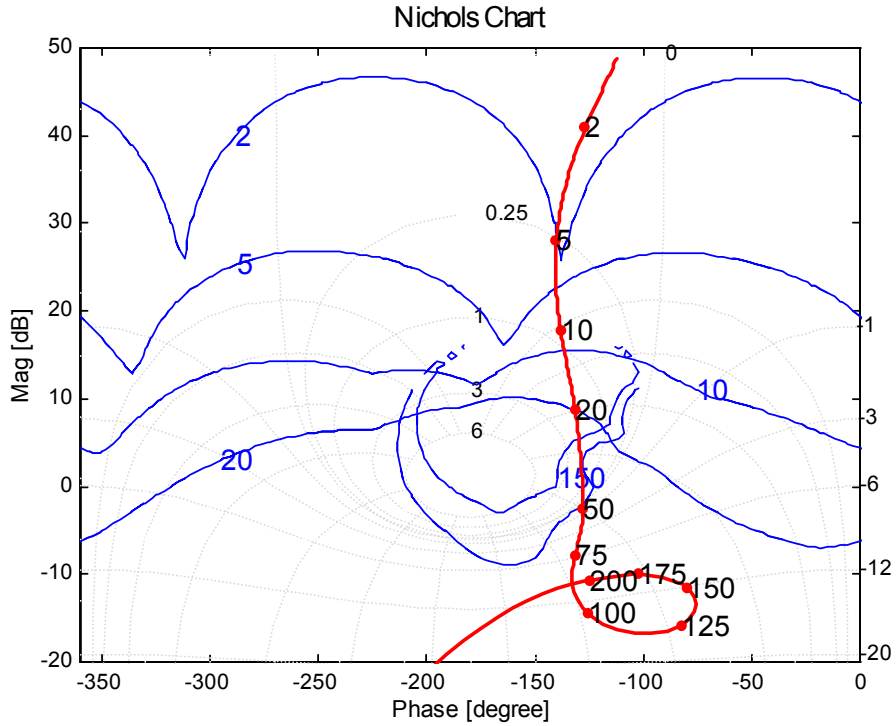

Figure 13-6 Total open loop transfer function and some Horowitz bounds.

The regulator transfer function was selected to be a PI controller in series with two second-order links

$$G_{Breg}(s) = k_{Breg}\frac{(1+sT_{Breg})}{sT_{Breg}}\frac{\left(\frac{s^2}{\omega_{n1}}+2\zeta_{n1}s+\omega_{n1}\right)}{\left(\frac{s^2}{\omega_{d1}}+2\zeta_{d1}s+\omega_{d1}\right)}\frac{\left(\frac{s^2}{\omega_{n2}}+2\zeta_{n2}s+\omega_{n2}\right)}{\left(\frac{s^2}{\omega_{d2}}+2\zeta_{d2}s+\omega_{d2}\right)} \qquad (13\text{-}7)$$

with the parameters

$k_{Breg} = 0.55$ rad/pu, $T_{Breg} = 80$ ms

$\omega_{d1} = 110$ rad/s, $\omega_{n1} = 60$ rad/s, $\zeta_{d1} = 0.54$, $\zeta_{n1} = 0.67$

$\omega_{d2} = 245$ rad/s, $\omega_{n2} = 165$ rad/s, $\zeta_{d2} = 1.4$, $\zeta_{n2} = 0.18$

The second order links serves the purpose of adding some phase to the transfer function for frequencies exceeding 30 rad/s and further to keep down the gain at 200 rad/s.

Figure 13-7 shows the step responses for the ensemble of parameter combinations (243 different combinations).

Figure 13-7 Step response without prefilter for the whole ensemble of systems.

Figure 13-8 depicts six different cases, representing the extreme results obtained, from the collection of systems.

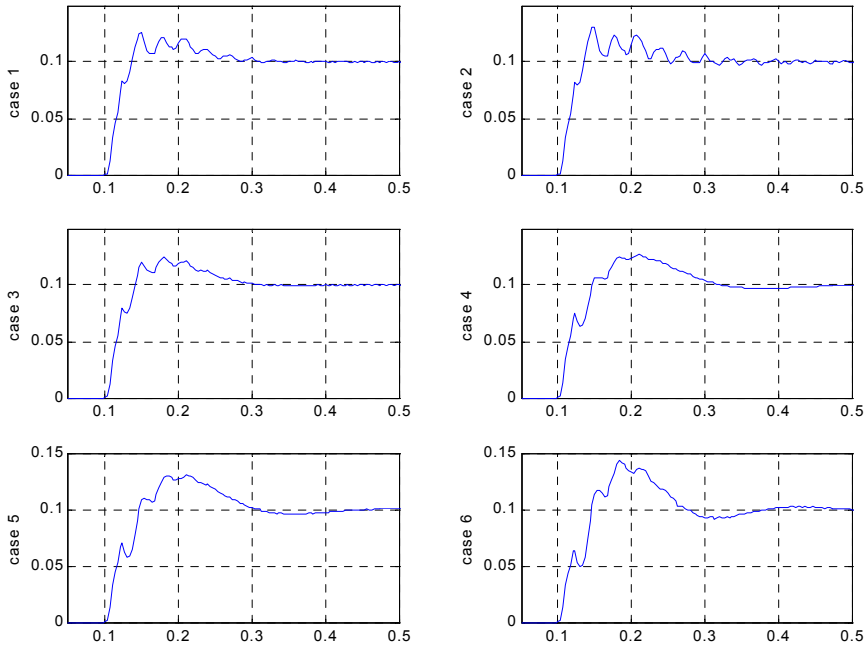

Figure 13-8 Six selected step responses for various parameter combinations.

The associated parameters for these cases are given in Table 13-I.

Table 13-I Parameter values for the selected cases

	x_L (pu)	r_L (pu)	D_f (pu)	τ (ms)	k_B	x_F (pu)
case 1	14.2	1.6	1.00	3	1.5	3.33
case 2	14.2	0.7	1.00	3	1.5	3.33
case 3	10.8	2.6	1.00	3	1.5	3.33
case 4	7.4	2.6	1.00	3	1.5	3.33
case 5	7.4	1.6	1.00	3	1.5	3.33
case 6	7.4	0.7	1.00	3	1.5	3.33

It appears from the graphs that the rise time is in the order of 50 ms or less, but that an overshoot up to 40 % appears in some cases.

This can also be seen in figure 13-9, where the small circles indicate the variation of the closed loop transfer function for the regulator and the uncertain system for different parameter combinations (template). The graph also shows the corresponding frequency-domain closed loop specification.

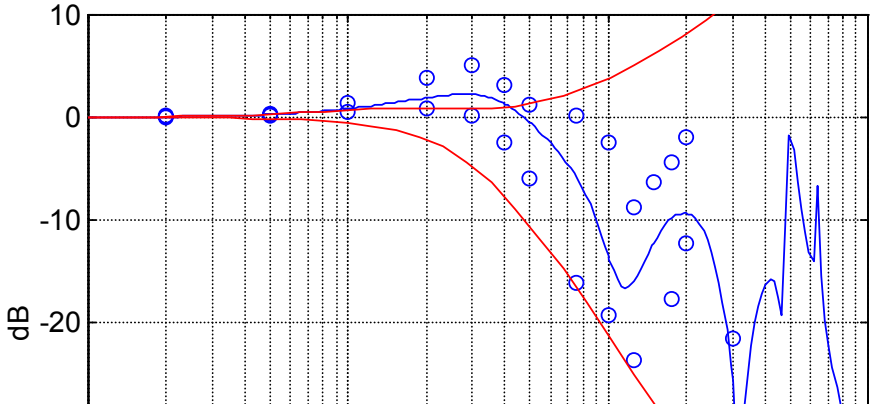

Figure 13-9 Envelop of closed loop transfer functions (circles) and closed loop nominal and specification limits (solid lines) in the frequency domain.

It can be concluded that a prefilter with a gain reduction in the range of 30 rad/s can reduce the overshot. As an example such a prefilter can be have the transfer function

$$F_{XR}(s) = \frac{1}{\left(1+\frac{s}{\omega_{PF1}}\right)} \cdot \frac{\left(\frac{s}{\omega_{PFn2}}\right)^2 + 2\zeta_{PFn2}\frac{s}{\omega_{PFn2}} + 1}{\left(\frac{s}{\omega_{PFd2}}\right)^2 + 2\zeta_{PFd2}\frac{s}{\omega_{PFd2}} + 1} \tag{13-8}$$

with the parameters

$\omega_{PF1} = 150\ rad/s$

$\omega_{PFd2} = 44\ rad/s$

$\omega_{PFn2} = 36$

$\zeta_{PFd2} = 1.15$

$\zeta_{PFn2} = 0.55$

The step response of the prefilter is shown in figure 13-10.

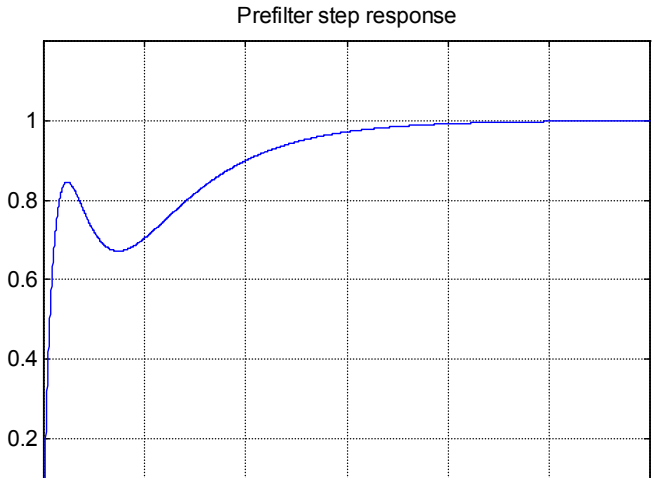

Figure 13-10 Prefilter step response

The closed loop transfer function in figure 13-9 modifies to the one in figure 13-11, when the prefilter is taken into account.

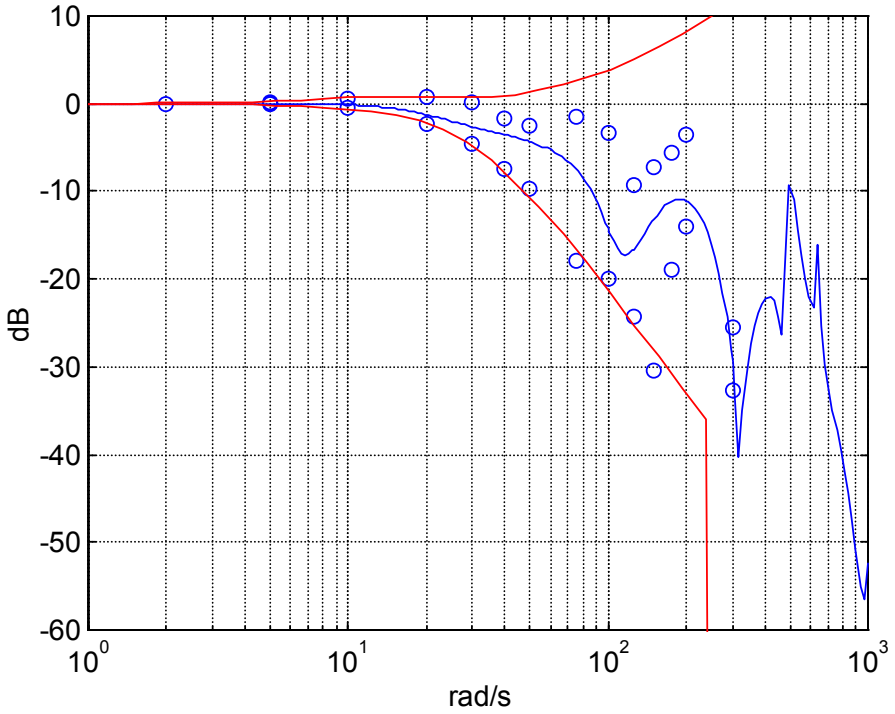

Figure 13-11 Modified closed loop transfer function variation (circles) and nominal and specification limits (solid lines)

Finally we obtain the step responses that are depicted in figure 13-12 for all parameter combinations and in figure 13-13 for the special cases according to Table 13.I.

Figure 13-12 Step response with prefilter for the whole ensemble of systems.

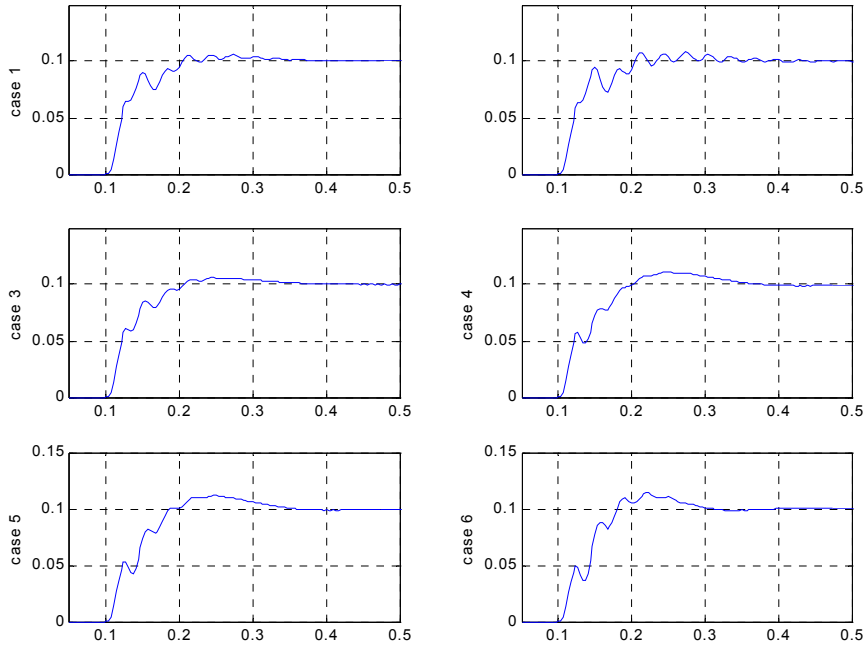

Figure 13-13 Six selected step responses for various parameter combinations.

The step responses obtained approximately fulfils the original specification with respect to rise time, settling time and overshot. The TCSC servo response may be approximately represented, e.g. in power oscillation damping simulations, by an equivalent first order filter with a time constant of 50 ms.

CHAPTER 14
TCSC AND SUBSYNCHRONOUS RESONANCE

14.1 BACKGROUND

In chapter 12 and 13 we have analysed in some detail the control behaviour of the TCSC. These studies mainly focus on the boost control, its stability and speed of response. The investigations have shown that the small signal model derived in the thesis provides a handy tool for tuning the control system. It has also been shown that a robust design with respect to varying conditions in the transmission system can be obtained, e.g. by using the methods developed in QFT.

In chapter 5 we have touched upon the subject of how the TCSC reacts when a current composant with subsynchronous frequency is being injected in addition to the normal 50 or 60 Hz line current. It was shown that the TCSC, when controlled according to the SVR scheme, ideally exhibits resistive-inductive apparent impedance to the system at subsynchronous frequencies. This is an important fact due to its implications with respect to the possible occurrence of a phenomenon known as subsynchronous resonance (SSR). The origin of one principal type of SSR will be dealt with in the following section.

The purpose of the investigations in this chapter is to apply the developed small-signal model in order to make a somewhat deeper analysis of the conditions at subsynchronous frequencies. One specific objective of great interest is to evaluate the impact of the boost control system (including the synchronization system) on the preconditions for SSR.

14.2 TORSIONAL INTERACTION SSR

It has been known for several decades that fixed series capacitors under certain conditions may interact with the generator-turbine shaft system in a connected thermal power station and spontaneously excite exponentially increasing torque oscillations. The phenomenon is known as Torsional Interaction Subsynchronous

Resonance or shorter TI-SSR. The SSR family also comprises some other related incidents like “Induction Generator Effect” and “Transient Torque Effect” [B5]. Similar SSR problems may be associated with other transmission installations e.g HVDC.

The TI-SSR can only occur if three conditions are fulfilled

- the shaft system must have a mechanical resonance at a subsynchronouns frequency f_m
- the generator mass must participate and be one of the swinging masses in the oscillation mode at frequency f_m
- a matching electrical resonance must exist in the transmission system at the “complementary” frequency $f_N - f_m$

Figure 14-1 illustrates the important constituents, which in combination establish the conditions for TI-SSR.

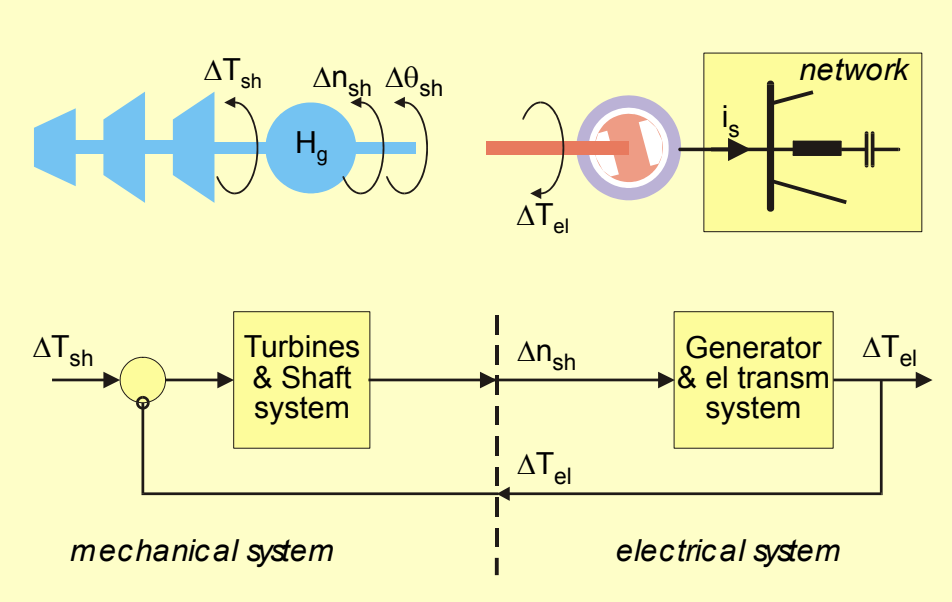

Figure 14-1 Subsystems interacting at subsynchronous resonance.

The mechanical shaft system is shown on the left-hand side. The shaft connecting the generator with the turbines exerts a mechanical torque on the generator mass. Typically several masses representing different turbine stages (low-pressure, high pressure etc.) must be represented in the model. When a torsional swing mode is excited the masses perform small amplitude twisting movements relative each other. The phase angle of the generator mass becomes modulated, causing a flux variation in the stator circuit. The flux deviation creates a voltage variation in the stator and, depending on the network impedance (or rather its admittance), a line current disturbance results. The latter is particularly noteworthy if an electrical resonance exists in the connected network.

The flux in the generator and the stator current create an electrical torque, which decelerates the generator mass, and which in the *IL_SYNC* coordinate system is given in normalized units by the expression

$$\widetilde{T}_{el}(t) = \mathrm{Im}\left[\widetilde{\vec{i}}_S^{\,R}(t)\widetilde{\vec{\psi}}_S^{\,R*}(t)\right] \tag{14-1}$$

For small deviations we get

$$\Delta\widetilde{T}_{el}(t) = \mathrm{Im}\left[\widetilde{\vec{\psi}}_S^{\,R*}\Delta\widetilde{\vec{i}}_S^{\,R}(t)\right] + \mathrm{Im}\left[\widetilde{\vec{I}}_S^{\,R}\Delta\widetilde{\vec{\psi}}_S^{\,R*}(t)\right] \tag{14-2}$$

where the steady state quantities have been denoted by phasor arrows. The torque variation acts on the generator mass and a feedback loop is being established, as shown in the lower part of figure 14-1. Our interest will now be concentrated on the transfer function between the impressed shaft speed modulation, Δn_{sh}, and the electrical torque, $\Delta\widetilde{T}_{el}$, that it brings about. In other words we will look at the gain and phase relation in the open loop feedback branch that represents the generator and the electrical transmission system. From this characteristic the possibility of SSR conditions can be visualized in the electrical damping curve for the system.

The influence of the TCSC on the possible SSR conditions relates to its impact on the electrical resonance conditions in the network. In the frequency range where the TCSC exhibits resistive-inductive apparent reactance no electrical resonance can be established between the TCSC and the line inductance.

14.3 GENERIC GENERATOR MODEL

The generator models used in power system analysis often are quite complicated with several winding systems along both the direct and the quadrature axis [B5]. These sophisticated models are motivated when low-frequency electro-mechanical transients shall be modeled with sufficient accuracy. Such transients namely mainly involve low rotor frequencies up to a few Hz. For SSR conditions the rotor frequency is much higher, typically in the range from 15 to 40 Hz. At these rotor frequencies the resistance in the damper windings has little impact. These windings therefore serve as a magnetic screen, which captures the rotor flux and prevents it from being varied. The leakage between the stator winding and the damper windings is represented by the subtransient reactance and the rotor flux behind that reactance can be considered to be constant in a rotor-fixed coordinate system. If the subtransient reactance is lumped together with the line reactance the remaining machine model simply becomes a rotating constant flux. Figure 14-2 illustrates this simple generic generator model.

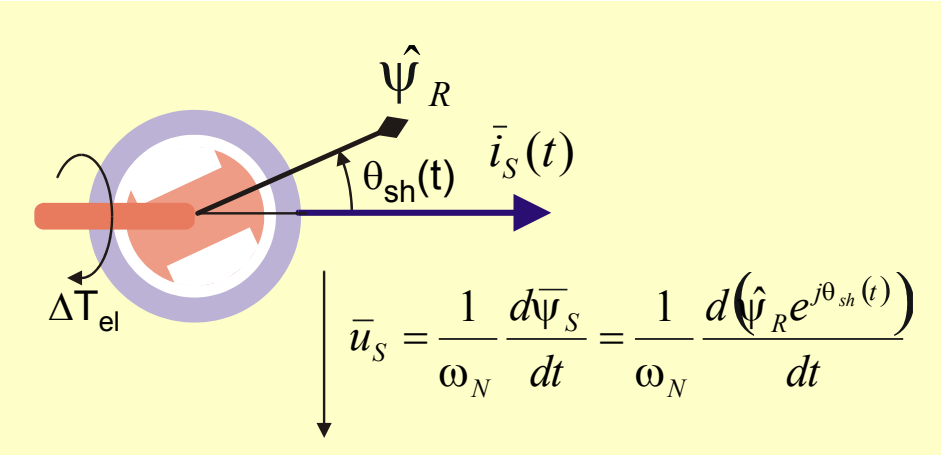

Figure 14-2 Generic simple generator model.

Let the normalized rotor flux be $\tilde{\hat{\psi}}_R$ and assume that it is constant. The shaft angle is $\theta_{sh}(t)$ in the *FIXED* coordinate system. Due to the rotor movement the flux in the stator circuit in the *FIXED* coordinate system becomes

$$\tilde{\bar{\psi}}_S^S(t) = \tilde{\hat{\psi}}_R e^{j\theta_{sh}(t)} \tag{14-3}$$

The induced stator voltage is the time derivative of the stator flux so that

$$\tilde{\bar{u}}_S^S(t) = \frac{1}{\omega_N}\frac{d\tilde{\bar{\psi}}_S^S}{dt} = j\tilde{\hat{\psi}}_R \frac{\dot{\theta}_{sh}}{\omega_N} e^{j\theta_{sh}(t)} \tag{14-4}$$

(Due to the use of normalized quantities, "per unit values", a visible factor ω_N shows up in formulas that involve time derivation).

Introduce the normalized mechanical shaft speed n_{sh} according to the definition

$$n_{sh}(t) = \frac{\dot{\theta}_{sh}(t)}{\omega_N} \tag{14-5}$$

Now assume that the shaft speed contains small sinusoidal deviations with frequency Ω so that

$$n_{sh}(t) = 1 + \mathrm{Re}\left\{\Delta\hat{n} e^{j\Omega t}\right\} \tag{14-6}$$

where $\Delta\hat{n}$ is a complex constant. Due to the relation (14-5) the angle will also be modulated. Integration of (14-6) yields

$$\begin{aligned}\theta_{sh}(t) &= \theta_{sh0} + \omega_N t + \mathrm{Re}\left\{\frac{\omega_N}{j\Omega}\Delta\hat{n}e^{j\Omega t}\right\} \\ \theta_{sh0} &= const\end{aligned} \tag{14-7}$$

We put (14-7) into (14-3) to get the flux variation caused by the rotor shaft speed modulation

$$\begin{aligned}\tilde{\tilde{\psi}}_S^S(t) &= \tilde{\hat{\psi}}_R e^{j\left\{\theta_{sh0}+\omega_N t+\mathrm{Re}\left[\frac{\omega_N}{j\Omega}\Delta\hat{n}e^{j\Omega t}\right]\right\}} = \tilde{\hat{\psi}}_R e^{j\theta_{sh0}} e^{j\omega_N t} e^{j\,\mathrm{Re}\left[\frac{\omega_N}{j\Omega}\Delta\hat{n}e^{j\Omega t}\right]} \approx \\ &\approx \tilde{\hat{\psi}}_R e^{j\theta_{sh0}} e^{j\omega_N t}\left\{1 + j\,\mathrm{Re}\left[\frac{\omega_N}{j\Omega}\Delta\hat{n}e^{j\Omega t}\right]\right\}\end{aligned} \tag{14-8}$$

This yields in the *FIXED* coordinate system

$$\Delta\tilde{\tilde{\psi}}_S^S(t) \approx j\tilde{\hat{\psi}}_R e^{j\theta_{sh0}} e^{j\omega_N t}\,\mathrm{Re}\left[\frac{\omega_N}{j\Omega}\Delta\hat{n}e^{j\Omega t}\right] \tag{14-9}$$

and, due to (6-6), in the *IL_SYNC* coordinate system

$$\Delta\tilde{\tilde{\psi}}_S^R(t) \approx j\tilde{\hat{\psi}} e^{j\theta_{sh0}}\,\mathrm{Re}\left[\frac{\omega_N}{j\Omega}\Delta\hat{n}e^{j\Omega t}\right] \tag{14-10}$$

In order to get the deviation voltage caused by the rotor speed variation we insert (14-5) - (14-7) in (14-4). We get

$$\tilde{\tilde{u}}_S^S(t) = j\tilde{\tilde{\psi}}_R\left[1 + \mathrm{Re}\left(\Delta\hat{n}e^{j\Omega t}\right)\right] e^{j\left[\theta_{sh0}+\omega_N t+\mathrm{Re}\left(\frac{\omega_N}{j\Omega}\Delta\hat{n}e^{j\Omega t}\right)\right]} \tag{14-11}$$

Due to (6-6) the total voltage in the *IL_SYNC* coordinate system, aligned with the steady state line current, becomes

$$\underline{\tilde{u}}_S^R(t) = j\underline{\tilde{\psi}}_R e^{j\theta_{sh0}}\left[1+\mathrm{Re}\left(\Delta\hat{n}e^{j\Omega t}\right)\right]e^{j\,\mathrm{Re}\left(\frac{\omega_N}{j\Omega}\Delta\hat{n}e^{j\Omega t}\right)} \tag{14-12}$$

Denote

$$\underline{\tilde{\psi}}_R = \tilde{\hat{\psi}}_R e^{j\theta_{sh0}} \tag{14-13}$$

For small deviations we can approximate (14-12) as

$$\begin{aligned}
&\underline{\tilde{u}}_S^R(t) = j\underline{\tilde{\psi}}_R\left[1+\mathrm{Re}\left(\Delta\hat{n}e^{j\Omega t}\right)\right]e^{j\,\mathrm{Re}\left(\frac{\omega_N}{j\Omega}\Delta\hat{n}e^{j\Omega t}\right)} \approx \\
&\approx j\underline{\tilde{\psi}}_R\left[1+\mathrm{Re}\left(\Delta\hat{n}e^{j\Omega t}\right)\right]\left[1+j\,\mathrm{Re}\left(\frac{\omega_N}{j\Omega}\Delta\hat{n}e^{j\Omega t}\right)\right] \approx \\
&\approx j\underline{\tilde{\psi}}_R + j\underline{\tilde{\psi}}_R\left[\mathrm{Re}\left(\Delta\hat{n}e^{j\Omega t}\right)+j\,\mathrm{Re}\left(\frac{\omega_N}{j\Omega}\Delta\hat{n}e^{j\Omega t}\right)\right]
\end{aligned} \tag{14-14}$$

We can subtract the steady state voltage $j\underline{\tilde{\psi}}_R$ from (14-14). What remains then is the deviation voltage in *IL_SYNC*

$$\boxed{\Delta\underline{\tilde{u}}_S^R(t) = j\underline{\tilde{\psi}}_R\left[\mathrm{Re}\left(\Delta\hat{n}e^{j\Omega t}\right)+j\,\mathrm{Re}\left(\frac{\omega_N}{j\Omega}\Delta\hat{n}e^{j\Omega t}\right)\right]} \tag{14-15}$$

The formula (14-15) directly delivers the voltage deviation in two orthogonal directions. We will utilize the equation in this form in the following. However, the formula may alternatively be developed into

$$\boxed{\Delta\underline{\tilde{u}}_S^R(t) \approx \frac{j\underline{\tilde{\psi}}_R}{2}\left\{\Delta\hat{n}\left(1+\frac{\omega_N}{\Omega}\right)e^{j\Omega t}+\Delta\hat{n}^*\left(1-\frac{\omega_N}{\Omega}\right)e^{-j\Omega t}\right\}} \tag{14-16}$$

In this latter form one can immediately identify the super- and sub-synchronous voltage components.

14.4 CONNECTION TO THE NETWORK

We shall consider the situation depicted in figure 13-1, where a TCSC is connected in a resistive-inductive line with a fixed series capacitor between two nodes.

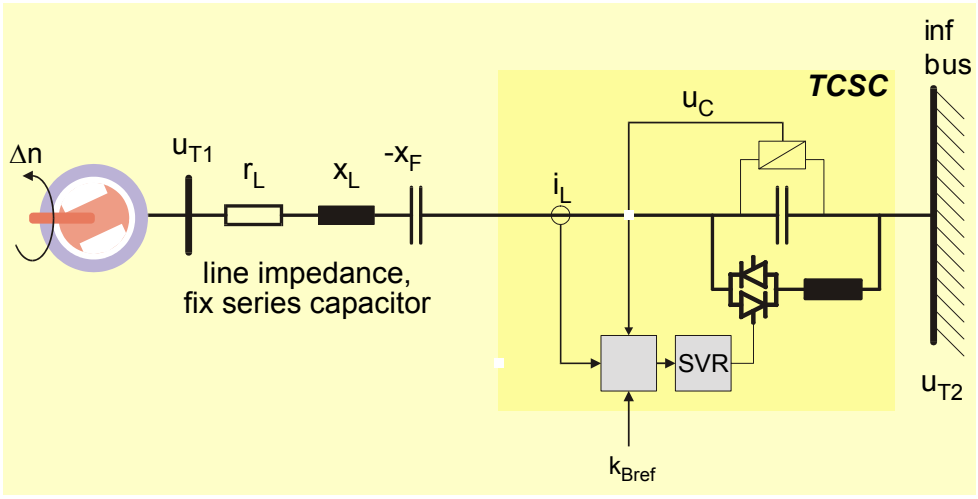

Figure 14-3 Outline of the generic study case.

Assume that a generic generator is connected to the left hand side node and that it feeds power into an infinite bus at the right hand side. This setup is outlined in figure 14-3.

14.4.1 Steady state conditions

We may assume that the amplitude of the steady state voltage $\vec{U}_{T2}^{R}$ is known and that the power delivered to the line terminal in the receiving end (the right-hand terminal) has been given as $P_{rec}+jQ_{rec}$. Then we can calculate the line current amplitude $\hat{I}_L$. The steady state line current phasor $\vec{I}_L^{R}$ is aligned with the real axis in the *IL_SYNC* coordinate system due to the definition of the latter. The argument of the terminal voltage U_{T2} therefore fulfils

$$\arg \vec{U}_{T2}^{R} = \arg(P_{rec} + jQ_{rec}) \tag{14-17}$$

Both the terminal voltage and the line current now have been fully determined. In the *IL_SYNC* coordinate system the steady state equation is

$$\underline{\tilde{U}}_{T1}^{R} = \underline{\tilde{U}}_{T2}^{R} + \left[\tilde{r}_L + j\left(\tilde{x}_L - \tilde{x}_F - \tilde{x}_{TCSC}\right)\right]\underline{\tilde{I}}_{L}^{R} \tag{14-18}$$

Here the quantities have been normalized. When the network equations shall be interfaced with the TCSC equations they must be normalized using the steady state line current and the physical reactance of the TCSC capacitor bank as base values. The *IL_SYNC* coordinate system is aligned with the line current, so the line current's normalized value in this case simply is unity. Further the TCSC steady state normalized voltage equals the steady state boost factor k_B. Thus

$$\underline{\tilde{U}}_{T1}^{R} = \underline{\tilde{U}}_{T2}^{R} + \tilde{r}_L + j\left(\tilde{x}_L - \tilde{x}_F - k_B\right) \tag{14-19}$$

Using (13.14) we get in *IL_SYNC* coordinates that

$$\underline{\tilde{U}}_{T1}^{R} = \underline{\tilde{U}}_{S}^{R} = je^{j\theta_{sh0}}\tilde{\psi}_R \tag{14-20}$$

Thus the rotor flux amplitude and phase can be obtained as

$$\begin{aligned} \tilde{\psi}_R &= \left|\underline{\tilde{U}}_{T1}^{R}\right| \\ \theta_{sh0} &= \arg \underline{\tilde{U}}_{T1}^{R} - \frac{\pi}{2} \end{aligned} \tag{14-21}$$

14.4.2 Fixed series compensation

In a first case we assume that the line is only compensated by a **fixed** series capacitor. The equations for the transmission system were discussed earlier in chapter 13. Equation (13-2) can be used in this case if we put $\Delta\tilde{u}_{Cd}^{R} = 0, \Delta\tilde{u}_{Cq}^{R} = 0$. Then we get

$$\frac{d}{dt}\begin{pmatrix}\Delta\widetilde{i}_{Ld}^{R}\\ \Delta\widetilde{i}_{Lq}^{R}\\ \Delta\widetilde{u}_{Fd}^{R}\\ \Delta\widetilde{u}_{Fq}^{R}\end{pmatrix}=A_{TL0}\begin{pmatrix}\Delta\widetilde{i}_{Ld}^{R}\\ \Delta\widetilde{i}_{Lq}^{R}\\ \Delta\widetilde{u}_{Fd}^{R}\\ \Delta\widetilde{u}_{Fq}^{R}\end{pmatrix}+B_{TL0}\begin{pmatrix}\Delta\widetilde{u}_{Td}^{R}\\ \Delta\widetilde{u}_{Tq}^{R}\end{pmatrix}$$
$$\begin{pmatrix}\Delta\widetilde{i}_{Ld}^{R}\\ \Delta\widetilde{i}_{Tq}^{R}\end{pmatrix}=C_{TL0}\begin{pmatrix}\Delta\widetilde{i}_{Ld}^{R}\\ \Delta\widetilde{i}_{Lq}^{R}\\ \Delta\widetilde{u}_{Fd}^{R}\\ \Delta\widetilde{u}_{Fq}^{R}\end{pmatrix} \tag{14-22}$$

with

$$A_{TL0}=\begin{pmatrix}-\frac{\omega_N r_L}{x_L} & \omega_N & -\frac{\omega_N}{x_L} & 0\\ -\omega_N & -\frac{\omega_N r_L}{x_L} & 0 & -\frac{\omega_N}{x_L}\\ \omega_N x_F & 0 & 0 & \omega_N\\ 0 & \omega_N x_F & -\omega_N & 0\end{pmatrix}\qquad B_{TL0}=\begin{pmatrix}\frac{\omega_N}{x_L} & 0\\ 0 & \frac{\omega_N}{x_L}\\ 0 & 0\\ 0 & 0\end{pmatrix} \tag{14-23}$$
$$C_{TL0}=\begin{pmatrix}1 & 0 & 0 & 0\\ 0 & 1 & 0 & 0\end{pmatrix}$$

The frequency domain transfer function can be immediately obtained by solving (14-22). The following result is obtained

$$\begin{pmatrix}\Delta\widetilde{u}_{Td}^{R}\\ \Delta\widetilde{u}_{Tq}^{R}\end{pmatrix}=\mathrm{Re}\begin{pmatrix}ae^{j\Omega t}\\ be^{j\Omega t}\end{pmatrix}\quad\Rightarrow\quad\begin{pmatrix}\Delta\widetilde{i}_{Ld}^{R}\\ \Delta\widetilde{i}_{Lq}^{R}\end{pmatrix}=\mathrm{Re}\begin{pmatrix}\left(aK_{TL}^{R,d->d}+bK_{TL}^{R,q->d}\right)e^{j\Omega t}\\ \left(aK_{TL}^{R,d->q}+bK_{TL}^{R,q->q}\right)e^{j\Omega t}\end{pmatrix} \tag{14-24}$$
$$\begin{pmatrix}K_{TL}^{R,d->d} & K_{TL}^{R,q->d}\\ K_{TL}^{R,d->q} & K_{TL}^{R,q->q}\end{pmatrix}=C_{TL0}\left(j\Omega-A_{TL0}\right)^{-1}B_{TL0}$$

14.4.3 TCSC and fixed series compensation

When the TCSC is inserted the calculation gets more complicated. The equations governing this system in the frequency domain are given by (13-5) and (13-6). Let us introduce the following notation for these equations

$$\begin{aligned} A_{(12.5)}\Delta X_{(12.5)} &= B_{(12.5)}\Delta U_{(12.5)} \\ \Delta k_{B,m} &= C_{(12.6)}\Delta X_{(12.5)} \end{aligned} \tag{14-25}$$

Here we can insert the boost regulator feedback transfer function G_{Breg} and put

$$\Delta\theta_{Breg} = -G_{Breg}\Delta k_{B,m} = -G_{Breg}C_{(12.6)}\Delta X_{(12.5)} \tag{14-26}$$

This yields (using MATLAB's notation)

$$\begin{aligned} \left[A_{(12.5)} + G_{Breg}B_{(12.5)}(:,3)C_{(12.6)}\right]\Delta X_{(12.5)} &= B_{(12.5)}(:,1:2)\Delta U_{(12.5)}(1:2) \\ \Delta k_{B,m} &= C_{(12.6)}\Delta X_{(12.5)} \end{aligned} \tag{14-27}$$

This equation system can now be inverted to get the desired transfer functions from the line terminal bus voltage components into the line current components. One arrives at the similar expression as in (14-24).

$$\begin{pmatrix} \Delta\widetilde{u}_{Td}^{R} \\ \Delta\widetilde{u}_{Tq}^{R} \end{pmatrix} = \mathrm{Re}\begin{pmatrix} ae^{j\Omega t} \\ be^{j\Omega t} \end{pmatrix} \quad \Rightarrow \quad \begin{pmatrix} \Delta\widetilde{i}_{Ld}^{R} \\ \Delta\widetilde{i}_{Lq}^{R} \end{pmatrix} = \mathrm{Re}\begin{pmatrix} \left(aK_{TL}^{R,d->d} + bK_{TL}^{R,q->d}\right)e^{j\Omega t} \\ \left(aK_{TL}^{R,d->q} + bK_{TL}^{R,q->q}\right)e^{j\Omega t} \end{pmatrix} \tag{14-28}$$

14.4.4 Line current deviations

The steady state voltage $j\widetilde{\widetilde{\psi}}_R$ is given by (14-20). We get

$$j\widetilde{\widetilde{\psi}}_R = j\hat{\widetilde{\psi}}_R e^{j\theta_{sh0}} = -\hat{\widetilde{\psi}}_R \sin\theta_{sh0} + j\hat{\widetilde{\psi}}_R \cos\theta_{sh0} \tag{14-29}$$

The impressed voltage deviations now can be obtained from (14-15)

$$\begin{aligned} \Delta\widetilde{u}_{Td}^{R} = \Delta\widetilde{u}_{Sd}^{R} &= \hat{\widetilde{\psi}}_R \,\mathrm{Re}\left\{\left(-\sin\theta_{sh0} + j\frac{\omega_N}{\Omega}\cos\theta_{sh0}\right)\Delta\hat{n}e^{j\Omega t}\right\} \\ \Delta\widetilde{u}_{Tq}^{R} = \Delta\widetilde{u}_{Sq}^{R} &= \hat{\widetilde{\psi}}_R \,\mathrm{Re}\left\{\left(\cos\theta_{sh0} + j\frac{\omega_N}{\Omega}\sin\theta_{sh0}\right)\Delta\hat{n}e^{j\Omega t}\right\} \end{aligned} \tag{14-30}$$

Plugging this result into equation (14-24) or (14-28) yields

$$\Delta\widetilde{i}_{Ld}^{R} = \widetilde{\hat{\psi}}_{R}\,\mathrm{Re}\left\{L_{sh,d}^{R}\,\Delta\hat{n}e^{j\Omega t}\right\}$$
$$L_{sh,d}^{R} = K_{TL}^{R,d->d}\left(-\sin\theta_{sh0} + j\frac{\omega_N}{\Omega}\cos\theta_{sh0}\right) + K_{TL}^{R,q->d}\left(\cos\theta_{sh0} + j\frac{\omega_N}{\Omega}\sin\theta_{sh0}\right) \quad (14\text{-}31)$$

$$\Delta\widetilde{i}_{Lq}^{R} = \widetilde{\hat{\psi}}_{R}\,\mathrm{Re}\left\{L_{sh,q}^{R}\,\Delta\hat{n}e^{j\Omega t}\right\}$$
$$L_{sh,q}^{R} = K_{TL}^{R,d->q}\left(-\sin\theta_{sh0} + j\frac{\omega_N}{\Omega}\cos\theta_{sh0}\right) + K_{TL}^{R,q->q}\left(\cos\theta_{sh0} + j\frac{\omega_N}{\Omega}\sin\theta_{sh0}\right) \quad (14\text{-}32)$$

14.5 ELECTRICAL TORQUE

The variation of the electrical torque, which is caused by the modulation of the shaft speed, is governed by the general equation (14-2). Figure 14-4 illustrates how the steady state quantities and the linear deviations interact to create the electrical torque deviation from their steady state values.

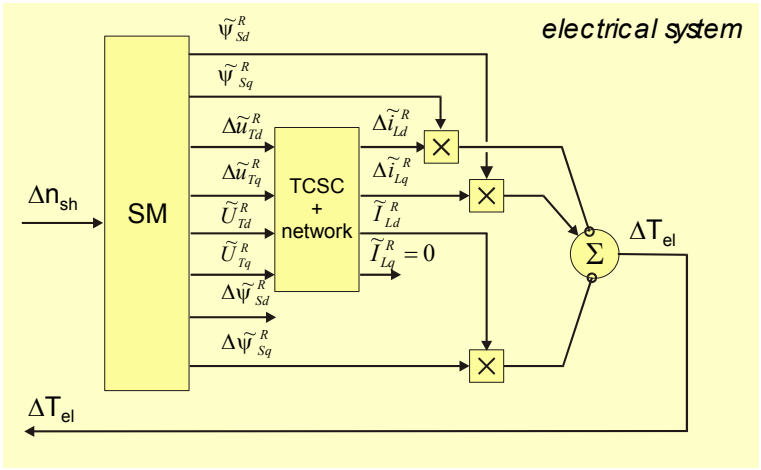

Figure 14-4 Generation of electrical torque deviation {SSRmod2.wmf}.

A first contribution to the electrical torque is obtained by the interaction between the deviation of the flux and the steady state line current. The flux variation is obtained from (14-10). We get

$$\Delta\widetilde{T}_{el1} = \mathrm{Im}\left[\widetilde{\vec{I}}_{S}^{R}\,\Delta\widetilde{\vec{\psi}}_{S}^{R*}\right] = \mathrm{Im}\left[\widetilde{\vec{I}}_{L}^{R}\,\Delta\widetilde{\vec{\psi}}_{S}^{*R}\right] = -\mathrm{Im}\left[\widetilde{\vec{I}}_{L}^{R*}\,\Delta\widetilde{\vec{\psi}}_{S}^{R}\right] =$$
$$= -\mathrm{Im}\left\{\widetilde{\vec{I}}_{L}^{R*}\left(j\widetilde{\vec{\psi}}_{R}e^{j\theta_{sh0}}\right)\mathrm{Re}\left[\frac{\omega_N}{j\Omega}\Delta\hat{n}e^{j\Omega t}\right]\right\} \quad (14\text{-}33)$$

where $\widetilde{\vec{I}}_L^R$ is the phasor that represents the steady state line current. Due to its definition the *IL_SYNC* system is aligned with the steady state line current, so the steady state phasor is real and equals $\hat{I}_L$, which happens to be the current base. Thus it turns out that $\widetilde{\vec{I}}_L^R$ equals unity. Equation (14-33) therefore reduces to

$$\Delta\widetilde{T}_{el1} = -\widetilde{\hat{\psi}}_R \cos\theta_{sh0} \operatorname{Re}\left[\frac{\omega_N}{j\Omega}\Delta\hat{n}e^{j\Omega t}\right] \tag{14-34}$$

Note that this contribution to the torque variation has the same frequency as variation of the shaft speed. It should also be recognized that this torque variation **does not depend on the network's impedance** characteristics at frequencies deviating from the rated network frequency.

The second and more important contribution to the electrical torque is produced by the interaction between the line current deviations and the steady state flux in the generator. The formula is given by

$$\Delta\widetilde{T}_{el2} = \operatorname{Im}\left[\widetilde{\vec{\psi}}_S^{R*}\Delta\widetilde{\vec{i}}_S^{\,R}\right] = \widetilde{\psi}_{Sd}^R\Delta\widetilde{i}_{Sq}^R - \widetilde{\psi}_{Sq}^R\Delta\widetilde{i}_{Sd}^R = \widetilde{\psi}_{Sd}^R\Delta\widetilde{i}_{Lq}^R - \widetilde{\psi}_{Sq}^R\Delta\widetilde{i}_{Ld}^R \tag{14-35}$$

The steady state flux is given by

$$\begin{aligned}\widetilde{\psi}_{Sd}^R &= \widetilde{\hat{\psi}}_R\cos\theta_{sh0}\\ \widetilde{\psi}_{Sq}^R &= \widetilde{\hat{\psi}}_R\sin\theta_{sh0}\end{aligned} \tag{14-36}$$

The line current deviations are obtained (14-31) and (14-32). Thus we arrive at

$$\Delta\widetilde{T}_{el2} = \widetilde{\hat{\psi}}_R^2 \operatorname{Re}\left\{\left[\cos\theta_{sh0}L_{sh,q}^R - \sin\theta_{sh0}L_{sh,d}^R\right]\Delta\hat{n}e^{j\Omega t}\right\} \tag{14-37}$$

Addition of (14-34) and (14-37) yields the final result

$$\boxed{\begin{aligned}\Delta\widetilde{T}_{el} &= \operatorname{Re}\left\{M_{sh}\Delta\hat{n}e^{j\Omega t}\right\}\\ M_{sh} &= \widetilde{\hat{\psi}}_R^2\left(L_{sh,q}^R\cos\theta_{sh0} - L_{sh,d}^R\sin\theta_{sh0}\right) + j\,\widetilde{\hat{\psi}}_R\frac{\omega_N}{\Omega}\cos\theta_{sh0}\end{aligned}} \tag{14-38}$$

14.6 ELECTRICAL DAMPING CURVE

Formula (14-38) reveals that a speed modulation of the generator shaft with a certain frequency in steady state causes an electrical torque variation with that same frequency. Inspection of the formulas for the speed variation and the angle variation

$$\begin{aligned} \Delta n_{sh} &= \mathrm{Re}\left[\Delta\hat{n}e^{j\Omega t}\right] \\ \Delta\theta_{sh} &= \mathrm{Re}\left[-j\frac{\omega_N}{\Omega}\Delta\hat{n}e^{j\Omega t}\right] \end{aligned} \tag{14-39}$$

indicates that the transfer function in (14-38) can be resolved in one part, which is proportional to the speed variation and another part that is proportional to the angle variation

$$\Delta\widetilde{T}_{el} = \mathrm{Re}\left(M_{sh}\right)\Delta n_{sh}(t) - \mathrm{Im}\left(\frac{\Omega}{\omega_N}M_{sh}\right)\Delta\theta_{sh}(t) \tag{14-40}$$

Putting

$$\begin{aligned} D_{el} &= \mathrm{Re}\left(M_{sh}\right) \\ K_{el} &= -\mathrm{Im}\left(\frac{\Omega}{\omega_N}M_{sh}\right) \end{aligned} \tag{14-41}$$

these two quantities can be identified as the **"electrical damping factor"** D_{el} in [(pu torque)/(pu speed)], and the **"electrical spring constant"** K_{el} in [(pu torque)/rad]. Note that the per unit base in the above formulas is related to the current and reactance of the TCSC, so that the power base and the torque base are

$$\begin{aligned} S_{base} &= 3X_C I_{L,rms}^2 \\ T_{base} &= \frac{S_{base}}{\omega_N} \end{aligned} \tag{14-42}$$

The electrical damping curve is calculated as a function of frequency. A negative dip in this curve at a certain frequency indicates that an SSR condition may exist

if the shaft system has a mechanical torsional resonance at that particular frequency.

The theory derived in the preceding sections now shall be illustrated by some examples.

Example 14-1

In the first example the radial line in figure 14-3 is compensated only by a fixed series capacitor. The following values have been assumed:

- 500 kV system voltage, 50 Hz
- steady state line current 1500 A rms
- 400 km line with reactance 0.30 Ω/km and resistance 25 mΩ/km; this gives a total line reactance of 120 Ω/phase and a line resistance of 10 Ω/phase
- source impedance corresponding to 5000 MVA short-circuit capacity in the feeding end and infinite capacity in the receiving terminal; this gives a source reactance of 50 Ω/phase; it is assumed that the source resistance is 10 % of the reactance i.e. 5 Ω/phase.
- fixed capacitor compensates 50 % of the line reactance i.e. –60 Ω/phase

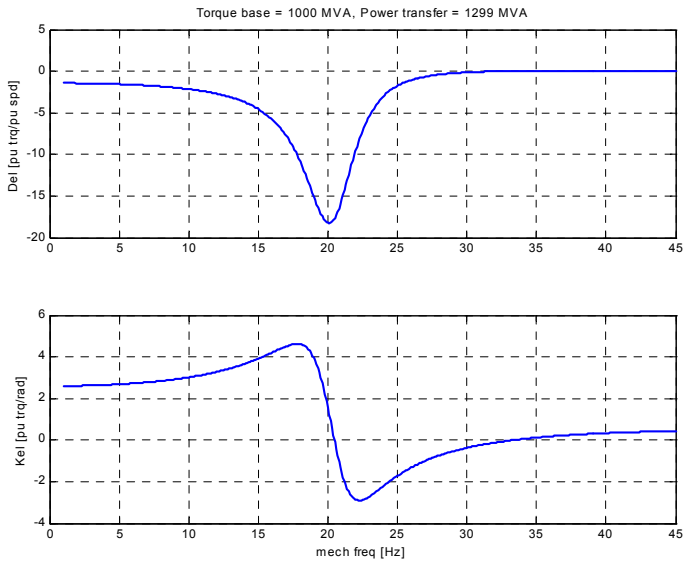

Figure 14-5 Electrical characteristics for fixed series compensation.

Figure 14-5 depicts the graphs showing electrical damping D_{el} and spring constant K_{el}. Once again it shall be stressed that the model does not represent the damping winding arrangements in the generator rotor, which would improve the damping at low mechanical frequencies. However, severe negative damping occurs in the frequency range around 20 Hz (mechanical torsion frequency).

Example 14-2

Assume that part of the inserted capacitance is provided by a TCSC. We split the series capacitor bank in the preceding example into a fixed bank providing 30 Ω/phase and a TCSC providing the remaining 30 Ω/phase at a boost level k_B = *1.2* or k_B = *2.0*. First we assume that both the PLL and the boost regulator operate with very low gains. The characteristics obtained then rely upon the use of the SVR scheme in the TCSC control. Note that the thyristor firing instants are not necessarily equidistant under SVR control. They are rather determined according to the equation discussed in section 4.6 in such a way that the consecutive capacitor voltage zero-crossings appear equidistantly.

Figure 14-6 shows the obtained characteristics for the generator. The thick lines are associated with the case of boost factor k_B = *1.2* and the thin lines with k_B = *2.0*. It should be noted that the discrepancy between these cases is quite small. This fact originates from the use of the SVR principle. **The same result will not be obtained when a fixed firing angle is used.**

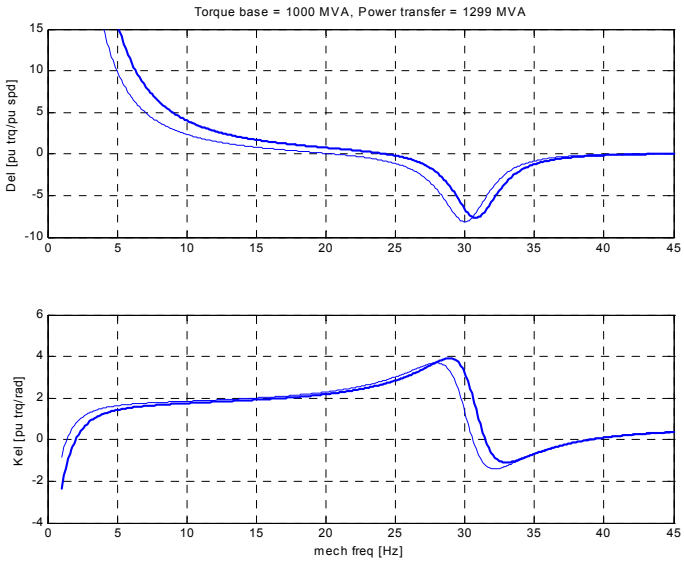

Figure 14-6 50/50 combination of fixed SC and SVR-TCSC; no PLL a; no boost regulator. Boost factor 1.2 (thick line) and 2.0 (thin line)

The effect of replacing half the inserted fixed series capacitor reactance by a TCSC is that the critical undamping frequency range is pushed towards a higher mechanical frequency, in the actual case from 20 Hz to 30 Hz. This means that the high degree of compensation can be applied even for generators having a torsional resonance up to approximately 25 Hz instead of about 15 Hz, when fixed compensation only is utilized. The electrical undamping amplitude also has decreased somewhat. Finally it can be noticed that some positive damping is

being provided by the TCSC at low mechanical frequencies; please note however that the model is inappropriate at very low rotor frequencies.

Example 14-3

Figure 14-7 presents some results from an investigation of the impact of the boost regulator dynamics on the electrical damping of the generator in example 14-2.

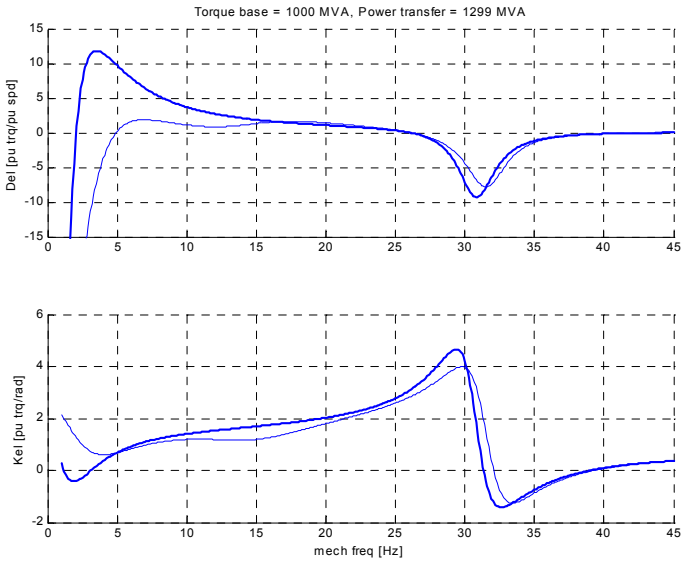

Figure 14-7 *50/50 combination of fixed SC and SVR-TCSC; no PLL; boost factor 1.2; boost regulator with medium gain (thick line) and high gain (thin line)*

The graphs show that the boost controller has only a small impact on the characteristics for mechanical frequencies exceeding approximately 15 Hz. In general the electrical damping curve is being determined by the inherent characteristics of the SVR-TCSC control for higher frequencies. The controller of course have a big impact on the generator at low mechanical frequencies, however the simple machine model can not be used for such frequencies. The general trend, that the low frequency range where the electrical spring constant is positive, expands with increasing regulator gain seems reasonable. If power oscillation becomes a problem it can be taken care of by a higher-level system, which generates a reactance reference that stabilizes the generator. In order to provide and tune such a system however appropriate generator models must be used.

Example 14-4

For the generator in example 14-3 having medium boost regulator gain we shall now investigate the impact of the synchronizing system.

Figure 14-8 depicts the calculation results. They show that a fast acting PLL may reduce the damping at low mechanical frequencies (10-15 Hz). A fast-acting PLL also tends to push the critical frequency range with negative electrical damping somewhat towards higher mechanical frequencies, but as a tradeoff the magnitude of the undamping peaks increases.

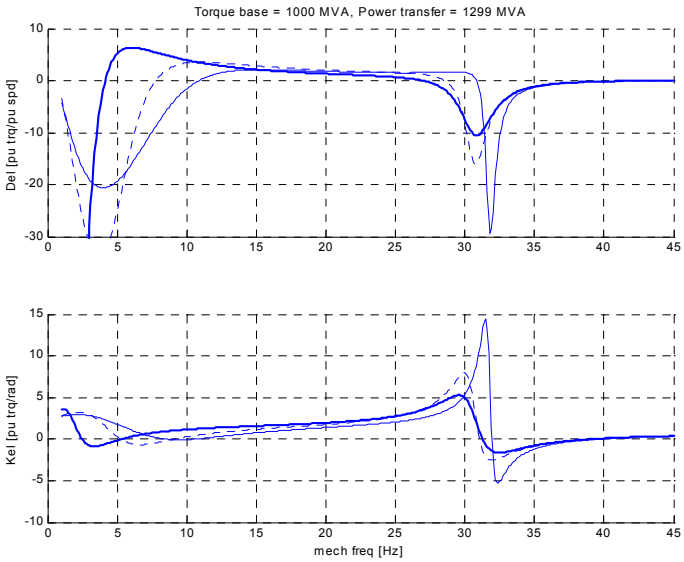

Figure 14-8 50/50 combination of fixed SC and SVR-TCSC; boost factor 1.2; boost regulator with medium gain; slow PLL (thick line), medium PLL (dashed), fast PLL (thin line)

Example 14-5

As a final example we shall consider the case that the series compensation is provided by TCSC only. Then it seems necessary that the TCSC operates with a low boost factor as the inserted harmonic voltage increases in proportion to $k_B - 1$. Assume that the TCSC operates with a medium gain boost regulator and that the synchronization system operates with medium speed.

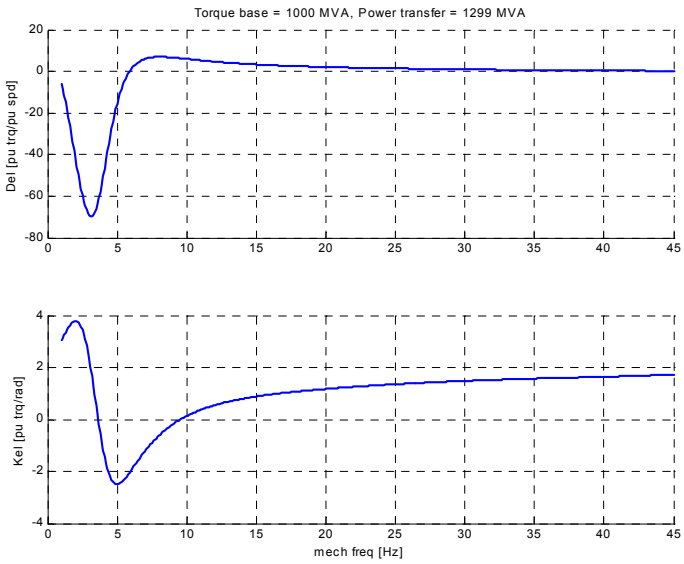

Figure 14-9 All-TCSC series compensation; boost factor 1.2; medium boost regulator gain; medium speed PLL

Figure 14-9 shows the calculation results. The figure shows that the series compensator exhibits positive damping for the whole range of mechanical torsional resonances exceeding *5 Hz*.

14.7 CONCLUSION

It has been shown above that the model derived in this chapter provides some very interesting results with respect to the conditions for SSR when series compensation is provided partly or totally by means of TCSC. The use of the SVR scheme has some important advantages over conventional direct control of the firing angle of the thyristors

- the electrical damping is mainly determined by the inherent characteristics obtained by using the SVR algorithm to determine the thyristor firing instants
- the tuning of the regulators and synchronization system then becomes less critical for the SSR behaviour
- linear controllers can be used in the boost regulator minimizing the dependence of parameters
- the characteristics of the TCSC behaviour with respect to SSR to a large extent is independent of the boost factor
- the TCSC can provide adequate SSR behaviour even when it operates with low boost factor

CHAPTER 15
SUMMARY OF THE THESIS

The intentions and the aim of the work, which has been reported in the preceding chapters of this thesis, have been to submit a monograph on the Thyristor Controlled Series Capacitor presenting the concept, the potential applications of the device and to discuss some relevant aspects of its modelling and control. Below some central themes of the work will be high-lighted.

15.1 CONCEPT

▪ simplification

The Synchronous Voltage Reversal (SVR) method to control the thyristor firing instants is based on the concept of **equivalent, instantaneous reversals** of the capacitor voltage. This idea simplifies the description of the TCSC operation tremendously and provides an understanding of the inherent dynamics of the device. It is surprising how far one can reach with such a simple model. In fact, it provides not only a good qualitative description but it also reveals quantitative results that are in good agreement with detailed simulations.

▪ inherent characteristics

It is often taken for granted that the output of the regulator (in this case the boost regulator) should be the thyristor control angle α. The SVR method, which has been presented in the thesis, shows that it might be advantageous to use other signals as outputs from the regulator. In the case of SVR the output signal determines the time instant of the capacitor voltage zero-crossing. It is an important fact the TCSC **acquires inherent characteristics** from the selection of the thyristor firing method.

This has been discussed in chapter 5 with respect to the use of the SVR method. The result in figure 5-2 gives a good illustration. At the onset of a DC current

component in the line current the forward and reverse thyristors adapt to different firing angles **immediately** and without any participation of the boost regulator or any other capacitor voltage symmetrizing control member.

Most TCSCs exhibit an apparent inductive impedance at subsynchronous frequencies, when it is operating with high boost level. Due to the firing mechanism used in the SVR control the characteristics of the TCSC is almost **independent of the actual boost level** and accordingly this characteristic, which is advantageous from an SSR point of view, is being preserved even at low boost levels.

It is believed that the best use of TCSC for SSR mitigation purposes is to implement such a low-level firing mechanism, which provides suitable inherent characteristics of the TCSC independent of the regulators operating at a higher level in the control system. This certainly does not provide an active damping of SSR oscillations, but it makes the series compensated line appear similarly to a line compensated to a lower degree or not compensated at all.

It appears that active damping of SSR oscillations by use of TCSC would require a speed signal measured directly on the turbine-generator shaft system to be available at the TCSC site. But series capacitors are never or seldom located at power generation plants, and therefore it is unlikely that such signals would be available.

15.2 MODELLING AND TUNING

Control system synthesis and investigations of performance require dynamical models not only of the TCSC main circuit but also of the auxiliary systems providing boost factor measurement and synchronization.

▪ phasor estimation

In the thesis the dynamical performance of a certain class of phasor estimators have been derived. Although a large number of methods can be applied to extract the fundamental frequency components of measured scalar or complex signals it is likely that their dynamical performance are rather similar.

▪ performance of TCSC boost control

The achievable performance of the TCSC boost control system certainly is limited by the available speed of response of the measuring devices, which all depend in some way on phasor (fundamental frequency component) extraction.

▪ uncertainties

The need for feedback control emerges from **uncertainties**. In this study two categories of uncertainties have been considered.

- The first category relates to uncertainties associated with the modelling. The simplification of the TCSC main-circuit description and the idealized description of the operation introduces unmodelled time delays. Losses in the main circuit can only be considered using approximations etc.
- The second category is the normal operational environment in which the power transmission equipment has to operate. The power system has a changing topology, where transmission lines are being inserted and taken out of service, transformers are being inserted or switched out and generators are connected or disconnected. In the thesis this has been considered by varying the source impedance at the terminals of the line where the TCSC is inserted.

▪ control system design using QFT

In the thesis the Quantitative Feedback Theory (QFT) method has been applied to deal with the uncertainties. It is the author's opinion that this method offers a practical way to synthesize and tune a robust regulator. It is also likely that the use of the frequency domain offers advantages when one shall model a large object like a power system and define uncertainties related to it.

15.3 OUT-LOOK

Although the work in this thesis has been entirely focussing on the TCSC some of the questions discussed are common to almost any power converter used in the transmission system. One such issue is the problem to extract the fundamental component of measured quantities. Such measured values are required for controlling converters independent of if they are based on conventional thyristor technology or Voltage Source Converter (VSC) technology.

The concept of the converter-oriented coordinate system described in chapter 6 originally was intended to establish a framework for time-domain simulation of the TCSC. The idea was to lessen the computational burden by approximating the capacitor voltage reversals by the equivalent, instantaneous voltage reversals. This would make it possible to simulate TCSC in a bigger system with a reasonable effort.

Hopefully, this thesis also has indicated that a simplified description of a power electronic system may be utilized in order to gain understanding of its dynamical performance. Occasionally it might also generate ideas of unconventional control approaches, which may give the apparatus desirable inherent characteristics.

APPENDIX A

Capacitor voltage fundamental frequency Fourier component

Here we shall evaluate formula (7-29) for the average relative capacitor voltage deviation in the sampling interval in some detail. The given formula is

$$\Delta\widetilde{\widetilde{u}}_{C,av}^{R}(t_k)=\frac{3}{\pi}\int_{-\frac{\pi}{6}}^{\frac{\pi}{6}}e^{-j\varphi}\Delta\widetilde{\widetilde{u}}_{C}^{k}(\varphi)d\varphi \qquad \text{(A-1)}$$

Studying figure 7-6 it can be seen that the deviation between the disturbed and the undisturbed capacitor voltage contains two different contributions

- the difference between the curves in the subintervals preceding and following the reversal; this contribution does not depend on the boost level in the steady state operating point around which the system has been linearized
- the voltage deviation caused by the displacement of the reversal; the amplitude of this voltage difference is given by the voltage step height in steady state operation, i.e. the difference between post- and pre-reversal voltages in the undisturbed conditions

In view of the above we may rewrite (A-1) as

$$\Delta\widetilde{\bar{u}}_{C,av}^{R}(t_k)=\frac{3}{\pi}\int_{-\frac{\pi}{6}}^{0}e^{-j\varphi}\left[\Delta\widetilde{\bar{u}}_{C}^{k}\left(-\frac{\pi}{6}\right)+\int_{-\frac{\pi}{6}}^{\varphi}\Delta\widetilde{\bar{i}}_{L}^{k}(\eta)d\eta\right]d\varphi+$$
$$+\frac{3}{\pi}\int_{0}^{\frac{\pi}{6}}e^{-j\varphi}\left[\Delta\widetilde{\bar{u}}_{C}^{k}\left(\frac{\pi}{6}\right)-\int_{\varphi}^{\frac{\pi}{6}}\Delta\widetilde{\bar{i}}_{L}^{k}(\eta)d\eta\right]d\varphi+ \qquad \text{(A-2)}$$
$$+\frac{3}{\pi}\left[\Delta\widetilde{\bar{u}}_{C,post}^{k}-\Delta\widetilde{\bar{u}}_{C,pre}^{k}\right]\Delta\theta_k$$

The terms containing the capacitor voltages in the interval endpoints can be evaluated immediately. The result is

$$\frac{3}{\pi}\Delta\widetilde{\bar{u}}_{C}^{k}\left(-\frac{\pi}{6}\right)\int_{-\frac{\pi}{6}}^{0}e^{-j\varphi}d\varphi=\frac{3}{\pi}\Delta\widetilde{\bar{u}}_{C}^{k}\left(-\frac{\pi}{6}\right)j\left(1-e^{j\frac{\pi}{6}}\right)$$
$$\frac{3}{\pi}\Delta\widetilde{\bar{u}}_{C}^{k}\left(\frac{\pi}{6}\right)\int_{0}^{\frac{\pi}{6}}e^{-j\varphi}d\varphi=\frac{3}{\pi}\Delta\widetilde{\bar{u}}_{C}^{k}\left(\frac{\pi}{6}\right)j\left(e^{-j\frac{\pi}{6}}-1\right) \qquad \text{(A-3)}$$

In the terms related to the relative line current deviation we will use the general approach of describing the line current inside the sampling interval, which has been described in section 7.5 with the formula (7-16). Then we get

$$\frac{3}{\pi}\left\{\int_{-\frac{\pi}{6}}^{0}e^{-j\varphi}\left[\int_{-\frac{\pi}{6}}^{\varphi}\Delta\widetilde{\bar{i}}_{L}^{k}(\eta)d\eta\right]d\varphi-\int_{-\frac{\pi}{6}}^{0}e^{-j\varphi}\left[\int_{\varphi}^{\frac{\pi}{6}}\Delta\widetilde{\bar{i}}_{L}^{k}(\eta)d\eta\right]d\varphi\right\}=$$
$$=\frac{3}{\pi}\Delta\widetilde{\bar{i}}_{L}^{k}(0)\left\{\int_{-\frac{\pi}{6}}^{0}e^{-j\varphi}\left[\int_{-\frac{\pi}{6}}^{\varphi}e^{j\xi\eta}d\eta\right]d\varphi-\int_{-\frac{\pi}{6}}^{0}e^{-j\varphi}\left[\int_{\varphi}^{\frac{\pi}{6}}e^{j\xi\eta}d\eta\right]d\varphi\right\} \qquad \text{(A-4)}$$

The integrals can be evaluated using e.g. partial integration

$$\frac{3}{\pi}\Delta\tilde{\tilde{i}}_L^k(0)\left\{\int_{-\frac{\pi}{6}}^{0} e^{-j\varphi}\left[\int_{-\frac{\pi}{6}}^{\varphi} e^{j\xi\eta}d\eta\right]d\varphi - \int_{-\frac{\pi}{6}}^{0} e^{-j\varphi}\left[\int_{\varphi}^{\frac{\pi}{6}} e^{j\xi\eta}d\eta\right]d\varphi\right\} =$$
$$= \frac{3}{\pi}\Delta\tilde{\tilde{i}}_L^k(0)\left\{j\int_{-\frac{\pi}{6}}^{0} e^{j\xi\eta}d\eta - j\int_{-\frac{\pi}{6}}^{0} e^{-j\varphi}e^{j\xi\varphi}d\varphi + j\int_{0}^{\frac{\pi}{6}} e^{j\xi\eta}d\eta - j\int_{0}^{\frac{\pi}{6}} e^{-j\varphi}e^{j\xi\varphi}d\varphi\right\} \quad \text{(A-5)}$$

Now the integrals can be evaluated giving the result

$$\frac{3}{\pi}\Delta\tilde{\tilde{i}}_L^k(0)\left\{\int_{-\frac{\pi}{6}}^{0} e^{-j\varphi}\left[\int_{-\frac{\pi}{6}}^{\varphi} e^{j\xi\eta}d\eta\right]d\varphi - \int_{-\frac{\pi}{6}}^{0} e^{-j\varphi}\left[\int_{\varphi}^{\frac{\pi}{6}} e^{j\xi\eta}d\eta\right]d\varphi\right\} =$$
$$= j\Delta\tilde{\tilde{i}}_L^k(0)\left\{\frac{\sin\left(\frac{\xi\pi}{6}\right)}{\frac{\xi\pi}{6}} - \frac{\sin\left(\frac{(1-\xi)\pi}{6}\right)}{\frac{(1-\xi)\pi}{6}}\right\} \quad \text{(A-6)}$$

We can summarize the averaged relative capacitor voltage deviation formula as follows

$$\begin{pmatrix}\Delta\tilde{u}_{Cd,av}^R(t_k)\\ \Delta\tilde{u}_{Cq,av}^R(t_k)\end{pmatrix} = F_{beg}\Delta\tilde{\tilde{u}}_C^k\left(-\frac{\pi}{6}\right) + F_{end}\Delta\tilde{\tilde{u}}_C^k\left(\frac{\pi}{6}\right) + G_{IL}\begin{pmatrix}\Delta\tilde{i}_{Ld}^R(t_k)\\ \Delta\tilde{i}_{Lq}^R(t_k)\end{pmatrix} + G_\theta P_{10}\Delta\theta_k \quad \text{(A-7)}$$

where

$$P_{10} = \begin{pmatrix}1\\0\end{pmatrix} \quad \text{(A-8)}$$

$$F_{beg} = \frac{3}{2\pi}\begin{pmatrix}1 & \sqrt{3}-2 & 0\\ 2-\sqrt{3} & 1 & 0\end{pmatrix} \qquad F_{end} = \frac{3}{2\pi}\begin{pmatrix}1 & 2-\sqrt{3} & 0\\ \sqrt{3}-2 & 1 & 0\end{pmatrix} \quad \text{(A-9)}$$

$$G_{IL} = \begin{pmatrix} 0 & -g_{IL} \\ g_{IL} & 0 \end{pmatrix} \qquad g_{IL} = \frac{\sin\frac{\xi\pi}{6}}{\frac{\xi\pi}{6}} - \frac{\sin\frac{(1-\xi)\pi}{6}}{\frac{(1-\xi)\pi}{6}} \tag{A-10}$$

$$G_{\theta} = \frac{3}{\pi}\left(\tilde{u}^{k}_{Cx,post} - \tilde{u}^{k}_{Cx,pre}\right) \tag{A-11}$$

The relative capacitor voltage difference $\tilde{u}^{k}_{Cx,post} - \tilde{u}^{k}_{Cx,pre}$ is two third of the total capacitor voltage step at the reversal in steady state operation. The reason is that the total step includes also the step in the zero sequence component. The latter step has half the height of the step $\tilde{u}^{k}_{Cx,post} - \tilde{u}^{k}_{Cx,pre}$ according to equation (7-4). Thus

$$G_{\theta} = \frac{2}{\pi}\left(\tilde{u}^{k}_{Cu,post} - \tilde{u}^{k}_{Cu,pre}\right) \approx \frac{4}{\pi}\tilde{u}^{k}_{Cu,post} \tag{A-12}$$

where the last approximation is motivated by figure 4-7. Now equation (4-3) gives that the expression on the right-hand side actually can be expressed in terms of the boost factor in steady state, so we end up with the simple expression

$$G_{\theta} = k_B - 1 \tag{A-13}$$

APPENDIX B
Phasor Estimator in FIXED coordinates

- **Algorithm**

The "constants" in equation (10-3) can be extracted by rearranging the equation and applying lowpass filtering. This process yields the following algorithm to obtain the estimates $\tilde{\vec{S}}^{av}(t), \tilde{\vec{S}}^{p}(t), \tilde{\vec{S}}^{n}(t)$ of the phasors.

$$\boxed{\begin{aligned}
\tilde{\vec{S}}^{av}(t) &= H_{av}(p)\left\{\hat{s}(t) - \tilde{\vec{S}}^{p}(t)e^{j\theta_{CS}(t)} - \tilde{\vec{S}}^{n*}(t)e^{-j\theta_{CS}(t)}\right\} \\
\tilde{\vec{S}}^{p}(t) &= H_{p}(p)\left\{e^{-j\theta_{CS}(t)}\left[\hat{s}(t) - \tilde{\vec{S}}^{av}(t) - \tilde{\vec{S}}^{n*}(t)e^{-j\theta_{CS}(t)}\right]\right\} \\
\tilde{\vec{S}}^{n*}(t) &= H_{n}(p)\left\{e^{j\theta_{CS}(t)}\left[\hat{s}(t) - \tilde{\vec{S}}^{av}(t) - \tilde{\vec{S}}^{p}(t)e^{j\theta_{CS}(t)}\right]\right\}
\end{aligned}} \qquad \text{(B-1)}$$

The operators $H_{av}(p)$, $H_p(p)$, $H_n(p)$ represent low pass linear operator function of the operator $p = \frac{d}{dt}$.

Equation (B-1) defines a dynamical system where $\tilde{\vec{S}}^{av}(t), \tilde{\vec{S}}^{p}(t), \tilde{\vec{S}}^{n}(t)$ are states and $\hat{s}(t), \theta_{CS}(t)$ inputs. The dynamical system appears to be time-varying as exponentials in θ_{CS} occur as coefficients. A better representation can be obtained if we make a variable substitution and transform the phasor estimates to the fixed coordinate system. Then put

$$\begin{aligned}
\hat{w}^{av}(t) &= \tilde{\vec{S}}^{av}(t) \\
\hat{w}^{p}(t) &= \tilde{\vec{S}}^{p}(t)e^{j\theta_{CS}(t)} \\
\hat{w}^{n*}(t) &= \tilde{\vec{S}}^{n*}(t)e^{-j\theta_{CS}(t)}
\end{aligned} \qquad \text{(B-2)}$$

Equation (B-1) then transforms into

$$\begin{aligned}
\hat{w}^{av}(t) &= H_{av}(p)\hat{s}(t) - H_{av}(p)\hat{w}^{p}(t) - H_{av}(p)\hat{w}^{n^*}(t) \\
\hat{w}^{p}(t) &= e^{j\theta_{CS}(t)}\left\{H_p(p)\left\{e^{-j\theta_{CS}(t)}\left[\hat{s}(t) - \hat{w}^{av}(t) - \hat{w}^{n^*}(t)\right]\right\}\right\} = \\
&= H_p(p - j\omega_{CS})\left[\hat{s}(t) - \hat{w}^{av}(t) - \hat{w}^{n^*}(t)\right] \\
\hat{w}^{n^*}(t) &= e^{-j\theta_{CS}(t)}\left\{H_p(p)\left\{e^{j\theta_{CS}(t)}\left[\hat{s}(t) - \hat{w}^{av}(t) - \hat{w}^{p}(t)\right]\right\}\right\} = \\
&= H_n(p + j\omega_{CS})\left[\hat{s}(t) - \hat{w}^{av}(t) - \hat{w}^{p}(t)\right]
\end{aligned} \tag{B-3}$$

The following linear equation system results

$$\begin{aligned}
&\begin{pmatrix} 1 & H_{av}(p) & H_{av}(p) \\ H_p(p - j\omega_{CS}) & 1 & H_p(p - j\omega_{CS}) \\ H_n(p + j\omega_{CS}) & H_n(p + j\omega_{CS}) & 1 \end{pmatrix} \begin{pmatrix} \hat{w}^{av}(t) \\ \hat{w}^{p}(t) \\ \hat{w}^{n^*}(t) \end{pmatrix} = \\
&= \begin{pmatrix} H_{av}(p) \\ H_p(p - j\omega_{CS}) \\ H_n(p + j\omega_{CS}) \end{pmatrix} \hat{s}(t)
\end{aligned} \tag{B-4}$$

It shall be noted that if the lowpass filters are time-invariant then all the elements in the matrices are operators with **time-independent** coefficients.

- **Frequency domain model**

We can conclude that the phasor estimation algorithm is characterized by linear transfer functions with time-independent coefficients from the input vector $\hat{s}(t)$ to the output vectors $\hat{w}^{av}(t), \hat{w}^{p}(t), \hat{w}^{n^*}(t)$. If the input signal is exponential with frequency ω, then also the steady state output signals become exponential with the same frequency. Thus we have

$$\begin{aligned}
\hat{s}(t) &= Ae^{j\omega t} \\
\hat{w}^{av}(t) &= Be^{j\omega t} \\
\hat{w}^{p}(t) &= C_1 e^{j\omega t} \\
\hat{w}^{n^*}(t) &= C_2 e^{j\omega t}
\end{aligned} \tag{B-5}$$

Accordingly three different transfer functions can be defined

- $G_{av}(j\omega)=\frac{B}{A}$, which describes the impact of the input signal on the estimated average output value
- $G_p(j\omega)=\frac{C_1}{A}$, which describes the impact of the input signal on the estimated positive sequence output
- $G_n(j\omega)=\frac{C_2}{A}$, which describes the impact of the input signal on the estimated negative sequence output

From (B-4) we get

$$\begin{pmatrix} G_{av}(j\omega) \\ G_p(j\omega) \\ G_n(j\omega) \end{pmatrix} = M^{-1}N \tag{B-6}$$

where

$$\begin{aligned} M &= \begin{pmatrix} 1 & H_{av}(j\omega) & H_{av}(j\omega) \\ H_p(j(\omega-\omega_{CS})) & 1 & H_p(j(\omega-\omega_{CS})) \\ H_n(j(\omega+\omega_{CS})) & H_n(j(\omega+\omega_{CS})) & 1 \end{pmatrix} \\ N &= \begin{pmatrix} H_{av}(j\omega) \\ H_p(j(\omega-\omega_{CS})) \\ H_n(j(\omega+\omega_{CS})) \end{pmatrix} \end{aligned} \tag{B-7}$$

- **Time domain model**

Equation (B-4) shows that the phasor estimator is a linear filter with time-independent coefficients. As such it can be represented by a state space model. In the following such a model shall be defined.

Each one of the operators $H_{av}(p)$, $H_p(p)$, $H_n(p)$ represents a lowpass linear filter and each one can be represented by a state space model

$$\begin{aligned} H_{av}(p) &\Leftrightarrow [A_{av},B_{av},C_{av},D_{av}]: \quad \dot{x}_{av}=A_{av}x_{av}+B_{av}u_{av} \quad y_{av}=C_{av}x_{av} \\ H_p(p) &\Leftrightarrow [A_p,B_p,C_p,D_p]: \quad \dot{x}_p=A_px_p+B_pu_p \quad y_p=C_px_p \\ H_n(p) &\Leftrightarrow [A_n,B_n,C_n,D_n]: \quad \dot{x}_n=A_nx_n+B_nu_n \quad y_n=C_nx_n \end{aligned} \tag{B-8}$$

($D_{av}=0$, $D_p=0$, $D_n=0$ because the filters have lowpass characteristics.)

Equation (B-3) yields

$$\begin{aligned}\hat{w}^{av}(t) &= H_{av}(p)\left[\hat{s}(t)-\hat{w}^{p}(t)-\hat{w}^{n*}(t)\right]\\ \hat{w}^{p}(t) &= H_{p}(p-j\omega_{CS})\left[\hat{s}(t)-\hat{w}^{av}(t)-\hat{w}^{n*}(t)\right]\\ \hat{w}^{n*}(t) &= H_{n}(p+j\omega_{CS})\left[\hat{s}(t)-\hat{w}^{av}(t)-\hat{w}^{p}(t)\right]\end{aligned} \tag{B-9}$$

Using the representation (B-8) we can interpret (B-9) as

$$\begin{aligned} p x_{av} = \dot{x}_{av} &= A_{av}x_{av} + B_{av}\left[\hat{s}(t)-\hat{w}^{p}(t)-\hat{w}^{n*}(t)\right]\\ \hat{w}^{av} &= C_{av}x_{av}\\ (p-j\omega_{CS})x_p = \dot{x}_p - j\omega_{CS}x_p &= A_p x_p + B_p\left[\hat{s}(t)-\hat{w}^{av}(t)-\hat{w}^{n*}(t)\right]\\ \hat{w}^{p} &= C_p x_p\\ (p+j\omega_{CS})x_n = \dot{x}_n + j\omega_{CS}x_n &= A_n x_n + B_n\left[\hat{s}(t)-\hat{w}^{p}(t)-\hat{w}^{n*}(t)\right]\\ \hat{w}^{n*} &= C_n x_n\end{aligned} \tag{B-10}$$

Reduction of the equations yields

$$\begin{aligned}\dot{x}_{av} &= A_{av}x_{av} + B_{av}\left[\hat{s}(t)-C_p x_p - C_n x_n\right]\\ \dot{x}_p &= (A_p + j\omega_{CS})x_p + B_p\left[\hat{s}(t)-C_{av}x_{av}-C_n x_n\right]\\ \dot{x}_n &= (A_n - j\omega_{CS})x_n + B_n\left[\hat{s}(t)-C_{av}x_{av}-C_p x_p\right]\\ \hat{w}^{av} &= C_{av}x_{av}\\ \hat{w}^{p} &= C_p x_p\\ \hat{w}^{n*} &= C_n x_n\end{aligned} \tag{B-11}$$

In matrix form

$$\boxed{\begin{aligned}\begin{pmatrix}\dot{x}_{av}\\ \dot{x}_p\\ \dot{x}_n\end{pmatrix} &= \begin{pmatrix}A_{av} & -B_{av}C_p & -B_{av}C_n\\ -B_pC_{av} & A_p+j\omega_{CS} & -B_pC_n\\ -B_nC_{av} & -B_nC_p & A_n-j\omega_{CS}\end{pmatrix}\begin{pmatrix}x_{av}\\ x_p\\ x_n\end{pmatrix} + \begin{pmatrix}B_{av}\\ B_p\\ B_n\end{pmatrix}\hat{s}(t)\\ \begin{pmatrix}\hat{w}^{av}\\ \hat{w}^{p}\\ \hat{w}^{n*}\end{pmatrix} &= \begin{pmatrix}C_{av} & & \\ & C_p & \\ & & C_n\end{pmatrix}\begin{pmatrix}x_{av}\\ x_p\\ x_n\end{pmatrix}\end{aligned}} \tag{B-12}$$

APPENDIX C
Phasor Estimator in IL_SYNC coordinates

- **Algorithm**

When the rotating coordinate system specifically is the *IL_SYNC* system its speed is constant and equals the network frequency. If we also consider (6-5) we get in this case

$$\begin{aligned}\omega_{CS}(t) &\equiv \omega_N \\ \theta_{CS}(t) &= \omega_N t\end{aligned} \tag{C-1}$$

If the electrical quantity is being observed in the *IL_SYNC* system the input signal is the space vector $\hat{s}^R(t)$. In view of (6-6) and (10-2) it comprises the following components

$$\hat{s}^R(t) = \vec{S}^{av}(t)e^{-j\omega_N t} + \vec{S}^{p}(t) + \vec{S}^{n*}(t)e^{-j2\omega_N t} \tag{C-2}$$

The estimation algorithm (10-3) now becomes

$$\boxed{\begin{aligned}\tilde{\vec{S}}^{av}(t) &= H_{av}(p)\left\{\hat{s}^R(t)e^{j\omega_N t} - \tilde{\vec{S}}^{p}(t)e^{j\omega_N t} - \tilde{\vec{S}}^{n*}(t)e^{-j\omega_N t}\right\} \\ \tilde{\vec{S}}^{p}(t) &= H_{p}(p)\left\{\hat{s}^R(t) - \tilde{\vec{S}}^{av}(t)e^{-j\omega_N t} - \tilde{\vec{S}}^{n*}(t)e^{-j2\omega_N t}\right\} \\ \tilde{\vec{S}}^{n*}(t) &= H_{n}(p)\left\{\hat{s}^R(t)e^{j2\omega_N t} - \tilde{\vec{S}}^{av}(t)e^{j\omega_N t} - \tilde{\vec{S}}^{p}(t)e^{j2\omega_N t}\right\}\end{aligned}} \tag{C-3}$$

Again a transformation of the states provides a linear equation with time independent coefficients. Put

$$\begin{aligned}\hat{v}^{av}(t) &= \tilde{\vec{S}}^{av}(t)e^{-j\omega_N t}\\ \hat{v}^{p}(t) &= \tilde{\vec{S}}^{p}(t)\\ \hat{v}^{n*}(t) &= \tilde{\vec{S}}^{n*}(t)e^{-j2\omega_N t}\end{aligned} \tag{C-4}$$

and get

$$\begin{aligned}\hat{v}^{av}(t) &= e^{-j\omega_N t}H_{av}(p)\left\{e^{j\omega_N t}\left[\hat{s}^{R}(t)-\hat{v}^{p}(t)-\hat{v}^{n*}(t)\right]\right\} =\\ &= H_{av}(p+j\omega_N)\left[\hat{s}^{R}(t)-\hat{v}^{av}(t)-\hat{v}^{p}(t)\right]\\ \hat{v}^{p}(t) &= H_{p}(p)\left[\hat{s}^{R}(t)-\hat{v}^{av}(t)-\hat{v}^{n*}(t)\right]\\ \hat{v}^{n*}(t) &= e^{-j2\omega_N t}H_{n}(p)\left\{e^{j2\omega_N t}\left[\hat{s}^{R}(t)-\hat{v}^{av}(t)-\hat{v}^{p}(t)\right]\right\} =\\ &= H_{n}(p+j2\omega_N)\left[\hat{s}^{R}(t)-\hat{v}^{av}(t)-\hat{v}^{p}(t)\right]\end{aligned} \tag{C-5}$$

In matrix form

$$\begin{pmatrix}1 & H_{av}(p+j\omega_N) & H_{av}(p+j\omega_N)\\ H_{p}(p) & 1 & H_{p}(p)\\ H_{n}(p+j2\omega_N) & H_{n}(p+j2\omega_N) & 1\end{pmatrix}\begin{pmatrix}\hat{v}^{av}(t)\\ \hat{v}^{p}(t)\\ \hat{v}^{n*}(t)\end{pmatrix} = \begin{pmatrix}H_{av}(p+j\omega_N)\\ H_{p}(p)\\ H_{n}(p+j2\omega_N)\end{pmatrix}\hat{s}^{R}(t) \tag{C-6}$$

- **Frequency domain model**

We may define linear transfer functions with time-independent coefficients from the input vector $\hat{s}^{R}(t)$ to the output vectors $\hat{v}^{av}(t), \hat{v}^{p}(t), \hat{v}^{n*}(t)$. If the input signal is exponential with frequency Ω, then also the steady state output signals become exponential with the same frequency. Thus we have

$$\begin{aligned}\hat{s}^{R}(t) &= De^{j\Omega t}\\ \hat{v}^{av}(t) &= Ee^{j\Omega t}\\ \hat{v}^{p}(t) &= F_1 e^{j\Omega t}\\ \hat{v}^{n*}(t) &= F_2 e^{j\Omega t}\end{aligned} \tag{C-7}$$

Accordingly three different transfer functions can be defined

- $G_{av}^{R}(j\Omega)=\frac{E}{D}$, which describes the impact of the input signal on the estimated average output value
- $G_{p}^{R}(j\Omega)=\frac{F_1}{D}$, which describes the impact of the input signal on the estimated positive sequence output
- $G_{n}^{R}(j\Omega)=\frac{F_2}{D}$, which describes the impact of the input signal on the estimated negative sequence output

From (C-6) we get

$$\begin{pmatrix} G_{av}^{R}(j\Omega) \\ G_{p}^{R}(j\Omega) \\ G_{n}^{R}(j\Omega) \end{pmatrix} = P^{-1}Q \tag{C-8}$$

where

$$\begin{aligned} P &= \begin{pmatrix} 1 & H_{av}(j(\Omega+\omega_N)) & H_{av}(j(\Omega+\omega_N)) \\ H_p(j\Omega) & 1 & H_p(j\Omega) \\ H_n(j(\Omega+2\omega_N)) & H_n(j(\Omega+2\omega_N)) & 1 \end{pmatrix} \\ Q &= \begin{pmatrix} H_{av}(j(\Omega+\omega_N)) \\ H_p(j\Omega) \\ H_n(j(\Omega+2\omega_N)) \end{pmatrix} \end{aligned} \tag{C-9}$$

- **Component-wise transfer functions in frequency domain**

The transfer functions in (C-8) reflect the **complex-to-complex** input-output signal relations. But in many applications the process exhibits different properties for the real and imaginary axis components. Further the control system might be configured to act only on the real or on the imaginary component. Then it becomes impractical to formulate the relations between complex input and output signals. It is preferred to describe directly the relations between the **components** of the input signal and the components of the output signal. Therefore it becomes interesting to express the transfer functions between each one of the input components to each one of the output components. In the following we consider only the output function $\hat{v}^p$. Define

$$\begin{aligned}\hat{s}^R(t) &= s_d^R(t) + js_q^R(t)\\ \hat{v}^p &= \tilde{\tilde{S}}^p = \tilde{S}_d^p + j\tilde{S}_q^p\end{aligned} \tag{C-10}$$

The complex-complex transfer function $G_p^R(j\Omega)$ gives the relation between $\hat{s}^R(j\Omega)$ and $\hat{v}^p(j\Omega)$ at frequency Ω (in *IL_SYNC* coordinates)

$$\tilde{S}_d^p + j\tilde{S}_q^p = G_p^R\left(s_d^R + js_q^R\right) \tag{C-11}$$

If the components of the input function are sinusoidal at frequency Ω, they can be expressed as

$$\begin{aligned}s_d^R(t) &= \mathrm{Re}\left\{Ae^{j\Omega t}\right\} = \frac{A}{2}e^{j\Omega t} + \frac{A^*}{2}e^{-j\Omega t}\\ s_q^R(t) &= \mathrm{Re}\left\{Be^{j\Omega t}\right\} = \frac{B}{2}e^{j\Omega t} + \frac{B^*}{2}e^{-j\Omega t}\end{aligned} \tag{C-12}$$

where A and B are some constants. In this case the output functions become

$$\tilde{S}_d^p(t) + j\tilde{S}_q^p(t) = \frac{(A+jB)G_p^R(j\Omega)}{2}e^{j\Omega t} + \frac{\left(A^* + jB^*\right)G_p^R(-j\Omega)}{2}e^{-j\Omega t} \tag{C-13}$$

For the components we get

$$\begin{aligned}\tilde{S}_d^p(t) &= \mathrm{Re}\left\{\frac{(A+jB)G_p^R(j\Omega)}{2}e^{j\Omega t} + \frac{\left(A^* + jB^*\right)G_p^R(-j\Omega)}{2}e^{-j\Omega t}\right\}\\ &= \mathrm{Re}\left\{\frac{(A+jB)G_p^R(j\Omega)}{2}e^{j\Omega t} + \frac{(A-jB)\left[G_p^R(-j\Omega)\right]^*}{2}e^{j\Omega t}\right\} =\\ &= \mathrm{Re}\left\{A\frac{G_p^R(j\Omega) + \left[G_p^R(-j\Omega)\right]^*}{2}e^{j\Omega t} - B\frac{G_p^R(j\Omega) - \left[G_p^R(-j\Omega)\right]^*}{2j}e^{j\Omega t}\right\}\end{aligned} \tag{C-14}$$

$$
\begin{aligned}
\widetilde{S}_q^p(t) &= \mathrm{Im}\left\{\frac{(A+jB)G_p^R(j\Omega)}{2}e^{j\Omega t}+\frac{\left(A^*+jB^*\right)G_p^R(-j\Omega)}{2}e^{-j\Omega t}\right\} \\
&= \mathrm{Re}\left\{\frac{(A+jB)G_p^R(j\Omega)}{2j}e^{j\Omega t}+\frac{\left(A^*+jB^*\right)G_p^R(-j\Omega)}{2j}e^{-j\Omega t}\right\} = \\
&= \mathrm{Re}\left\{\frac{(A+jB)G_p^R(j\Omega)}{2j}e^{j\Omega t}-\frac{(A-jB)\left[G_p^R(-j\Omega)\right]^*}{2j}e^{j\Omega t}\right\} = \\
&= \mathrm{Re}\left\{A\frac{G_p^R(j\Omega)-\left[G_p^R(-j\Omega)\right]^*}{2j}e^{j\Omega t}+B\frac{G_p^R(j\Omega)+\left[G_p^R(-j\Omega)\right]^*}{2}e^{j\Omega t}\right\}
\end{aligned}
\tag{C-15}
$$

We get the following formulas for the component-component transfer functions

$$
\begin{aligned}
G_p^{R,d->d}(j\Omega) &= \frac{\widetilde{S}_d^p}{s_d^R} = \frac{G_p^R(j\Omega)+\left[G_p^R(-j\Omega)\right]^*}{2} \\
G_p^{R,d->q}(j\Omega) &= \frac{\widetilde{S}_q^p}{s_d^R} = \frac{G_p^R(j\Omega)-\left[G_p^R(-j\Omega)\right]^*}{2j} \\
G_p^{R,q->d}(j\Omega) &= \frac{\widetilde{S}_d^p}{s_q^R} = -\frac{G_p^R(j\Omega)-\left[G_p^R(-j\Omega)\right]^*}{2j} \\
G_p^{R,q->q}(j\Omega) &= \frac{\widetilde{S}_q^p}{s_q^R} = \frac{G_p^R(j\Omega)+\left[G_p^R(-j\Omega)\right]^*}{2}
\end{aligned}
\tag{C-16}
$$

- **Time domain model**

Equation (C-5) shows that the phasor estimator is a linear filter with time-independent coefficients. As such it can be represented by a state space model. In the following such a model shall be defined.

Each one of the operators $H_{av}(p)$, $H_p(p)$, $H_n(p)$ represents a lowpass linear filter and each one can be represented by a state space model

$$
\begin{aligned}
H_{av}(p) &\Leftrightarrow \left[A_{av},B_{av},C_{av},D_{av}\right]: \quad \dot{x}_{av}=A_{av}x_{av}+B_{av}u_{av} \quad y_{av}=C_{av}x_{av} \\
H_p(p) &\Leftrightarrow \left[A_p,B_p,C_p,D_p\right]: \quad \dot{x}_p=A_px_p+B_pu_p \quad y_p=C_px_p \\
H_n(p) &\Leftrightarrow \left[A_n,B_n,C_n,D_n\right]: \quad \dot{x}_n=A_nx_n+B_nu_n \quad y_n=C_nx_n
\end{aligned}
\tag{C-17}
$$

($D_{av}=0$, $D_p=0$, $D_n=0$ because the filters have lowpass characteristics.)

Equation (C-5) yields

$$\begin{aligned}\hat{v}^{av}(t) &= H_{av}(p+j\omega_N)\left[\hat{s}^R(t)-\hat{v}^{av}(t)-\hat{v}^p(t)\right]\\ \hat{v}^p(t) &= H_p(p)\left[\hat{s}^R(t)-\hat{v}^{av}(t)-\hat{v}^{n*}(t)\right]\\ \hat{v}^{n*}(t) &= H_n(p+j2\omega_N)\left[\hat{s}^R(t)-\hat{v}^{av}(t)-\hat{v}^p(t)\right]\end{aligned} \tag{C-18}$$

Using the representation (C-10) we can interpret (C-11) as

$$\begin{aligned}(p+j\omega_N)x_{av} &= \dot{x}_{av}+j\omega_N x_{av} = A_{av}x_{av}+B_{av}\left[\hat{s}^R(t)-\hat{v}^p(t)-\hat{v}^{n*}(t)\right]\\ \hat{v}^{av} &= C_{av}x_{av}\\ px_p &= \dot{x}_p = A_p x_p + B_p\left[\hat{s}^R(t)-\hat{v}^p(t)-\hat{v}^{n*}(t)\right]\\ \hat{v}^p &= C_p x_p\\ (p+j2\omega_N)x_n &= \dot{x}_n+j2\omega_N x_n = A_n x_n + B_n\left[\hat{s}^R(t)-\hat{v}^p(t)-\hat{v}^{n*}(t)\right]\\ \hat{v}^{n*} &= C_n x_n\end{aligned} \tag{C-19}$$

Reduction of the equations yield

$$\begin{aligned}\dot{x}_{av} &= (A_{av}-j\omega_N)x_{av}+B_{av}\left[\hat{s}^R(t)-C_p x_p - C_n x_n\right]\\ \dot{x}_p &= A_p x_p + B_p\left[\hat{s}^R(t)-C_{av}x_{av}-C_n x_n\right]\\ \dot{x}_n &= (A_n-j2\omega_N)x_n+B_n\left[\hat{s}^R(t)-C_{av}x_{av}-C_p x_p\right]\\ \hat{v}^{av} &= C_{av}x_{av}\\ \hat{v}^p &= C_p x_p\\ \hat{v}^{n*} &= C_n x_n\end{aligned} \tag{C-20}$$

In matrix form

$$\boxed{\begin{aligned}\begin{pmatrix}\dot{x}_{av}\\ \dot{x}_p\\ \dot{x}_n\end{pmatrix} &= \begin{pmatrix}A_{av}-j\omega_N & -B_{av}C_p & -B_{av}C_n\\ -B_pC_{av} & A_p & -B_pC_n\\ -B_nC_{av} & -B_nC_p & A_n-j2\omega_N\end{pmatrix}\begin{pmatrix}x_{av}\\ x_p\\ x_n\end{pmatrix}+\begin{pmatrix}B_{av}\\ B_p\\ B_n\end{pmatrix}\hat{s}^R(t)\\ \begin{pmatrix}\hat{v}^{av}\\ \hat{v}^p\\ \hat{v}^{n*}\end{pmatrix} &= \begin{pmatrix}C_{av} & & \\ & C_p & \\ & & C_n\end{pmatrix}\begin{pmatrix}x_{av}\\ x_p\\ x_n\end{pmatrix}\end{aligned}} \tag{C-21}$$

The matrix form immediately translates into a version using the components of the input and output vectors as

$$\begin{pmatrix} \dot{x}_{avd} \\ \dot{x}_{pd} \\ \dot{x}_{nd} \\ \dot{x}_{avq} \\ \dot{x}_{pq} \\ \dot{x}_{nq} \end{pmatrix} = \begin{pmatrix} A_{av} & -B_{av}C_p & -B_{av}C_n & \omega_N & 0 & 0 \\ -B_pC_{av} & A_p & -B_pC_n & 0 & 0 & 0 \\ -B_nC_{av} & -B_nC_p & A_n & 0 & 0 & 2\omega_N \\ -\omega_N & 0 & 0 & A_{av} & -B_{av}C_p & -B_{av}C_n \\ 0 & 0 & 0 & -B_pC_{av} & A_p & -B_pC_n \\ 0 & 0 & -2\omega_N & -B_nC_{av} & -B_nC_p & A_n \end{pmatrix} \begin{pmatrix} x_{avd} \\ x_{pd} \\ x_{nd} \\ x_{avq} \\ x_{pq} \\ x_{nq} \end{pmatrix} + \begin{pmatrix} B_{av} & 0 \\ B_p & 0 \\ B_n & 0 \\ 0 & B_{av} \\ 0 & B_p \\ 0 & B_n \end{pmatrix} \begin{pmatrix} s_d^R(t) \\ s_q^R(t) \end{pmatrix}, \quad \begin{pmatrix} \tilde{S}_d^p(t) \\ \tilde{S}_q^p(t) \end{pmatrix} = \begin{pmatrix} v_d^p(t) \\ v_q^p(t) \end{pmatrix} = \begin{pmatrix} 0 & C_p & 0 & 0 & 0 & 0 \\ 0 & 0 & 0 & 0 & C_p & 0 \end{pmatrix} \begin{pmatrix} x_{avd} \\ x_{pd} \\ x_{nd} \\ x_{avq} \\ x_{pq} \\ x_{nq} \end{pmatrix} \tag{C-22}$$

APPENDIX D

Phasor Estimator for single-phase signal

Assume that a scalar input signal *s(t)* is measured. It may e.g. be a phase current, a capacitor voltage or anything similar. The signal is expected to be comprised by an offset signal, $S^{av}(t)$, and a sinusoidal contribution. A rotating coordinate system is defined by the angle function, $\theta_{CS}(t)$, and in this frame the sinusoidal part may be represented by a complex phasor, $\vec{S}^{ph}$. Thus the input signal has theform

$$s(t) = S^{av} + \mathrm{Re}\left[\vec{S}^{ph} e^{j\theta_{CS}(t)}\right] \tag{D-1}$$

We want to extract the generating phasor $\vec{S}^{ph}$ and the average value S^{av}.

It has been described in chapter 10 how the results in Appendix B can be utilized, because the input signal may be written as

$$s(t) = S^{av} + \frac{\vec{S}^{ph}}{2} e^{j\theta_{CS}(t)} + \frac{\vec{S}^{ph*}}{2} e^{-j\theta_{CS}(t)} \tag{D-2}$$

according to (10-9).

- **Frequency domain model**

Assume that the input signal has frequency ω, so that it can be written

$$s(t) = \mathrm{Re}\left[A e^{j\omega t}\right] \tag{D-3}$$

The output functions (see figure 10-7) become

$$\begin{aligned}\widetilde{S}^{av}(t) &= AG_{av}(j\omega) \\ \widetilde{\widetilde{S}}^{ph}(t) &= AG_{p}(j\omega)e^{j(\omega-\omega_{CS})t} + A^{*}G_{p}(-j\omega)e^{-j(\omega+\omega_{CS})t}\end{aligned} \tag{D-4}$$

where the transfer functions are given by equations (B-6) and (B-7). We may define

$$\boxed{\begin{aligned}G_{ph}(j\omega) &= G_{p}(j\omega) \\ G_{phx}(j\omega) &= \left[G_{p}(-j\omega)\right]^{*}\end{aligned}} \tag{D-5}$$

Then

$$\begin{aligned}\widetilde{S}^{av}(t) &= AG_{av}(j\omega) \\ \widetilde{\widetilde{S}}^{ph}(t) &= AG_{ph}(j\omega)e^{j(\omega-\omega_{CS})t} + \left[AG_{phx}(j\omega)e^{j(\omega+\omega_{CS})t}\right]^{*}\end{aligned} \tag{D-6}$$

In the formulas the transfer function $G_{ph}(j\omega)$ provides the desired output, while $G_{phx}(j\omega)$ represents the transfer function that we would like to suppress as much as possible.

- **Time domain model**

In a single phase Phasor Estimation the two lowpass filters generating positive and negative sequence output signals have identical charactersistics. Thus

$$H_{p}(p) = H_{n}(p) = H_{ph}(p) \tag{D-7}$$

Direct inspection in (10-3) and (10-4) yields that, when the phasor filters are identical, the output function $w^{av}(t)$ is real-valued and the output functions $\hat{w}^{p}(t), \hat{w}^{n^{*}}(t)$ are each other's complex conjugate.

In Appendix B, equations (B-11) and (B-12), we derived a time domain model of the three-phase Phasor Estimator. Now all lowpass phasor filters are identical so we can put

$$\begin{aligned}A_{p} &= A_{n} = A_{ph} \\ B_{p} &= B_{n} = B_{ph} \\ C_{p} &= C_{n} = C_{ph}\end{aligned} \tag{D-8}$$

All these matrices $[A_{av}, B_{av}, C_{av}, A_{ph}, B_{ph}, C_{ph}]$ are real-valued and so is the input function $s(t)$. Then the states x_p and x_n are complex conjugates. The state equation in (B-11) then can be reduced as follows

$$\boxed{\begin{aligned} \dot{x}_{av} &= A_{av}x_{av} + B_{av}\left[s(t) - 2C_{ph}x_{phd}\right] \\ \dot{x}_{phd} &= A_{ph}x_{phd} - \omega_{CS}x_{phq} + B_{ph}\left[s(t) - C_{av}x_{av} - C_{ph}x_{phd}\right] \\ \dot{x}_{phq} &= A_{ph}x_{phq} + \omega_{CS}x_{phd} + B_{ph}C_{ph}x_{phq} \end{aligned}} \tag{D-9}$$

where x_{phd} and x_{phq} are the real and imaginary part of the phasor states. In matrix form

$$\boxed{\begin{pmatrix} \dot{x}_{av} \\ \dot{x}_{phd} \\ \dot{x}_{phq} \end{pmatrix} = \begin{pmatrix} A_{av} & -2B_{av}C_{ph} & 0 \\ -B_{ph}C_{av} & A_{ph} - B_{ph}C_{ph} & -\omega_{CS}I \\ 0 & \omega_{CS}I & A_{ph} + B_{ph}C_{ph} \end{pmatrix} \begin{pmatrix} x_{av} \\ x_{phd} \\ x_{phq} \end{pmatrix} + \begin{pmatrix} B_{av} \\ B_{ph} \\ 0 \end{pmatrix} s(t)} \tag{D-10}$$

The output signals are given by

$$\boxed{\begin{aligned} w^{av}(t) &= C^{av}x_{av} \\ \widehat{w}^{p}(t) &= C^{ph}\left[x_{phd} + jx_{phq}\right] \\ \widetilde{\widetilde{S}}(t) &= \widehat{w}^{p}(t)e^{-j\theta_{CS}(t)} \end{aligned}} \tag{D-11}$$

APPENDIX E
Phasor Estimation using RLS algorithm

The problem to extract the average value S^{av} and the phasor $\vec{S}^{ph} = S_d^{ph} + jS_q^{ph}$ that approximates the input scalar function *s(t)* has been defined in chapter 10 in equations (10-13) – (10-16). The solution is given by the recursive scheme

$$\boxed{\begin{aligned} &r_{e,k} = \lambda + \varphi_k^t P_{k-1}\varphi_k, \quad P_{-1} = \Pi_0 \\ &K_{p,k} = P_{k-1}\varphi_k r_{e,k}^{-1} \\ &P_k = \frac{\left(I - K_{p,k}\varphi^t\right)P_{k-1}}{\lambda} \\ &\Theta_k = \Theta_{k-1} + K_{p,k}\left(s_k - \varphi^t\Theta_{k-1}\right), \quad \Theta_{-1} = 0 \end{aligned}} \tag{E-1}$$

Here the forgetting factor λ has been introduced in order to make the algorithm respond dynamically to changes in the input signal. The bandwidth of the estimation using sampling time t_s is given by the cutoff frequency ω_{CO}

$$\omega_{CO} = \frac{1-\lambda}{t_s} \tag{E-2}$$

Let the coordinate system be rotating with fixed angular frequency ω_{CS} and assume that (10-11) applies. The regressors $\varphi(t)$ given in (10-14) are periodic and in steady state the gain $K_{p,k}$ converges to a constant for the average component and sinusoidal time functions for the phasor components. Assume that the sampling time is short compared with the cycle time. The steady state solution to (E-1) then has the form in (10-17) with the gain

$$K(t) = \begin{pmatrix} \lambda_{AV} \\ \lambda_{PH}\cos(\omega_{CS}t + \mu) \\ -\lambda_{PH}\sin(\omega_{CS}t + \mu) \end{pmatrix} \tag{E-3}$$

The constants depend on the cutoff frequency $\omega_{CO,AV}$ for the average component and $\omega_{CO,PH}$ for the phasor components according to the formulas in (E-4).

$$\begin{aligned} \lambda_{AV} &= \omega_{CO,AV} \\ \xi_F &= \frac{\omega_{CO,PH}}{\omega_{CS}} \\ \lambda_{PH} &= \omega_{CO,PH}\sqrt{4 + 5\xi_F^2 + \xi_F^4} \\ \mu &= \arctan\left(\frac{3\xi_F}{2 - \xi_F^2}\right) \end{aligned} \tag{E-4}$$

- **Direct time-domain model**

Equation (10-17) together with the gain factor in (E-3) constitutes one time domain model, which maps the scalar input function *s(t)* into the phasor estimate $\vec{S}^{ph}$.

Example E-1

We select the cutoff frequencies *10 Hz* for the average and *15 Hz* for the phasor estimation. Figure E-1 depicts the time domain response of the phasor estimation at a suddenly applied *50 Hz* sinusoidal input signal. Coordinate system also rotates with the same frequency.

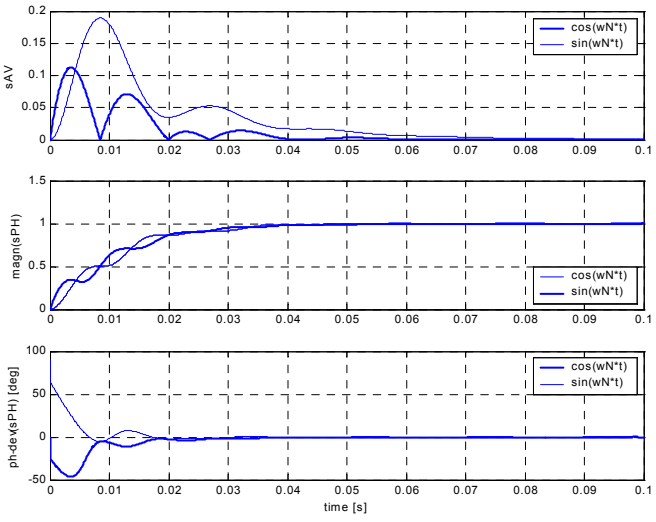

Figure E-1 Time –domain response of phasor estimation using RLS steady-state gain.

The calculated response to suddenly applied cosine or sine input signal is depicted in figure E-1. This figure can be compared with the results presented in figure 10-8. It seems that the performance of different methods to extract the phasor are rather similar.

- **Linear time-invariant time-domain model**

The estimated phasor can be transformed back to the *FIXED* coordinate by the transformation

$$S_\alpha^{ph} + jS_\beta^{ph} = \vec{S}_{\alpha\beta}^{ph} = e^{j\omega_{CS}t}\vec{S}^{ph} = e^{j\omega_{CS}t}\left(\vec{S}_q^{ph} + j\vec{S}_q^{ph}\right) \tag{E-5}$$

The following time-domain model then applies

$$\boxed{\begin{aligned}\frac{d}{dt}\begin{pmatrix} S^{av} \\ S_\alpha^{ph} \\ S_\beta^{ph} \end{pmatrix} &= \begin{pmatrix} -\lambda_{AV} & -\lambda_{AV} & 0 \\ -\lambda_{PH}\cos\mu & -\lambda_{PH}\cos\mu & -\omega_{CS} \\ \lambda_{PH}\sin\mu & \omega_{CS}+\lambda_{PH}\sin\mu & 0 \end{pmatrix}\begin{pmatrix} S^{av} \\ S_\alpha^{ph} \\ S_\beta^{ph} \end{pmatrix} + \begin{pmatrix} \lambda_{AV} \\ \lambda_{PH}\cos\mu \\ -\lambda_{PH}\sin\mu \end{pmatrix} s(t) \\ \vec{S}^{ph} &= S_d^{ph} + jS_q^{ph} = \left(S_\alpha^{ph} + jS_\beta^{ph}\right)e^{-j\omega_{CS}t}\end{aligned}} \tag{E-6}$$

The interesting feature with the model (E-6) is that it is a linear, time-invariant (LTI) model .

- **Frequency-domain**

Due to its LTI property any input signal *s(t),* which is sinusoidal with frequency ω, produces sinusoidal output signals in (E.6) that have the same frequency ω. The lower formula in (E-6) shows that the following set of signal components is obtained

$$\begin{aligned} s(t) &= \mathrm{Re}\left\{Ae^{j\omega t}\right\} \\ S^{av}(t) &= \mathrm{Re}\left\{Be^{j\omega t}\right\} \\ S_d^{ph}(t) &= \mathrm{Re}\left\{C_1 e^{j(\omega-\omega_{CS})t} + C_2^* e^{-j(\omega+\omega_{CS})t}\right\} \\ S_q^{ph}(t) &= \mathrm{Im}\left\{C_1 e^{j(\omega-\omega_{CS})t} + C_2^* e^{-j(\omega+\omega_{CS})t}\right\} = \mathrm{Re}\left\{-jC_1 e^{j(\omega-\omega_{CS})t} - jC_2^* e^{-j(\omega+\omega_{CS})t}\right\} \end{aligned} \tag{E-7}$$

The following relations apply

$$\begin{pmatrix} G^{av}(j\omega) \\ G_P^{ph}(j\omega) \\ G_{PX}^{ph}(j\omega) \end{pmatrix} = \begin{pmatrix} B/A \\ C_1/A \\ C_2/A \end{pmatrix} = M^{-1}N \tag{E-8}$$

where

$$M = \begin{pmatrix} \lambda_{AV} + j\omega & \lambda_{AV} & \lambda_{AV} \\ \lambda_{PH}e^{-j\mu} & \lambda_{PH}e^{-j\mu} + 2j(\omega - \omega_{CS}) & \lambda_{PH}e^{-j\mu} \\ \lambda_{PH}e^{j\mu} & \lambda_{PH}e^{j\mu} & \lambda_{PH}e^{j\mu} + 2j(\omega + \omega_{CS}) \end{pmatrix}$$

$$N = \begin{pmatrix} \lambda_{AV} \\ \lambda_{PH}e^{-j\mu} \\ \lambda_{PH}e^{j\mu} \end{pmatrix} \tag{E-9}$$

Example E-2

The desired contribution to the output estimated phasor components is provided by the transfer function $G_P^{ph}(j\omega)$. The transfer function $G_{PX}^{ph}(j\omega)$ represents the undesired disturbance contribution. Figure E-2 shows the calculated transfer functions for the phasor estimator in Example E-1. The curves can be compared with those in figure 10-8.

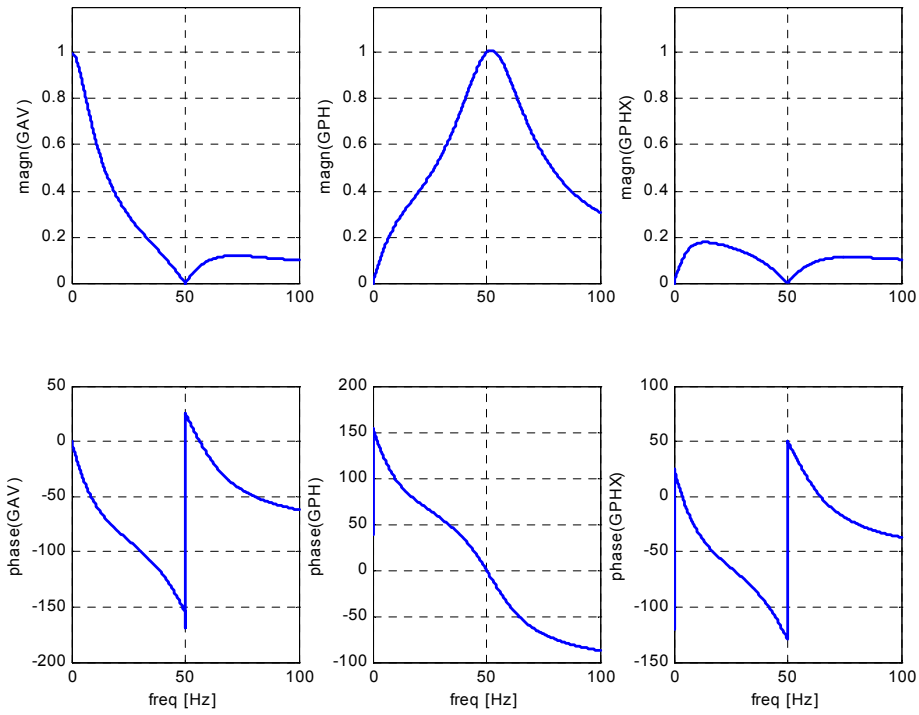

Figure E-2 Transfer functions for the RLS-based phasor estimator.

APPENDIX F

Time domain model of PLL

In this appendix the time domain model of the PLL as implemented in figure 11-8 will be derived. For this purpose we shall assume that the PLL frequency regulator (including the integrator from frequency to angle) is represented by a linear state-space system according to (F-1) below.

$$\begin{aligned} \dot{z}_{PLL} &= A'_{PLL}\, z_{PLL} + B'\Delta\varphi_{PLL} \\ \Delta\theta_{PLL} &= C'_{PLL}\, z_{PLL} + D'_{PLL}\,\Delta\varphi_{PLL} \end{aligned} \tag{F-1}$$

The adequate phasor estimator model can be obtained from Appendix C formula (C-22)

$$\begin{aligned} \dot{z}_{PE} &= A'_{PE}\, z_{PE} + B'_{PE}\begin{pmatrix} \Delta\widetilde{i}_{Ld}^{R} \\ \Delta\widetilde{i}_{Lq}^{R} - \Delta\theta_{PLL} \end{pmatrix} \\ \Delta\varphi_{PLL} &= C'_{PE}\, z_{PE} \end{aligned} \tag{F-2}$$

where

$$A'_{PE} = \left(\begin{array}{ccc|ccc} A_{av} & -B_{av}C_p & -B_{av}C_n & \omega_N & 0 & 0 \\ -B_pC_{av} & A_p & -B_pC_n & 0 & 0 & 0 \\ -B_nC_{av} & -B_nC_p & A_n & 0 & 0 & 2\omega_N \\ \hline -\omega_N & 0 & 0 & A_{av} & -B_{av}C_p & -B_{av}C_n \\ 0 & 0 & 0 & -B_pC_{av} & A_p & -B_pC_n \\ 0 & 0 & -2\omega_N & -B_nC_{av} & -B_nC_p & A_n \end{array}\right)$$

$$B'_{PE} = \begin{pmatrix} B_{av} & 0 \\ B_p & 0 \\ B_n & 0 \\ 0 & B_{av} \\ 0 & B_p \\ 0 & B_n \end{pmatrix} \qquad C'_{PE} = \left(\begin{array}{ccc|ccc} 0 & 0 & 0 & 0 & C_p & 0 \end{array}\right) \tag{F-3}$$

The combination of (F-1) and (F-2) yields the total state-space system

$$\begin{aligned} \dot{x}_{PLL} &= A_{PLL}x_{PLL} + B_{PLL}\begin{pmatrix} \Delta\tilde{i}_{Ld}^{R} \\ \Delta\tilde{i}_{Lq}^{R} \end{pmatrix} \\ \Delta\theta_{PLL} &= C_{PLL}x_{PLL} \end{aligned} \tag{F-4}$$

where

$$x_{PLL} = \begin{pmatrix} z_{PLL} \\ z_{PE} \end{pmatrix} \tag{F-5}$$

and

$$\begin{aligned} A_{PLL} &= \begin{pmatrix} A'_{PLL} & B'_{PLL}C'_{PE} \\ -B'_{PE}P_{01}C'_{PLL} & A'_{PE} - B'_{PE}P_{01}D'_{PLL}C'_{PE} \end{pmatrix} \qquad P_{01} = \begin{pmatrix} 0 \\ 1 \end{pmatrix} \\ B_{PLL} &= \begin{pmatrix} 0 & 0 \\ 0 & B'_{PE} \end{pmatrix} \qquad C_{PLL} = \begin{pmatrix} C'_{PLL} & D'_{PLL}C'_{PE} \end{pmatrix} \end{aligned} \tag{F-6}$$

REFERENCES

- **Books**

[B1] P.K. Kovács, "Transient Phenomena in Electrical Machines", Elsevier, ISBN 0-444-99663-X

[B2] K.J Åström, B. Wittenmark, "Adaptive Control", Addison-Wesley, ISBN 0-201-55866-1

[B3] T. Kailath, A.H. Sayed, B. Hassibi, "Linear Estimation", Prentice Hall, ISBN 0-13-022464-2

[B4] O. Yaniv, "Quantitative Feedback design of linear and nonlinear control systems", Kluwer Academic Publishers, ISBN 0-7923-8529-2

[B5] P.M. Anderson, B.L. Agrawal, J.E. Van Ness, "Subsynchronous resonance in power systems", IEEE Press, ISBN 0-87942-258-0

- **Papers about TCSC installations**

[I1] R.M. Maliszewski, B.M. Pasternack, H.N. Scherer Jr., M. Chamia, H.Frank, L.Paulsson, "Power flow control in a highly integrated transmission network", Cigré 1990, paper 37-303

[I2] A.J.F. Keri, B.J. Ware, R.A. Byron, A.S. Mehraban, M. Chamia, P. Halvarsson, L. Ängquist, "Improving transmission system performance using controlled series capacitors", Cigré 1992, paper 14/37/38-07

[I3] A.H. Montoya, D.R. Torgerson, B.A. Vossler, W. Feldmann, G. Juette, K. Sadek, A. Schultz, "230 kV Advanced Series Compensation, Kayenta substation – Arizona, project overview", EPRI FACTS Workshop Cincinatti, Ohio, November 14-16, 1990

[I4] N. Christl, R. Hedin, K. Sadek, P. Lutzelberger, P.E. Krause, S.M. McKenna, A.H. Montoya, D. Torgerson, "Advanced Series Compensation (ASC) with thyristor controlled impedance", Cigré 1992, paper 4/37/38-05

[I5] J. Urbanek, R.J.Piwko, E.V. Larsen, B.L. Damsky, B.C: Furumasu, W.A. Mittelstadt, J. Eden, "Thyristor Controlled Series Compensation prototype installation at the Slatt 500 kV substation", IEEE PES, paper 92 SM 467-1 PWRD

[I6] R.J. Piwko, C.A. Wegner, B.C. Furumasu, B.L. Damsky, J.D. Eden, "The Slatt Thyristor-Controlled Series Capacitor project – design, installation, commissining and system testing", Cigré 1994, paper 14-104

[I7] D. Holmberg, M. Danielsson, P. Halvarsson, L. Ängquist, "The Stöde Thyristor Controlled Series Capacitor", Cigré 1998, paper 14-105

[I8] C. Gama, L. Ängquist, G. Ingeström, M. Noroozian, "Commissioning and operative experience of TCSC for damping power oscillation in the Brazilian North-South interconnection", Cigré 2000, paper 14-104

- **Papers about TCSC modelling**

[M1] N. Christl, P. Luetzelberger, M. Pereira, K. Sadek, A.H. Montoya, D.R. Torgerson, B.A. Vossler, "Advanced Series Compensation with variable impedance", EPRI FACTS Workshop, Cincinatti, Ohio, November 14-16, 1990

[M2] S.G. Helbing, G.G. Karady, "Investigation of an advanced form of series compensation", IEEE PES, paper 93 SM 431-7 PWRD

[M3] S.G. Jalili, R.H. Lasseter, "Harmonic instabilities in Advanced Series Compensators", EPRI FACTS2 Conference, Boston, 1992

[M4] S.G. Jalili, R.H. Lasseter, I. Dobson, "Dynamic response of a Thyristor Controlled Switched Capacitor", IEEE PES, paper 94 WM 065-3 PWRD

[M5] S.G. Jalili, R.A. Hedin, M. Pereira, K. Sadek, "A stability model for the Advanced Series Compensator (ASC)", IEEE PES, paper 95 SM 404-4 PWRD

[M6] H.A. Othman, L. Ängquist, "Analytical modeling of Thyristor-Controlled Series Capacitors for SSR Studies", IEEE PES, paper 95 WM 171-9 PWRS

[M7] A. Ghosh, G. Ledwich, "Modelling and control of thyristor-controlled series compensators", IEE Proc.- Gener. Transm. Distr., Vol. 142, No.3, May 1995

[M8] Perkins, Iravani, "Dynamical Modeling of a TCSC with application to SSR analysis", IEEE PES paper PE-477-PWRS-0-01-1997

[M9] P. Mattavelli, G.C. Verghese, A.M. Stankovic, "Phasor Dynamics of Thyristor-Controlled Series Capacitor systems", IEEE PES paper 96 SM 532-2 PWRS

[M10] L. Ängquist, G. Ingeström, H.-Å. Jönsson, "Dynamical performance of TCSC schemes", Cigré 1996, paper 14-302

- **Papers about TCSC applications and performance**

[A1] E. Larsen, C. Bowler, B. Damsky, S. Nilsson, "Benefits of Thyristor Controlled Series Compensation", Cigré 1992, paper 14/37/38-04

[A2] M. Noroozian, G. Andersson, "Power flow control by use of controllable series components", IEEE PES paper 92 SM 466-3 PWRD

[A3] L. Ängquist, B. Lundin, J. Samuelsson, "Power oscillation damping using controlled reactive power compensation – a comparison between series and shunt approaches", IEEE PES paper 92 SM 539-7 PWRS

[A4] S. Nyati, C.A. Wegner, R.W. Delmerico, R.J. Piwko, D.H. Baker, A. Edris, "Effectiveness of Thyristor Controlled Series Capacitor in enhancing power system dynamics: an analog simulator study", IEEE PES paper 93 SM 432-5 PWRD

[A5] E.V. Larsen, K. Clark, S.A. Miske Jr, J. Urbanek, "Characteristics and rating considerations of Thyristor Controlled Series Compensation", IEEE PES paper 93 SM 433-3 PWRD

[A6] C.A. Gama, J.L. Scavassa, W.M. da Silva, J.M.M. da Silva, J.R. Ponte, "Prospective application of advanced series compensation to improve transmission system performance", Cigré 1994, paper 14-204

[A7] W. Zhu, R. Spee, R.R. Mohler, G.G.Alexander, W.A. Mittelstadt, D. Maratukulam, "An EMTP study of SSR using the Thyristor Controlled Series Capacitor", IEEE PES paper 94 SM 477-0 PWRD

[A8] M. Noroozian, G. Andersson, "Damping of inter-area and local modes by use of controllable components", IEEE PES paper 95 WM 267-5 PWRD

[A9] D.N. Kosterev, W.A. Mittelstadt, R.R: Mohler, W.J. Kolodziej, "An application study for sizing and rating controlled and conventional series compensation", IEEE PES paper 95 SM 401-0 PWRD

[A10] R.J. Piwko, C.A. Wegner, S.J. Kinney, J.D. Eden, "Subsynchronous resonance performance tests of the Slatt thyristor-Controlled Series Capacitor, IEEE PES paper 95 SM 402-8 PWRD

[A11] R. Rajaraman, I. Dobson, R.H. Lasseter, Y. Shern, "Computing the damping of subsynchronous oscilaltions due ot a Thyristor Controlled Series Capacitor", IEEE PES paper 95 SM 403-6

[A12] D.J. Trudnowski, M.K. Donnelly, J.F. Hauer, "Estimating damping effectiveness of BPA's Thyristor Controlled Series Capacitor by applying time and frequency domain methods to measure response", IEEE PES paper 95 SM 519-9 PWRS

[A13] G. Ban, L. Prikler, G.G. Karady, B. Banfai, "investigation of the transients in the Advanced Series Compensation scheme", Cigré 1996, paper 14-201

[A14] H. Okamoto, A, Kurita, K. Clark, E.V. Larsen, N.W. Miller, "Modeling and performance of multiple multi-mode TCSCs in ATP", Cigré 1996, paper 14-307

[A15] R. Rajaraman, I. Dobson, “Damping estimates of subsynchronous and power swing oscillations in power systems with thyristor switching devices”, IEEE PES paper 96 WM 255-0 PWRS

[A16] C. Gama, R.L. Leoni, J. Gribel, R. Fraga, M.J. Eiras, W. Ping, A. Ricardo, J. Cavalcanti, R. Tenorio, “Brazilian North-South Interconnection - application of Thyristor Controlled Series Compensation (TCSC) to damp inter-area oscillation mode”, Cigré 1998, paper 14-101

[A17] R. Rajaraman, I. Dobson, “Justification of torque per unit velocity methods of analyzing subsynchronous resonance and a swing mode in power systems”, IEEE Trans. on Circuits and Systems-I: Fundamental Theory and Applications, Vol., 45, No. 10, October 1998

[A18] P. Mattavelli, A.M. Stankovic, G.C. Verghese, “SSR analysis with dynamic phasor model of Thyristor-Controlled Series Capacitor”, IEEE Trans. on Power Systems, Vol. 14, No. 1, February 1999

[A19] N. Martins, H.J.C.P. Pinto, J.J. Paserba, “Using a TCSC for line power scheduling and system oscillation damping – small signala and transient stability studies”, paper 0-7803-5938-0/00, 2000 IEEE

[A20] L. Ängquist, C. Gama, “Damping Algortihm based on Phasor Estimation”, paper 0-7803-6674-3, 2000 IEEE (IEEE PES WM 2001 paper 63-04)

[A21] D.J. McDonald, J. Urbanek, B.L. Damsky, “Modeling and testing of a thyristor for Thyristor Controlled Series Compenstaion (TCSC), IEEE PES paper 93 WM 074-5 PWRD

- **Papers about signal estimation and three-phase representation**

[S1] D.S. Bayard, “A general theory of linear time-invariant adaptive feedforward systems with harmonic regressors”, IEEE Trans on Automatic Control, Vol. 45, No. 11, Nov. 2000

[S2] H.S. Song, K. Nam, “Instantaneous phase-angle algorithm under unbalanced voltage-sag conditions”, IEE Proc. – Gener. Transm. Distr., Vol 147, No. 6, November 2000

[S3] A. Ferrero, L. Giuliano, J.L. Willems, “ A new space-vector transformation for four-conductor systems”, ETEP Vol. 10, No. 3, May/June 2000

- **Patent**

[P1] “Control equipment for a series capacitor connected into an electric power line” SE 504 302, EP0689272, US 5801459,CA2150319,DE6950920

LIST OF SYMBOLS

Coordinate systems

FIXED	Coordinate system with phases *a,b,c*
IL_SYNC	Rotating coordinate system aligned with the undisturbed line current
CONV_ORI	Sequence of frames coordinated with the switching of the converter

General

Capital letters	rms values or magnitude of phasors
Capital letters ´ $\vec{A}$ ´	phasor/vector
Capital letters ´ $\hat{A}$ ´	peak value
Capital letters ´ $\widetilde{A}$ ´	estimated value
Lower case letters	instantaneous values
Lower case letters ‘ $\bar{a}(t)$ ’	three-dimensional vectors
Lower case letters ‘ $\bar{a}(t)$ ’	two-dimensional vectors, “space vectors”
Lower case letters ‘ $\widetilde{a}(t)$ ’	normalized quantity
Δ	deviation from steady state operating point

Subscripts

a,b,c	phase quantities in *FIXED* coordinates
α,β,γ	components in the *FIXED* coordinates
d,q,0	components in the rotating *IL_SYNC* coordinates
u,v,w	phase quantities in the *CONV_ORI* sequence of frames
x,y,z	components in the *CONV_ORI* sequence of frames

l-l	line-line
meas	measured value
N	nominal/rated value
post	value immediately after reversal
pre	value immediately before reversal
ref	reference value

Superscripts

*	complex conjugate
av	average
k (numeric)	frame *k* in *CONV_IL* sequence of frames
n	negative-sequence
p	positive sequence
R	rotating coordinate system *IL_SYNC*
t	transponate

Specific Symbols

A_{rev}	matrix representing the voltage reversal
B_P	matrix representing impact of line current on capacitor voltage
C	series capacitor capacitance
D_{el}	electrical damping coefficient [pu torque/pu speed variation]
D_f	loss factor for voltage reversal
F_{beg}, F_{end}	matrices for obtaining averaged capacitor voltage output from states
F, F_{XR}	transfer function for prefilter (acting on boost reference)
G_{IL}	matrix representing direct impact of line current on capacitor voltage
G_θ	matrix representing direct impact of control angle on capacitor voltage
G_P	transfer function for scalar input signal
G_P^R	complex-complex transfer function in *IL_SYNC* coordinates
$G_{PE}^{R,d->d}, G_{PE}^{R,d->q}$ $G_{PE}^{R,q->d}, G_{PE}^{R,q->q}$	transfer functions between components in *IL_SYNC* coordinates
H_{av}, H_p, H_n	lowpass filter operators for complex input signals
H_{av}, H_{ph}	lowpass filter operators for scalar input signals
H_{PLL}	transfer function in PLL frequency regulator (from angle error to angular frequency)

$H_{PLLd}^{cl}, H_{PLLq}^{cl}$	closed loop transfer function from line current's *d*- and *q*-components to PLL's output = the measured line current phase
G_{Breg}	transfer function in boost regulator
I	unit matrix
i_L	line current
$\hat{I}_L$	steady state line current amplitude
I_{Lsub}	subsynchronous line current component
i_V	valve current
h	sampling time (may be half or sixth cycle at network frequency)
K_{el}	electrical spring constant [pu torque/rad]
k_B	boost factor
$\Delta k_{B,m}$	measured boost factor (response to regulator)
$K_{TL}^{R,d->d}, K_{TL}^{R,q->d}$ $K_{TL}^{R,d->q}, K_{TL}^{R,q->q}$	transfer functions from bus voltage deviations to line current deviations between components in *IL_SYNC* coordinates
k_Z	factor for apparent impedance
L	inductance in TCSC valve branch
$L_{sh,d}^{R}, L_{sh,q}^{R}$	transfer functions from shaft speed deviation to line current deviation in *IL_SYNC* coordinates
L_{TCSC}	apparent inductance in low-frequency approximation
M_{sh}	transfer function from shaft speed deviation to electrical torque deivation
Δn	generator shaft speed deviation (in pu)
P_{next}	transformation matrix between consecutive member frames in *CONV_ORI* sequence
P_{x2d}	transformation matrix from state to output in *IL_SYNC*
P_{100}	column matrix with *1* in first row
p	differentiating operator *d/dt*
q	time shift operator
R_{TCSC}	apparent resistance in low-frequency approximation
$\underline{\tilde{S}}^{av}, \underline{\tilde{S}}^{p}, \underline{\tilde{S}}^{n*}$	estimated phasors from complex input signal
$\tilde{S}^{av}, \tilde{S}^{ph}$	estimated average and phasor from scalar input signal
T_{del}	delay time from reference pulse to voltage reversal
T_{el}	electrical torque in generator (braking)
ΔT_{el1}	electrical torque deviation due to steady-state line current and deviation in flux
ΔT_{el2}	electrical torque deviation due to steady-state flux and deviation in line current
t_k	reversal time with thyristor *k* involved
u_C	capacitor voltage

$\widetilde{\widehat{u}}^{R}_{C,av}$	average of space vector representing capacitor voltage in *IL_SYNC* coordinates (=Fourier fundamental frequency component)
u_{CF}	capacitor voltage at firing
u_{CM}	measured capacitor voltage
$\hat{u}_{Cm}$	amplitude of harmonic component in capacitor voltage
$\widetilde{\widehat{u}}^{S}_{S}$	stator voltage (normalized) in *FIXED* coordinates
$\Delta u_{Td}, \Delta u_{Tq}$	bus voltage deviations
u_Z, u_{CZ}	reversal voltage (at instantaneous reversal)
$\hat{U}_{add}$	additional voltage caused by thyristor action
$\widehat{v}^{av}, \widehat{v}^{p}, \widehat{v}^{n*}$	estimated phasors transformed to *IL_SYNC* coordinates
$\widehat{w}^{av}, \widehat{w}^{p}, \widehat{w}^{n*}$	estimated phasors transformed back to *FIXED* coordinates
X_0	reactance at resonance in LC circuit
Z_{app}	apparent impedance of TCSC
α	TCSC firing angle
β	TCSC control angle
λ	TCSC design parameter, ratio ω_0/ω_N
σ	TCSC conduction angle
ξ	factor that characterize the line current approximation within the sampling interval, *0*=constant in *FIXED*, *1*=constant in *IL_SYNC* coordinates
θ_{CS}	angle of coordinate system for phasor estimation
ω_{CS}	anglular frequency of coordinate system for phasor estimation
φ	argument for time functions in *CONV_IL* sequence of frames
$\Delta\varphi_C$	angular deviation of instantaneous voltage reversal from its equilibrium position
$\Delta\theta_{PLL}$	phase error between real line current argument and PLL's output
$\Delta\theta_k$	phase advance angle for capacitor voltage reversal (command from regulator and PLL)
θ_{sh}	shaft angle in *FIXED* coordinates
ω	angular frequency in *FIXED* coordinates (argument in transfer functions)
ω_0	resonance angular frequency in TCSC
ω_N	network angular frequency
Ω	angular frequency in *IL_SYNC* coordinates (argument in transfer functions)
$\hat{\psi}_R$	constant rotor flux in generator
$\widetilde{\widehat{\psi}}^{S}_{S}$	stator flux linkage (normalized) in *FIXED* coordinates